HIGH FREQUENCY BRAIN SIGNALS: FROM BASIC RESEARCH TO CLINICAL APPLICATION

EDITED BY: Jing Xiang, Ryouhei Ishii and Xiaofeng Yang
PUBLISHED IN: Frontiers in Human Neuroscience

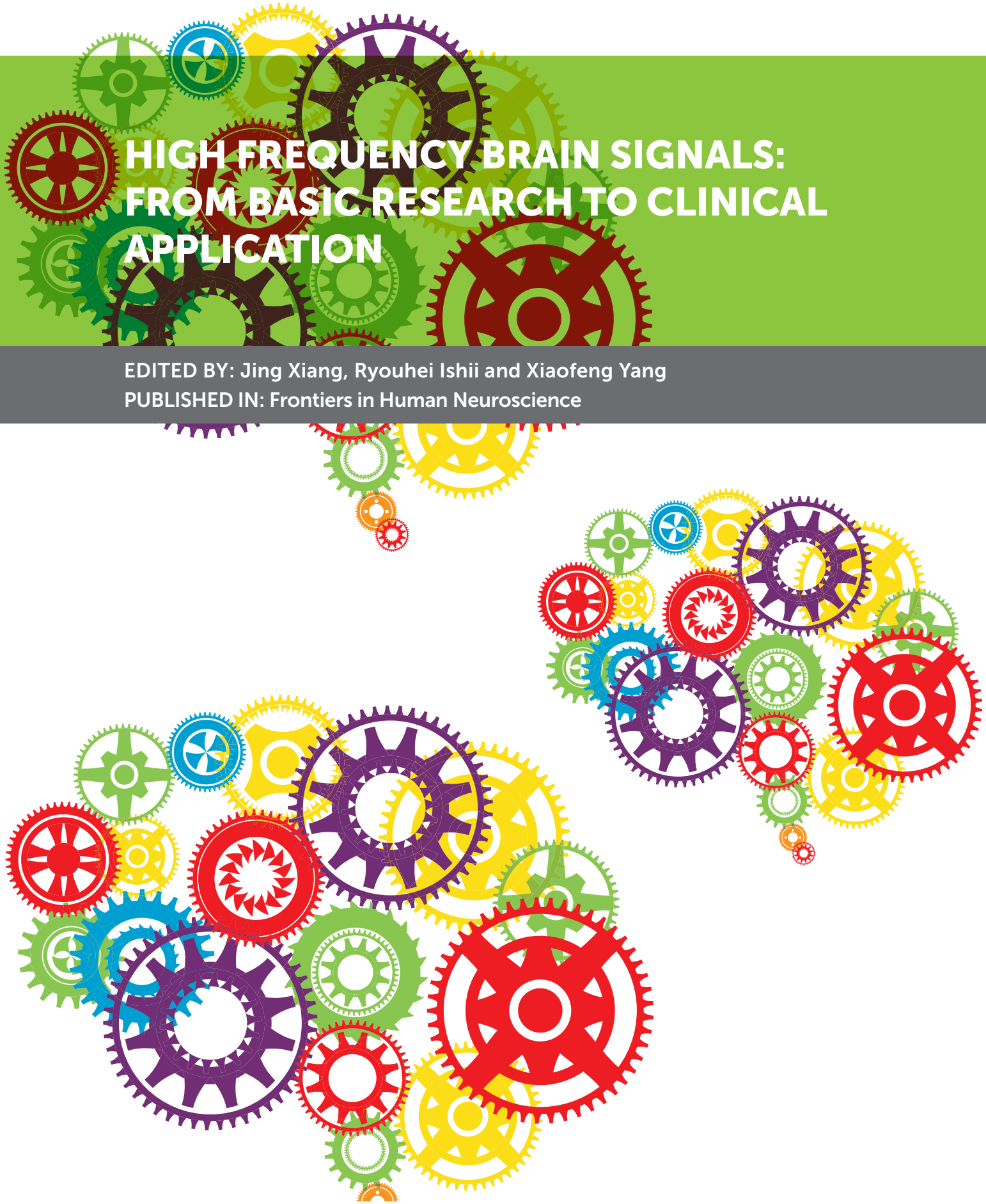

frontiers Research Topics

ISSN 1664-8714
ISBN 978-2-88976-009-1
DOI 10.3389/978-2-88976-009-1

About Frontiers

Frontiers is more than just an open-access publisher of scholarly articles: it is a pioneering approach to the world of academia, radically improving the way scholarly research is managed. The grand vision of Frontiers is a world where all people have an equal opportunity to seek, share and generate knowledge. Frontiers provides immediate and permanent online open access to all its publications, but this alone is not enough to realize our grand goals.

Frontiers Journal Series

The Frontiers Journal Series is a multi-tier and interdisciplinary set of open-access, online journals, promising a paradigm shift from the current review, selection and dissemination processes in academic publishing. All Frontiers journals are driven by researchers for researchers; therefore, they constitute a service to the scholarly community. At the same time, the Frontiers Journal Series operates on a revolutionary invention, the tiered publishing system, initially addressing specific communities of scholars, and gradually climbing up to broader public understanding, thus serving the interests of the lay society, too.

Dedication to Quality

Each Frontiers article is a landmark of the highest quality, thanks to genuinely collaborative interactions between authors and review editors, who include some of the world's best academicians. Research must be certified by peers before entering a stream of knowledge that may eventually reach the public - and shape society; therefore, Frontiers only applies the most rigorous and unbiased reviews.
Frontiers revolutionizes research publishing by freely delivering the most outstanding research, evaluated with no bias from both the academic and social point of view. By applying the most advanced information technologies, Frontiers is catapulting scholarly publishing into a new generation.

What are Frontiers Research Topics?

Frontiers Research Topics are very popular trademarks of the Frontiers Journals Series: they are collections of at least ten articles, all centered on a particular subject. With their unique mix of varied contributions from Original Research to Review Articles, Frontiers Research Topics unify the most influential researchers, the latest key findings and historical advances in a hot research area! Find out more on how to host your own Frontiers Research Topic or contribute to one as an author by contacting the Frontiers Editorial Office: frontiersin.org/about/contact

HIGH FREQUENCY BRAIN SIGNALS: FROM BASIC RESEARCH TO CLINICAL APPLICATION

Topic Editors:
Jing Xiang, Cincinnati Children's Hospital Medical Center, United States
Ryouhei Ishii, Osaka Prefecture University, Japan
Xiaofeng Yang, Bioland Laboratory, China

Citation: Xiang, J., Ishii, R., Yang, X., eds. (2022). High Frequency Brain Signals: From Basic Research to Clinical Application. Lausanne: Frontiers Media SA. doi: 10.3389/978-2-88976-009-1

Table of Contents

frontiers in Human Neuroscience

EDITORIAL
published: 30 March 2022
doi: 10.3389/fnhum.2022.872478

Editorial: High Frequency Brain Signals: From Basic Research to Clinical Application

Jing Xiang[1]*, *Ryouhei Ishii*[2] and *Xiaofeng Yang*[3]

[1] Department of Pediatrics and Neurology, Cincinnati Children's Hospital Medical Center, Cincinnati, OH, United States, [2] Graduate School of Comprehensive Rehabilitation, Osaka Prefecture University, Habikino, Japan, [3] Bioland Laboratory, Guangzhou Regenerative Medicine and Health, Guangzhou, China

Keywords: high frequency brain signal, high frequency oscillation, ripple, fast ripples, high gamma oscillation

Editorial on the Research Topic

High Frequency Brain Signals: From Basic Research to Clinical Application

High frequency brain signals (HFBS) can be divided into endogenous (spontaneous) HFBS and evoked HFBS. Endogenous HFBS are preliminarily detected in epilepsy patients. Endogenous HFBS in epilepsy include high frequency oscillations (HFOs), very high frequency oscillations (VHFOs), ripples, and fast ripples. Elicited or evoked HFBS are typically called high gamma (oscillations), which are functional activation and have been identified in the somatosensory, motor, visual, auditory, language and several other nerve systems. HFBS are typically recorded with invasive recordings, which include intracranial electroencephalography (iEEG), electrocorticography (ECoG) and stereoelectroencephalography (SEEG). Recent advances in magnetoencephalography (MEG) and scalp electroencephalography (EEG) have shown promising results for non-invasive detection of HFBS. Invasive recordings provide convincing data, although its applications are limited to accessible brain areas (low spatial sampling). Modern MEG can detect HFBS from the entire brain, which opens a new avenue for non-invasive detection and localization of HFBS.

Since epilepsy is one of the world's most common neurological disorders, it is important to find new biomarkers in epilepsy. Birk et al. showed that HFOs were significantly increased during ictal periods and significantly decreased during postictal periods compared to the ictal segment in a chronic focal epilepsy model in rats. Ictal ripples and fast ripples were significantly higher in severe seizures than in mild seizures. The results of this study indicate that HFOs can be used as biomarkers for measuring seizure severity in epilepsy. Ramon and Holmes showed that EEG ripples were markers of abnormally increased cortical excitability. Phase cone clustering patterns in EEG ripple bands were potential tools that could assist in localizing the epileptogenic zone (EZ).

Despite epilepsy being one of the most common neurologic disorders seen in children, there is no clear consensus regarding whether to treat or not to treat epileptiform discharges after a first unprovoked seizure. El Shakankiry and Arnold addressed the question by analyzing the coexistence of ripples/ HFOs with interictal epileptiform discharges in routinely acquired scalp EEG. The results showed that including analysis of HFOs in routine EEG interpretation could guide the decision to either start or discontinue anti-seizure medication. Yan et al. showed that the energy of HFOs could distinguish physiological HFOs from pathological ones more accurately than frequency. On scalp EEG, gamma oscillations could better detect susceptibility to epilepsy than ripple and FR oscillations. HFOs could trigger spasms. Of note, the analysis of average HFO energy could be used as a predictor of the effectiveness of epilepsy treatment in children.

One limitation in clinical applications of HFOs is that there is a significant inter-individual variation among patients. Qi et al. showed that the relative strength of HFO, especially fast ripples,

Edited and reviewed by:
Mingzhou Ding,
University of Florida, United States

***Correspondence:**
Jing Xiang
Jing.Xiang@cchmc.org

Specialty section:
This article was submitted to Brain Imaging and Stimulation, a section of the journal Frontiers in Human Neuroscience

Received: *09 February 2022*
Accepted: *11 March 2022*
Published: *30 March 2022*

Citation:
Xiang J, Ishii R and Yang X (2022) Editorial: High Frequency Brain Signals: From Basic Research to Clinical Application. Front. Hum. Neurosci. 16:872478. doi: 10.3389/fnhum.2022.872478

was a promising effective biomarker for identifying the EZ with minimum individual variation. Clinical resection of the brain areas generating HFOs with the highest relative strength could lead to a favorable seizure outcome. Li et al. showed that the combination of PET-MRI and HFOs provided significantly more information than each modality alone for precise localization of EZs. The periphery of the lesion marked by neuroimaging might be epileptic, but not every lesion contributed to seizures. Therefore, approaches in multimodality could detect EZ more accurately, and HFO analysis helped in defining real epileptic areas.

Multi-frequency analysis of HFBS is important for basic research and clinical applications. Ren et al. showed that both ripples and fast ripples superimposed more frequently on slow waves in EZ than in non-EZ. Although ripples preferred to occur on the down state of slow waves in both two groups, ripples in EZ tended to be closer to the down-state peak of slow wave than in non-EZ. Slow wave-containing ripples in EZ had a steeper slope and wider distribution ratio than those in the non-EZ. But for slow wave-containing FR, only a steeper slope could be observed. A combination of HFOs and slow wave in EZ and non-EZ from refractory focal epilepsy could improve surgical outcomes. Sun et al. showed that the termination of absence seizures was associated with a dynamic neuromagnetic process. Frequency-dependent changes in the functional connection could be observed during seizure termination. Neuromagnetic activity in different frequency bands might play different roles in the pathophysiological mechanism during absence seizures.

Localization of HFBS provides crucial information for clinical treatment of epilepsy. Xu et al. showed the usage of HFOs for radiofrequency thermocoagulation (RFTC) for surgical treatment of drug-resistant focal epilepsy. The results of this study showed that RFTC targeting at brain areas generating ictal high-frequency-discharge, fast-rhythm, and low-voltage could result in favorable surgical outcomes. Wang et al. showed that fast ripples could be extensively detected in tuberous sclerosis complex patients using SEEG. Interestingly, high fast ripple rate contacts were mostly localized in the junction region of the epileptogenic tuber, which could aid in the localization of epileptogenic tubers for surgical treatment.

HFBS can be detected in patients with persistent postural-perceptual dizziness (PPPD). Jiang et al. showed that the frontal cortex generated aberrant activities in 1–4, 80–250, and 250–500 Hz in PPPD patients compared with healthy controls. The finding indicated that alterations in the frontal cortex played a critical role in the pathophysiological mechanism of PPPD.

AUTHOR CONTRIBUTIONS

All authors listed have made a substantial, direct and intellectual contribution to the work and approved it for publication.

ACKNOWLEDGMENTS

We thank all authors for their time, support and contributions to this topic.

Conflict of Interest: The authors declare that the research was conducted in the absence of any commercial or financial relationships that could be construed as a potential conflict of interest.

Publisher's Note: All claims expressed in this article are solely those of the authors and do not necessarily represent those of their affiliated organizations, or those of the publisher, the editors and the reviewers. Any product that may be evaluated in this article, or claim that may be made by its manufacturer, is not guaranteed or endorsed by the publisher.

frontiers in Human Neuroscience

ORIGINAL RESEARCH
published: 09 June 2020
doi: 10.3389/fnhum.2020.00186

Identifying the Epileptogenic Zone With the Relative Strength of High-Frequency Oscillation: A Stereoelectroencephalography Study

Lei Qi[1,2†], Xing Fan[1,3†], Xiaorong Tao[1,3], Qi Chai[1], Kai Zhang[1,3], Fangang Meng[1,3], Wenhan Hu[1], Lin Sang[2], Xiaoli Yang[2] and Hui Qiao[1,3]*

[1] Beijing Neurosurgical Institute, Capital Medical University, Beijing, China, [2] Beijing Fengtai Hospital, Beijing, China, [3] Department of Neurosurgery, Beijing Tiantan Hospital, Capital Medical University, Beijing, China

Background: High-frequency oscillation (HFO) represents a promising biomarker of epileptogenicity. However, the significant interindividual differences among patients limit its application in clinical practice. Here, we applied and evaluated an individualized, frequency-based approach of HFO analysis in stereoelectroencephalography (SEEG) data for localizing the epileptogenic zones (EZs).

Methods: Clinical and SEEG data of 19 patients with drug-resistant focal epilepsy were retrospectively analyzed. The individualized spectral power of all signals recorded by electrode array, i.e., the relative strength of HFO, was computed with a wavelet method for each patient. Subsequently, the clinical value of the relative strength of HFO for identifying the EZ was evaluated.

Results: Focal increase in the relative strength of HFO in SEEG recordings were identified in all 19 patients. HFOs identified inside the clinically identified seizure onset zone had more spectral power than those identified outside ($p < 0.001$), and HFOs in 250–500 Hz band (fast ripples) seemed to be more specific identifying the EZ than in those in 80–250 Hz band (ripples) ($p < 0.01$). The resection of brain regions generating HFOs resulted in a favorable seizure outcome in 17 patients (17/19; 89.5%), while in the cases of other patients with poor outcomes, the brain regions generating HFOs were not removed completely.

Conclusion: The relative strength of HFO, especially fast ripples, is a promising effective biomarker for identifying the EZ and can lead to a favorable seizure outcome if used to guide epilepsy surgery.

Keywords: high-frequency oscillation, wavelet analysis, stereo-EEG, seizure, epilepsy surgery

OPEN ACCESS

Edited by:
Jing Xiang,
Cincinnati Children's Hospital Medical Center, United States

Reviewed by:
Hailong Li,
Cincinnati Children's Research Foundation, United States
Amir Fared Al-Bakri,
University of Kentucky, United States

****Correspondence:***
Hui Qiao
hqiao1215@sina.com;
proqiao@sina.com

† These authors have contributed equally to this work

Specialty section:
This article was submitted to Brain Imaging and Stimulation, a section of the journal Frontiers in Human Neuroscience

Received: *18 March 2020*
Accepted: *27 April 2020*
Published: *09 June 2020*

Citation:
Qi L, Fan X, Tao X, Chai Q, Zhang K, Meng F, Hu W, Sang L, Yang X and Qiao H (2020) Identifying the Epileptogenic Zone With the Relative Strength of High-Frequency Oscillation: A Stereoelectroencephalography Study. Front. Hum. Neurosci. 14:186. doi: 10.3389/fnhum.2020.00186

INTRODUCTION

Fifty million people all over the world live with epilepsy, and 30% of epileptics suffer from drug-resistant epilepsy, which is defined as a failure to achieve seizure-free status by applying two (or more) appropriately chosen and administered antiepileptic drugs (Kwan et al., 2011; Kalilani et al., 2018). Currently, the optimal treatment for drug-resistant epilepsy is surgical intervention, and the outcome of epilepsy surgery depends greatly on the localization of the brain region that is

indispensable for initiating seizures, i.e., the epileptogenic zone (EZ) (Timoney and Rutka, 2017; Jehi, 2018).

The understanding of the EZ is evolving over time. In recent decades, epilepsy has been increasingly considered as a result of brain network disorder, and the concept of the EZ has expanded to "any region of the epileptogenic network," which opens a door for sophisticated neuroimaging and electrophysiological analyses (Spencer, 2002). To date, various techniques have been applied for investigating the epileptogenic network and identifying the EZ (Jehi, 2018; Nissen et al., 2018). Among those techniques, stereoelectroencephalography (SEEG) has been considered as the current "gold standard" for identifying the EZ by localizing the seizure onset zone in three dimensions (Gonzalez-Martinez, 2016; Bartolomei et al., 2017; Yang et al., 2018). Nevertheless, this "gold standard" still has much room for improvement. SEEG cannot detect seizure spikes efficiently all the time, and the conventional hallmark of epileptic activity, including spikes, is not a specific biomarker for the EZ (Rektor et al., 2009). Accordingly, simply removing the seizure onset zone identified at the time of surgery is not always sufficient to achieve a lasting good surgical outcome (Ramantani et al., 2018). It is necessary to find new specific biomarkers for the EZ to improve the outcome of epilepsy surgery.

Previous studies have verified that in seizures, preictal and interictal discharges show unique patterns on SEEG, and those patterns can be analyzed by specific signal analysis modalities, such as functional connectivity analysis and high-frequency oscillation (HFO) analysis (Bartolomei et al., 2017). HFO, which is defined as at least four oscillations with a frequency over 80 Hz, is suggested to be a promising biomarker of the EZ (Frauscher et al., 2017; Thomschewski et al., 2019). HFO can be divided into ripples (80–250 Hz), fast ripples (250–500 Hz), and very fast ripples (>500 Hz). According to recent studies, all three kinds of HFO have the potential to become valuable biomarkers for identifying the EZ (Brazdil et al., 2017; Hussain et al., 2017; Wang et al., 2017). However, significant interindividual differences are observed in HFO among patients, which prevent its widespread use in clinical practice (Xiang et al., 2009; Gliske et al., 2018). Theoretically, individually normalized HFO may do better in localizing the EZ than raw HFO (Xiang et al., 2009; Gliske et al., 2018).

The current study aimed to refine the HFO-based identification of the EZ by normalizing HFOs in SEEG recordings of each patient. An individualized, frequency-based approach for HFO normalization was applied. The normalization was accomplished by obtaining the relative strength (i.e., the relative spectral power) of each SEEG contact, which could be calculated by dividing the power of each contact by the averaged power of all the contacts. Subsequently, the correlation of the EZ identified by normalized HFOs with surgical outcome was discussed.

MATERIALS AND METHODS

Patients

Nineteen patients with drug-resistant focal epilepsy who underwent SEEG at the Department of Neurosurgery, Beijing Tiantan Hospital between January 2015 and December 2016 were retrospectively analyzed (mean age, 21.2; range, 3–33). The inclusion criteria were patients who underwent comprehensive presurgical non-invasive evaluations including seizure semiology analysis, scalp electroencephalography (EEG), magnetic resonance imaging (MRI), and positron emission computed tomography (PET-CT), and the placement of electrodes was confirmed by postimplantation CT. The exclusion criteria were as follows: (1) no clinical seizure was captured during SEEG monitoring; (2) the seizure onset zone remained undetermined after SEEG monitoring; and (3) the patient received either hemispherectomy or non-resective epilepsy surgery. The current study was approved by the institutional review board of Beijing Tiantan Hospital, and writing informed consents were obtained from all patients or their relatives.

SEEG Recording and Identification of the Seizure Onset Zone

The placement of SEEG depth electrodes (8–16 contacts for each electrode, 0.8 mm diameter, 3.5 mm intercontact distance) was performed by the same surgery team using the Integra CRW System (NeuroSight Arc 2.7.1, Integra Lifesciences Corporation, Plainsboro, NJ, United States). SEEG trajectory planning was done based on routine non-invasive evaluations including semeiology analysis, scalp EEG, MRI, and PET-CT (**Figure 1A**), and the accuracy of SEEG placement was confirmed by fusing postimplantation CT images with preimplantation MRI images (**Figure 1B**). SEEG data were recorded with a sampling rate of 2,000 Hz by a 256-channel NK EEG 2100 system (Nihon-Kohden, Tokyo, Japan). The duration of SEEG recording varied individually from 2 to 30 days to ensure that at least two seizures can be captured in each patient. The maximum number of seizures captured in a single patient was 18.

Ictal SEEG recordings of all seizures recorded in each patient were reviewed. The seizure onset zone was identified by at least two experienced epileptologists basing on the channels which recorded earliest rhythmic or semi rhythmic discharges (Singh et al., 2015). Conventional epileptic spikes and slow activities (1–100 Hz, 10 s/page) in SEEG data were used for the presurgical localization of the seizure onset zone, while HFOs were analyzed only for research purpose (**Figure 1C**). The planned extent of resection was determined by synthesizing seizure semiology and neuroimaging findings.

SEEG Data Preprocessing

Stereoelectroencephalography data were visually inspected and cleaned from artifacts and noises. Channels with persistent artifacts due to poor contact, environmental or line noise, movement, or others that might affect the results were excluded. Artifact-free epochs, which were at least 2 h away from a seizure, were selected for analyzing interictal activities, while 2-min epochs starting from the detected seizure onset were selected for analyzing ictal activities. Seizure onset was judged by a

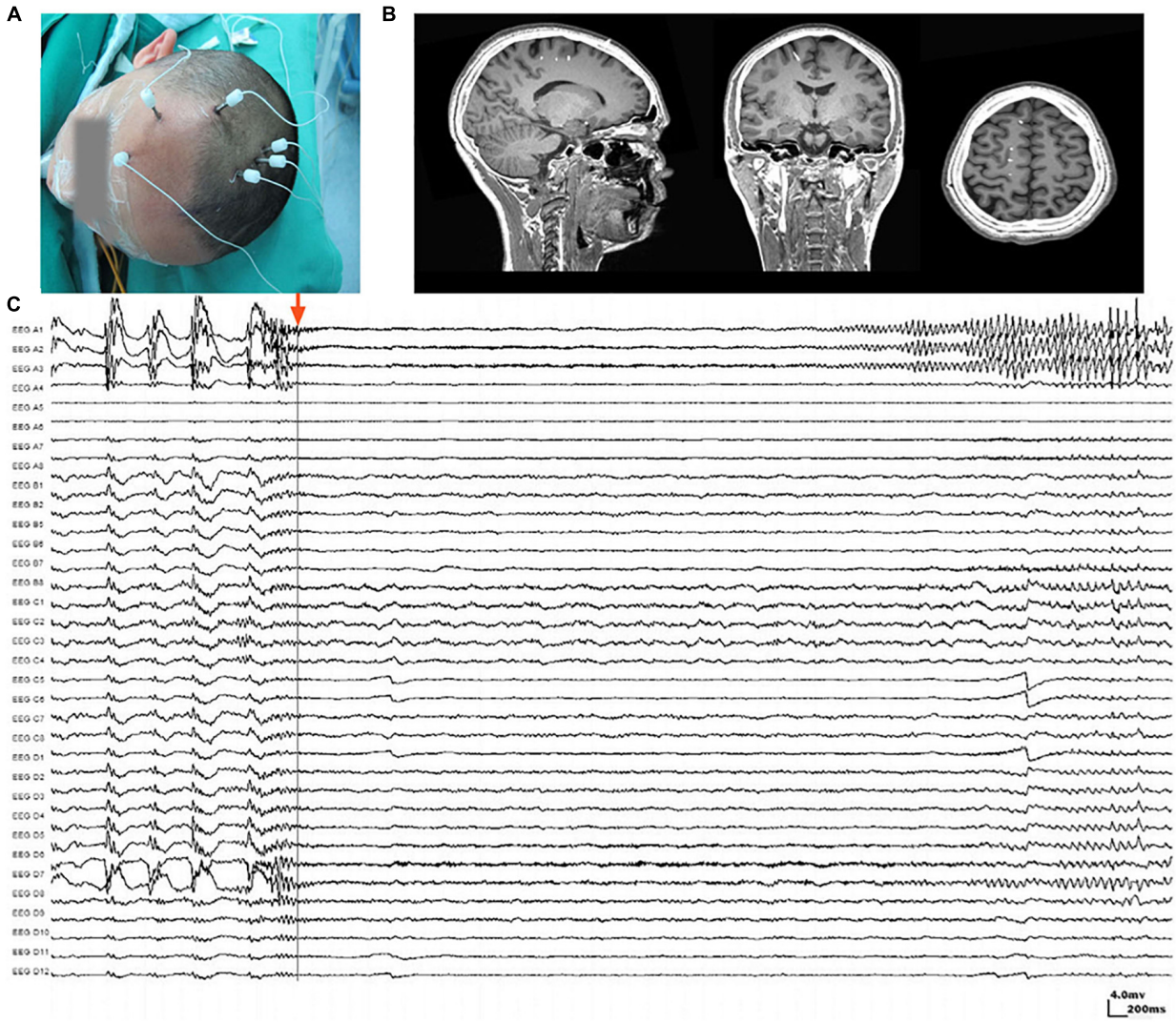

FIGURE 1 | Stereoelectroencephalography (SEEG) electrodes and recordings. **(A)** SEEG electrodes were implanted in a patient in the operating room. **(B)** Localization of SEEG electrode implantation was verified by coregistering preimplantation MRI images with postimplantation CT images. **(C)** A typical SEEG recording of one habitual seizure in patient W, visualized with a 1–100 Hz bandpass, 50 Hz notch filter, at 10 s/page, showing the low voltage fast (LVF) seizure onset type. Channels A1, A2, and A3, which first exhibited low-voltage fast activity, evolving into rhythmic spikes, are recognized as seizure onset zone.

combination of video recordings and typical SEEG patterns, such as spikes and sharp waves.

HFO Identification, Quantification, and Normalization

Electroencephalography Studio software (MEG Center, Cincinnati Children's Hospital Medical Center, Cincinnati, OH, United States) was used to semiautomatically check ripples (80–250 Hz) and fast ripples (250–500 Hz) by searching for increased activities in the corresponding bands (Xiang et al., 2014, 2015b). Subsequently, time–frequency analysis using Morlet continuous wavelet transform was performed for ripples and fast ripples separately to precisely measure the frequency and spectral signals (Xiang et al., 2014, 2015b). The analysis was applied to at least two seizures captured in each patient. For patients who experienced more than one type of seizure, the aforementioned procedures were performed for each type. Coregistered postimplantation CT and preimplantation MRI were used to determine the position of each electrode contact. The waveforms and spectrograms from each channel were then correlated to the corresponding position in structural images for analysis (**Figure 1**).

To quantify the HFOs generated by a brain region, we computed the spectral power of HFOs with band-pass filtered SEEG data with the conventional approach. To minimize the interindividual variations in baselines and amplitudes, we applied an individualized approach to estimate epileptogenic regions by computing "the relative strength" of HFOs. Mathematically, we divided the spectral power of SEEG signals from each contact by

the averaged power of all the contacts on all the electrodes over the entire "clean" segments. The SEEG data processed by this procedure was considered to be spatiotemporally normalized.

Identification of Brain Regions Generating Epileptic HFOs

The means and standard deviations (SD) of the relative strength of HFOs were computed. The threshold for differentiating pathological HFOs from physiological HFOs was defined as mean plus three times SD (Matsumoto et al., 2013), i.e., HFOs with a spectral peak power over the threshold were identified as pathological HFOs. The contacts that recorded pathological HFOs were considered to be pinpointing to the seizure onset zone.

Assessments of Resection and Surgical Outcome

Postoperative CT scans were obtained for all patients. To clarify the resection boundaries and their spatial relationship with the electrode contacts, the waveforms of all electrode contacts were identified onto the individual structural images. Postoperative CT and preimplantation MRI were coregistered and then compared with fusion images from postimplantation CT and preimplantation MRI by EEG Studio software.

All patients were followed up for at least 6 months (mean ± SD, 10 ± 2.72; range, 6–15) after surgery, and the surgical outcomes were assessed according to International League Against Epilepsy (ILAE) classifications of epilepsy surgery seizure outcome (Wieser et al., 2001; Durnford et al., 2011). Patients with ILAE classes 1–3 were considered to have a favorable outcome, while those with ILAE classes 4–6 were considered to have a poor outcome.

Statistical Analysis

Measurements were statistically analyzed with pair-wise comparisons (Student's *t* test) and multiple analysis of variance (ANOVA). The ratio of activities in brain regions among the electrodes was analyzed by Fisher's exact test. For multiple comparison, a Bonferroni correction was applied, e.g., since two frequency bands (ripples and fast ripples) were analyzed, only $p < 0.025$ (0.05/2) was considered significant.

RESULTS

Clinical Characteristics

A total of 142 SEEG electrodes including 1,654 contacts were implanted in all 19 patients, and 148 seizure-onset channels were identified by clinical neurophysiologists through a preoperative evaluation which is independent of study. Neuropathological examination of resected tissue samples revealed various types of epilepsy-related pathologies. The clinical and pathological characteristics of each patient are summarized in **Table 1**. Follow-up was achieved for all 19 patients, and 17 of them achieved a favorable seizure outcome (**Table 2**).

The Characteristics of HFOs

Artifacts and/or noises were observed in 27 out of 1,654 contacts (1.6%), and the data from these 27 contacts were excluded to ensure the quality of subsequent analysis. Ultimately, SEEG data from 1,627 contacts, including 63 ictal segments (data recorded during seizures), were analyzed. Examples of the identified HFOs are shown in **Figure 2**. Visual inspection of SEEG data revealed that the amplitude and rate of ripples and fast ripples varied from patient to patient during interictal periods. Even within the same patient, the amplitudes and rates of ripples and fast ripples could vary from time to time.

High-frequency oscillations were identified in all patients. Continuous ripples during ictal periods were observed in 10 of them (15 channels), while continuous fast ripples during ictal periods were only observed in two patients (three channels). In the 10 patients with continuous ripples, 14 out of the total 15 channels were located in the seizure onset zone, which were identified by presurgical evaluation. HFOs were observed both inside and outside the seizure onset zone in each patient.

Subsequently, time–frequency analysis was performed. For HFOs inside the seizure onset zone, the spectral power of HFO during ictal periods was significantly increased than that during interictal periods. **Figure 3** shows an example of identified HFOs from the interictal to the ictal state. Moreover, we also found that the frequency of ripples increased from interictal to ictal periods: the main frequency range during interictal periods was 85–100 Hz, whereas during the interictal–ictal transition, the main frequency range was 105–130 Hz, accompanied by 85–100 Hz. As for fast ripples, the main frequency range was stable at 250–380 Hz, no significant change was identified.

Relationship Between the Seizure Onset Zone and HFOs

The spectral data of ripples and fast ripples inside the conventionally defined seizure onset zone (by typical SEEG patterns like spikes and slow activities) showed significantly higher power values than those outside the seizure onset zone ($p < 0.01$). The spectral power for ripples were as follows: (1) interictal, $15.74 \pm 7.12\ \mu V^2/Hz$ vs. $10.54 \pm 4.12\ \mu V^2/Hz$ (inside vs. outside the seizure onset zone, for the following data as well) and (2) ictal, $49.02 \pm 94.30\ \mu V^2/Hz$ vs. $31.61 \pm 62.65\ \mu V^2/Hz$ ($p < 0.001$). The spectral power for fast ripples were as follows: (1) interictal, $8.15 \pm 4.60\ \mu V^2/Hz$ vs. $6.88 \pm 3.39\ \mu V^2/Hz$; and (2) ictal: $21.04 \pm 34.32\ \mu V^2/Hz$ vs. $16.21 \pm 24.26\ \mu V^2/Hz$ ($p < 0.001$). Additionally, the spectral data also showed an increase in HFO power from interictal to ictal periods. **Figure 4** shows the comparisons of HFO power during interictal and ictal periods and its spectral changes between the seizure onset zone and non-seizure onset zone. The spectrograms revealed an increase in HFO power in 105–130 Hz band (ripple) and 250–380 Hz band (fast ripple) during interictal and ictal periods.

To estimate the EZ, the number of channels with epileptic HFOs were quantified. During interictal periods, ripples were observed in 2.32 ± 2.88 channels, and fast ripples were observed in 1.58 ± 2.83 channels ($p < 0.01$). During ictal periods, the HFO involved regions tended to be larger, with ripple regions refer to

TABLE 1 | Clinical characteristics of the enrolled 19 patients.

Patients	Age/sex	Seizure type	MRI	PET-CT (hypo-metabolism)	EEG	Location	Pathology
1	24 years/FM	CFS	–	Temporal_Post_Inf_R	O4 & P4-T6	Temporal	FCD Ia
2	25 years/FM	GTCS	–	Postcentral sulus_R	F4 & Fz-Cz	Frontal	FCD Ia
3	29 years/M	CFS	Left temporal polar FCD	Temporal–parietal_L	F7-T3-T5	Frontal–temporal	FCD Ib
4	28 years/M	GTCS	–	Bitemporal (esp Left)	F3-F7	Temporal	FCD IIa
5	31 years/FM	GTCS + CFS	Frontal–parietal–temporal_L FL	Left temporal–insulae–parietal_Inf lobule	F3-F7	Frontal–temporal–insulae	FCD IIa
6	23 years/M	CFS	Frontal_R and Hippocampus_L	Temporal_L–parietal_Inf lobule	T5-P3	Frontal–temporal	FCD IIIa
7	33 years/FM	CFS	Straight gyrus_L FL	Straight gyrus_L	All channel	Frontal	FCD IIb
8	21 years/M	CFS	Left hippocampus–temporal polar	Temporal_ Mid_L	Left anterior head	Temporal	FCDIIIa
9	24 years/FM	GTCS	–	Temporal_Mid_B	All channels	Precentral suclus_R	FCD
10	29 years/M	CFS	–	–	Frontal-Temporal_B	Frontal–temporal	FCDIIa
11	17 years/FM	GTCS	–	Frontal_Mid_Inf_R	Unclear	Frontal	FCD
12	12 years/M	GTCS	Temporal_Mid_L incomplete resectomy	Left Temporal_Ant-TPO	Temporal_B	Temporal	FCDIIIb
13	3 years/M	CFS	–	Frontal_Mid_L	All channels	Frontal–temporal	FCD IIb
14	29 years/M	GTCS	Left temporal horn atrophy	Temporal_L	F7	Temporal	FCD
15	10 years/M	CFS	Temporal_L	Right frontal–temporal–pariental	F4-F8	Frontal–temporal	FCD IIb
16	10 years/M	CFS	White matter FL	Frontal_L–lateral ventricle_B	F4	Frontal_L–lateral ventricle_B	TSC
17	8 years/M	CFS + GTCS	–	NA	F3-F7	Frontal	FCD Ia
18	16 years/M	CFS	–	Temporal_Mid_R–parietal cortex_L	F4-F8	Frontal	FCD Ia
19	30 years/M	GTCS	Insulae_R FL	Temporal_B	All channels	Insulae	FCD Ia

CFS, complex focal seizure; GTCS, general tonic–colonic seizure; FL, focal lesion; L, left; R, right; B, bilateral; TPO, temporal–parietal–occipital; FCD, focal cortical dysplasia; TSC, tuberous sclerosis complex.

8.00 ± 5.43 channels and fast ripple regions refer to 5.00 ± 3.80 channels. The overlap of the ripple regions inside the seizure onset zone was 0.71 ± 0.32 channel sites for interictal periods and 0.37 ± 0.20 channel sites for ictal periods, and the overlap of the fast ripple regions was 0.79 ± 0.27 channels for interictal periods and 0.23 ± 0.13 channels for ictal periods. Notably, the fast ripples were more spatially focal than the ripples. In addition, the overlap between the identified ripple and fast ripple regions was 0.16 ± 0.29 channels during interictal periods and 0.50 ± 0.31 channels during ictal periods, whereas the inverse overlap was 0.17 ± 0.31 channels during interictal periods and 0.71 ± 0.33 channels during ictal periods, which suggested that ripples and fast ripples were independent events in the epileptic brain.

Surgical Outcome and HFO Regions

Overall, 16 patients achieved seizure freedom and were classified as ILAE class 1. One patient experienced a seizure after surgery, which was different from his habitual seizures, and was classified as ILAE class 3. Two patients experienced frequent seizures postoperatively and were classified as ILAE class 5.

For the 17 (89.5%) patients with a favorable outcome, the proportion of the resected areas in ripple-generating brain regions (ripple resection rate) was 0.76 ± 0.41 for interictal periods and 0.38 ± 0.34 for ictal periods. The identified fast ripple resection rate was higher than the ripple resection rate in interictal periods (0.91 ± 0.16), but lower in ictal periods (0.33 ± 0.33). Notably, ripples and fast ripples were propagated after seizure onset, especially to the symptomatic regions. In addition, we reviewed interictal HFOs for all 17 patients with a favorable outcome and found that the region presenting the highest spectral values for fast ripples had been resected; however, for the two patients with poor outcomes, the brain regions generating fast ripples had not been removed completely. This result indicated that the resection of brain regions generating fast ripples was critical for the achievement of a favorable seizure outcome.

TABLE 2 | Relationship between HFOs, SOZ, and surgical outcomes.

Patients	Electrode count	Channel count	Surgical outcome (ILAE)	Number of channels in SOZ	Interictal					Ictal				
					Number of channels with up-threshold HFOs					Number of channels with up-threshold HFOs				
					R	R in SOZ	FR	FR in SOZ	R&FR	R	R in SOZ	FR	FR in SOZ	R&FR
1	6	72	1	15	6	5	5	3	4	4	2	5	1	2
2	10	114	1	2	1	0	0	0	0	7	1	2	0	2
3	10	146	1	4	1	1	0	0	0	12	2	6	1	5
4	6	68	1	9	0	0	1	0	0	5	2	6	0	2
5	8	80	3	6	4	1	3	1	2	6	0	5	0	5
6	10	110	1	5	3	2	1	1	1	13	2	10	1	10
7	7	76	1	3	2	1	1	1	0	6	1	3	0	2
8	9	124	1	11	3	1	1	0	0	15	8	5	0	4
9	4	36	1	3	0	0	1	1	0	5	0	5	0	5
10	10	118	5	9	12	1	0	0	0	23	4	15	0	13
11	6	84	1	14	5	4	0	0	0	3	1	4	1	3
12	8	86	1	8	1	0	0	0	0	15	2	4	0	4
13	4	46	1	11	1	1	1	1	0	7	5	2	0	2
14	6	64	1	16	3	3	12	5	3	12	8	12	6	10
15	6	54	1	8	0	0	0	0	0	4	0	0	0	0
16	11	136	1	3	0	0	0	0	0	2	0	0	0	0
17	6	50	1	12	2	2	4	0	0	5	3	7	1	2
18	8	102	5	6	0	0	0	0	0	7	3	3	0	2
19	7	88	1	12	2	2	2	2	1	2	0	2	0	2

R, ripples; FR, fast ripples; SOZ, seizure onset zone; HFOs, high-frequency oscillations. For example, in patient 1: the number 6 under R of interictal means that these six channels were detected up-threshold ripples. In these six channels detected ripples, there are five in SOZ. This also applies to FR.

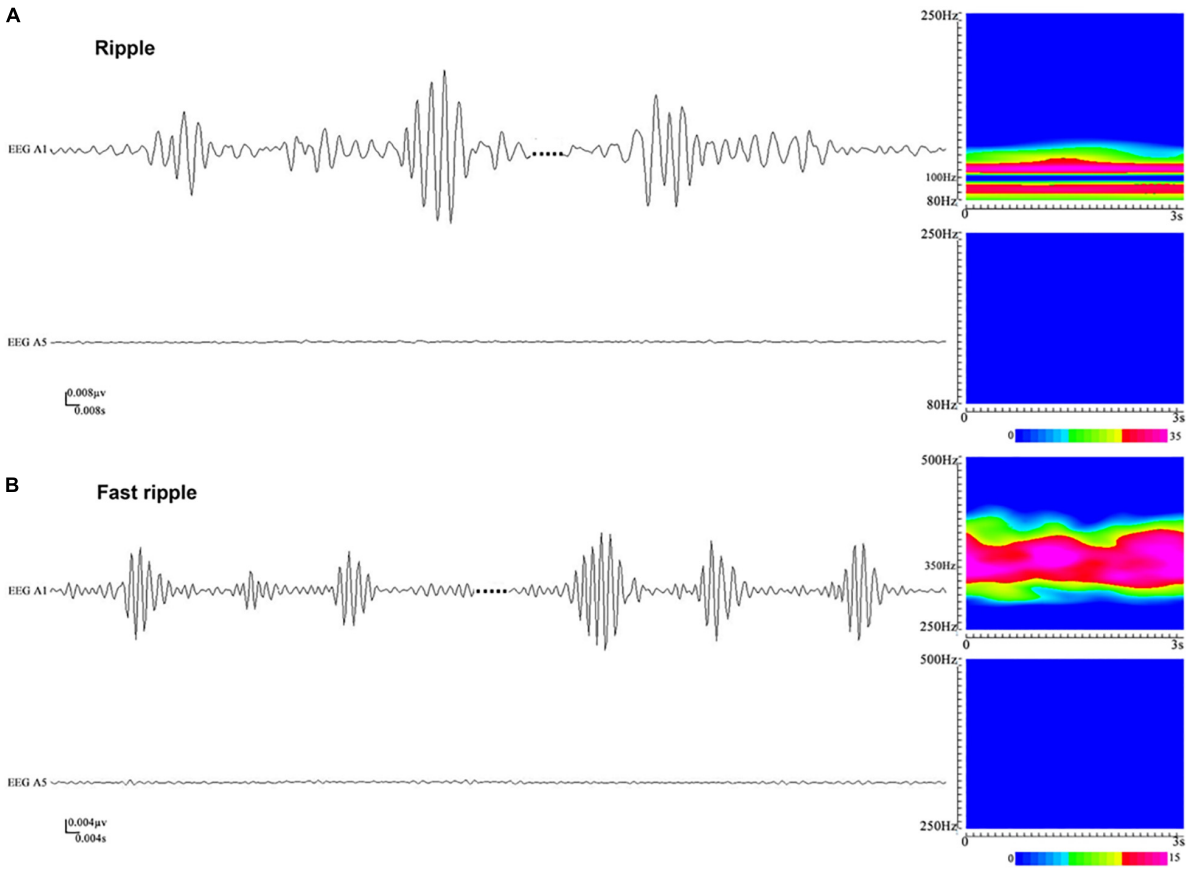

FIGURE 2 | An illustration of high-frequency oscillations (HFOs) in stereoelectroencephalography (SEEG) recordings. **(A)** Ripples in waveforms (80–250 Hz bandpass, 50 Hz notch filter, 0.008 μV/mm, 0.008 s/mm) and accumulated spectrograms. Channel A1, placed inside the seizure onset zone, shows ripples occurring discontinuously, with the frequencies in the range between 88 and 110 Hz. No ripples can be observed in channel A5, which is placed outside the seizure onset zone. **(B)** Fast ripples in waveforms (250–500 Hz bandpass, 50 Hz notch filter, 0.004 μV/mm, 0.004 s/mm) and accumulated spectrograms. Channel A1, placed inside the seizure onset zone, shows fast ripples with the frequencies centered at ∼350 Hz. No fast ripples can be observed in channel A5, placed outside the seizure onset zone.

DISCUSSION

In the current study, we analyzed SEEG data using an individualized, frequency-based approach for HFO analysis and demonstrated that the resection of the EZ estimated by the relative strength of HFOs was associated with a favorable seizure outcome. Notably, HFOs in 250–500 Hz were more specific for localizing the EZ. The results enhanced the clinical application value of HFO analysis in patients with drug-resistant epilepsy and provided a potential marker for guiding epilepsy surgery.

The detection of HFOs has been widely studied in intracranial EEG studies but rarely in SEEG studies (Chassoux, 2003; Amiri et al., 2016; Ferrari-Marinho et al., 2016; Fuertinger et al., 2016). Although both subdural and stereotactic electrode recordings can be used to identify the EZ, they exhibit some differences. The electrodes used for SEEG are thin, needle-like electrodes, which can be implanted stereotactically, i.e., with the aid of a stereotactic frame using precalculated coordinates that guarantee accurate targeting of specific deep regions in the brain. Currently, SEEG has been indicated as a preferable tool for the epileptogenic network exploration and is especially effective in detecting the epileptogenic activity originate from deep brain structures. Furthermore, previous reports have shown that a high rate of HFOs can be used for the localization of the EZ (Chaitanya et al., 2015; Ferrari-Marinho et al., 2016; Jacobs et al., 2016). Accordingly, a combination of SEEG recording and HFO analysis is considered to be a promising approach for identifying the EZ.

Generally, HFOs can be identified through visual inspection of bandpass-filtered data. However, this process is quite time consuming and highly dependent on the reviewers. For instance, the identification of HFO necessitates at least four consecutive oscillations above the "background or baseline," and the "baseline" is generally determined by reviewers subjectively. Additionally, previous studies showed that the characteristics of HFOs in epileptic brain varies greatly among individuals (Staba et al., 2014; Chaitanya et al., 2015; Ferrari-Marinho et al., 2016). As observed in the current study, the morphology, amplitude, and duration of HFOs varied not only among different individuals but also among time to time, site to site in the same

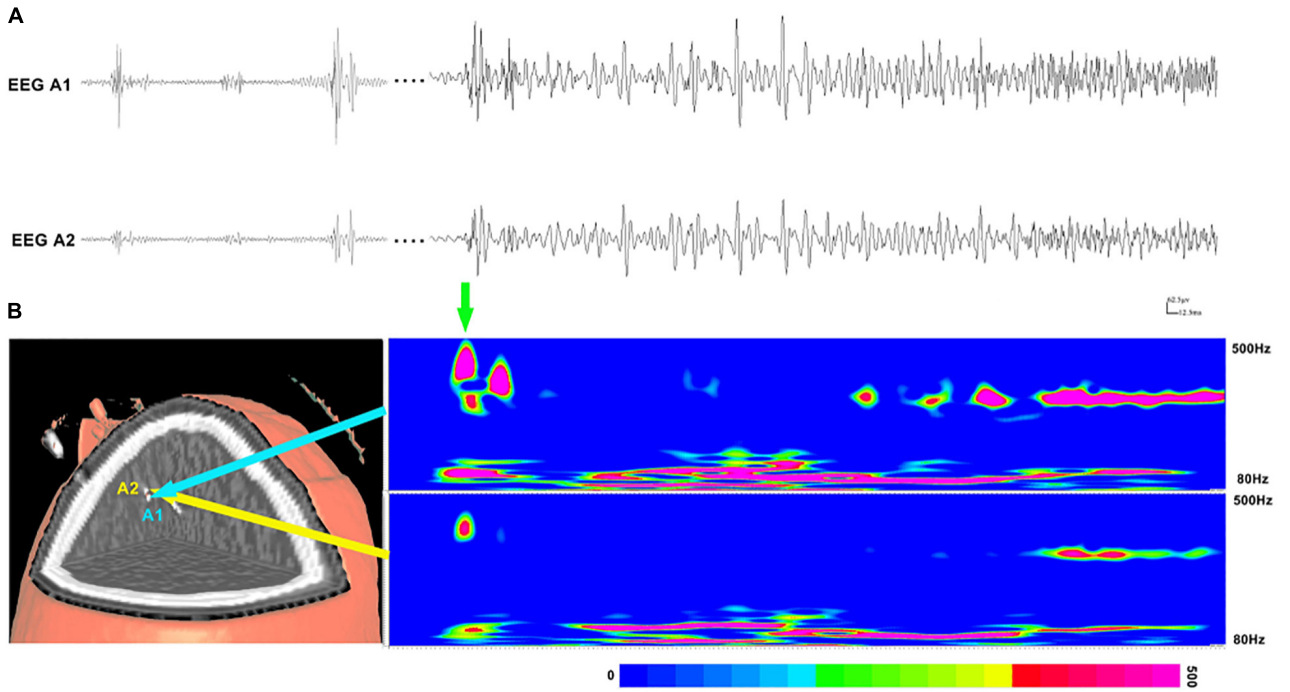

FIGURE 3 | Interictal and ictal HFOs inside the seizure onset zone of two neighboring electrodes. **(A)** High-frequency oscillations (HFOs) (bandpass filtered at 80–500 Hz) in waveforms occur intermittently in interictal periods and occur continuously in the ictal period. **(B)** Time–frequency analysis reveals that the increases in ripples and fast ripples start before ictal onset (the green arrow point). The corresponding sites of the electrodes are shown on the left.

patient. All these factors present significant barriers to the clinical application of HFO analysis for the localization of the EZ.

In the current study, we improved the method for HFO analysis. With wavelet transforms, the spectrograms revealed that the spectral power of ripples was significantly increased in 105–130 Hz band, while the spectral power of fast ripples was relatively stable at 250–380 Hz band. To minimize interindividual variation, we computed the relative strength of HFOs of each electrode contact, and the EZ identified by the relative strength of HFOs and the seizure onset zone defined by preoperative evaluation were consistently matched. Importantly, the resection of brain regions with high relative strength of HFOs was correlated with a favorable surgical outcome. According to previous reports, epilepsy surgery, which is performed typically based on the seizure onset zone defined by spike-and-wave discharges (low-frequency signals), conventionally achieve seizure freedom in 40–70% of patients with medically refractory focal epilepsy (Engel et al., 2003). In the current study, seizure freedom was achieved in 89.5% of patients, and the brain regions with high relative strength of HFOs were removed completely in all of them, while the remaining two patients with poor outcomes showed residual brain regions generating HFOs after surgery. The results suggested that the relative strength of HFOs is an effective biomarker for identifying the EZ and can be used for the presurgical evaluation of patients with drug-resistant epilepsy. Compared with visual inspection, this approach is individually normalized, objective, quantitative, and time efficient (semiautomatically computed by a computer). Moreover, it provides a precise frequency description of epileptic activities.

It has been shown that HFOs can reliably localize the EZ in both mesial temporal and extratemporal epilepsy (Jacobs et al., 2009; Cho et al., 2014). In our study, the combination of postsurgical CT and spectrograms revealed that, compared with the EZ identified by the conventional spikes in routine EEG analysis, the EZ identified by HFO analysis was more focal, which was consistent with previous reports (Xiang et al., 2014, 2015a). Additionally, our analysis showed that fast ripples (250–500 Hz) were generally more focal than ripples (80–250 Hz), which indicated that fast ripples may have greater clinical value than ripples for identifying the EZ. The other relevant finding was that the changes in ripples and fast ripples were not always spatially overlapped, indicating that the ripples and fast ripples are mutually independent biomarkers for identifying the EZ.

The results of the present study also demonstrated the dynamic changes in HFOs. HFOs were observed to be significantly increased from the interictal to ictal period. Consistent bursts of ripples and fast ripple could be observed during ictal periods, and sudden increases of fast ripples were typically identified inside seizure onset zone. Such dynamic changes in HFOs inside the seizure onset zone could be used to indicate the interictal–ictal transition. In other words, the dynamic changes in HFOs could be used to predict epileptic state changes. This finding also provide support to the notion that HFOs represent the network-driven activity of the brain in epilepsy.

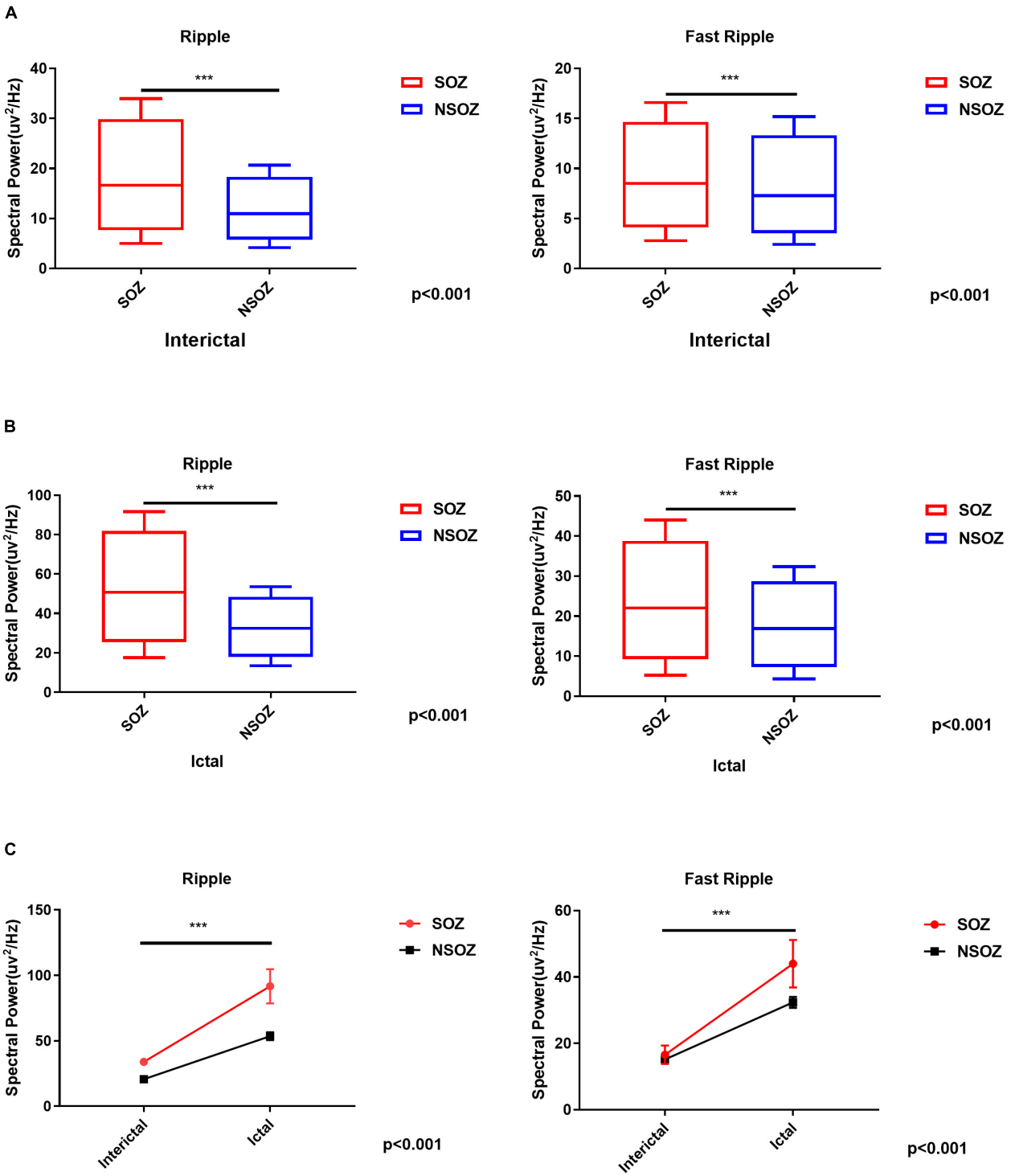

FIGURE 4 | Comparisons of the mean ripple and fast ripple spectral power between the seizure onset zone and non-seizure onset zone during **(A)** interictal and **(B)** ictal periods. **(C)** Mixed-design analyses of variance show dynamic increases of mean ripple and fast ripple spectral power from interictal to ictal periods between the seizure onset zone and non-seizure onset zone. ***$p < 0.001$.

The current investigation was limited by its retrospective nature. Moreover, SEEG electrodes implantation is highly relied on the preimplantation plan, which can greatly affect the positional distribution of the contacts, making presurgical evaluation of the EZ a challenging task. In addition, our work is limited to analyzing the correlation between the identified HFOs

and the conventional seizure onset zone, and characterizing the relationship between HFOs and the surgical outcome. Such limitation arises from the fact that there is no current "gold standard" for identifying HFOs (Spring et al., 2017). Overall, the promising results lead us to believe that HFO analysis can be refined to improve the identification of the EZ and will play a key role in the presurgical evaluation of epilepsy surgery in the near future. Further studies are required to determine a reliable, effective quantitative marker of HFO activity for delineating the true EZ.

DATA AVAILABILITY STATEMENT

The datasets generated for this study are available on request to the corresponding author.

ETHICS STATEMENT

The studies involving human participants were reviewed and approved by the Institutional Review Board of Beijing Tiantan Hospital. Written informed consent to participate in this study was provided by the participants, and where necessary, the legal guardian/next of kin.

AUTHOR CONTRIBUTIONS

LQ and XF were the major contributors in data analysis and manuscript writing. KZ, LS, WH, and XY contributed to the diagnosis and treatment of patients. XT and HQ contributed to checking the manuscript. All authors read and approved the manuscript.

FUNDING

This study was supported by the Capital Foundation of Medical Developments, grant number 2018-2-1075.

ACKNOWLEDGMENTS

We appreciate the staff of the Epilepsy Center at Beijing Tian Tai Hospital and thank the patients who participated in this study.

REFERENCES

Amiri, M., Lina, J. M., Pizzo, F., and Gotman, J. (2016). High Frequency Oscillations and spikes: separating real HFOs from false oscillations. *Clin. Neurophysiol.* 127, 187–196. doi: 10.1016/j.clinph.2015.04.290

Bartolomei, F., Lagarde, S., Wendling, F., Mcgonigal, A., Jirsa, V., Guye, M., et al. (2017). Defining epileptogenic networks: contribution of SEEG and signal analysis. *Epilepsia* 58, 1131–1147. doi: 10.1111/epi.13791

Brazdil, M., Pail, M., Halamek, J., Plesinger, F., Cimbalnik, J., Roman, R., et al. (2017). Very high-frequency oscillations: novel biomarkers of the epileptogenic zone. *Ann. Neurol.* 82, 299–310. doi: 10.1002/ana.25006

Chaitanya, G., Sinha, S., Narayanan, M., and Satishchandra, P. (2015). Scalp high frequency oscillations (HFOs) in absence epilepsy: an independent component analysis (ICA) based approach. *Epilepsy Res.* 115, 133–140. doi: 10.1016/j.eplepsyres.2015.06.008

Chassoux, F. (2003). Stereo-EEG: the Sainte-Anne experience in focal cortical dysplasias. *Epileptic Disord.* 5(Suppl. 2), S95–S103.

Cho, J. R., Koo, D. L., Joo, E. Y., Seo, D. W., Hong, S. C., Jiruska, P., et al. (2014). Resection of individually identified high-rate high-frequency oscillations region is associated with favorable outcome in neocortical epilepsy. *Epilepsia* 55, 1872–1883. doi: 10.1111/epi.12808

Durnford, A. J., Rodgers, W., Kirkham, F. J., Mullee, M. A., Whitney, A., Prevett, M., et al. (2011). Very good inter-rater reliability of Engel and ILAE epilepsy surgery outcome classifications in a series of 76 patients. *Seizure* 20, 809–812. doi: 10.1016/j.seizure.2011.08.004

Engel, J. Jr., Wiebe, S., French, J., Sperling, M., Williamson, P., Spencer, D., et al. (2003). Practice parameter: temporal lobe and localized neocortical resections for epilepsy: report of the Quality Standards Subcommittee of the American Academy of Neurology, in association with the American Epilepsy Society and the American Association of Neurological Surgeons. *Neurology* 60, 538–547. doi: 10.1212/01.wnl.0000055086.35806.2d

Ferrari-Marinho, T., Perucca, P., Dubeau, F., and Gotman, J. (2016). Intracranial EEG seizure onset-patterns correlate with high-frequency oscillations in patients with drug-resistant epilepsy. *Epilepsy Res.* 127, 200–206. doi: 10.1016/j.eplepsyres.2016.09.009

Frauscher, B., Bartolomei, F., Kobayashi, K., Cimbalnik, J., Van 'T Klooster, M. A., Rampp, S., et al. (2017). High-frequency oscillations: the state of clinical research. *Epilepsia* 58, 1316–1329.

Fuertinger, S., Simonyan, K., Sperling, M. R., Sharan, A. D., and Hamzei-Sichani, F. (2016). High-frequency brain networks undergo modular breakdown during epileptic seizures. *Epilepsia* 57, 1097–1108. doi: 10.1111/epi.13413

Gliske, S. V., Irwin, Z. T., Chestek, C., Hegeman, G. L., Brinkmann, B., Sagher, O., et al. (2018). Variability in the location of high frequency oscillations during prolonged intracranial EEG recordings. *Nat. Commun.* 9:2155. doi: 10.1038/s41467-018-04549-2

Gonzalez-Martinez, J. A. (2016). The stereo-electroencephalography: the epileptogenic zone. *J. Clin. Neurophysiol.* 33, 522–529. doi: 10.1097/wnp.0000000000000327

Hussain, S. A., Mathern, G. W., Hung, P., Weng, J., Sankar, R., and Wu, J. Y. (2017). Intraoperative fast ripples independently predict postsurgical epilepsy outcome: comparison with other electrocorticographic phenomena. *Epilepsy Res.* 135, 79–86. doi: 10.1016/j.eplepsyres.2017.06.010

Jacobs, J., Levan, P., Chatillon, C. E., Olivier, A., Dubeau, F., and Gotman, J. (2009). High frequency oscillations in intracranial EEGs mark epileptogenicity rather than lesion type. *Brain* 132, 1022–1037. doi: 10.1093/brain/awn351

Jacobs, J., Vogt, C., Levan, P., Zelmann, R., Gotman, J., and Kobayashi, K. (2016). The identification of distinct high-frequency oscillations during spikes delineates the seizure onset zone better than high-frequency spectral power changes. *Clin. Neurophysiol.* 127, 129–142. doi: 10.1016/j.clinph.2015.04.053

Jehi, L. (2018). The epileptogenic zone: concept and definition. *Epilepsy Curr.* 18, 12–16. doi: 10.5698/1535-7597.18.1.12

Kalilani, L., Sun, X., Pelgrims, B., Noack-Rink, M., and Villanueva, V. (2018). The epidemiology of drug-resistant epilepsy: a systematic review and meta-analysis. *Epilepsia* 59, 2179–2193. doi: 10.1111/epi.14596

Kwan, P., Schachter, S. C., and Brodie, M. J. (2011). Drug-resistant epilepsy. *N. Engl. J. Med.* 365, 919–926.

Matsumoto, A., Brinkmann, B. H., Matthew Stead, S., Matsumoto, J., Kucewicz, M. T., Marsh, W. R., et al. (2013). Pathological and physiological high-frequency oscillations in focal human epilepsy. *J. Neurophysiol.* 110, 1958–1964. doi: 10.1152/jn.00341.2013

Nissen, I. A., Stam, C. J., Van Straaten, E. C. W., Wottschel, V., Reijneveld, J. C., Baayen, J. C., et al. (2018). Localization of the epileptogenic zone using interictal MEG and machine learning in a large cohort of drug-resistant epilepsy patients. *Front. Neurol.* 9:647. doi: 10.3389/fneur.2018.00647

Ramantani, G., Kadish, N. E., Mayer, H., Anastasopoulos, C., Wagner, K., Reuner, G., et al. (2018). Frontal lobe epilepsy surgery in childhood and adolescence:

predictors of long-term seizure freedom. Overall cognitive and adaptive functioning. *Neurosurgery* 83, 93–103. doi: 10.1093/neuros/nyx340

Rektor, I., Zakopcan, J., Tyrlikova, I., Kuba, R., Brazdil, M., Chrastina, J., et al. (2009). Secondary generalization in seizures of temporal lobe origin: Ictal EEG pattern in a stereo-EEG study. *Epilepsy Behav.* 15, 235–239. doi: 10.1016/j.yebeh.2009.03.032

Singh, S., Sandy, S., and Wiebe, S. (2015). Ictal onset on intracranial EEG: do we know it when we see it? State of the evidence. *Epilepsia* 56, 1629–1638. doi: 10.1111/epi.13120

Spencer, S. S. (2002). Neural networks in human epilepsy: evidence of and implications for treatment. *Epilepsia* 43, 219–227. doi: 10.1046/j.1528-1157.2002.26901.x

Spring, A. M., Pittman, D. J., Aghakhani, Y., Jirsch, J., Pillay, N., Bello-Espinosa, L. E., et al. (2017). Interrater reliability of visually evaluated high frequency oscillations. *Clin. Neurophysiol.* 128, 433–441. doi: 10.1016/j.clinph.2016.12.017

Staba, R. J., Stead, M., and Worrell, G. A. (2014). Electrophysiological biomarkers of epilepsy. *Neurotherapeutics* 11, 334–346. doi: 10.1007/s13311-014-0259-0

Thomschewski, A., Hincapie, A. S., and Frauscher, B. (2019). Localization of the epileptogenic zone using high frequency oscillations. *Front. Neurol.* 10:94. doi: 10.3389/fneur.2019.00094

Timoney, N., and Rutka, J. T. (2017). Recent advances in epilepsy surgery and achieving best outcomes using high-frequency oscillations, diffusion tensor imaging, Magnetoencephalography, Intraoperative Neuromonitoring, focal cortical Dysplasia, and bottom of Sulcus Dysplasia. *Neurosurgery* 64, 1–10. doi: 10.1093/neuros/nyx239

Wang, S., So, N. K., Jin, B., Wang, I. Z., Bulacio, J. C., Enatsu, R., et al. (2017). Interictal ripples nested in epileptiform discharge help to identify the epileptogenic zone in neocortical epilepsy. *Clin. Neurophysiol.* 128, 945–951. doi: 10.1016/j.clinph.2017.03.033

Wieser, H. G., Blume, W. T., Fish, D., Goldensohn, E., Hufnagel, A., King, D., et al. (2001). ILAE Commission Report. Proposal for a new classification of outcome with respect to epileptic seizures following epilepsy surgery. *Epilepsia* 42, 282–286. doi: 10.1046/j.1528-1157.2001.35100.x

Xiang, J., Korman, A., Samarasinghe, K. M., Wang, X., Zhang, F., Qiao, H., et al. (2015a). Volumetric imaging of brain activity with spatial-frequency decoding of neuromagnetic signals. *J. Neurosci. Methods* 239, 114–128. doi: 10.1016/j.jneumeth.2014.10.007

Xiang, J., Liu, Y., Wang, Y., Kirtman, E. G., Kotecha, R., Chen, Y., et al. (2009). Frequency and spatial characteristics of high-frequency neuromagnetic signals in childhood epilepsy. *Epileptic Disord.* 11, 113–125. doi: 10.1684/epd.2009.0253

Xiang, J., Luo, Q., Kotecha, R., Korman, A., Zhang, F., Luo, H., et al. (2014). Accumulated source imaging of brain activity with both low and high-frequency neuromagnetic signals. *Front. Neuroinform.* 8:57. doi: 10.3389/fninf.2014.00057

Xiang, J., Tenney, J. R., Korman, A. M., Leiken, K., Rose, D. F., Harris, E., et al. (2015b). Quantification of interictal neuromagnetic activity in absence epilepsy with accumulated source imaging. *Brain Topogr.* 28, 904–914. doi: 10.1007/s10548-014-0411-5

Yang, C., Luan, G., Wang, Q., Liu, Z., Zhai, F., and Wang, Q. (2018). Localization of epileptogenic zone with the correction of pathological networks. *Front. Neurol.* 9:143. doi: 10.3389/fneur.2018.00143

Conflict of Interest: The authors declare that the research was conducted in the absence of any commercial or financial relationships that could be construed as a potential conflict of interest.

frontiers in Human Neuroscience

ORIGINAL RESEARCH
published: 26 June 2020
doi: 10.3389/fnhum.2020.00221

Multifrequency Dynamics of Cortical Neuromagnetic Activity Underlying Seizure Termination in Absence Epilepsy

*Jintao Sun, Yuan Gao, Ailiang Miao, Chuanyong Yu, Lu Tang, Shuyang Huang, Caiyun Wu, Qi Shi, Tingting Zhang, Yihan Li, Yulei Sun and Xiaoshan Wang**

Department of Neurology, The Affiliated Brain Hospital of Nanjing Medical University, Nanjing Medical University, Nanjing, China

Purpose: This study aimed to investigate the spectral and spatial signatures of neuromagnetic activity underlying the termination of absence seizures.

Methods: Magnetoencephalography (MEG) data were recorded from 18 drug-naive patients with childhood absence epilepsy (CAE). Accumulated source imaging (ASI) was used to analyze MEG data at the source level in seven frequency ranges: delta (1–4 Hz), theta (4–8 Hz), alpha (8–12 Hz), beta (12–30 Hz), gamma (30–80 Hz), ripple (80–250 Hz), and fast ripple (250–500 Hz).

Result: In the 1–4, 4–8, and 8–12 Hz ranges, the magnetic source during seizure termination appeared to be consistent over the ictal period and was mainly localized in the frontal cortex (FC) and parieto-occipito-temporal junction (POT). In the 12–30 and 30–80 Hz ranges, a significant reduction in source activity was observed in the frontal lobe during seizure termination as well as a decrease in peak source strength. The ictal peak source strength in the 1–4 Hz range was negatively correlated with the ictal duration of the seizure, whereas in the 30–80 Hz range, it was positively correlated with the course of epilepsy.

Conclusion: The termination of absence seizures is associated with a dynamic neuromagnetic process. Frequency-dependent changes in the FC were observed during seizure termination, which may be involved in the process of neural network interaction. Neuromagnetic activity in different frequency bands may play different roles in the pathophysiological mechanism during absence seizures.

Keywords: childhood absence epilepsy, magnetoencephalography, termination, cerebral cortex, multifrequency

OPEN ACCESS

Edited by:
Jing Xiang,
Cincinnati Children's Hospital Medical Center, United States

Reviewed by:
Yingying Wang,
University of Nebraska–Lincoln, United States
Ton J. Degrauw,
Emory University, United States

***Correspondence:**
Xiaoshan Wang
wangxiaoshan52@163.com

Specialty section:
This article was submitted to Brain Imaging and Stimulation, a section of the journal Frontiers in Human Neuroscience

Received: *30 March 2020*
Accepted: *15 May 2020*
Published: *26 June 2020*

Citation:
Sun J, Gao Y, Miao A, Yu C, Tang L, Huang S, Wu C, Shi Q, Zhang T, Li Y, Sun Y and Wang X (2020) Multifrequency Dynamics of Cortical Neuromagnetic Activity Underlying Seizure Termination in Absence Epilepsy. Front. Hum. Neurosci. 14:221. doi: 10.3389/fnhum.2020.00221

INTRODUCTION

Childhood absence epilepsy (CAE) is a common pediatric epilepsy syndrome. Children with CAE often suffer absence seizures during which children lose consciousness and stare blankly. Children with CAE have a risk for psychosocial and behavioral comorbidities and may develop persistent absence seizures or other types of epilepsy (Kessler and McGinnis, 2019). CAE mostly occurs in school-age children, ranging from 6 to 12 years of age, and the morbidity of CAE is higher in females than in males.

Childhood absence epilepsy is considered primary generalized epilepsy. On electroencephalography (EEG), seizures are characterized by a highly recognizable pattern of generalized (bilateral, symmetric, and synchronous) 3-Hz spike and wave discharges (SWDs) (Kessler and McGinnis, 2019). However, an increasing number of studies have found that CAE was more likely to have focal brain origins that were responsible for absence seizures (Westmijse et al., 2009; Kim et al., 2011; Tenney et al., 2013; Rozendaal et al., 2016; Kokkinos et al., 2017).

The involvement of the cortex during absence seizures in CAE has been reported in many studies (Tenney et al., 2013; Miao et al., 2014a; Tang et al., 2016; Jun et al., 2019). Moreover, cortical impairment has also been reported even in the interictal period (Xiang et al., 2015b; Qiu et al., 2016; Drenthen et al., 2019). Previous reports on source changes in the pre-ictal period have demonstrated that SWDs built up gradually rather than occurring suddenly and that the cortex played a leading role in the initiation of absence seizures (Gupta et al., 2011; Jacobs-Brichford et al., 2014; Wu et al., 2017b).

Although the changes in brain activity before the onset of absence seizures have been intensively investigated, the characteristics of neural activity underlying the termination of absence seizures remain poorly understood. Similar to the onset of absence seizures, the termination of absence seizures is well known to be an important part of the evolution of absence seizures, and knowledge of the features of seizure termination may help to further understand the potential self-regulatory mechanism for absence seizures, develop novel therapeutic strategies, and eventually improve the long-term prognosis of CAE. Previous studies focusing on the termination of seizures were mainly conducted at the cellular and energy metabolism levels (Lado and Moshe, 2008; Boison and Steinhauser, 2018; Kovacs et al., 2018). With the progress of technology, neuroimaging has provided new insight for the study of seizure termination. Recently, several studies have reported that the cortex was involved in the termination of SWDs (Benuzzi et al., 2015; Sysoeva et al., 2016; Jiang et al., 2019). However, the specific cortical regions involved in the termination of absence seizures are unclear.

Magnetoencephalography (MEG) is a non-invasive imaging technique that can be used to detect neuromagnetic signals from the brain. MEG and EEG have a similar high temporal resolution. However, MEG signals are usually unaffected by the skull and skin, which leads to a higher spatial resolution than that of EEG (Babiloni et al., 2009). Several studies have reported that MEG can localize epileptiform activity more accurately than EEG and provide reliable localization in the brain cortex (Alkawadri et al., 2018; Tamilia et al., 2019; van Klink et al., 2019). Moreover, MEG has been increasingly used in the evaluation of epileptogenic foci before epileptic surgery because of its non-invasive precise localization (De Tiege et al., 2017; Tamilia et al., 2017). In addition, the advantage over functional magnetic resonance imaging (fMRI) is that MEG can measure at millisecond temporal resolution, which renders it an ideal tool for the investigation of multifrequency epileptic activities (Moradi et al., 2003; Babiloni et al., 2009).

The present study was undertaken using MEG to analyze cortical neuromagnetic activity from 18 CAE patients from low- to high-frequency bands to investigate whether a pattern of specific cortical neural activity exists during the termination of absence seizures, which may be different from that during the ictal period.

MATERIALS AND METHODS

Eighteen patients with CAE were recruited from the Nanjing Brain Hospital and Nanjing Children's Hospital. The inclusion criteria were as follows: (1) a clinical diagnosis of CAE in line with the International League Against Epilepsy Proposal for Revised Classification of Epilepsies and Epileptic Syndromes; (2) typical bilateral, synchronous, symmetrical, approximately 3-Hz SWDs on a normal background in EEG with an ictal duration $\geq$3 s; (3) no history of receiving antiepileptic medication; and (4) no abnormal MRI results. The exclusion criteria were as follows: (1) CAE coexisting with other types of epilepsy or disease and (2) the presence of metal implants in the head. The medical ethics committees of Nanjing Children's Hospital, Nanjing Brain Hospital, and Nanjing Medical University provided permission for the present study. Informed assent was signed by all subjects, and consent was received from parents/guardians. All methods were performed in accordance with the relevant guidelines and regulations of the Declaration of Helsinki for human experimentation.

Magnetoencephalography Recordings

Magnetoencephalography data from all children with CAE acquired using a whole-head CTF 275 Channel MEG system (VSM Medical Technology Company, Canada) were recorded in a magnetically shielded room at the MEG Center of Nanjing Brain Hospital. Before MEG recording, three coils were affixed to the nasion and the left and right pre-auricular points of each patient to fix the head location in the MEG system. All subjects were told to remain still with their eyes closed during MEG recording. For each subject, the MEG recording duration was 120 s. At least six MEG data recordings were acquired for each subject with CAE, which ensured that complete and usable ictal data were available for further study. When the head movement was $\geq$5 mm or any artifact was present in the MEG data, the data were considered invalid and were recorded again. If ictal data were not captured by MEG recording, another MEG recording was performed, and the subjects were told to hyperventilate to provoke additional absence seizures. The rate of sampling for data acquisition was 6,000 Hz with noise cancelation of third-order gradients during the MEG recordings.

MRI Scan

Three-dimensional structural images were obtained by a 3.0-T MRI scanner (Siemens, Germany). Anatomic 3D T1-weighted images were obtained using a rapid gradient echo sequence (TR/TE = 1,900/2.48 ms). The imaging parameters were as follows: the field of view was 250 $\times$ 250 mm; the flip angle was 9°; and the matrix was 512 $\times$ 512. For each subject, 176

sagittal slices were collected. All subjects were instructed to minimize their head movements during scanning procedure, whereas markers were placed on the same three fiducial positions used for MEG to co-register the imaging data with the MEG data. All anatomical landmarks digitized in the MEG study were identifiable in the MRI.

Data Analysis

Magnetoencephalography data were first visually inspected for removing artifacts and motion-related noise. Then, visually inspected MEG data were band-pass filtered with 1–4 Hz bandwidth. The ictal segments were selected by identifying 3-Hz SWDs. We assessed the ictal segments using an audio-visual system in which we observed behavioral changes during absence seizures, such as staring, in the subjects with CAE. The first spike wave in SWDs was defined as the onset of a seizure, and the last slow wave component of SWDs was defined as the termination of the seizure. Epileptic waveforms were identified by two experienced epileptologists, and the interrater reliability was satisfactory for the identification of epileptic waveforms.

A total of two segments with a length of 3 s were selected to represent the ictal period and the period during termination of the seizure. Waveforms with a 10-s time window away from the ictal segment at least 30 s were considered interictal control data for further analysis (**Figure 1**).

The segments selected from the MEG data were analyzed in the following seven frequency bands: delta (1–4 Hz), theta (4–8 Hz), alpha (8–12 Hz), beta (12–30 Hz), gamma (30–80 Hz), ripple (80–250 Hz), and fast ripple (250–500 Hz). To eliminate power-line noise from the MEG data, notch filters for 50 Hz and its harmonics were applied.

Neuromagnetic sources were analyzed with an individual MRI-based head model. To objectively assess seizure-related epileptic activity in the brain, the whole brain was scanned with 3-mm resolution (115,136–115,562 voxels, depending on the size of the brain) (Xiang et al., 2014). Volumetric source imaging was computed for each frequency band for each subject. Detailed mathematical algorithms and validations have been described recently (Xiang et al., 2014, 2015a). To quantify source strength and reliability, each voxel in the source imaging comprised more than one parameter (multiple parameters per position). Specifically, each voxel had one parameter to represent the confidence volume and another parameter to describe the spectral power. The confidence volume was used for quality control: if the source voxel had a confidence volume smaller than 5 mm × 5 mm × 5 mm, the source voxel was considered reliable; otherwise, the source voxel was considered unreliable. Because the source strength was statistically analyzed (Xiang et al., 2015a; Shi et al., 2019), no units for the source measurements were provided. MEG source imaging was co-registered to MRI with the three fiducial points that had been placed prior to the MEG study and then spatially normalized for group analyses (Gilbert et al., 2012). Similar to a previous report (Xiang et al., 2009b), we performed comparisons at the source levels.

The definition of accumulated source imaging (ASI) was the volumetric summation of source activity over a period of time. The sources were localized by ASI using node-beam lead fields (Xiang et al., 2014). Because each node-beam lead field represented a form of either source-beamformer or subspace solution, the ASI had multiple source beamformers to separate correlated sources.

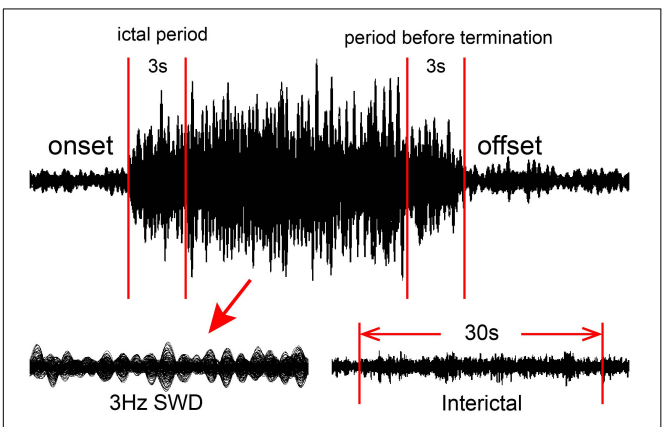

FIGURE 1 | Schematic of magnetoencephalography (MEG) waveform analysis. MEG data were recorded from 18 patients. For each eligible seizure, two 3-s segments were selected as the ictal period and the period during termination of the seizure, whereas one 100-s corresponding segment was selected as the interictal period.

Statistical Analysis

Fisher's exact test was utilized to assess the predominant source localization between different periods in each frequency band. Student's *t*-test was applied to compare changes in source strength between different periods in each frequency band. Partial correlation analysis was used to estimate correlations between clinical features and the peak source strength after adjustment for age and sex. The *p*-value threshold in our study was 0.05. For multiple comparisons, Bonferroni correction was applied. All statistical analyses were performed using SPSS 19.0 for Windows (SPSS Inc., Chicago, IL, United States).

RESULTS

Clinical Characteristics

Eighteen drug-naive patients with CAE were enrolled in this study (age range, 5–11 years; mean age, 8.4 ± 1.75 years; sex, 5 males and 13 females). The average course of epilepsy was 10.2 ± 7.60 months. The average seizure frequency was 6.6 ± 4.0 times/day. The clinical features of the subjects with CAE are shown in **Table 1**. A total of 33 ictal segments with an average ictal duration of 14.1 s (range, 6–36 s) were detected in the 18 subjects with CAE during MEG recording for the following analysis.

Source Localization Pattern

In the 1–4, 4–8, 8–12, and 12–30 Hz ranges, the magnetic source during seizure termination was mainly localized in the frontal cortex (FC) and parieto-occipito-temporal junction (POT) compared with that during the interictal period, which appeared to be consistent with the localization in the ictal period.

TABLE 1 | Characteristics of the patients with CAE.

Patient	Sex (F/M)	Age (years)	Duration of disease (months)	Frequency of seizures (times/day)	Time between diagnosis and the MEG test (day)
1	M	10	5	6	0
2	F	7	5	3	1
3	F	6	5	2–3	0
4	M	8	5	10	0
5	M	8	6	7	0
6	F	5	6	2–3	0
7	F	10	12	5	0
8	F	9	16	5–6	1
9	F	10	11	5	0
10	F	10	12	6–7	0
11	F	11	23	8	0
12	F	10	32	8	0
13	F	5	3	8	1
14	F	8	8	8	0
15	F	8	4	20	0
16	F	9	12	4–5	0
17	M	8	4	5	0
18	M	9	15	7–8	0

CAE, childhood absence epilepsy; MEG, magnetoencephalography; F, female; M, male.

No significant change in magnetic source localization in the POT was observed during seizure termination (**Figures 2**, **3**).

In the 12–30 and 30–80 Hz ranges, the source was mainly localized in the FC and deep brain area (DBA) in the ictal period. A significant difference in the source location in the FC was identified during seizure termination compared with the ictal and interictal periods ($p < 0.05$) (**Figures 2**, **3**).

In the 80–250 and 250–500 Hz ranges, the source was mainly localized in the FC and DBA. No significant difference was detected in the magnetic source location over all three periods (**Figures 2**, **3**).

Peak Source Strength of Neuromagnetic Activity

In the 1–4, 4–8, and 8–12 Hz ranges, the peak source strength during seizure termination was significantly higher than that during the interictal period ($p < 0.05$). No significant difference in peak source strength was found between the ictal period and during seizure termination (**Figure 4**).

In the 12–30 and 30–80 Hz ranges, the peak source strength during seizure termination decreased significantly compared with that during the ictal period and was still significantly higher than that during the ictal period ($p < 0.05$) (**Figure 4**).

In the 80–250 and 250–500 Hz ranges, no significant difference in peak source strength was found over all three periods (**Figure 4**).

Clinical Correlations

As shown in **Figure 5**, our data demonstrated that during the ictal period, the ictal peak source strength in the 1–4 Hz range

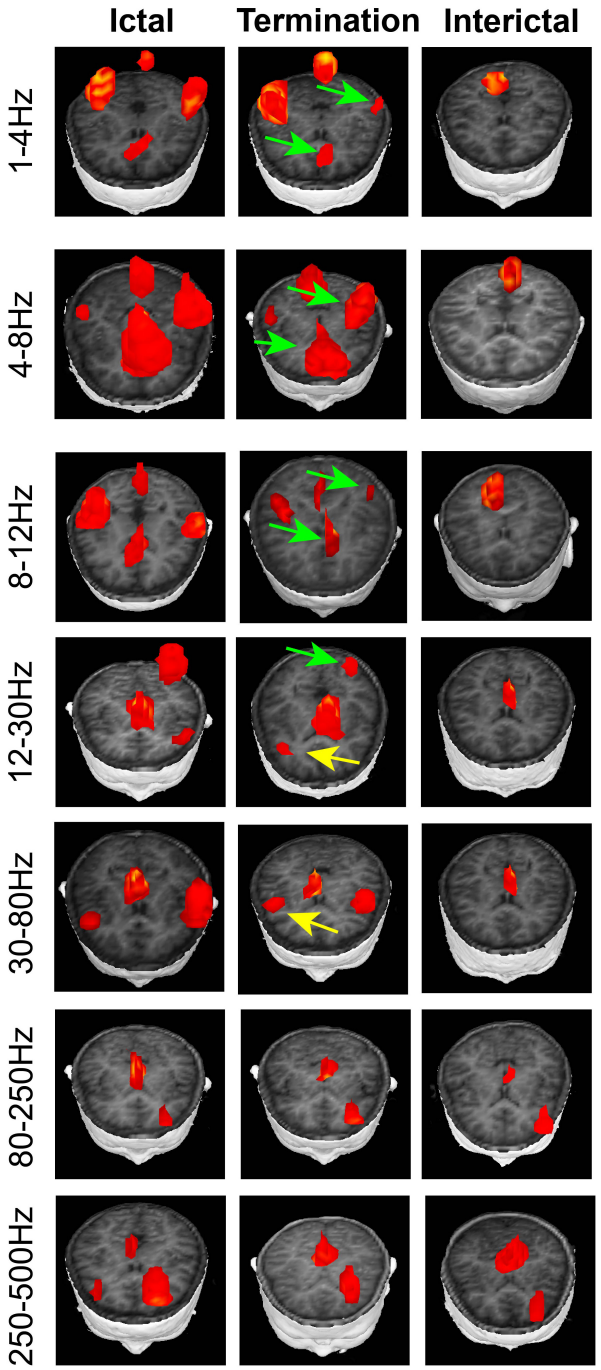

FIGURE 2 | Typical distribution of neuromagnetic source localization in the three periods in the seven frequency bands recorded from patients with CAE. In the 1–4, 4–8, 8–12, and 12–30 Hz ranges, the magnetic source during seizure termination mainly localized in the frontal cortex (FC) and parieto-occipito-temporal junction (POT) compared with that during the interictal period. In the 12–30 and 30–80 Hz ranges, a significant difference was identified in the source location in the FC during seizure termination compared with the ictal and interictal periods. Green arrows indicate the locations of neuromagnetic sources, which show significant differences between the period during seizure termination and the interictal period. Yellow arrows point to the regions that statistically changed during seizure termination compared with the ictal and interictal periods.

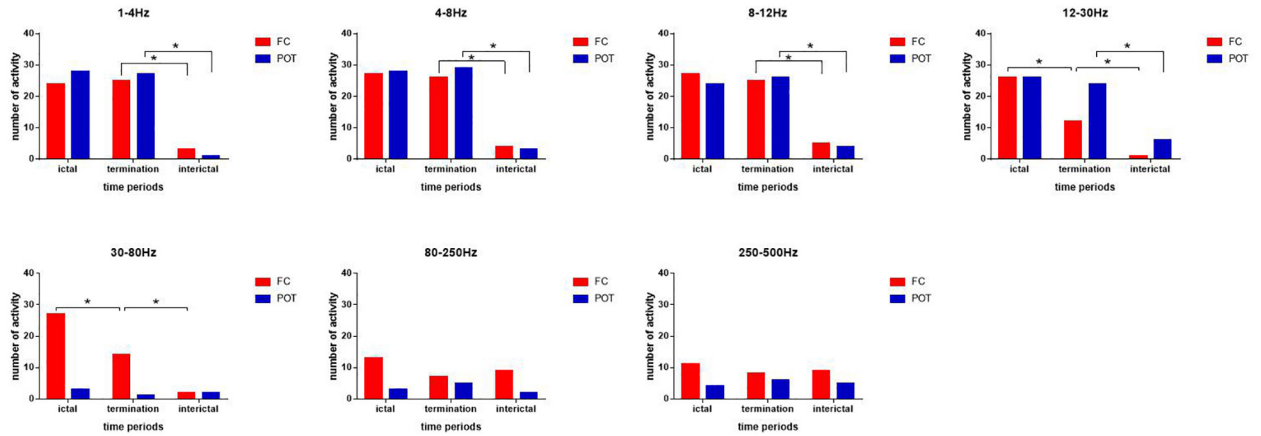

FIGURE 3 | Changes in the number of neuromagnetic source activities in the three periods for the seven frequency bands. The number of source locations is listed on the *y*-axis. Three periods are located on the *x*-axis. $^{*}p < 0.05$ after Bonferroni correction.

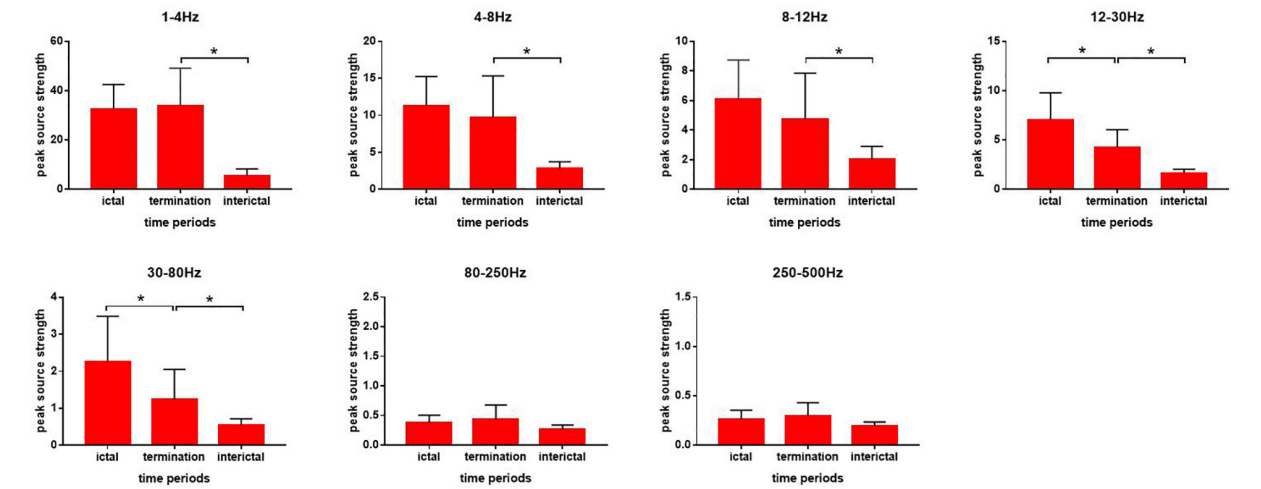

FIGURE 4 | Changes in the strength of neuromagnetic activity in the seven frequency bands during absence seizures. Source strength measurements are shown on the *y*-axis. Three periods are listed on the *x*-axis. $^{*}p < 0.05$ after Bonferroni correction.

was negatively correlated with the ictal duration of the seizure ($r = -0.645$, $p < 0.001$) after adjustment for age and sex, whereas in the 30–80 Hz range, it was positively correlated with the duration of epilepsy ($r = 0.603$, $p = 0.013$) after adjustment for age and sex. No significant correlation was found in the other frequency bands.

DISCUSSION

Our study investigated cortical neuromagnetic activity in subjects with CAE from low- to high-frequency ranges using MEG. The neuromagnetic activity revealed significant frequency-dependent differences during seizure termination compared with the ictal and interictal periods. The ictal peak source strength of neuromagnetic activity in specific frequency bands was correlated with the ictal duration of the seizure and the duration of epilepsy.

Most previous studies have suggested that the FC is more likely to play a critical role in the initiation and propagation of SWDs (Holmes et al., 2004; Szaflarski et al., 2010; Tenney et al., 2013; Miao et al., 2014a; Tang et al., 2016; Wu et al., 2017b). In the present study, we found lower activity in the FC during the termination of absence seizures than that during the ictal period, suggesting that the activity of the FC decreases significantly during the termination of absence seizures. An EEG-fMRI study demonstrated that the blood oxygenation level-dependent (BOLD) signal was decreased in the FC at seizure termination, indicating that the FC may be related to the termination of absence seizures (Benuzzi et al., 2015). Furthermore, our results showed that the decrease in activity in the FC mainly occurred in the 12–30 and 30–80 Hz frequency bands. In other words, we found a frequency-dependent neuromagnetic activity pattern during the termination of absence seizures. A previous study revealed a frequency-dependent feature of the ictal network in

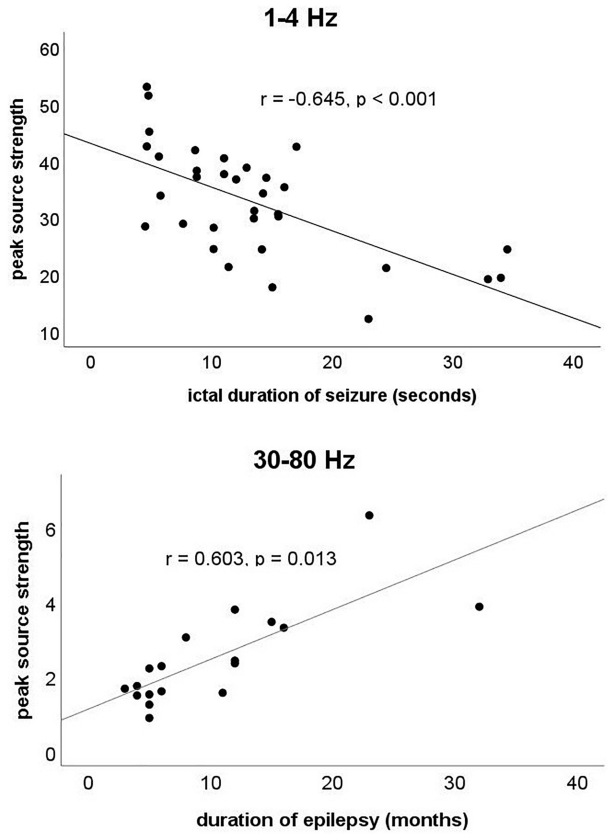

FIGURE 5 | The *y*-axis represents the ictal peak source strength. The *x*-axis at 1–4 Hz represents the ictal duration of the seizure, whereas at 30–80 Hz, the *x*-axis represents the duration of epilepsy. Partial correlation analysis showed that the ictal peak source strength in the 1–4 Hz range was negatively correlated with the ictal duration of the seizure ($r = -0.645$, $p < 0.001$) after adjustment for age and sex, whereas in the 30–80 Hz range, it was positively correlated with the duration of epilepsy ($r = 0.603$, $p = 0.013$) after adjustment for age and sex.

absence epilepsy, which may partially explain our results (Tenney et al., 2014, 2018). Similarly, another study reported that SWDs revealed alternating ictal patterns between localization during the spikes and generalization during the waves (Ossenblok et al., 2019). In addition, several studies have shown that part of the spike wave during absence seizures was generated by the FC (Clemens et al., 2007; Jun et al., 2019). Another study also reported that the first spike wave of SWDs was localized in the lateral FC during absence seizures (Tenney et al., 2013). Therefore, we speculate that the decrease in activity in the FC in the 12–30 and 30–80 Hz ranges may be related to decreased activity in the spike wave during seizure termination. Furthermore, our results suggest that the termination of absence seizures was a gradual process rather than a sudden event, which in line with previous studies (Luttjohann et al., 2014; Jiang et al., 2019).

The present study showed that the magnetic source locations in high-frequency ranges (80–250 and 250–500 Hz) were mainly in the FC and DBA. No significant difference in magnetic source location was observed over all three periods, suggesting that the pattern of neural activity in high-frequency bands differed from that in all other frequency bands (<80 Hz), which is supported by recent studies (Tang et al., 2016; Wu et al., 2017b; Jiang et al., 2019). In recent years, increasing research on high-frequency oscillations (HFOs) has been presented, and HFOs have been considered a new biomarker for epilepsy (Xiang et al., 2009a, 2010; Miao et al., 2014b; Tang et al., 2016). HFOs have been reported to be correlated with the pathophysiology of epilepsy and used to localize the epileptogenic zone in epileptic surgery (Haegelen et al., 2013; Kerber et al., 2014). Previous reports have demonstrated that source localization in high-frequency bands was more focal and stable than that in low-frequency bands (Miao et al., 2014b; Tang et al., 2016; Wu et al., 2017b). Furthermore, a study found that HFOs could precede the onset of a seizure and persist after the postictal period (Fuertinger et al., 2016). These related studies suggested the existence of different cellular and network mechanisms between HFOs and other neural activity (Draguhn et al., 1998; Traub et al., 2003; Roopun et al., 2010). HFOs are suited to interact with neighboring neurons, and lower frequencies are suitable for integration over a wider range (Sauseng and Klimesch, 2008; Xiang et al., 2015b; Tang et al., 2016; Wu et al., 2017a,b; Tenney et al., 2018). Therefore, we speculate that the activity of the FC in high-frequency bands may be related to the generation of absence seizures. Nevertheless, the specific function of HFOs still requires further investigation.

Our study found that the ictal peak source strength at 30–80 Hz was positively correlated with the duration of epilepsy. Previous studies have suggested that gamma oscillations were produced by the activity of fast-spiking inhibitory interneurons (Cardin et al., 2009; Sohal, 2012). One possible explanation for the correlation between peak source strength and the duration of epilepsy is that long-term chronic neuronal structural damage may be the structural basis for the increase in peak source strength caused by frequent abnormal discharges during the ictal period (Tang et al., 2016). In addition, we also found that the ictal peak source strength at 1–4 Hz was negatively correlated with the ictal duration of the seizure. Delta oscillations were mainly produced by cortical pyramidal neurons (Neckelmann et al., 2000; Cardin et al., 2009). Abnormal delta oscillations were found to be associated with impairment of consciousness during epileptic seizures, which may be due to an inhibitory effect on the excitability of the cortex (Shmuel et al., 2002, 2006; Pittau et al., 2013; Holler and Trinka, 2015; Unterberger et al., 2018). However, another study revealed that low-frequency oscillations could also inhibit neural activity in higher-frequency bands and promote seizure termination (Medvedev, 2002; Tenney et al., 2014). An interaction between different frequency bands may be achieved through cross-frequency coupling as reported by a previous study, which requires further investigation (Aru et al., 2015). Although our results are not sufficient to prove the specific mechanism of the correlation between peak source strength in different frequency bands and clinical features, we speculate that neural activity in different frequency bands may play different roles in absence epilepsy.

Limitations

Several limitations to our research exist. First, because absence seizures are unpredictable, collecting complete ictal data is difficult, resulting in a small sample size. However, we applied strict criteria and excluded other forms of idiopathic generalized epilepsy to establish a strictly homogeneous group of patients in terms of diagnosis for this study despite the limited sample size. Second, although recent studies have certified that MEG can detect the DBA (Papadelis et al., 2009; Leiken et al., 2014), the spatial resolution in the DBA on MEG remains debatable. In several studies, although the activities of the DBA were mainly regarded as the activities of the thalamus (Wu et al., 2017b; Jiang et al., 2019), we cannot rule out the possibility of artifacts and noise, which may disturb our results. Therefore, we removed the analysis and discussions of neuromagnetic activities related to the DBA in this study. This issue can be resolved with the advancement of MEG technology in the future. Third, the 3-s time windows selected in this study were not sufficiently short, preventing us from observing changes in neuromagnetic activity within 3 s during the termination of absence seizures. Further investigations with shorter time windows are essential in the future. Fourth, although we recorded MEG signals under the same experimental conditions and minimized artifacts using accumulated technology and other measures, artifacts from electromyography, magnetocardiography, and other signals may still be included in our results. More investigations in the future are required to determine whether artifacts are completely eliminated. Finally, the source imaging technology of software is limited and not wholly reliable. Thus, our results must be verified using other brain imaging software in future investigations.

CONCLUSION

In conclusion, we demonstrated that the termination of absence seizures is associated with a dynamic neuromagnetic process and that frequency-dependent changes in the activity of the FC during termination of absence seizures may be involved in the process of seizure termination. The ictal peak source strength in the 1–4 Hz range was negatively correlated with the ictal duration of the seizure, whereas in the 30–80 Hz range, it was positively correlated with the duration of epilepsy, suggesting that neuromagnetic activity in different frequency bands may play different roles in the pathophysiological mechanism of CAE. The specific mechanism of neural activity in multifrequency bands underlying seizure termination needs to be investigated further.

DATA AVAILABILITY STATEMENT

The raw data supporting the conclusions of this article will be made available by the authors, without undue reservation, to any qualified researcher.

ETHICS STATEMENT

The studies involving human participants were reviewed and approved by the medical ethics committees of Nanjing Brain Hospital, the medical ethics committees of Nanjing Children's Hospital and the medical ethics committees of Nanjing Medical University. Written informed consent to participate in this study was provided by the participants' legal guardian/next of kin. Written informed consent was obtained from the minor(s)' legal guardian/next of kin for the publication of any potentially identifiable images or data included in this article.

AUTHOR CONTRIBUTIONS

JS, YG, AM, and XW designed the research. JS, QS, AM, LT, and SH analyzed the data. YG, CY, TZ, YL, YS, and CW recruited the participants and acquired the images. JS wrote the manuscript. XW revised the manuscript. All authors approved the final submitted version and agreed to be accountable for its content.

FUNDING

This study was supported by the General Program of Natural Science Foundation of Jiangsu Province (Grant No. BK20191127) and the Health Department of Jiangsu Province (Grant No. H2018062).

ACKNOWLEDGMENTS

We would like to thank the physicians and researchers at the NBH and Nanjing Children's Hospital. We also thank all participants and their guardians for their support.

REFERENCES

Alkawadri, R., Burgess, R. C., Kakisaka, Y., Mosher, J. C., and Alexopoulos, A. V. (2018). Assessment of the utility of ictal magnetoencephalography in the localization of the epileptic seizure onset zone. *JAMA Neurol.* 75, 1264–1272. doi: 10.1001/jamaneurol.2018.1430

Aru, J., Aru, J., Priesemann, V., Wibral, M., Lana, L., Pipa, G., et al. (2015). Untangling cross-frequency coupling in neuroscience. *Curr. Opin. Neurobiol.* 31, 51–61. doi: 10.1016/j.conb.2014.08.002

Babiloni, C., Pizzella, V., Gratta, C. D., Ferretti, A., and Romani, G. L. (2009). Fundamentals of electroencefalography, magnetoencefalography, and functional magnetic resonance imaging. *Int. Rev. Neurobiol.* 86, 67–80. doi: 10.1016/S0074-7742(09)86005-4

Benuzzi, F., Ballotta, D., Mirandola, L., Ruggieri, A., Vaudano, A. E., Zucchelli, M., et al. (2015). An EEG-fMRI study on the termination of generalized spike-and-wave discharges in absence epilepsy. *PLoS One* 10:e0130943. doi: 10.1371/journal.pone.0130943

Boison, D., and Steinhauser, C. (2018). Epilepsy and astrocyte energy metabolism. *Glia* 66, 1235–1243. doi: 10.1002/glia.23247

Cardin, J. A., Carlen, M., Meletis, K., Knoblich, U., Zhang, F., Deisseroth, K., et al. (2009). Driving fast-spiking cells induces gamma rhythm and controls sensory responses. *Nature* 459, 663–667. doi: 10.1038/nature08002

Clemens, B., Bessenyei, M., Piros, P., Toth, M., Seress, L., and Kondakor, I. (2007). Characteristic distribution of interictal brain electrical activity in idiopathic generalized epilepsy. *Epilepsia* 48, 941–949. doi: 10.1111/j.1528-1167.2007.01030.x

De Tiege, X., Lundqvist, D., Beniczky, S., Seri, S., and Paetau, R. (2017). Current clinical magnetoencephalography practice across Europe: are we closer to use MEG as an established clinical tool? *Seizure* 50, 53–59. doi: 10.1016/j.seizure.2017.06.002

Draguhn, A., Traub, R. D., Schmitz, D., and Jefferys, J. G. (1998). Electrical coupling underlies high-frequency oscillations in the hippocampus in vitro. *Nature* 394, 189–192. doi: 10.1038/28184

Drenthen, G. S., Fonseca Wald, E. L. A., Backes, W. H., Debeij-Van Hall, M., Hendriksen, J. G. M., Aldenkamp, A. P., et al. (2019). Lower myelin-water content of the frontal lobe in childhood absence epilepsy. *Epilepsia* 60, 1689–1696. doi: 10.1111/epi.16280

Fuertinger, S., Simonyan, K., Sperling, M. R., Sharan, A. D., and Hamzei-Sichani, F. (2016). High-frequency brain networks undergo modular breakdown during epileptic seizures. *Epilepsia* 57, 1097–1108. doi: 10.1111/epi.13413

Gilbert, J. R., Shapiro, L. R., and Barnes, G. R. (2012). A peak-clustering method for MEG group analysis to minimise artefacts due to smoothness. *PLoS One* 7:e45084. doi: 10.1371/journal.pone.0045084

Gupta, D., Ossenblok, P., and van Luijtelaar, G. (2011). Space-time network connectivity and cortical activations preceding spike wave discharges in human absence epilepsy: a MEG study. *Med. Biol. Eng. Comput.* 49, 555–565. doi: 10.1007/s11517-011-0778-3

Haegelen, C., Perucca, P., Chatillon, C. E., Andrade-Valenca, L., Zelmann, R., Jacobs, J., et al. (2013). High-frequency oscillations, extent of surgical resection, and surgical outcome in drug-resistant focal epilepsy. *Epilepsia* 54, 848–857. doi: 10.1111/epi.12075

Holler, Y., and Trinka, E. (2015). Is there a relation between EEG-slow waves and memory dysfunction in epilepsy? A critical appraisal. *Front. Hum. Neurosci.* 9:341. doi: 10.3389/fnhum.2015.00341

Holmes, M. D., Brown, M., and Tucker, D. M. (2004). Are "generalized" seizures truly generalized? Evidence of localized mesial frontal and frontopolar discharges in absence. *Epilepsia* 45, 1568–1579. doi: 10.1111/j.0013-9580.2004.23204.x

Jacobs-Brichford, E., Horn, P. S., and Tenney, J. R. (2014). Mapping preictal networks preceding childhood absence seizures using magnetoencephalography. *J. Child Neurol.* 29, 1312–1319. doi: 10.1177/0883073813518107

Jiang, W., Wu, C., Xiang, J., Miao, A., Qiu, W., Tang, L., et al. (2019). Dynamic neuromagnetic network changes of seizure termination in absence epilepsy: a magnetoencephalography study. *Front. Neurol.* 10:703. doi: 10.3389/fneur.2019.00703

Jun, Y. H., Eom, T. H., Kim, Y. H., Chung, S. Y., Lee, I. G., and Kim, J. M. (2019). Source localization of epileptiform discharges in childhood absence epilepsy using a distributed source model: a standardized, low-resolution, brain electromagnetic tomography (sLORETA) study. *Neurol. Sci.* 40, 993–1000. doi: 10.1007/s10072-019-03751-4

Kerber, K., Dumpelmann, M., Schelter, B., Le Van, P., Korinthenberg, R., Schulze-Bonhage, A., et al. (2014). Differentiation of specific ripple patterns helps to identify epileptogenic areas for surgical procedures. *Clin. Neurophysiol.* 125, 1339–1345. doi: 10.1016/j.clinph.2013.11.030

Kessler, S. K., and McGinnis, E. (2019). A practical guide to treatment of childhood absence epilepsy. *Paediatr. Drugs* 21, 15–24. doi: 10.1007/s40272-019-00325-x

Kim, D. S., Nordli, D. R. Jr., and Zelko, F. (2011). Spectral power of 1-4 Hz frequency in the ictal phase of childhood absence epilepsy. *J. Clin. Neurophysiol.* 28, 463–468. doi: 10.1097/WNP.0b013e318231c2e1

Kokkinos, V., Koupparis, A. M., Koutroumanidis, M., and Kostopoulos, G. K. (2017). Spatiotemporal propagation patterns of generalized ictal spikes in childhood absence epilepsy. *Clin. Neurophysiol.* 128, 1553–1562. doi: 10.1016/j.clinph.2017.05.021

Kovacs, R., Gerevich, Z., Friedman, A., Otahal, J., Prager, O., Gabriel, S., et al. (2018). Bioenergetic mechanisms of seizure control. *Front. Cell. Neurosci.* 12:335. doi: 10.3389/fncel.2018.00335

Lado, F. A., and Moshe, S. L. (2008). How do seizures stop? *Epilepsia* 49, 1651–1664. doi: 10.1111/j.1528-1167.2008.01669.x

Leiken, K., Xiang, J., Zhang, F., Shi, J., Tang, L., Liu, H., et al. (2014). Magnetoencephalography detection of high-frequency oscillations in the developing brain. *Front. Hum. Neurosci.* 8:969. doi: 10.3389/fnhum.2014.00969

Luttjohann, A., Schoffelen, J. M., and van Luijtelaar, G. (2014). Termination of ongoing spike-wave discharges investigated by cortico-thalamic network analyses. *Neurobiol. Dis.* 70, 127–137. doi: 10.1016/j.nbd.2014.06.007

Medvedev, A. V. (2002). Epileptiform spikes desynchronize and diminish fast (gamma) activity of the brain. An "anti-binding" mechanism? *Brain Res. Bull.* 58, 115–128. doi: 10.1016/s0361-9230(02)00768-2

Miao, A., Tang, L., Xiang, J., Guan, Q., Ge, H., Liu, H., et al. (2014a). Dynamic magnetic source imaging of absence seizure initialization and propagation: a magnetoencephalography study. *Epilepsy Res.* 108, 468–480. doi: 10.1016/j.eplepsyres.2014.01.006

Miao, A., Xiang, J., Tang, L., Ge, H., Liu, H., Wu, T., et al. (2014b). Using ictal high-frequency oscillations (80-500Hz) to localize seizure onset zones in childhood absence epilepsy: a MEG study. *Neurosci. Lett.* 566, 21–26. doi: 10.1016/j.neulet.2014.02.038

Moradi, F., Liu, L. C., Cheng, K., Waggoner, R. A., Tanaka, K., and Ioannides, A. A. (2003). Consistent and precise localization of brain activity in human primary visual cortex by MEG and fMRI. *Neuroimage* 18, 595–609. doi: 10.1016/s1053-8119(02)00053-8

Neckelmann, D., Amzica, F., and Steriade, M. (2000). Changes in neuronal conductance during different components of cortically generated spike-wave seizures. *Neuroscience* 96, 475–485. doi: 10.1016/s0306-4522(99)00571-0

Ossenblok, P., van Houdt, P., Colon, A., Stroink, H., and van Luijtelaar, G. (2019). A network approach to investigate the bi-hemispheric synchrony in absence epilepsy. *Clin. Neurophysiol.* 130, 1611–1619. doi: 10.1016/j.clinph.2019.05.034

Papadelis, C., Poghosyan, V., Fenwick, P. B. C., and Ioannides, A. A. (2009). MEG's ability to localise accurately weak transient neural sources. *Clin. Neurophysiol.* 120, 1958–1970. doi: 10.1016/j.clinph.2009.08.018

Pittau, F., Fahoum, F., Zelmann, R., Dubeau, F., and Gotman, J. (2013). Negative BOLD response to interictal epileptic discharges in focal epilepsy. *Brain Topogr.* 26, 627–640. doi: 10.1007/s10548-013-0302-1

Qiu, W., Gao, Y., Yu, C., Miao, A., Tang, L., Huang, S., et al. (2016). Structural abnormalities in childhood absence epilepsy: voxel-based analysis using diffusion tensor imaging. *Front. Hum. Neurosci.* 10:483. doi: 10.3389/fnhum.2016.00483

Roopun, A. K., Simonotto, J. D., Pierce, M. L., Jenkins, A., Nicholson, C., Schofield, I. S., et al. (2010). A nonsynaptic mechanism underlying interictal discharges in human epileptic neocortex. *Proc. Natl. Acad. Sci. U.S.A.* 107, 338–343. doi: 10.1073/pnas.0912652107

Rozendaal, Y. J., van Luijtelaar, G., and Ossenblok, P. P. (2016). Spatiotemporal mapping of interictal epileptiform discharges in human absence epilepsy: a MEG study. *Epilepsy Res.* 119, 67–76. doi: 10.1016/j.eplepsyres.2015.11.013

Sauseng, P., and Klimesch, W. (2008). What does phase information of oscillatory brain activity tell us about cognitive processes? *Neurosci. Biobehav. Rev.* 32, 1001–1013. doi: 10.1016/j.neubiorev.2008.03.014

Shi, Q., Zhang, T., Miao, A., Sun, J., Sun, Y., Chen, Q., et al. (2019). Differences between interictal and ictal generalized spike-wave discharges in childhood absence epilepsy: a MEG study. *Front Neurol* 10:1359. doi: 10.3389/fneur.2019.01359

Shmuel, A., Augath, M., Oeltermann, A., and Logothetis, N. K. (2006). Negative functional MRI response correlates with decreases in neuronal activity in monkey visual area V1. *Nat. Neurosci.* 9, 569–577. doi: 10.1038/nn1675

Shmuel, A., Yacoub, E., Pfeuffer, J., Van de Moortele, P. F., Adriany, G., Hu, X., et al. (2002). Sustained negative BOLD, blood flow and oxygen consumption response and its coupling to the positive response in the human brain. *Neuron* 36, 1195–1210. doi: 10.1016/s0896-6273(02)01061-9

Sohal, V. S. (2012). Insights into cortical oscillations arising from optogenetic studies. *Biol. Psychiatry* 71, 1039–1045. doi: 10.1016/j.biopsych.2012.01.024

Sysoeva, M. V., Luttjohann, A., van Luijtelaar, G., and Sysoev, I. V. (2016). Dynamics of directional coupling underlying spike-wave discharges. *Neuroscience* 314, 75–89. doi: 10.1016/j.neuroscience.2015.11.044

Szaflarski, J. P., DiFrancesco, M., Hirschauer, T., Banks, C., Privitera, M. D., Gotman, J., et al. (2010). Cortical and subcortical contributions to absence seizure onset examined with EEG/fMRI. *Epilepsy Behav.* 18, 404–413. doi: 10.1016/j.yebeh.2010.05.009

Tamilia, E., AlHilani, M., Tanaka, N., Tsuboyama, M., Peters, J. M., Grant, P. E., et al. (2019). Assessing the localization accuracy and clinical utility of electric and magnetic source imaging in children with epilepsy. *Clin. Neurophysiol.* 130, 491–504. doi: 10.1016/j.clinph.2019.01.009

Tamilia, E., Madsen, J. R., Grant, P. E., Pearl, P. L., and Papadelis, C. (2017). Current and emerging potential of magnetoencephalography in the detection and localization of high-frequency oscillations in epilepsy. *Front. Neurol.* 8:14. doi: 10.3389/fneur.2017.00014

Tang, L., Xiang, J., Huang, S., Miao, A., Ge, H., Liu, H., et al. (2016). Neuromagnetic high-frequency oscillations correlate with seizure severity in absence epilepsy. *Clin. Neurophysiol.* 127, 1120–1129. doi: 10.1016/j.clinph.2015.08.016

Tenney, J. R., Fujiwara, H., Horn, P. S., Jacobson, S. E., Glauser, T. A., and Rose, D. F. (2013). Focal corticothalamic sources during generalized absence seizures: a MEG study. *Epilepsy Res.* 106, 113–122. doi: 10.1016/j.eplepsyres.2013.05.006

Tenney, J. R., Fujiwara, H., Horn, P. S., Vannest, J., Xiang, J., Glauser, T. A., et al. (2014). Low- and high-frequency oscillations reveal distinct absence seizure networks. *Ann. Neurol.* 76, 558–567. doi: 10.1002/ana.24231

Tenney, J. R., Kadis, D. S., Agler, W., Rozhkov, L., Altaye, M., Xiang, J., et al. (2018). Ictal connectivity in childhood absence epilepsy: associations with outcome. *Epilepsia* 59, 971–981. doi: 10.1111/epi.14067

Traub, R. D., Pais, I., Bibbig, A., LeBeau, F. E., Buhl, E. H., Hormuzdi, S. G., et al. (2003). Contrasting roles of axonal (pyramidal cell) and dendritic (interneuron) electrical coupling in the generation of neuronal network oscillations. *Proc. Natl. Acad. Sci. U.S.A.* 100, 1370–1374. doi: 10.1073/pnas.0337529100

Unterberger, I., Trinka, E., Kaplan, P. W., Walser, G., Luef, G., and Bauer, G. (2018). Generalized nonmotor (absence) seizures-What do absence, generalized, and nonmotor mean? *Epilepsia* 59, 523–529. doi: 10.1111/epi.13996

van Klink, N., Mooij, A., Huiskamp, G., Ferrier, C., Braun, K., Hillebrand, A., et al. (2019). Simultaneous MEG and EEG to detect ripples in people with focal epilepsy. *Clin. Neurophysiol.* 130, 1175–1183. doi: 10.1016/j.clinph.2019.01.027

Westmijse, I., Ossenblok, P., Gunning, B., and van Luijtelaar, G. (2009). Onset and propagation of spike and slow wave discharges in human absence epilepsy: a MEG study. *Epilepsia* 50, 2538–2548. doi: 10.1111/j.1528-1167.2009.02162.x

Wu, C., Xiang, J., Jiang, W., Huang, S., Gao, Y., Tang, L., et al. (2017a). Altered effective connectivity network in childhood absence epilepsy: a multi-frequency MEG study. *Brain Topogr.* 30, 673–684. doi: 10.1007/s10548-017-0555-1

Wu, C., Xiang, J., Sun, J., Huang, S., Tang, L., Miao, A., et al. (2017b). Quantify neuromagnetic network changes from pre-ictal to ictal activities in absence seizures. *Neuroscience* 357, 134–144. doi: 10.1016/j.neuroscience.2017.05.038

Xiang, J., Korman, A., Samarasinghe, K. M., Wang, X., Zhang, F., Qiao, H., et al. (2015a). Volumetric imaging of brain activity with spatial-frequency decoding of neuromagnetic signals. *J. Neurosci. Methods* 239, 114–128. doi: 10.1016/j.jneumeth.2014.10.007

Xiang, J., Liu, Y., Wang, Y., Kirtman, E. G., Kotecha, R., Chen, Y., et al. (2009a). Frequency and spatial characteristics of high-frequency neuromagnetic signals in childhood epilepsy. *Epileptic Disord.* 11, 113–125. doi: 10.1684/epd.2009.0253

Xiang, J., Liu, Y., Wang, Y., Kotecha, R., Kirtman, E. G., Chen, Y., et al. (2009b). Neuromagnetic correlates of developmental changes in endogenous high-frequency brain oscillations in children: a wavelet-based beamformer study. *Brain Res.* 1274, 28–39. doi: 10.1016/j.brainres.2009.03.068

Xiang, J., Luo, Q., Kotecha, R., Korman, A., Zhang, F., Luo, H., et al. (2014). Accumulated source imaging of brain activity with both low and high-frequency neuromagnetic signals. *Front. Neuroinform.* 8:57. doi: 10.3389/fninf.2014.00057

Xiang, J., Tenney, J. R., Korman, A. M., Leiken, K., Rose, D. F., Harris, E., et al. (2015b). Quantification of interictal neuromagnetic activity in absence epilepsy with accumulated source imaging. *Brain Topogr.* 28, 904–914. doi: 10.1007/s10548-014-0411-5

Xiang, J., Wang, Y., Chen, Y., Liu, Y., Kotecha, R., Huo, X., et al. (2010). Noninvasive localization of epileptogenic zones with ictal high-frequency neuromagnetic signals. *J. Neurosurg. Pediatr.* 5, 113–122. doi: 10.3171/2009.8.PEDS09345 doi: 10.3171/2009.8.peds09345

Conflict of Interest: The authors declare that the research was conducted in the absence of any commercial or financial relationships that could be construed as a potential conflict of interest.

frontiers in Human Neuroscience

ORIGINAL RESEARCH
published: 26 August 2020
doi: 10.3389/fnhum.2020.00335

Association Between Interictal High-Frequency Oscillations and Slow Wave in Refractory Focal Epilepsy With Good Surgical Outcome

Guoping Ren[1,2†], Jiaqing Yan[3†], Yueqian Sun[1,2,4], Jiechuan Ren[1,2], Jindong Dai[5], Shanshan Mei[5], Yunlin Li[5], Xiaofei Wang[5], Xiaofeng Yang[4,6,7] and Qun Wang[1,2,4*]*

[1] Department of Neurology, Beijing Tiantan Hospital, Capital Medical University, Beijing, China, [2] China National Clinical Research Center for Neurological Diseases, Beijing, China, [3] College of Electrical and Control Engineering, North China University of Technology, Beijing, China, [4] Laboratory of Brain Disorders, Collaborative Innovation Center for Brain Disorders, Beijing Institute of Brain Disorders, Capital Medical University, Ministry of Science and Technology, Beijing, China, [5] Department of Functional Neurosurgery, Beijing Haidian Hospital, Beijing, China, [6] Neuroelectrophysiological Laboratory, Xuanwu Hospital, Capital Medical University, Beijing, China, [7] Guangzhou Regenerative Medicine and Health Guangdong Laboratory, Guangzhou, China

OPEN ACCESS

Edited by:
Mario Tombini,
Campus Bio-Medico University, Italy

Reviewed by:
James Tao,
University of Chicago, United States
Nan Zhang,
University of Science and Technology of China, China

***Correspondence:**
Qun Wang
wangq@ccmu.edu.cn
Jiaqing Yan
redyjq@gmail.com

† These authors have contributed equally to this work and share first authorship

Specialty section:
This article was submitted to Brain Imaging and Stimulation, a section of the journal Frontiers in Human Neuroscience

Received: *07 June 2020*
Accepted: *29 July 2020*
Published: *26 August 2020*

Citation:
Ren G, Yan J, Sun Y, Ren J, Dai J, Mei S, Li Y, Wang X, Yang X and Wang Q (2020) Association Between Interictal High-Frequency Oscillations and Slow Wave in Refractory Focal Epilepsy With Good Surgical Outcome. Front. Hum. Neurosci. 14:335. doi: 10.3389/fnhum.2020.00335

High-frequency oscillations (HFOs) have been proposed as a promising biomarker of the epileptogenic zone (EZ). But accurate delineation of EZ based on HFOs is still challenging. Our study compared HFOs from EZ and non-EZ on the basis of their associations with interictal slow waves, aiming at exploring a new way to localize EZ. Nineteen medically intractable epilepsy patients with good surgical outcome were included. Five minute interictal intracranial electroencephalography (EEG) epochs of slow-wave sleep were randomly selected; then ripples (80–200 Hz), fast ripples (FRs; 200–500 Hz), and slow waves (0.1–4 Hz) were automatically analyzed. The EZ and non-EZ were identified by resection range during the surgeries. We found that both ripples and FRs superimposed more frequently on slow waves in EZ than in non-EZ ($P < 0.01$). Although ripples preferred to occur on the down state of slow waves in both two groups, ripples in EZ tended to be closer to the down-state peak of slow wave than in non-EZ (-174 vs. -231 ms, $P = 0.008$). As for FR, no statistical difference was found between the two groups ($P = 0.430$). Additionally, slow wave-containing ripples in EZ had a steeper slope (1.7 vs. 1.5 μV/ms, $P < 0.001$) and wider distribution ratio (32.3 vs. 30.1%, $P < 0.001$) than those in the non-EZ. But for slow wave-containing FR, only a steeper slope (1.7 vs. 1.4 μV/ms, $P < 0.001$) was observed. Our study innovatively compared the different features of association between HFOs and slow wave in EZ and non-EZ from refractory focal epilepsy with good surgical outcome, proposing a new method to localize EZ and facilitating the surgical plan.

Keywords: high-frequency oscillations, slow wave, refractory focal epilepsy, good surgical outcome, epileptogenic zone

INTRODUCTION

High-frequency oscillations (HFOs) have been proposed as a promising biomarker of the epileptogenic zone (EZ) (Bragin et al., 1999; Jirsch et al., 2006; Thomschewski et al., 2019; Frauscher, 2020). It is categorized as ripples (80–200 Hz) and fast ripples (FRs; 200–500 Hz). The rate of HFOs is higher in the seizure onset zone or EZ than that outside these areas, and removal of tissue containing pathological HFOs is associated with good surgical outcome (Jacobs et al., 2010; Thomschewski et al., 2019). However, HFOs occur both inside and outside the EZ (Sakuraba et al., 2016; Pail et al., 2017), and FR outside the EZ may eliminate after removal of FR inside the EZ, which indicates the existence of epileptogenic network (van't Klooster et al., 2017). Moreover, the normal brain functional activity such as learning, memory, and emotional activities can also induce physiological HFOs (Blanco et al., 2011; Buzsáki and Silva, 2012). This characteristic further improves the difficulty to accurately localize EZ on the basis of HFOs in clinical practice.

Many researches explored the methods to precisely identify EZ on the basis of interictal HFOs. They tried to find a detection threshold in order to detect channels with a frequent occurrence of interictal HFOs (Cho et al., 2014; Holler et al., 2015; Gonzalez Otarula et al., 2018; Jiang et al., 2018). Some studies also computed energy of HFOs to delineate EZ (Leung et al., 2015; Brazdil et al., 2017). Moreover, the suppressive effect of rapid eye movement sleep on interictal HFOs might also provide specific markers of epileptogenicity (Sakuraba et al., 2016). But the results of these methods were discordant, and the occurrence rate and energy of HFOs would be influenced by many factors, such as their locations in the brain and the physiological activity.

The relationship between slow wave and interictal HFOs was widely discussed in nearly a decade. Interictal coupling of HFOs and slow oscillations could predict the seizure-onset pattern in mesiotemporal lobe epilepsy (Amiri et al., 2019). A study in 123 patients showed that a stronger amplitude coupling between high-frequency activity (>150 Hz) and the phase of the slow wave (3–4 Hz) in non-resected tissues relative to that in resected tissues was independently associated with a reduced probability of good outcome (Motoi et al., 2018). Physiologic HFO activity increased during the "up state" and decreased during the "down state" of slow oscillations during deep sleep (Le Van Quyen et al., 2010), but epileptic HFOs appeared increasingly during the "down state" or the transition to it (Frauscher et al., 2015). By implementing the coupling to slow waves, the performance to classify epileptic or non-epileptic HFOs was enhanced (von Ellenrieder et al., 2016). However, in the researches, they focused on distinguishing HFOs from seizure onset zone, irritative zone, and normal brain rather than accurate identification of EZ. The precise localization of EZ is key to receive good surgical outcome and bring benefits to patients in clinical practice.

Therefore, we proceed this retrospective study to compare the relationship between HFOs and slow waves during non-rapid eye movement (NREM) sleep from EZ and non-EZ, aiming at developing a new method to identify EZ precisely.

MATERIALS AND METHODS

Patient Population

We selected consecutive patients with pharmacoresistant epilepsy who went through continuous intracerebral electroencephalography (EEG) recordings and EZ removal surgery at the Epilepsy Centre of Beijing Haidian Hospital between January 2013 and December 2015. The inclusion criteria consisted of the following: (1) availability of at least one continuous whole night recording and (2) followed up at least 2 years and received surgical outcome of Engel I. The criteria for exclusion were as follows: (1) there were obvious artifacts in EEG and (2) patients who experienced two or more brain resection surgeries. Patients over 18 and the legal guardian/next of kin for those under 18 gave informed consent in agreement with the Research Ethics Board of Beijing Haidian Hospital. Patients were still under antiepileptic drug therapy at the time of the recording, but doses of the drugs were adjusted according to seizure frequency.

Electrode Placement and Intracranial Electroencephalography Recording

Several kinds of electrodes were implanted in putative epileptogenic areas on the basis of previous non-invasive presurgical evaluation. A combination of cortical strips and grid electrodes (contact diameter 4 mm with a 2.5 mm exposure, spacing between contact centers 10 mm; Beijing Huakehengsheng Healthcare Co., Ltd., Beijing, China) and depth electrodes (1.2 mm diameter, eight contacts 2 mm in length, 10 mm between contacts; Beijing Huakehengsheng Healthcare Co., Ltd., Beijing, China) were implanted. Preimplantation magnetic resonance imaging (MRI) and postimplantation computer tomography (CT) scans were used to locate each contact anatomically along the electrode trajectory.

Data were recorded from the day after electrode implantation. Data for HFO analysis were acquired at 2,000 Hz with a 32- or 256-channel Nicolet recording system (Natus Medical Incorporated, San Carlos, CA, United States). The recording was performed in a monitoring unit under video surveillance and lasted for 2 days.

Delineation of Epileptogenic Zone and Non-epileptogenic Zone

As a part of the clinical routine, the resection range was determined by neurologists and neurosurgeon according to long-term intracranial EEG monitoring. Removed channels were confirmed by comparing the fusion of presurgical MRI and CT and postsurgical MRI. In five subjects whose motor, somatosensory, or visual areas were covered with implanted grid electrodes, functional regions were defined by cortical mapping. Specifically, the functional areas included motor cortex (Patients 2, 5, 7, and 12), somatosensory cortex (Patients 2, 5, 7, and 15), and visual cortex (Patient 15). EZ was defined as the area of cortex that generates seizures, which should be removed to be seizure free. In our study, all the included patients had surgical outcome of Engel I; therefore, we

considered the removed tissue was EZ and the non-resected area was non-EZ.

Data Selection and High-Frequency Oscillation Detection

We chose a segment in slow-wave sleep (N3 stage of sleep) because NREM sleep is the state of vigilance that best identifies the EZ interictally (Klimes et al., 2019), and also in this period there is less muscle activity and more HFOs. The specific method was the same with our previous study (Ren et al., 2018). Then we randomly selected a 5 min segment during the slow-wave sleep period from each patient. All data were selected from interictal periods occurring at least 2 h from a seizure. Data with artifacts and noise, such as sharp transients with enormous amplitudes (higher than normal spikes) or irregular signals, were not selected. The data were transformed to a bipolar montage for further analysis. HFOs were automatically detected by our preliminary algorithm on the basis of maximum distributed peak points (Jiang et al., 2018; Ren et al., 2018). In the detector, the "false" HFOs caused by band-pass filtering of sharp transient events (Gibbs effect) were excluded (Jiang et al., 2018). As ripples and FRs have different generation mechanisms and electrophysiological characteristics (Jiruska et al., 2017), the algorithm was designed to analyze the ripple and FR separately.

Slow-Wave Detection

Slow waves were detected in each intracranial channel separately by an automated detector. In bipolar intracranial channels, the polarity of slow wave depends on the local configuration of the cortex with respect to the electrode contacts. As physiologic activity in the gamma bands decreases during the down state of slow wave (Grenier et al., 2001; Mukovski et al., 2007), we computed the average gamma band (30–80 Hz) power in the positive and negative half-waves of slow wave to determine the polarity of the down state in each intracranial channel (von Ellenrieder et al., 2016). The polarity of the down state in each channel was selected as the one with lower average power in gamma band (von Ellenrieder et al., 2016). If the down state was the positive half-waves of slow wave, then signal of the channel will be turned into the opposite polarity. Thus, the down state of slow wave was the negative half-wave, which was same with scalp EEG.

We used the zero-phase finite impulse response filter (hamming window with 881 points) to band-pass the data from 0.1 to 4 Hz. Then the slow waves were detected according to the criteria that were used previously in scalp or intracranial EEG (Valderrama et al., 2012; von Ellenrieder et al., 2016): (1) a negative wave between two succeeding zero-crossings separated by 0.125–1 s and presenting only one main peak $\leq$80 mV and other negative peaks not exceeding 50% of the main one (in absolute value); (2) a subsequent (or antecedent) positive wave between two succeeding zero-crossings separated by 0.125–1 s; (3) a negative-to-positive (or positive-to-negative) peak-to-peak amplitude $\geq$140 mV. To include only the most prominent half-waves in each channel, we only kept the 25% highest absolute amplitude. Consequently, slow waves were detected as negative half-waves, with their corresponding preceding and following positive half-waves (von Ellenrieder et al., 2016). The slow waves were divided into three parts: preceding positive half-wave, negative half-wave, and following positive half-wave (**Figure 1**).

Association Between High-Frequency Oscillations and Slow Waves

Firstly, we computed the ratio of HFOs superimposed on slow waves in each channel. If HFOs occurred at the following positive half-wave of a slow wave and the preceding positive half-wave of the subsequent slow wave at the same time, they would be eliminated automatically because it was difficult to identify which slow wave did the HFOs superimpose on. Moreover, if two succeeding HFOs occur in the same part of one slow wave, only the feature of the relationship between foregoing HFO and slow wave will be computed to avoid repeatability.

Then these characteristics were explored: (1) the distribution probability of HFOs in the three phases of slow waves; (2) the timing between the onset of each HFO and the peak of the down state of the slow waves; and (3) the relationship between the relative density of HFOs and the amplitude of slow waves. The slow-wave amplitude was calculated as the percentage of the absolute value of the negative peak; and (4) the slopes and spread rates of isolated slow waves that contain HFOs. The slope was defined as the amplitude of the most negative peak divided by the time from the previous zero-crossing to the negative peak. The spread rate referred to the number ratio of channels that showed slow wave-containing HFOs simultaneously to all recording channels.

Statistical Analysis

Data were analyzed using sigmaplot 12.0 (Systat Software, Inc., United States). The non-normal distribution data were compared by Mann–Whitney rank sum test. The composition ratio of HFO distribution in the three phases of slow wave in the two groups was compared by chi-square test. A $P < 0.05$ was considered statistically significant.

RESULTS

Nineteen subjects were included in the study (10 females) (see **Table 1** for demographic and clinical data). The total number of channels was 757, with 420 (55.5%) in EZ and 337 (44.5%) in non-EZ.

High-Frequency Oscillation Detection

A total of 20,238 ripples (12,756 in EZ and 7,482 in non-EZ) and 5,189 FRs (3,146 in EZ and 2,043 in non-EZ) were automatically detected. The median ripple rate in channels recording from the EZ was 3.9 (range 0–39.8) per minute and from the non-EZ 2.2 (range 0–45.4) per minute. In the case of FR, the median was 0.2 (range 0–23.4) per minute and 0 (range 0–37.0) per minute. The rate of both ripples and FRs in EZ were significantly higher than that in non-EZ ($P < 0.001$) (**Figure 2**).

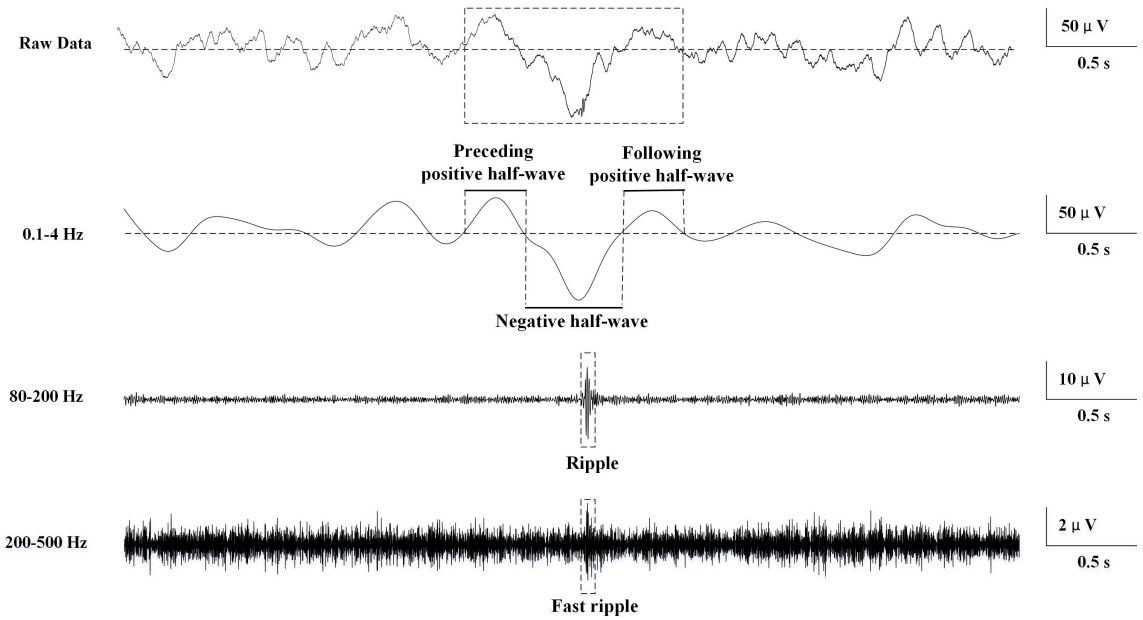

FIGURE 1 | Schematic of automatic slow wave, ripple, and fast ripple (FR) detection. The first row was the raw data. The second row was band-passed from 0.1 to 4 Hz, and slow wave was automatically detected. The three phases of the slow wave were labeled. The third row was band-passed from 80 to 200 Hz, and ripple was automatically detected. The fourth row was band-passed from 200 to 500 Hz, and FR was automatically detected.

Slow-Wave Detection

A total of 20,478 slow waves (12,995 in EZ and 7,483 in non-EZ) were automatically detected. The median rate of detected slow waves in each EZ or non-EZ channel was 6.2 (range 0–18) or 4.4 (range 0–15.4) per minute, respectively. The rate of slow wave in EZ was significantly higher than that in non-EZ ($P < 0.001$).

Association Between High-Frequency Oscillations and Slow Waves

A total of 2,303 and 1,177 ripples were found superimposed on slow wave in EZ and non-EZ, respectively. Among them, 117 (5.1%) in EZ and 74 (6.3%) in non-EZ were excluded because of overlapping on two succeeding slow waves simultaneously; 85 (3.7%) in EZ and 43 (3.7%) in non-EZ were automatically eliminated due to superimposing in the same phase of a slow wave with another ripple. Then the median slow wave-ripple (SW-ripple) rate in channels recording from the EZ was 0.6 (range 0–10) per minute and from the non-EZ 0.2 (range 0–11.4) per minute.

A total of 653 and 308 FRs were found superimposed on slow wave in EZ and non-EZ channels, respectively. Among them, 21 (3.2%) in EZ and 11 (3.6%) in non-EZ were excluded because of overlapping on two succeeding slow waves simultaneously; 56 (8.6%) in EZ and 26 (8.4%) in non-EZ were automatically eliminated due to superimposing in the same phase of a slow wave with another FR. Then the median slow wave-FR (SW-FR) rate in channels recording from the EZ was 0 (range 0–4.4) per minute and from the non-EZ 0 (range 0–6.0) per minute (**Figure 2**).

The number of ripples in the three phases of slow wave were 572, 1106 (52.6%), and 423; and 350, 514 (48.5%), and 196 in EZ and non-EZ, respectively. Ripples in two groups were both likely to superimpose on the negative half-wave of the slow wave, but the composition ratio of ripple distribution in the three phases of slow wave was statistically different between the two groups ($P = 0.003$). The number of FR in the three phases of slow wave was 129, 368 (63.9%), and 79; and 74, 157 (57.9%), and 40 in EZ and non-EZ, respectively. FRs in the two groups were also likely to superimpose on the negative half-wave of the slow wave, and the composition ratio of FR distribution in the three phases of slow wave was not statistically different between the two groups ($P = 0.217$) (**Figure 3**).

The duration from the starting point of ripples to the negative peak of slow wave in EZ was shorter than that in the non-EZ (-174.0 vs. -231.0 ms, $P = 0.008$). As for FR, no statistical difference was found between the two groups ($P = 0.430$). **Figure 4** shows the density of ripples per 50 ms as a function of the time to the peak of the down state of the slow waves.

During the HFOs superimposed on the negative half-wave of slow waves, the relative density of ripples and FRs in EZ and non-EZ was the highest during the nearly same slow-wave amplitude percentile (50–90%) (**Figure 5**).

The slope of slow wave-containing ripples in EZ was steeper than that in the non-EZ (1.7 vs. 1.5 μV/ms, $P < 0.001$). As for FR, the slope of slow wave-containing FR in EZ was also steeper than that in the non-EZ (1.7 vs. 1.4 μV/ms, $P < 0.001$) (**Figure 6**).

The spread ratio of isolated slow wave that contain ripples in EZ was higher than that in the non-EZ (32.3 vs. 30.1%, $P < 0.001$). As for FR, no statistical difference was found between the two groups ($P = 0.788$) (**Figure 6**).

TABLE 1 | The clinical information of included patients.

ID	Gender	Age, years	MRI	Implantation sites	Removed sites
1	Male	16	L HS	L T, L LF, L H, L A	L AT, L partial H, L A
2	Male	33	Abnormal signal in R F	R MFG, R PreG, R PosG, R SFG, R Pos T, R P O	R Pos T, R P O
3	Female	25	Old bleeding foci in L P O	L F T, L T P	L P, L Wernicke zone
4	Female	14	Normal	L SFG, L MFG, L IFG, L M F, L T, L H	L SFG, L MFG, L IFG, L M F
5	Male	12	Abnormal signal in L F, L P cortex	L Lat F, L B F, L T, L I	L Lat F, L B F
6	Female	24	Normal	L M F, L SFG, L PreG, L P, L B F, L Lat F, L F, L M F	L M F, L SFG, L Pos T, L P
7	Male	11	Bilateral HS	R P, R O, R P O	R P, R O
8	Male	35	Normal	R F, R SFG, R B F, R T, RH, R A	R F, R SFG, R B F, R AT, R H, R A
9	Female	42	R HS, bilateral CA	R T, R F P, bilateral H, bilateral A	R AT, R H, R A
10	Male	24	Normal	L F, L T, L A, L H	L F, L AT
11	Female	39	Normal	Bilateral F, bilateral T, bilateral H, bilateral A	L AT, L partial H, L Lat OG
12	Male	21	Normal	Bilateral SFG, bilateral MFG, bilateral IFG, bilateral M F, bilateral B F, bilateral T, bilateral B T	L F, L M F
13	Female	36	OPCA	R L F, R M F, R B F, R T, R P, R H, R A	R Lat F, R M F, R B F
14	Male	16	Atrophy in L H and the whole cortex	Bilateral F, R B F, bilateral T, R I, L OFC, R H, R A	R B F, R I
15	Female	26	Bilateral CA	L F P, L middle T, L Pos T, L P O	L Pos T, L P O
16	Male	20	Encephalomalacia foci in L T P O	L F, L T, L P, L O	L P O
17	Female	8	Normal	R F, R O, R P, R T, R M F, R H	R P, R O
18	Female	27	Normal	L F, L P, L T, L H, L A	L F P, L Pos T
19	Female	13	AC in L T and L LF, abnormal signal in bilateral OHLV	R CS, R P, R P O, R T	R O

L, left; HS, hippocampal sclerosis; T, temporal; LF, lateral fissure; H, hippocampus; A, amygdala; AT, anterior temporal; R, right; F, frontal; MFG, middle frontal gyrus; PreG, precentral gyrus; PosG, postcentral gyrus; SFG, superior frontal gyrus; Pos, posterior; P, parietal; O, occipital; IFG, inferior frontal gyrus; M, mesial; Lat, lateral; B, basis; I, insular; CA, cerebellar atrophy; OG, orbitofrontal gyrus; OPCA, olivo-ponto-cerebellar atrophy; OFC, orbit frontal cortex; AC, arachnoid cyst; OHLV, occipital horn of lateral ventricle; CS, central sulcus.

DISCUSSION

In this research, we compared the different associations between HFOs and the slow waves during sleep in EZ and non-EZ. We found that the rate of HFOs overlapping with slow waves was higher in EZ than that in non-EZ. HFOs tended to occur at negative half-wave of slow wave in both two zones, but ripples in EZ were much closer to the negative peak of slow wave than that in the non-EZ. Slow wave-containing ripples in EZ had a steeper slope and wider distribution ratio than those in the non-EZ. But for slow wave-containing FR, only a steeper slope was identified.

We observed that HFOs in the EZ tended to occur before the peak of the deactivated down state of the slow wave, which was concordant with the previous reports (Frauscher et al., 2015; von Ellenrieder et al., 2016; Song et al., 2017; Samiee et al., 2018). Likewise, we demonstrated the same result in the non-EZ. It is proved that some FRs in non-EZ and EZ might be related by epileptic network (van't Klooster et al., 2017); thus, it is reasonable that they had similar characteristics when they were closed in distance. Also, the irritative zones might not always be resected completely in epilepsy surgery, so the non-EZ probably included not only normal brain regions but also irritative zones. Previous studies found that the coupling of HFOs with the phase of the slow wave in normal brain regions occurred at the transition to the "up" state (Frauscher et al., 2015; von Ellenrieder et al., 2016), but in the irritative zone, it tended to occur more often before the peak of the deactivated or down state of the slow wave (von Ellenrieder et al., 2016). Therefore, in our study, the characteristics of relationship between HFOs and slow wave in non-EZ might be the comprehensive result from irritative and normal brain zones.

Although HFOs occurred more often at negative half-wave of slow wave in both EZ and non-EZ, ripples in EZ were significantly closer to the negative peak of slow wave than that in non-EZ. The actual underlying mechanisms leading to this observation were not clear. Partial evidence suggested that slow-wave oscillations might enhance synaptic excitability and hyper-excitability, which would in turn facilitate the development of pathological hypersynchrony and eventually form epileptiform activity (Schall et al., 2008; Nazer and Dickson, 2009; Samiee et al., 2018).

Moreover, in the EZ, slow wave that contain HFOs had a steeper slope. Previously, the slope was a proxy measure of the rapidity of neural firing synchronization, which reflected synaptic strength (Esser et al., 2007; Riedner et al., 2007). Here,

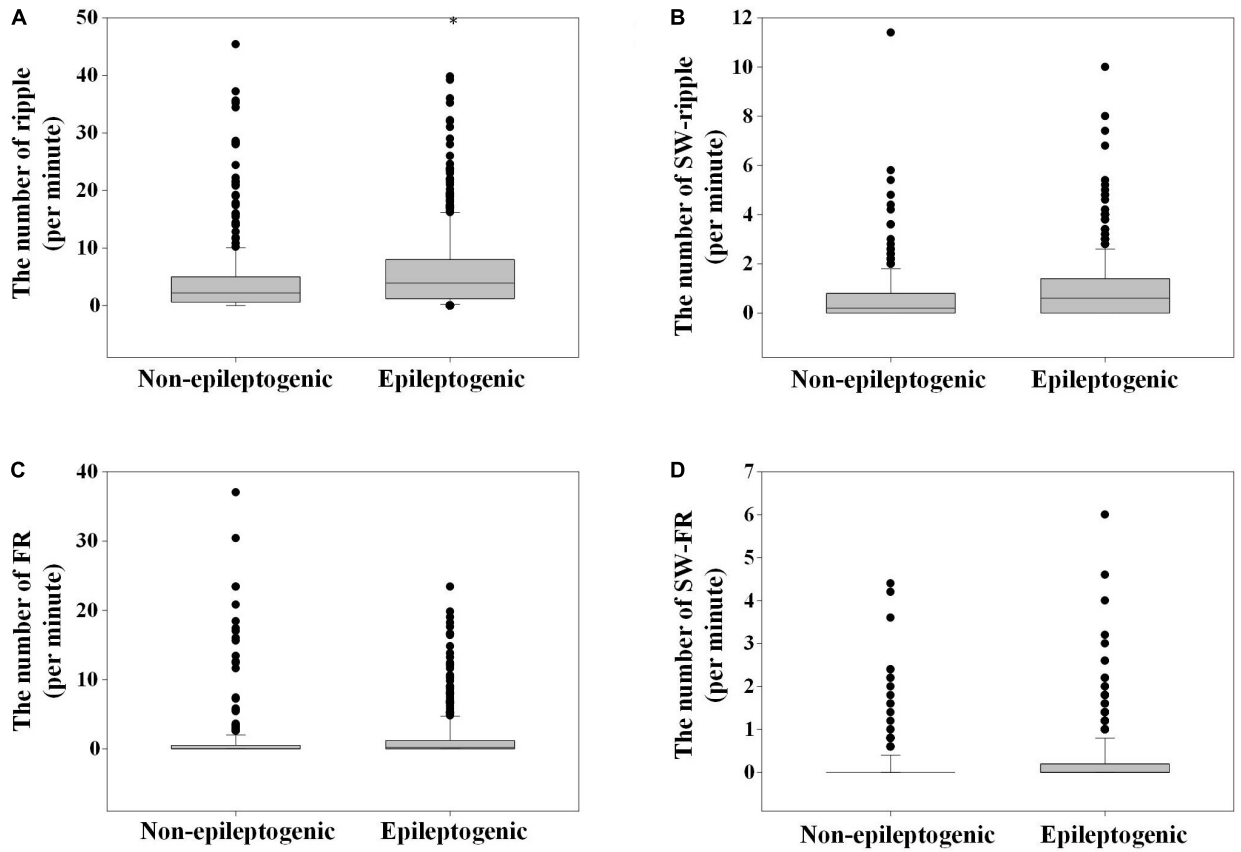

FIGURE 2 | The number of ripples, fast ripple (FR), slow wave (SW)-ripple, and SW-FR in non-epileptogenic and epileptogenic zone (EZ). The rates of ripples **(A)**, SW-ripple **(B)**, FR **(C)**, and SW-FR **(D)** in EZ were significantly higher than those in non-EZ ($P < 0.001$). SW-ripple or SW-FR refers to ripple or FR that superimposed on slow wave.

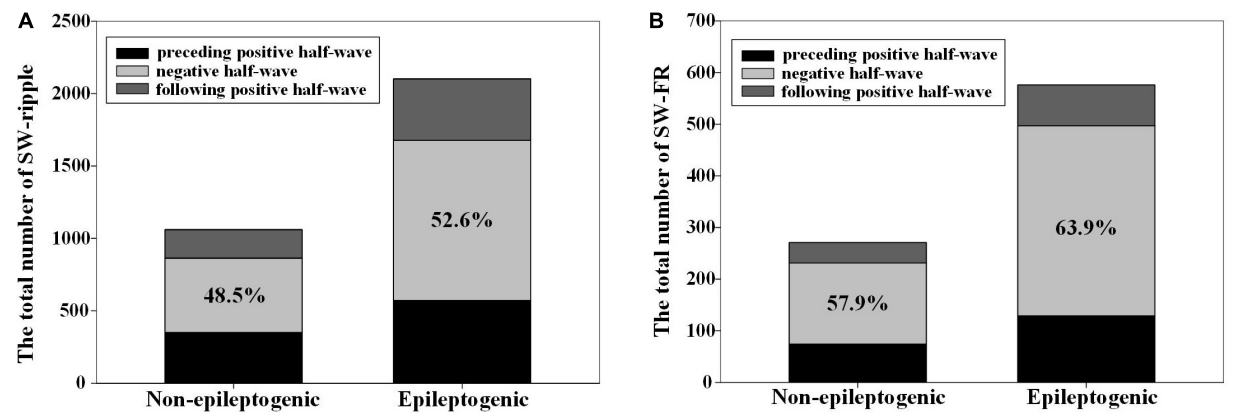

FIGURE 3 | The distribution of high-frequency oscillations (HFOs) in the three different phases of slow wave. **(A)** Ripples in epileptogenic zone (EZ) and non-EZ were both likely to superimpose on the negative half-wave of the slow wave, but the composition ratio of HFO distribution in the three phases of slow wave was statistically different between EZ and non-EZ ($P = 0.003$). **(B)** Fast ripple (FR) in EZ and non-EZ tended to superimpose on the negative half-wave of the slow wave, and the composition ratio of HFO distribution in the three phases of slow wave was not statistically different between EZ and non-EZ ($P = 0.217$). Slow wave (SW)-ripple or SW-FR refers to ripple or FR that superimposed on slow wave.

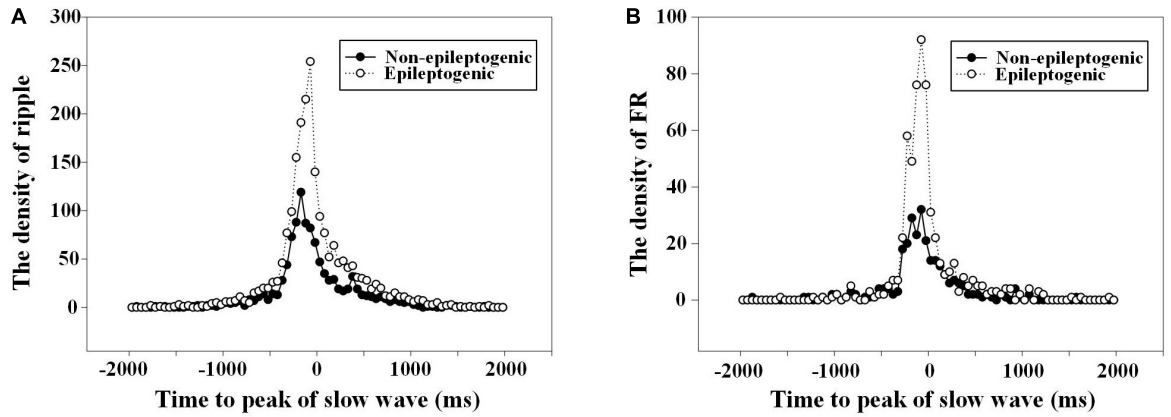

FIGURE 4 | The density of high-frequency oscillations (HFOs) fluctuated with the time to the slow wave peak. **(A)** Density of ripples (80–200 Hz) per 50 ms as a function of the time to the peak (at $t = 0$) of the down state of the slow waves. The duration from the starting point of ripples to the negative peak of slow wave in epileptogenic zone (EZ) was closer than that in the non-EZ (−174.0 vs. −231.0 ms, $P = 0.008$). There was two times' increase in the occurrence of ripples in channels recording from EZ 75 ms before the down state peak of the slow waves. **(B)** Density of fast ripple (FR) (200–500 Hz) per 50 ms as a function of the time to the peak (at $t = 0$) of the down state of the slow waves. No statistical difference was found between FR in EZ and non-EZ (−166.0 vs. −150.5 ms, $P = 0.430$).

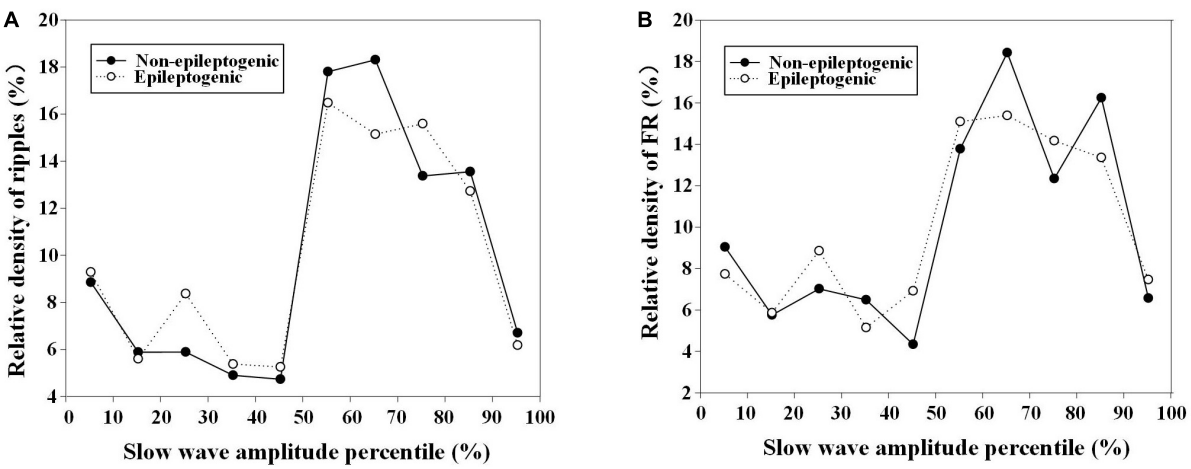

FIGURE 5 | Relationship between relative density of high-frequency oscillations (HFOs) with slow-wave amplitude percentile in epileptogenic and non-epileptogenic zone (non-EZ). **(A)** The relative density of ripples at different slow-wave amplitude percentile. The relative density of ripples in EZ and non-EZ was the highest during 50–80% slow-wave amplitude percentile. **(B)** The relative density of fast ripple (FR) at different slow-wave amplitude percentile. The highest densities were distributed during 50–90%.

we calculated the slope from the preceding crossing zero to the peak of the down state. The rate at which this transition occurred across the population was determined by synaptic activity. The rate at which a population of neurons left the up state was based on the rate at which synaptic activity was removed from the network as neurons one by one entered the down state, which was in turn determined by synaptic strength (Riedner et al., 2007). Hence, it is deducible that the steeper slope of the slow wave in the EZ might indicate a higher synaptic strength, which might facilitate the occurrence of HFOs (Jiruska et al., 2017; Cepeda et al., 2020).

We also concluded that slow wave-containing ripples in EZ had wider distribution ratio than that in the non-EZ. Low-frequency rhythms, such as slow waves, were formed by a large-scale cellular network, while high-frequency rhythms were formed by a small-scale cellular network (von Stein and Sarnthein, 2000). It was demonstrated that large networks of neurons fired in synchrony and produced local-field oscillatory signals in the gamma ripple band that were triggered by slow-wave oscillations (Samiee et al., 2018). Therefore, the widespread slow waves that contain HFOs in the EZ might reflect more vulnerable tissue that could transform into epileptogenic focus.

In our study, some drawbacks existed. At primary, the number of patients was limited. Secondly, we just deduced the EZ according the resection range from patients with good

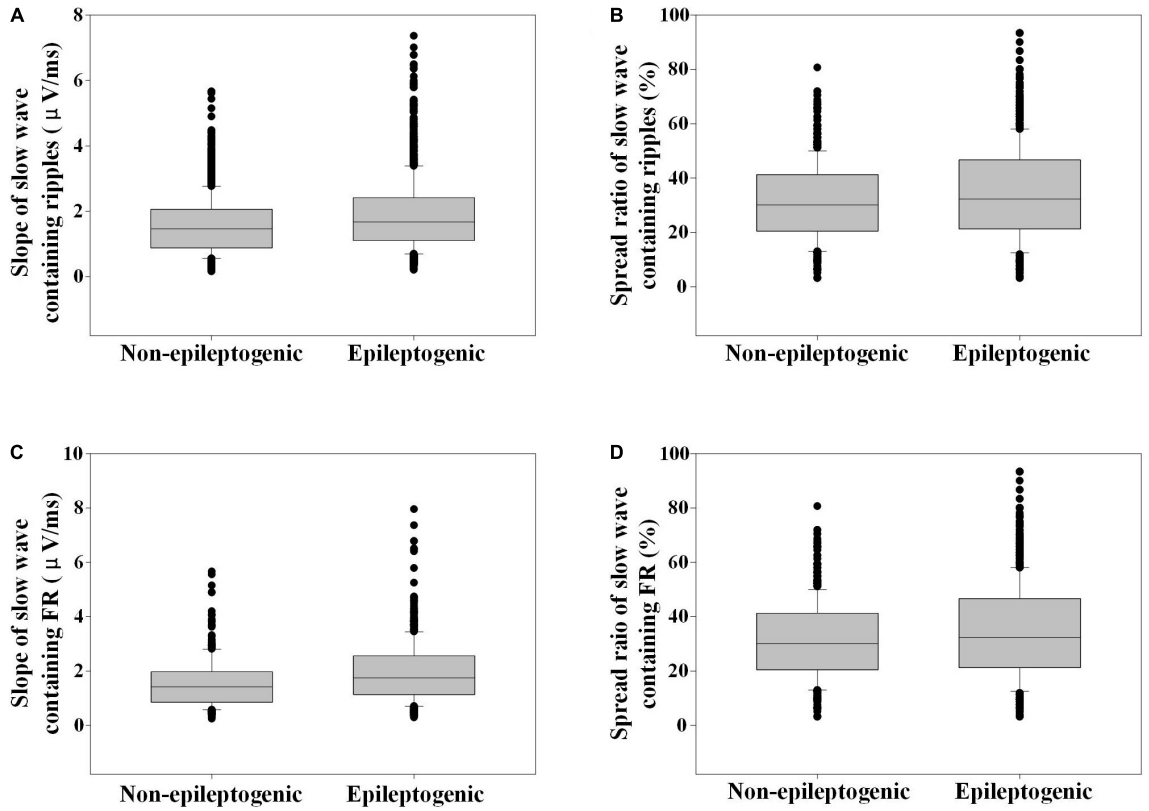

FIGURE 6 | Slope and spread ratio of slow wave-containing high-frequency oscillations (HFOs) in epileptogenic and non-epileptogenic zone (non-EZ). **(A)** The slope of slow wave that contains ripples in EZ was steeper than that in the non-EZ (1.7 vs. 1.5 μV/ms, $P < 0.001$). **(B)** The spread ratio of isolated slow wave that contains ripple in EZ was higher than that in the non-EZ (32.3 vs. 30.1%, $P < 0.001$). **(C)** The slope of slow wave that contains fast ripple (FR) in EZ was steeper than that in the non-EZ (1.7 vs. 1.4 μV/ms, $P < 0.001$). **(D)** The spread ratios of isolated slow wave that contain FR were not statistically different between the two groups (31.0 vs. 28.7%, $P = 0.788$).

surgical outcome, but the realistic size of EZ might be less than the surgery resection range. Thirdly, absolute amplitude was used to detect intracranial slow wave, which needed more discussion.

CONCLUSION

In this study, we explored the association between HFOs and interictal slow wave in refractory focal epilepsy with good surgical outcome. We found that HFOs in EZ and non-EZ had different characteristics: although ripples preferred to occur on the down state of slow waves in both EZ and non-EZ, ripples in EZ tended to be closer to the down-state peak of slow wave than in non-EZ. Besides, slow wave-containing ripples in EZ had a steeper slope and wider distribution ratio than those in the non-EZ. But for slow wave-containing FR, only a steeper slope was observed. These different features between EZ and non-EZ are probably due to the synaptic hyper-excitability or the higher synaptic strength in EZ. Using the different relationship between HFOs and slow wave may be an efficient way to differ HFOs in EZ from non-EZ. More efforts are needed to verify the validity.

DATA AVAILABILITY STATEMENT

The raw data supporting the conclusions of this article will be made available by the authors, without undue reservation, to any qualified researcher.

ETHICS STATEMENT

The studies involving human participants were reviewed and approved by the Research Ethics Board of Beijing Haidian Hospital. Written informed consent to participate in this study was provided by the participants' legal guardian/next of kin. Written informed consent was obtained from the individual(s), and minor(s)' legal guardian/next of kin, for the publication of any potentially identifiable images or data included in this article.

AUTHOR CONTRIBUTIONS

GR and JY analyzed the data. GR wrote a draft of the manuscript. All authors contributed to designing the study and collecting the

data, interpreted the results, reviewed and revised the manuscript, and confirmed its final version.

FUNDING

The study was financially supported by the National Natural Science Foundation of China (81801280 to GR, 61803003 to JY, 81601126 to JR, and 81971202 to XY), Youth Research Fund of Beijing Tiantan Hospital affiliated to Capital Medical University (2017-YQN-01 to GR), Capital Health Research and Development of Special grant (2016-1-2011 and 2020-1-2013 to QW), Beijing-Tianjin-Hebei Cooperative Basic Research Program (H2018206435 to QW), and the National Key R&D Program of China grant (2017YFC1307500 to QW).

ACKNOWLEDGMENTS

We would like to thank Xiaonan Li for the fruitful discussions.

REFERENCES

Amiri, M., Frauscher, B., and Gotman, J. (2019). Interictal coupling of HFOs and slow oscillations predicts the seizure-onset pattern in mesiotemporal lobe epilepsy. *Epilepsia* 6, 1160–1170. doi: 10.1111/epi.15541

Blanco, J. A., Stead, M., Krieger, A., Stacey, W., Maus, D., Marsh, E., et al. (2011). Data mining neocortical high-frequency oscillations in epilepsy and controls. *Brain* 10(Pt. 10), 2948–2959. doi: 10.1093/brain/awr212

Bragin, A., Engel, J. Jr., Wilson, C. L., Fried, I., and Buzsaki, G. (1999). High-frequency oscillations in human brain. *Hippocampus* 2, 137–142. doi: 10.1002/(SICI)1098-106319999:2<137::AID-HIPO5<3.0.CO;2-0

Brazdil, M., Pail, M., Halamek, J., Plesinger, F., Cimbalnik, J., Roman, R., et al. (2017). Very high-frequency oscillations: novel biomarkers of the epileptogenic zone. *Ann. Neurol.* 2, 299–310. doi: 10.1002/ana.25006

Buzsáki, G., and Silva, F. L. (2012). High frequency oscillations in the intact brain. *Prog. Neurobiol.* 3, 241–249. doi: 10.1016/j.pneurobio.2012.02.004

Cepeda, C., Levinson, S., Nariai, H., Yazon, V. W., Tran, C., Barry, J., et al. (2020). Pathological high frequency oscillations associate with increased GABA synaptic activity in pediatric epilepsy surgery patients. *Neurobiol. Dis.* 134:104618. doi: 10.1016/j.nbd.2019.104618

Cho, J. R., Koo, D. L., Joo, E. Y., Seo, D. W., Hong, S. C., Jiruska, P., et al. (2014). Resection of individually identified high-rate high-frequency oscillations region is associated with favorable outcome in neocortical epilepsy. *Epilepsia* 11, 1872–1883. doi: 10.1111/epi.12808

Esser, S. K., Hill, S. L., and Tononi, G. (2007). Sleep homeostasis and cortical synchronization: I. Modeling the effects of synaptic strength on sleep slow waves. *Sleep* 12, 1617–1630. doi: 10.1093/sleep/30.12.1617

Frauscher, B. (2020). Localizing the epileptogenic zone. *Curr. Opin. Neurol.* 2, 198–206. doi: 10.1097/WCO.0000000000000790

Frauscher, B., von Ellenrieder, N., Ferrari-Marinho, T., Avoli, M., Dubeau, F., and Gotman, J. (2015). Facilitation of epileptic activity during sleep is mediated by high amplitude slow waves. *Brain* 138(Pt. 6), 1629–1641. doi: 10.1093/brain/awv073

Gonzalez Otarula, K. A., Khoo, H. M., von Ellenrieder, N., Hall, J. A., Dubeau, F., and Gotman, J. (2018). Spike-related haemodynamic responses overlap with high frequency oscillations in patients with focal epilepsy. *Brain* 141, 731–743. doi: 10.1093/brain/awx383

Grenier, F., Timofeev, I., and Steriade, M. (2001). Focal synchronization of ripples (80-200 Hz) in neocortex and their neuronal correlates. *J. Neurophysiol.* 4, 1884–1898. doi: 10.1152/jn.2001.86.4.1884

Holler, Y., Kutil, R., Klaffenbock, L., Thomschewski, A., Holler, P. M., Bathke, A. C., et al. (2015). High-frequency oscillations in epilepsy and surgical outcome. A meta-analysis. *Front. Hum. Neurosci.* 9:574. doi: 10.3389/fnhum.2015.00574

Jacobs, J., Zijlmans, M., Zelmann, R., Chatillon, C. E., Hall, J., Olivier, A., et al. (2010). High-frequency electroencephalographic oscillations correlate with outcome of epilepsy surgery. *Ann. Neurol.* 2, 209–220. doi: 10.1002/ana.21847

Jiang, C., Li, X., Yan, J., Yu, T., Wang, X., Ren, Z., et al. (2018). Determining the quantitative threshold of high-frequency oscillation distribution to delineate the epileptogenic zone by automated detection. *Front. Neurol.* 9:889. doi: 10.3389/fneur.2018.00889

Jirsch, J. D., Urrestarazu, E., LeVan, P., Olivier, A., Dubeau, F., and Gotman, J. (2006). High-frequency oscillations during human focal seizures. *Brain* 129(Pt 6), 1593–1608. doi: 10.1093/brain/awl085

Jiruska, P., Alvarado-Rojas, C., Schevon, C. A., Staba, R., Stacey, W., Wendling, F., et al. (2017). Update on the mechanisms and roles of high-frequency oscillations in seizures and epileptic disorders. *Epilepsia* 8, 1330–1339. doi: 10.1111/epi.13830

Klimes, P., Cimbalnik, J., Brazdil, M., Hall, J., Dubeau, F., Gotman, J., et al. (2019). NREM sleep is the state of vigilance that best identifies the epileptogenic zone in the interictal electroencephalogram. *Epilepsia* 60, 2404–2415. doi: 10.1111/epi.16377

Le Van Quyen, M., Staba, R., Bragin, A., Dickson, C., Valderrama, M., Fried, I., et al. (2010). Large-scale microelectrode recordings of high-frequency gamma oscillations in human cortex during sleep. *J. Neurosci.* 23, 7770–7782. doi: 10.1523/JNEUROSCI.5049-09.2010

Leung, H., Zhu, C. X., Chan, D. T., Poon, W. S., Shi, L., Mok, V. C., et al. (2015). Ictal high-frequency oscillations and hyperexcitability in refractory epilepsy. *Clin. Neurophysiol.* 11, 2049–2057. doi: 10.1016/j.clinph.2015.01.009

Motoi, H., Miyakoshi, M., Abel, T. J., Jeong, J. W., Nakai, Y., Sugiura, A., et al. (2018). Phase-amplitude coupling between interictal high-frequency activity and slow waves in epilepsy surgery. *Epilepsia* 59, 1954–1965. doi: 10.1111/epi.14544

Mukovski, M., Chauvette, S., Timofeev, I., and Volgushev, M. (2007). Detection of active and silent states in neocortical neurons from the field potential signal during slow-wave sleep. *Cereb. Cortex* 2, 400–414. doi: 10.1093/cercor/bhj157

Nazer, F., and Dickson, C. T. (2009). Slow oscillation state facilitates epileptiform events in the hippocampus. *J. Neurophysiol.* 3, 1880–1889. doi: 10.1152/jn.90795.2008

Pail, M., Rehulka, P., Cimbalnik, J., Dolezalova, I., Chrastina, J., and Brazdil, M. (2017). Frequency-independent characteristics of high-frequency oscillations in epileptic and non-epileptic regions. *Clin. Neurophysiol.* 128, 106–114. doi: 10.1016/j.clinph.2016.10.011

Ren, G. P., Yan, J. Q., Yu, Z. X., Wang, D., Li, X. N., Mei, S. S., et al. (2018). Automated detector of high frequency oscillations in epilepsy based on maximum distributed peak points. *Int. J. Neural. Syst.* 28:1750029. doi: 10.1142/S0129065717500290

Riedner, B. A., Vyazovskiy, V. V., Huber, R., Massimini, M., Esser, S., Murphy, M., et al. (2007). Sleep homeostasis and cortical synchronization: III. A high-density EEG study of sleep slow waves in humans. *Sleep* 12, 1643–1657. doi: 10.1093/sleep/30.12.1643

Sakuraba, R., Iwasaki, M., Okumura, E., Jin, K., Kakisaka, Y., Kato, K., et al. (2016). High frequency oscillations are less frequent but more specific to epileptogenicity during rapid eye movement sleep. *Clin. Neurophysiol.* 1, 179–186. doi: 10.1016/j.clinph.2015.05.019

Samiee, S., Levesque, M., Avoli, M., and Baillet, S. (2018). Phase-amplitude coupling and epileptogenesis in an animal model of mesial temporal lobe epilepsy. *Neurobiol. Dis.* 114, 111–119. doi: 10.1016/j.nbd.2018.02.008

Schall, K. P., Kerber, J., and Dickson, C. T. (2008). Rhythmic constraints on hippocampal processing: state and phase-related fluctuations of synaptic

excitability during theta and the slow oscillation. *J. Neurophysiol.* 2, 888–899. doi: 10.1152/jn.00915.2007

Song, I., Orosz, I., Chervoneva, I., Waldman, Z. J., Fried, I., Wu, C., et al. (2017). Bimodal coupling of ripples and slower oscillations during sleep in patients with focal epilepsy. *Epilepsia* 11, 1972–1984. doi: 10.1111/epi.13912

Thomschewski, A., Hincapie, A. S., and Frauscher, B. (2019). Localization of the epileptogenic zone using high frequency oscillations. *Front. Neurol.* 10:94. doi: 10.3389/fneur.2019.00094

Valderrama, M., Crepon, B., Botella-Soler, V., Martinerie, J., Hasboun, D., Alvarado-Rojas, C., et al. (2012). Human gamma oscillations during slow wave sleep. *PLoS One* 4:e33477. doi: 10.1371/journal.pone.0033477

van't Klooster, M. A., van Klink, N. E. C., Zweiphenning, W., Leijten, F. S. S., Zelmann, R., Ferrier, C. H., et al. (2017). Tailoring epilepsy surgery with fast ripples in the intraoperative electrocorticogram. *Ann. Neurol.* 5, 664–676. doi: 10.1002/ana.24928

von Ellenrieder, N., Frauscher, B., Dubeau, F., and Gotman, J. (2016). Interaction with slow waves during sleep improves discrimination of physiologic and pathologic high-frequency oscillations (80-500 Hz). *Epilepsia* 6, 869–878. doi: 10.1111/epi.13380

von Stein, A., and Sarnthein, J. (2000). Different frequencies for different scales of cortical integration: from local gamma to long range alpha/theta synchronization. *Int. J. Psychophysiol.* 3, 301–313. doi: 10.1016/s0167-8760(00)00172-0

Conflict of Interest: The authors declare that the research was conducted in the absence of any commercial or financial relationships that could be construed as a potential conflict of interest.

frontiers in Human Neuroscience

ORIGINAL RESEARCH
published: 23 December 2020
doi: 10.3389/fnhum.2020.615744

Increased Phase Cone Turnover in 80–250 Hz Bands Occurs in the Epileptogenic Zone During Interictal Periods

Ceon Ramon[1,2]* *and Mark D. Holmes*[2]

[1]Department of Electrical & Computer Engineering, University of Washington, Seattle, WA, United States, [2]Regional Epilepsy Center, Harborview Medical Center, University of Washington, Seattle, WA, United States

OPEN ACCESS

Edited by:
Jing Xiang,
Cincinnati Children's Hospital Medical Center, United States

Reviewed by:
Douglas Rose,
Cincinnati Children's Hospital Medical Center, United States
Xiaoqian Yu,
Cincinnati Children's Hospital Medical Center, United States

***Correspondence:**
Ceon Ramon
ceon@uw.edu

Some preliminary results were presented as a conference poster at the 68th Annual Meeting of the American Epilepsy Society, 05–09 December 2014, Seattle, WA, United States

Specialty section:
This article was submitted to Brain Imaging and Stimulation, a section of the journal Frontiers in Human Neuroscience

Received: 09 October 2020
Accepted: 26 November 2020
Published: 23 December 2020

Citation:
Ramon C and Holmes MD (2020) Increased Phase Cone Turnover in 80–250 Hz Bands Occurs in the Epileptogenic Zone During Interictal Periods. Front. Hum. Neurosci. 14:615744. doi: 10.3389/fnhum.2020.615744

We found that phase cone clustering patterns in EEG ripple bands demonstrate an increased turnover rate in epileptogenic zones compared to adjacent regions. We employed 256 channel EEG data collected in four adult subjects with refractory epilepsy. The analysis was performed in the 80–150 and 150–250 Hz ranges. Ictal onsets were documented with intracranial EEG recordings. Interictal scalp recordings, free of epileptiform patterns, of 240-s duration, were selected for analysis for each subject. The data was filtered, and the instantaneous phase was extracted after the Hilbert transformation. Spatiotemporal contour plots of the unwrapped instantaneous phase with 1.0 ms intervals were constructed using a montage layout of the 256 electrode positions. Stable phase cone patterns were selected based on criteria that the sign of spatial gradient did not change for a minimum of three consecutive time samples and the frame velocity was consistent with known propagation velocities of cortical axons. These plots exhibited increased dynamical formation and dissolution of phase cones in the ictal onset zones, compared to surrounding cortical regions, in all four patients. We believe that these findings represent markers of abnormally increased cortical excitability. They are potential tools that may assist in localizing the epileptogenic zone.

Keywords: EEG ripple, EEG phase cones, epilepsy and phase cones, high-frequency brain signals, cortical phase transitions, phase clusters

INTRODUCTION

Cortical dynamics play an important role to study the behavior of the brain under normal and epileptic conditions. Recently we have shown the oscillatory patterns of phase cone formations near the epileptic spikes (Ramon et al., 2018). Similarly, it is also a possibility that these phase cone patterns might also be higher in epileptogenic areas during interictal periods. This is what we have investigated in this report and found to be true for the high-frequency ripple bands of 80–150 and 150–250 Hz. These findings also complement our earlier results that the phase synchronization index in the low gamma (30–50 Hz) band during interictal periods is higher in the epileptogenic zones.

The phase jumps and related phase cone structures need some introduction. These phase jumps also called phase slips (Pikovsky et al., 2001), arise due to the state transitions of the coordinated activity of cortical neurons in a local neighborhood at mesoscopic (∼0.5–1.0 mm) scales and can be utilized to study the dynamical behavior of the cortex under different cognitive conditions (Freeman and Barrie, 2000; Freeman and Rogers, 2002). The electrical activity of the cerebral cortex, in general, is in a dynamic state of criticality (Beggs and Timme, 2012), and the slightest external input, e.g., visual stimuli, or an internal input, e.g., a thought, could induce a state transition which will give rise to a sudden phase jump. This critical behavior of the cerebral cortex is very similar to the triple point of water at the boundary of solid, liquid, and gas phases. Another example will be the sandpile model of self-organized criticality (Bak et al., 1987) in which one keeps adding grains of sand to a sandpile till it collapses. A very simple example will be a pot of boiling water. In the beginning, there will be the formation of small bubbles at a few places at the bottom of the pot which begin to rise toward the top surface of the water. As temperature rises, few more streams of bubbles rise to the surface and one begins to see the spatial formation of a group of bubbles on the surface of the water. This continues till the whole pot of water begins to boil. The spatiotemporal formation of phase cones on the cortical surface is very similar. In the beginning, few isolated phase cones appear on the cortical surface and as more neurons begin to go through phase transitions, there will be the appearance of more phase cones. Some of these phase cones will be isolated and grow in size while others will subside. Also, some phase cones will be stable and will begin to expand slowly in size on the cortical surface (Freeman, 2008). This is a simile of cortical phase cones to the bubbles in a pot of boiling water.

These concepts of criticality have been applied to study the nonlinear brain dynamics (Freeman and Vitiello, 2006, 2010; Freeman, 2008), the cinematic behavior of cortical phase transitions (Kozma and Freeman, 2017), and the behavior of epileptic spikes (Ramon et al., 2018). Thus, phase jumps play an important role to study brain dynamics from the EEG data. These state transitions are also often called phase transitions, cortical phase transitions, or EEG phase transitions in the neuroscience and EEG literature.

These phase transition-related activities show up as small perturbations, i.e., glitches in the EEG data. On the application of Hilbert transform to the EEG data, one gets a sawtooth pattern of the instantaneous phase that can be unwrapped to give an almost linearly increasing phase with respect to time that will have small slow variations. The linear or nonlinear trends in the unwrapped phase can be removed by differencing or taking a derivative (d/dt) of the time-series of the unwrapped phase. The phase jump will then show up as a sharp peak or valley whenever there is a slight perturbation in the EEG trace, particularly near the zero crossing line. A peak will represent the growing coordination of firing of neurons in the local neighborhood while a valley will represent the loss of coordination between nearby neurons (Freeman, 2003).

These phase jumps and related spatial phase cones were first observed in the ECoG data (8 × 8 grid, 0.79-mm interelectrode distance) of rabbits (Freeman and Barrie, 2000; Freeman and Rogers, 2002; Freeman, 2003), then in the ECoG data (1 × 1 cm microgrid array with 64 electrodes, 8 × 8 grid, 1.25 mm separation) placed on the right inferior temporal gyrus of a human subject (Freeman et al., 2006a,b), and more recently in 64 channel scalp EEG (Ruiz et al., 2010) and in the high density, 256 channel, scalp EEG data of human subjects (Ramon and Holmes, 2013a, 2015; Ramon et al., 2013, 2018). In spatiotemporal frames, one can see the amplitude and phase-modulated waves in the theta (3–7 Hz) and alpha (7–12 Hz) bands with carrier frequencies in the beta (12–30 Hz) and gamma (30–80 Hz) bands (Freeman, 2004; Myers et al., 2014; Kozma and Freeman, 2017). Aperiodic phase resetting at alpha-theta rates in the scalp EEG of human subjects has also been observed (Freeman et al., 2003). This scalp EEG data was collected with a curvilinear array of 64 electrodes, 3 mm apart, extending 18.9 cm, and placed on the forehead across the midline just below the frontal hairline (Freeman et al., 2003). A common theme in these studies has been to search for spatiotemporal behavior of phase cone structures in the traditional EEG (theta, alpha, beta, and gamma) bands during cognitive tasks, near to the epileptic spikes and during interictal periods. The oscillatory patterns of the phase cone activity near to the epileptic spikes in the low gamma band, 30–50 Hz, and in the ripple band of 80–150 Hz have been examined earlier by us (Ramon et al., 2018). However, no detailed study in the ripple bands (80–150 and 150–250 Hz) during interictal periods has been performed before except reporting of some preliminary results in conference abstracts (Holmes and Ramon, 2014; Holmes et al., 2015). Our newer results are reported here and show that the phase cone activity in the ripple bands during interictal periods is higher as compared to the nearby areas and it could become a complementary noninvasive tool to localize epileptogenic zones from interictal EEG data for presurgical planning purposes.

MATERIALS AND METHODS

Subjects Data

Data sets of four subjects were used for this study. These subjects were all patients at the Harborview Medical Center, the University of Washington for presurgical epilepsy monitoring, and later on, three subjects went through invasive subdural grid and strip electrode recordings. All data sets were collected with the approved Human Subjects Guidelines at the University of Washington. Written permission was obtained from each subject to use these data sets for research purposes. Before invasive recordings, during presurgical evaluations, high-density 256-channel scalp EEG data, also called hdEEG, were collected with an EEG system developed by Electrical Geodesics, Incorporated (EGI), Eugene, OR, USA (now Magstim EGI[1]). For an adult head, from the center of one electrode to the other, the interelectrode separation is approximately 2.0 cm (Tucker, 1993). The data were collected with a sampling rate of 1.0 kHz, i.e., the time difference between two consecutive samples was 1.0 ms. The hdEEG data of each subject during sleep was collected between

[1] www.egi.com

2 and 4 h or so. For all four subjects, in the waking state, there was a symmetric 9–10 Hz posterior alpha rhythm that attenuates symmetrically with eye-opening. A central mu rhythm was seen on either side from time to time. Drowsiness was characterized by waxing and waning of the alpha rhythm, slow lateral eye movements, and intermittent generalized theta activity. Stage II sleep was characterized by symmetric V-waves, K-complexes, sleep spindles, and positive occipital sharp transients of sleep. Interictal epileptiform abnormalities (spike and sharp waves) were observed, mainly during drowsiness and stage II sleep. There were no clinical or electrographic seizures. The interictal data for analysis was selected during the waking state and/or during the drowsiness which was free from Stage II sleep-related spindles et cetera.

Interictal invasive subdural ECoG were also collected for three of the four subjects later on with 8 × 8 grid electrodes and strip electrodes to localize the seizure areas. The electrodes on the grid or strips had an exposed surface area defined by 2.3 mm diameter and with center-to-center, inter-electrode separation of 1.0 cm (Johnson et al., 2012). The epileptic sites were localized from seizure activity in ECoG and/or in hdEEG data sets.

Subject #1 was an adult 35 years old female who was a candidate for surgery. The epileptic spikes and seizures were observed over left central-parietal areas, in the vicinity of the somatosensory cortex. Subject #2 was a 20-year-old male with drug-resistant focal epilepsy with complex left partial midline seizures and was a candidate for surgery. Subject #3 had epileptic spikes and seizure activity over midline/anterior frontal regions, with shifting hemispheric preponderance. The activity area was mapped with hdEEG and subdural electrocorticograms (ECoG) recordings. He was a 26-year-old male and was a candidate for surgery. Subject #4 was a 26-year-old female who had seizure activity in left frontal-temporal and inferior midline areas as observed in hdEEG recordings. She declined to go for surgery. All data sets were de-identified and then used for analysis.

Data Analysis

Interictal scalp hdEEG recordings, free of epileptiform patterns, of 240-s duration, were selected for analysis for each subject. All data sets were at least half an hour away from any epileptiform activity. The data were filtered in broadband of 70–300 Hz with an equiripple filter. The eye-blink and muscle artifacts were removed by use of principal component analysis (PCA) techniques by use of EEGLAB software. The data was then filtered in the appropriate EEG ripple band of 80–150 Hz or 150–250 Hz and Hilbert transform was applied to extract the instantaneous phase and then it was unwrapped which gives almost a linearly increasing time series of the phase.

The equiripple filter was designed based on the Parks-McClellan algorithm (McClellan and Parks, 2005) and was implemented in a MATLAB environment. It is an equiripple linear phase FIR (finite impulse response) filter. The ripples in the passband and the stopbands are of equal height which can be specified while designing the filter. Our bandpass filters were designed with 0 ± 0.25 dB gain in the passband and −60 dB gain (or loss one could say) in the stopband. The transition bands were 1.0 Hz. As an example, the 80–150 Hz passband filter had the following design parameters: sampling frequency, Fs = 1 kHz, F_{stop1} = 79 Hz, F_{pass1} = 80 Hz, F_{pass2} = 150 Hz, F_{stop2} = 151 Hz, passband gain = 0.0 dB, ripple = 0.5 dB, stopband gain = −60 dB. The filter order was 2201. Similarly, other filters were designed by use of the Filter Designer toolbox in MATLAB. The EEG data were filtered with the "filtfilt" function in MATLAB which does not introduce any phase distortions in the filtered data by filtering in both the forward and reverse directions.

The Hilbert transform is a very common technique to extract the analytic amplitude and phase from the EEG data (Barlow, 1993; Freeman et al., 2003; Freeman, 2007; Myers and Padmanabha, 2017; Mortezapouraghdam et al., 2018). With the Hilbert transform, a $\pm\pi$ phase shift is introduced at each sinusoidal peaks/valleys and also wherever there is a slight perturbation in the EEG trace. The instantaneous phase, also often called the analytic phase in the EEG literature, comes out as a sawtooth pattern after taking the Hilbert to transform which after unwrapping gives a linearly increasing phase with slight glitches corresponding to the perturbations in the EEG trace. The unwrapping was done by use of the "unwrap" command in MATLAB. It adds 2π at every reset point in the sawtooth pattern of the instantaneous phase (Mortezapouraghdam et al., 2018). More details about the algorithm and the MATLAB script are described in the documentation for the "Unwrap" in the DSP Systems Toolbox, and are also described in the literature (Karam and Oppenheim, 2007).

In our analysis, the linear trend in the unwrapped phase was removed by taking the first-order derivative (d/dt) of the unwrapped phase. From this, the instantaneous phase-frequency was computed. An example of these steps is given in **Figure 1**.

The top plot shows the EEG in 80–150 Hz band at one of the electrodes in the left central midline area. It has high-frequency spindles which are very common (Mooij et al., 2017; Boran et al., 2019, 2020). The second plot from the top is the instantaneous phase after taking the Hilbert transform of the EEG data and the third plot from the top is the unwrapped phase. The derivative of the unwrapped phase was converted into the instantaneous frequency in cycles/s (or Hz) by dividing by 2π, which is given in the bottom plot which has several peaks related to the cortical phase transitions. Some peaks are sharp which will form transient spatiotemporal phase cones and will disappear quickly. Some peaks are slightly wider as compared with sharp peaks and will tend to form stable spatiotemporal phase cones which could last for several digitization points, e.g., 2–5 ms, for the data collected at 1 kHz. In general, it is very common to look for stable phase cone patterns for three consecutive digitization steps (Ramon and Holmes, 2013a; Ramon et al., 2013, 2018; Ruiz et al., 2010).

These phase jumps were extracted for all 256 channels over the 240-s long data set. Out of which stable phase cone structures were extracted with ms resolution. These procedures have been described earlier by us (Ramon et al., 2018) and also by others (Ruiz et al., 2010; Freeman, 2015). A summary is given here.

Several criteria were applied to select stable phase cone patterns. These included: (1) phase-frequency was within the temporal band, e.g., 80–150 Hz or 150–250 Hz; (2) sign of spatial gradient and maximum or the minimum did not change

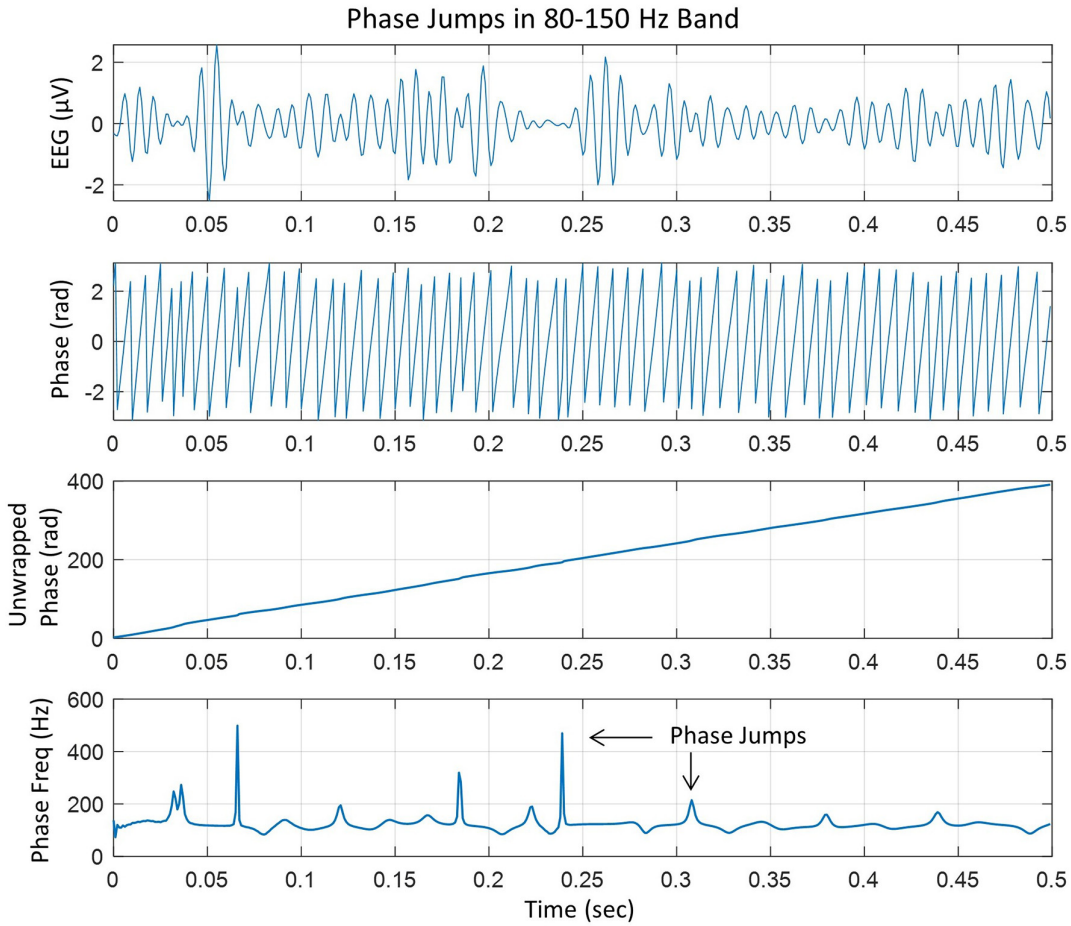

FIGURE 1 | (Top) EEG trace filtered in the 80–150 Hz ripple band, (second plot from the top) phase in radians extracted after taking Hilbert transform of the EEG trace, (third plot from the top) unwrapped phase in radians which is almost linear with slight variations, and (bottom plot), taking the derivative of the unwrapped phase and dividing by 2π to get the instantaneous phase-frequency in cycles/s or Hz. The peaks are phase jumps that appear whenever there is a slight perturbation, particularly near the zero crossing line in the EEG trace.

for at least three consecutive time samples; and (3) the frame velocity should be within the range of conduction velocities of cortical axons, 1–10 m/s (Swadlow, 1994; Swadlow and Waxman, 2012; Ramon et al., 2018). The rate of change in phase with distance (rad/mm) was computed from the spatial location of the electrodes on the scalp. An idealized layout of seven electrodes on the scalp surface is given in **Figure 2**. It shows one central electrode and six nearby electrodes. The interelectrode separation is about 2 cm which gives about 4 cm separation between diametrically opposite electrodes. An idealized representation of a phase cone on a group of six electrodes is also shown. The diameter of the phase cone was approximately equal to 4 cm or less. This choice was made to look for the local formation of stable phase cones which do not expand to the whole cortical surface of about 20 cm diameter for an adult head. This gives a finer spatial resolution to localize the epileptogenic sites.

Based on these criteria, stable clusters of frames in each second long EEG data were computed and an averaged rate of phase cone clusters over 240 s was computed. Color intensity plots of an averaged rate of phase clusters were constructed using a montage of the layout of 256 electrode positions displayed as if one was looking on top of the subject's head. In all the spatial plots in the "Results" section, the nose is on the top, the back of the neck is at the bottom, the left of the subject is on the left side of the plot and the right side of the subject is on the right side of the plot.

Surrogate Data Analysis

Surrogate data testing was performed to make sure that our results are real and are not due to chance occurrences. Procedures for performing this analysis are described elsewhere (Prichard, 1994; Kugiumtzis, 2002; Lancaster et al., 2018). The main points are that the signal processing steps, including filtering differentiation, etc., should be kept the same for the real and the surrogate data. Otherwise, comparative analysis between the real and the surrogate data could be biased. The most simple procedure is to generate random data from a subset

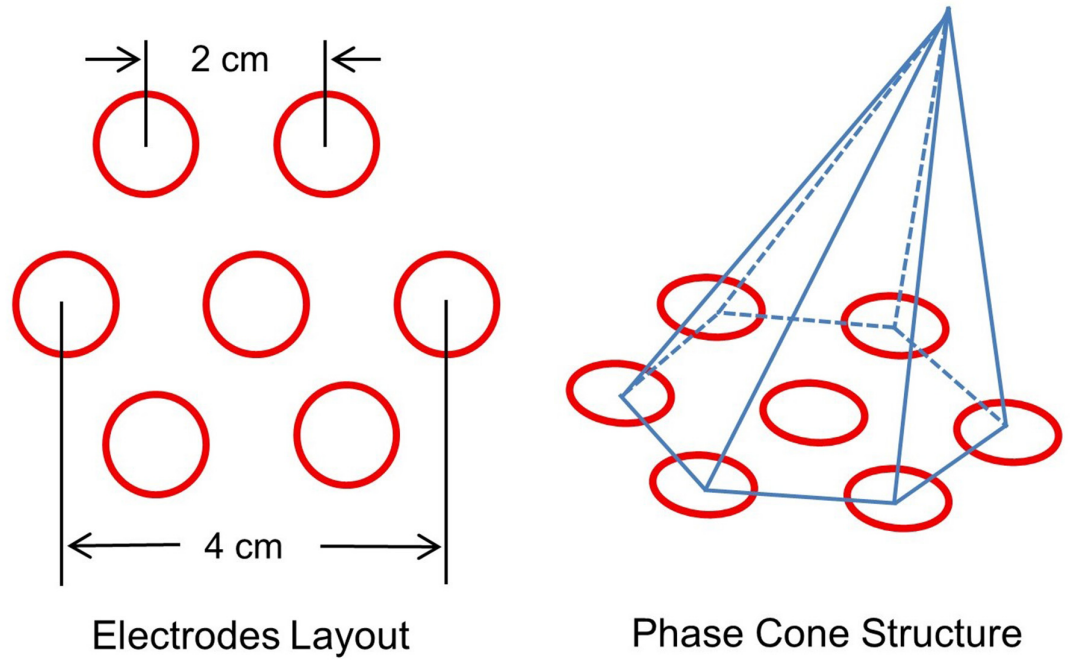

FIGURE 2 | (Left) Layout of a center electrode and six nearby electrodes, and (right) a schematic representation of the phase cone which arises due to the coordinated activity of cortical neurons at mesoscopic scales. The interelectrode separation is 2.0 cm.

of real data and perform the same analysis on both data sets. If the results are significantly different then the phenomena or process under investigation is genuine and not a chance occurrence. For our work, the surrogate data was generated by randomly shuffling the real EEG data. A 240 s long filtered 256 channel EEG data, as described above, from one of the subjects was converted into a vector, randomly shuffled using the "randperm" command in MATLAB, and then rearranged as 256 channel surrogate EEG data. This data was then used to compute the rate of formation of stable phase cones (counts/s) over 240 s interictal period. The maximum rate of the formation of stable phase cones on all electrodes was extracted. This process was repeated for 100 trials. The averaged value of the maximum rate of stable phase cones over 100 trials was: 2.31 $\pm$ 0.98 (n = 100) counts/s for the ripple band of 80–150 Hz. This process was repeated for the fast ripple band of 150–250 Hz. The averaged value of the maximum rate of stable phase cones over 100 trials was: 12.12 $\pm$ 3.15 (n = 100) counts/s. These values ($<$ = 12.12 counts/s) for the randomly shuffled EEG data are much lower as compared with the actual EEG data (50–310 counts/s) shown in the figures in the "Results" section. Thus, our results are genuine, above the random noise, and are due to neurophysiological processes in the brain.

RESULTS

For subject #1, the stable phase cone clusters are given in **Figure 3**. The left two plots are for the stable phase cone patterns for the 80–150 and 150–250 Hz bands, respectively. The right plot is the cortical surface with subdural grid and strip electrodes for ECoG recordings. The red ellipse in the left central-parietal areas is the main area where the majority of the seizures and epileptogenic activities, such as spikes were observed intermittently for 5 days. The hot spots of the stable phase cone clusters in the 80–150 Hz band (left plot in **Figure 3**) are enclosed in the red circle depicting the possible seizure area. The maximum value of 158 counts/s is at the x, y coordinate location of (34, 42). The horizontal (x) and vertical (y) axes are in arbitrary length units based on the normalized location of 256 electrode positions on a flat surface. The stable phase cone activity is spread in a wide area. This possibly could be related to the epileptogenic cortical network activity during interictal periods which possibly could be spread on an interconnected wide area cortical networks. However, the hot spots of maximum activity are in the epileptogenic zone which was identified from ECoG recordings. Compared to this, the stable phase cone clustering activity in the fast ripple band of 150–250 Hz is confined to a single spot (183 counts/s) approximately at the same coordinate location of (37, 42). Refer to the middle plot. This plot does not show a widespread network activity as seen in the 80–150 Hz band (left plot). There is another bright lengthy spot in the right front central (x = 70–100, y = 70–105) area. This possibly could also be due to the large area cortical networks involved in the cortical phase transitions. This is explored in detail in the "Discussion" section.

For subject #2, the stable phase cone cluster activity is given in **Figure 4**. During ECoG recordings, the seizure activity

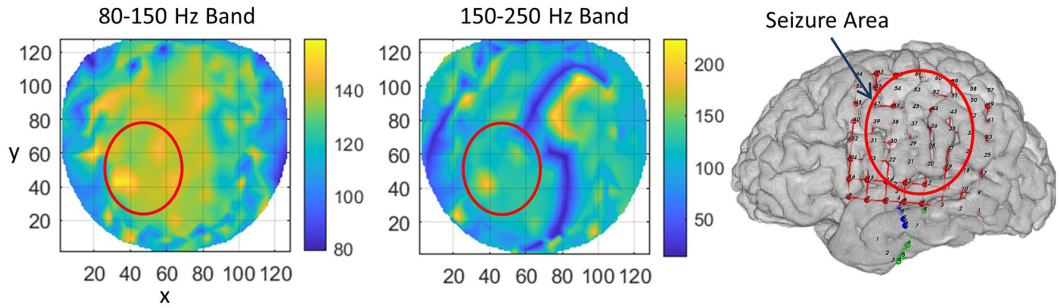

FIGURE 3 | The rate of formation (counts/s) of stable phase cone clusters averaged over a 240-s interictal period for subject #1 in the 80–150 Hz and 150–250 Hz bands are given in the left and middle plots, respectively. The color bar indicates the rate in counts/s. (Right plot) The grid layout for electrocorticograms (ECoG) data collection with red ellipse showing the area where seizures and epileptogenic activities were observed.

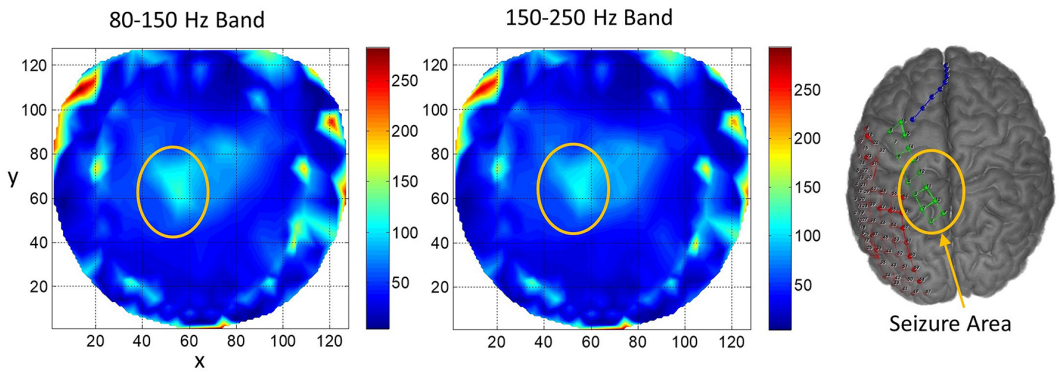

FIGURE 4 | The rate of formation (counts/s) of stable phase cone clusters averaged over a 240-s interictal period for the subject #2 in the 80–150 and 150–250 Hz bands are given in the left and middle plots, respectively. The color bar indicates the rate in counts/s. (Right plot) The grid and strip electrodes layout for ECoG data collection. The yellow-orange ellipse marks the area where seizures and epileptogenic activities were observed.

was observed in the complex left partial midline areas. It is marked with a yellow-orange ellipse. For both bands, the rate of formation (counts/s) of stable phase cone clusters is higher in the epileptogenic area as compared with nearby areas. The peak rate is about 115 counts/s for the 80–150 Hz band and about 107 counts/s for the 150–250 Hz band. These are averaged values over 240 s. There is diffused phase cone activity outside the elliptical area, particularly in the north-east direction spread over x = 60–85 and y = 55–90. This will correspond to the right midline central area of the brain. Most probably, this activity is related to the cortical networks in the vicinity of the main focus of the epileptogenic area marked with an ellipse. There are bright spots (∼270 counts/s) in the left front temporal area and also in the right front temporal and right central temporal areas. These probably are due to muscle artifacts which can be suppressed by the use of image processing techniques. However, we decided to include it here in these plots to show that phase cone formations are strong for muscle artifacts. Overall, the rate of formation of stable phase cone clusters is also strong in the epileptogenic areas.

Subject #3 had epileptic spikes and seizure activity over midline/anterior frontal regions, with shifting hemispheric preponderance. This region is marked with a rectangle. Refer to **Figure 5**. There are several hot spots in both bands in the rectangular area which signify the higher rate of formation of phase cone clusters as compared with nearby areas and most probably are related to the silent interictal epileptogenic activity. There are some scattered bright spots in the left central area which possibly could be the continuation of the left frontal epileptogenic activity. There is a bright spot around the coordinate location of (74, 23) which could be due to some other activity in the brain and not related to epileptogenic activity in the frontal regions. It is a possibility that it is a separate epileptogenic activity which was not observed in the hdEEG recordings but showed up in the interictal phase cone analysis. Sometimes it does happen that the stochastic analysis of EEG power does not show the exact and complete spatial patterns of epileptogenic activity while they show up in more detail with the stochastic analysis of EEG phase synchronization (Ramon et al., 2008). The diffused midline central activity area, possibly, could be an epileptogenic activity or unidentified background brain activity during the Stage I sleep. However, this needs to be confirmed with additional studies.

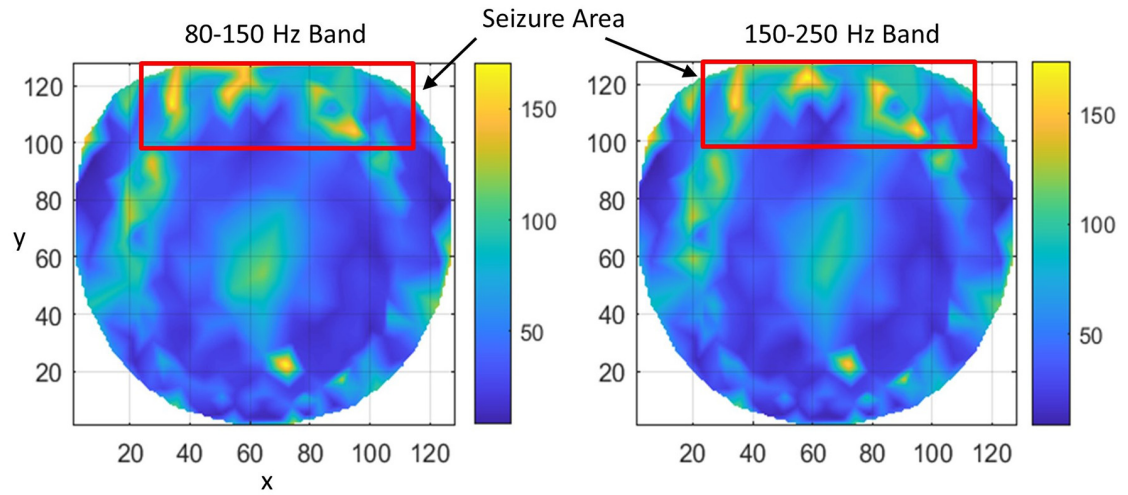

FIGURE 5 | The rate of formation (counts/s) of stable phase cone clusters averaged over a 240-s interictal period for subject #3 in the 80–150 and 150–250 Hz bands are given in the left and right plots, respectively. The color bar indicates the rate in counts/s. The seizure activity area is marked with a red rectangle which shows several hot spots.

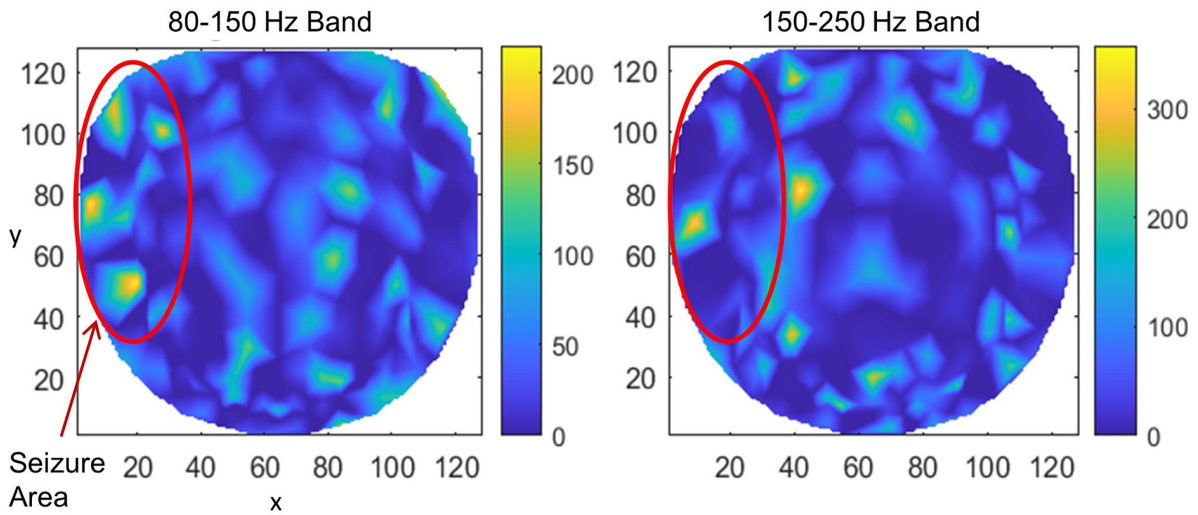

FIGURE 6 | The rate of formation (counts/s) of stable phase cone clusters averaged over a 240-s interictal period for subject #4 in the 80–150 and 150–250 Hz bands are given in the left and right plots, respectively. The color bar indicates the rate in counts/s. The epileptic spikes and seizure activity area is marked with a red ellipse. The left plot shows several hot spots in the left temporal frontal, central and parietal areas. The activity in the 150–250 Hz band, the right plot, has one hot spot in the left temporal central area and another hot spot at the right side of the red circle which could also be related to the silent interictal epileptic activity.

Results for subject #4 are given in **Figure 6**. This subject had epileptic spikes and seizure activity in the left frontal-temporal and inferior midline areas. In the left plot for 80–150 Hz band, there are three distinct hot spots where the rate of formation of stable phone cones is very high (150 −210 counts/s) as compared with nearby areas where the rate is low (0–50 counts/s). This activity is mainly confined to the left frontal, central, and parietal temporal areas. The cortical activity in the inferior midline area could get picked up by the scalp electrodes in the left temporal areas which possibly could be the additional sources of the formation of the observed hot spots in the left temporal areas. The activity in the 150–250 Hz band is limited only to one hot spot in the left temporal central with a peak rate of 307 counts/s averaged over a 240-s interictal period. There is another hot spot at the right side of the red circle at the x, y coordinate location of (40, 80). Its peak rate is 342 counts/s and is also probably related to the silent epileptic network activity during the interictal period. There are other numerous visible spots in the range of 100–135 counts/s for the 80–150 Hz band and between 180–250 counts/s for the 150–250 Hz band. These, most

TABLE 1 | Change in peak value of the phase cone rate (counts/s) in the epileptogenic zone as compared with the nearby background rate.

	80–150 Hz			150–250 Hz		
	Background	**Epilepsy**	**% Change**	**Background**	**Epilepsy**	**% Change**
Subject #1	100	158	58%	72	183	154%
Subject #2	45	115	155%	47	107	128%
Subject #3	37	160	332%	34	162	376%
Subject #4	25	210	740%	50	307	514%
Mean % change (all subjects)			321 ± 301			293 ± 185
Statistical Significance	$p < 0.03$			$p < 0.045$		

probably, are related to the spontaneous background activity of the brain and not related to any epileptogenic activity.

The peak values in the epileptogenic zone were compared with nearby baseline values for all four subjects. These values are given in **Table 1**. The peak values are significantly higher in the epileptogenic zones. This was determined by the paired *t*-test between the values (counts/s) for the background and epilepsy, i.e., epileptogenic zone.

DISCUSSIONS

The overall summary of our results is that the rate of formation of stable phase cone cluster patterns during interictal periods is higher in the epileptogenic zones in the 80–150 and 150–250 Hz bands and are above the value of 12.12 counts/s for the surrogate data. This we have shown in four subjects. These are encouraging preliminary findings and need to be confirmed with a larger subject population. These findings suggest that there is a silent background epileptic network activity in the high frequency (80–250 Hz) EEG band during interictal periods which possibly could be a physiological marker to localize and isolate epileptogenic zones. Such information derived during interictal periods could become a useful tool for brain electrical stimulation to control the onset of epileptic seizures.

The observed phase cone activity in both high frequency (80–150 and 150–250 Hz) bands is often spread outside of the mapped epileptogenic zones. This could be due to the large area cortical networks involved in the cortical phase transitions that give rise to the spatiotemporal formation of phase cones (Freeman and Vitiello, 2006; Freeman, 2008). The phase cone activity related to the background cognitive processes in the brain is also observed along with the epileptogenic activity in the spatial plots. We have not seen any studies which quantify the phase cone formations due to spontaneous brain activity in healthy subjects or subjects with epilepsy. Thus, it is difficult to quantify and separate the epileptic activity from the background brain activity. This has to be a topic for a carefully designed future study. However, in general, the rate of phase cone formations related to the background brain activity during the Stage I sleep will be much lower than the epileptogenic activity. This is what we are observing in all four subjects. These observations are listed in **Table 1**. In summary, the observed hot spots in the epileptogenic zones are definitely related to the silent epileptic activity during interictal periods which are above the spontaneous brain activity during the stage I sleep.

The muscle artifacts are a problem, particularly on the facial and back of the neck electrodes. The frequency spectra of the electromyographic (EMG) signal and the EEG are very similar (Whitham et al., 2011; Muthukumaraswamy, 2013) which makes it difficult to use signal processing techniques to separate the muscle activity from the brain activity in the scalp EEG data. The independent component analysis (ICA) or PCA are two of the best tools to remove these artifacts from the EEG data. In some subjects, the electrodes on the face, forehead, and back of the neck, below the skull, pick up a lot of muscle activity along with the basal brain activity. However, even with PCA or ICA analysis, it is difficult to get rid of all the muscle activity in these electrodes. Often in the component spectra of PCA or ICA, one can see the residual muscle activity along with a strong component of the brain activity. In spatial component maps, the focus of the activity is generally observed in the vicinity of the skin, skull bone, and the neocortex, and it is difficult to separate the dipoles related to the muscle artifact from the brain activity. So, one has to make a judicious choice to keep some of the ICA or PCA components that have mixed brain and muscle activity. These electrodes will show the phase cone activity due to muscle activity and also due to brain activity. Only in the data of subject #2, we had strong muscle activity on outer rim electrodes (face, near to ears, and the neck). This subject had complex left partial midline seizures so the muscle activity at the outer rim electrodes was not a confounding factor. For the other three subjects, we did not have this problem.

Our work reported here complements our previous work on the stable phase cone formations during interictal periods in the theta (3–7 Hz), alpha (7–12 Hz), beta (12–30 Hz), and low gamma (30–50 Hz) bands (Ramon et al., 2008; Ramon and Holmes, 2013a). It also complements the oscillatory patterns of phase cone formations near epileptic spikes (Ramon et al., 2018). These combined studies show that the rate of formation of stable phase cones is higher in the vicinity of epileptogenic zones in different low and high-frequency EEG bands. Also, we have shown earlier that the stochastic behavior of phase synchronization index exhibits a complex behavior, and the phase-amplitude cross-frequency couplings are reduced and spatial patterns are fragmented during interictal periods in the epileptogenic zones (Ramon and Holmes, 2012, 2013a,b). These studies were performed in the lower (3–50 Hz) EEG frequency

bands. The stochastic behavior of the phase synchronization index was higher in the beta (12–30 Hz) and low gamma (30–50 Hz) bands but depressed in the theta (3–7 Hz) and alpha (7–12 Hz) bands. These earlier findings of the stochastic behavior of the phase synchronization index are also of interest and should be extended to examine this behavior in the high frequency (80–250 Hz) EEG bands to localize the epileptogenic sites in the brain in a noninvasive fashion. In summary, we believe that the findings described in this article, namely, that focal area of increased phase cone turnover are markers of abnormal cortical excitability, and as such, may eventually be utilized as tools to assist in the noninvasive localization of epileptogenic cortices.

DATA AVAILABILITY STATEMENT

All datasets used in this study are available from the authors without undue reservation. In addition, in the near future we will submit our datasets to some repository, such as, GitHub.

ETHICS STATEMENT

The studies involving human participants were reviewed and approved by Human Subjects Division, University of Washington, Seattle, WA 98195, USA. The patients/participants provided their written informed consent to participate in this study.

AUTHOR CONTRIBUTIONS

Data was collected by MH. Data analysis was done by CR and MH. Discussions of results and writing was done jointly by both authors. All authors contributed to the article and approved the submitted version.

ACKNOWLEDGMENTS

Some of the computing facilities at the University of Washington and Neuroscience Gateway at the San Diego Supercomputing Center were used for preprocessing and analysis of the EEG data.

REFERENCES

Bak, P., Tang, C., and Wiesenfeld, K. (1987). Self-organized criticality: an explanation of 1/f noise. *Phys. Rev. Lett.* 59, 381–384. doi: 10.1103/PhysRevLett.59.381

Barlow, J. S. (1993). *The Electroencephalogram: Its Patterns and Origins*. Cambridge, MA: MIT Press.

Beggs, J. M., and Timme, N. (2012). Being critical of criticality in the brain. *Front. Physiol.* 3:163. doi: 10.3389/fphys.2012.00163

Boran, E., Sarnthein, J., Krayenbühl, N., Ramantani, G., and Fedele, T. (2019). High-frequency oscillations in scalp EEG mirror seizure frequency in pediatric focal epilepsy. *Sci. Rep.* 9:16560. doi: 10.1038/s41598-019-52700-w

Boran, E., Sarnthein, J., Krayenbühl, N., Ramantani, G., and Fedele, T. (2020). Publisher correction: high-frequency oscillations in scalp EEG mirror seizure frequency in pediatric focal epilepsy. *Sci. Rep.* 10:1632. doi: 10.1038/s41598-020-58621-3

Freeman, W. J. (2003). A neurobiological theory of meaning in perception part II: spatial patterns of phase in gamma EEG from primary sensory cortices reveal the properties of mesoscopic wave packets. *Int. J. Bifurc. Chaos.* 13, 2513–2535. doi: 10.1142/S0218127403008144

Freeman, W. J. (2004). Origin, structure and role of background EEG activity. Part 1. Analytic amplitude. *Clin. Neurophysiol.* 115, 2077–2088. doi: 10.1016/j.clinph.2004.02.029

Freeman, W. J. (2007). Hilbert transform for brain waves. *Scholarpedia* 2:1338. doi: 10.4249/scholarpedia.1338

Freeman, W. J. (2008). A pseudo-equilibrium thermodynamic model of information processing in nonlinear brain dynamics. *Neural Netw.* 21, 257–265. doi: 10.1016/j.neunet.2007.12.011

Freeman, W. J. (2015). Mechanism and significance of global coherence in scalp EEG. *Curr. Opin. Neurobiol.* 31, 199–205. doi: 10.1016/j.conb.2014.11.008

Freeman, W. J., and Barrie, J. M. (2000). Analysis of spatial patterns of phase in neocortical gamma EEGs in rabbit. *J. Neurophysiol.* 84, 1266–1278. doi: 10.1152/jn.2000.84.3.1266

Freeman, W. J., Burke, B. C., and Holmes, M. D. (2003). Aperiodic phase re-setting in scalp EEG of beta-gamma oscillations by state transitions at alpha-theta rates. *Hum. Brain Mapp.* 19, 248–272. doi: 10.1002/hbm.10120

Freeman, W. J., Holmes, M. D., West, G. A., and Vanhatalo, S. (2006a). Fine spatiotemporal structure of phase in human intracranial EEG. *Clin. Neurophysiol.* 117, 1228–1243. doi: 10.1016/j.clinph.2006.03.012

Freeman, W. J., Holmes, M. D., West, G. A., and Vanhatalo, S. (2006b). Dynamics of human neocortex that optimizes its stability and flexibility. *Int. J. Intell. Syst.* 21, 881–901. doi: 10.1002/int.20167

Freeman, W. J., and Rogers, L. J. (2002). Fine temporal resolution of analytic phase reveals episodic synchronization by state transitions in gamma EEGs. *J. Neurophysiol.* 87, 937–945. doi: 10.1152/jn.00254.2001

Freeman, W. J., and Vitiello, G. (2006). Nonlinear brain dynamics as macroscopic manifestation of underlying many-body field dynamics. *Phys. Life Rev.* 3, 93–118. doi: 10.1016/j.plrev.2006.02.001

Freeman, W. J., and Vitiello, G. (2010). Vortices in brain waves. *Int. J. Modern Phys. B* 24, 3269–3295. doi: 10.1142/S0217979210056025

Holmes, M. D., Ramon, C., and Jenson, K. (2015). "EEG ripple band power, phase synchronization and phase clustering in epileptogenic zones in 256-channel interictal scalp EEG data," in *69th Annual American Epilepsy Society (AES) Meeting*, Philadelphia, PA, USA.

Holmes, M., and Ramon, C. (2014). "Interictal phase clustering of high frequency oscillations derived from 256-channel scalp EEG correlates with the epileptogenic zone," in *68th Annual American Epilepsy Society Meeting*, Seattle, WA, USA.

Johnson, L. A., Blakely, T., Hermes, D., Hakimian, S., Ramsey, N. F., and Ojemann, J. G. (2012). Sleep spindles are locally modulated by training on a brain-computer interface. *Proc. Natl. Acad. Sci. U S A* 109, 18583–18588. doi: 10.1073/pnas.1207532109

Karam, Z. N., and Oppenheim, A. V. (2007). "Computation of the one-dimensional unwrapped phase," in *15th International Conference on Digital Signal Processing, Cardiff, 2007*, (Piscataway, NJ: IEEE), 304–307. doi: 10.1109/ICDSP.2007.4288579

Kozma, R., and Freeman, W. J. (2017). Cinematic operation of the cerebral cortex interpreted *via* critical transitions in self-organized dynamic systems. *Front. Syst. Neurosci.* 11:10. doi: 10.3389/fnsys.2017.00010

Kugiumtzis, D. (2002). "Surrogate Data test on time series," in *Modelling and Forecasting Financial Data. Studies in Computational Finance*, Vol. 2, eds A. S. Soofi and L. Cao (Boston, MA: Springer), 267–282. doi: 10.1007/978-1-4615-0931-8_13

Lancaster, G., Iatsenko, D., Pidde, A., Ticcinelli, V., and Stefanovska, A. (2018). Surrogate data for hypothesis testing of physical systems. *Phys. Rep.* 748, 1–60. doi: 10.1016/j.physrep.2018.06.001

McClellan, J. H., and Parks, T. W. (2005). A personal history of the parks-McClellan algorithm. *IEEE Signal Process. Mag.* 22, 82–86. doi: 10.1109/MSP.2005.1406492

Mooij, A. H., Raijmann, R., Jansen, F. E., Braun, K., and Zijlmans, M. (2017). Physiological ripples (± 100 Hz) in spike-free scalp eegs of children with and without epilepsy. *Brain Topogr.* 30, 739–746. doi: 10.1007/s10548-017-0590-y

Mortezapouraghdam, Z., Corona-Strauss, F. I., Takahashi, K., and Strauss, D. J. (2018). Reducing the effect of spurious phase variations in neural oscillatory signals. *Front. Comput. Neurosci.* 12:82. doi: 10.3389/fncom.2018.00082

Muthukumaraswamy, S. D. (2013). High-frequency brain activity and muscle artifacts in MEG/EEG: a review and recommendations. *Front. Hum. Neurosci.* 7:138. doi: 10.3389/fnhum.2013.00138

Myers, M. H., Kozma, R., Davis, J. J., and Ilin, R. (2014). "Phase cone detection optimization in EEG data," in *2014 International Joint Conference on Neural Networks (IJCNN)*, (Beijing, China: IEEE), 2504–2511.

Myers, M. H., and Padmanabha, A. (2017). Quantitative EEG signatures through amplitude and phase modulation patterns. *J. Med. Signals Sens.* 7, 123–129.

Pikovsky, A., Rosenblum, M., and Kurths, J. (2001). *Synchronization: A Universal Concept in Non-Linear Sciences.* Cambridge, UK: Cambridge University Press.

Prichard, D. (1994). The correlation dimension of differenced data. *Phys. Lett. A* 191, 245–250. doi: 10.1016/0375-9601(94)90134-1

Ramon, C., and Holmes, M. D. (2012). Noninvasive epileptic seizure localization from stochastic behavior of short duration interictal high density scalp EEG data. *Brain Topogr.* 25, 106–115. doi: 10.1007/s10548-011-0188-8

Ramon, C., and Holmes, M. D. (2013a). Stochastic behavior of phase synchronization index and cross-frequency couplings in epileptogenic zones during interictal periods measured with scalp dEEG. *Front. Neurol.* 4:57. doi: 10.3389/fneur.2013.00057

Ramon, C., and Holmes, M. D. (2013b). Noninvasive localization of epileptic sites from stable phase synchronization patterns on different days derived from short duration interictal scalp dEEG. *Brain Topogr.* 26, 1–8. doi: 10.1007/s10548-012-0236-z

Ramon, C., and Holmes, M. D. (2015). Spatiotemporal phase clusters and phase synchronization patterns derived from high density EEG and ECoG recordings. *Curr. Opin. Neurobiol.* 31, 127–132. doi: 10.1016/j.conb.2014.10.001

Ramon, C., Holmes, M. D., and Freeman, W. J. (2013). Increased phase clustering in epileptogenic areas measured with 256-channel dense array EEG. *J. Neurol. Transl. Neurosci.* 2:1029.

Ramon, C., Holmes, M. D., Freeman, W. J., McElroy, R., and Rezvanian, E. (2008). Comparative analysis of temporal dynamics of EEG and phase synchronization of EEG to localize epileptic sites from high density scalp EEG interictal recordings. *Annu. Int. Conf. IEEE Eng. Med. Biol. Soc.* 2008, 4548–4550. doi: 10.1109/IEMBS.2008.4650224

Ramon, C., Holmes, M. D., Wise, M. V., Tucker, D., Jenson, K., and Kinn, S. R. (2018). Oscillatory patterns of phase cone formations near to epileptic spikes derived from 256-channel scalp EEG data. *Comput. Math. Methods Med.* 2018:9034543. doi: 10.1155/2018/9034543

Ruiz, Y., Pockett, S., Freeman, W. J., Gonzalez, E., and Li, G. (2010). A method to study global spatial patterns related to sensory perception in scalp EEG. *J. Neurosci. Methods* 191, 110–118. doi: 10.1016/j.jneumeth.2010.05.021

Swadlow, H. A. (1994). Efferent neurons and suspected interneurons in motor cortex of the awake rabbit: axonal properties, sensory receptive fields and subthreshold synaptic inputs. *J. Neurophysiol.* 71, 437–453. doi: 10.1152/jn.1994.71.2.437

Swadlow, H. A., and Waxman, S. G. (2012). Axonal conduction delays. *Scholarpedia* 7:1451. doi: 10.4249/scholarpedia.1451

Tucker, D. M. (1993). Spatial sampling of head electrical fields: the geodesic sensor net. *Electroencephalogr. Clin. Neurophysiol.* 87, 154–163. doi: 10.1016/0013-4694(93)90121-b

Whitham, E. M., Fitzgibbon, S. P., Lewis, T. W., Pope, K. J., Delosangeles, D., Clark, C. R., et al. (2011). Visual experiences during paralysis. *Front. Hum. Neurosci.* 5:160. doi: 10.3389/fnhum.2011.00160

Conflict of Interest: The authors declare that the research was conducted in the absence of any commercial or financial relationships that could be construed as a potential conflict of interest.

frontiers in Human Neuroscience

ORIGINAL RESEARCH
published: 08 June 2021
doi: 10.3389/fnhum.2021.677840

Localization of the Epileptogenic Zone by Multimodal Neuroimaging and High-Frequency Oscillation

Xiaonan Li[1,2,3], Tao Yu[2], Zhiwei Ren[2], Xueyuan Wang[2], Jiaqing Yan[4], Xin Chen[2], Xiaoming Yan[2], Wei Wang[1,2,3], Yue Xing[1,2,3], Xianchang Zhang[5], Herui Zhang[3], Horace H. Loh[3], Guojun Zhang[2] and Xiaofeng Yang[1,2,3]**

[1] Laboratory of Brain Disorders, Collaborative Innovation Center for Brain Disorders, Ministry of Science and Technology, Beijing Institute of Brain Disorders, Capital Medical University, Beijing, China, [2] Xuanwu Hospital, Capital Medical University, Beijing, China, [3] Bioland Laboratory, Guangzhou, China, [4] College of Electrical and Control Engineering, North China University of Technology, Beijing, China, [5] MR Collaboration, Siemens Healthcare Ltd., Beijing, China

Accurate localization of the epileptogenic zone (EZ) is a key factor to obtain good surgical outcome for refractory epilepsy patients. However, no technique, so far, can precisely locate the EZ, and there are barely any reports on the combined application of multiple technologies to improve the localization accuracy of the EZ. In this study, we aimed to explore the use of a multimodal method combining PET-MRI, fluid and white matter suppression (FLAWS)—a novel MRI sequence, and high-frequency oscillation (HFO) automated analysis to delineate EZ. We retrospectively collected 15 patients with refractory epilepsy who underwent surgery and used the above three methods to detect abnormal brain areas of all patients. We compared the PET-MRI, FLAWS, and HFO results with traditional methods to evaluate their diagnostic value. The sensitivities, specificities of locating the EZ, and marking extent removed versus not removed [RatioChann(ev)] of each method were compared with surgical outcome. We also tested the possibility of using different combinations to locate the EZ. The marked areas in every patient established using each method were also compared to determine the correlations among the three methods. The results showed that PET-MRI, FLAWS, and HFOs can provide more information about potential epileptic areas than traditional methods. When detecting the EZs, the sensitivities of PET-MRI, FLAWS, and HFOs were 68.75, 53.85, and 87.50%, and the specificities were 80.00, 33.33, and 100.00%. The RatioChann(ev) of HFO-marked contacts was significantly higher in patients with good outcome than those with poor outcome ($p < 0.05$). When intracranial electrodes covered all the abnormal areas indicated by neuroimaging with the overlapping EZs being completely removed referred to HFO analysis, patients could reach seizure-free ($p < 0.01$). The periphery of the lesion marked by neuroimaging may be epileptic, but not every lesion contributes to seizures. Therefore, approaches in multimodality can detect EZ more accurately, and HFO analysis may help in defining real epileptic areas that may be missed in the neuroimaging results. The implantation of intracranial electrodes guided by non-invasive PET-MRI and FLAWS findings as well as HFO analysis would be an optimized multimodal approach for locating EZ.

Keywords: epileptogenic zone, neuroimaging, high-frequency oscillations, PET-MRI, FLAWS, multimodal method

OPEN ACCESS

Edited by:
Felix Scholkmann,
University Hospital Zürich, Switzerland

Reviewed by:
Ahmet Ademoglu,
Boğaziçi University, Turkey
James Ward Antony,
Princeton University, United States

***Correspondence:**
Xiaofeng Yang
xiaofengyang@yahoo.com
Guojun Zhang
zgj62051@163.com

Specialty section:
This article was submitted to Brain Imaging and Stimulation, a section of the journal Frontiers in Human Neuroscience

Received: *08 March 2021*
Accepted: *23 April 2021*
Published: *08 June 2021*

Citation:
Li X, Yu T, Ren Z, Wang X, Yan J, Chen X, Yan X, Wang W, Xing Y, Zhang X, Zhang H, Loh HH, Zhang G and Yang X (2021) Localization of the Epileptogenic Zone by Multimodal Neuroimaging and High-Frequency Oscillation. Front. Hum. Neurosci. 15:677840. doi: 10.3389/fnhum.2021.677840

INTRODUCTION

For patients with drug-refractory epilepsy, surgical removal of the epileptogenic zone (EZ), which is defined as the brain regions necessary and sufficient for initiating seizures (Rosenow and Luders, 2001), is the best option to eliminate seizures (Jacobs et al., 2010). Because the definition of the EZ is only a theoretical concept, as of now, there are no techniques that can accurately delineate an EZ. Recently, some new techniques, which could help in identifying the EZs have attracted increasing attention, including PET-MRI (positron emission tomography-magnetic resonance imaging), special MRI sequences, a neuroimaging postprocessing technique, and an automatic analysis of high-frequency oscillations (HFOs) (Salamon et al., 2008; Holler et al., 2015; Soares et al., 2016; Sun et al., 2018).

PET imaging provides important insights into the functional integrity and activity of neural systems, as it is a sensitive and non-invasive method for measuring brain metabolism. However, PET imaging has limitations of a lower spatial relationship and false lateralization (Chugani et al., 1993; Hur et al., 2013). Newly developed PET and MRI coregistration approaches combined the tissue contrast of MRI and the metabolic characterization of FDG-PET, which would help to delineate surgical resection margins correlated with the structural anatomy and improve surgical outcomes based on discernible MRI findings (Salamon et al., 2008). In addition, hybrid PET/MR scanners could combine the superior soft tissue contrast of MRI and the metabolic characterization of FDG-PET into a single exam without the need for the additional ionizing radiation inherent to PET/CT systems (Paldino et al., 2017), thus, further promoting its clinical usage.

In the analysis of MRI results, the method of separating gray matter (GM), white matter (WM), and cerebrospinal fluid (CSF) in the brain has been very important in a variety of clinical studies and neuroscience research fields, as it enables the quantification of tissue volume and visualization of anatomical structures (Grieve et al., 2013; Erickson et al., 2014; Gautam et al., 2014; Schick, 2016). Recently, a novel sequence known as fluid and white matter suppression (FLAWS) was developed to obtain three different anatomical images with high spatial resolution in one scan (Tanner et al., 2012). It first acquires two sets of 3D images using two inversion times, with TI1 suppressing the WM signal and TI2 suppressing the CSF signal. Based on these two sets of images, a set of synthetic minimum FLAWS-contrast images is subsequently calculated, which suppresses both the WM and CSF signals (gray matter specific). Gray matter-specific contrast images have been reported to detect abnormal brain structures more accurately than do conventional MRIs (Wang et al., 2018), which is important for epilepsy surgery.

Over the past 20 years, several studies reported an association between the removal of areas showing high rates of HFOs and a good surgical outcome (Jacobs et al., 2010; Akiyama et al., 2011; Fujiwara et al., 2016; Frauscher et al., 2017; Jiang et al., 2018; Ren et al., 2018), suggesting that HFOs are a promising biomarker of epileptogenic tissues. HFOs are generally viewed as spontaneous EEG patterns at frequencies ranging from 80 to 500 Hz. They consist of at least four oscillations that are clearly differentiated from the background activity, classified into ripples (80–200 Hz) and fast ripples (FRs; 200–500 Hz).

No technique has yet been able to precisely locate the EZ, and a few reports have described the application of multiple technologies to form a multimodal method with improved accuracy in localizing the EZ. Therefore, in this study, we aim to retrospectively explore the possibility of using a multimodal method that combines PET-MRI, FLAWS, and an automated analysis of HFOs to delineate the EZ. We also aimed to determine the accuracy of different combinations of technologies in locating the EZ.

MATERIALS AND METHODS

Patient Selection

In this study, 55 patients were consecutively enrolled from March 2016 to July 2019. All patients underwent long-term intracranial electroencephalogram (iEEG) monitoring. The inclusion criteria were as follows: (1) the patient underwent at least two of the following three examinations: PET-MRI, FLAWS, and HFOs; (2) the epileptogenic region was resected or ablated; and (3) at least 12 months of postsurgical follow-up was completed.

This study was approved by the ethics committee of Xuanwu Hospital of Capital Medical University, and all patients have signed the informed consent form.

Positron Emission Tomography-Magnetic Resonance Imaging Scanning and Image Processing

Positron Emission Tomography and Magnetic Resonance Imaging Infusion Image Collection

Some patients underwent a regular MRI scan of the brain using a MAGNETOM Trio Tim 3T MR scanner (Siemens Healthcare, Erlangen, Germany) and received [^{18}F] FDG PET-CT scans to extract the PET signal from the PET-CT images for imaging registration. Structural images were acquired with a three-dimensional T1-weighted sequence (TR = 1,600 ms, TE = 2.15 ms, flip angle = 9°, thickness = 1.0 mm, and FOV = 256 mm × 256 mm). The registration was conducted using SPM12 software[1].

Hybrid Positron Emission Tomography-Magnetic Resonance Imaging Scan

Some patients received a hybrid PET-MRI scan, which simultaneously obtains higher resolution PET images and MRI images. The process was performed on an integrated simultaneous Signa PET-MRI imaging system (GE Healthcare, Milwaukee, WI, United States). The MRI portion of the hybrid PET-MRI was acquired with a 3.0-T MRI using a 19-channel head coil that obtained all sequences of MRI, including the BRAVO sequence that is the same as MPR images. Parameters for the routine anatomic acquisitions were as follows: axial T2-weighted fast spin-echo (TR = 9,600 ms, TE = 149 ms, matrix

[1]https://www.fil.ion.ucl.ac.uk/spm/software/spm12/

size = 256 × 256, slice thickness = 3.0 mm, and gap = 1.0 mm); axial T1-weighted fast spin-echo (TR = 3,286 ms, TE = 24 ms, matrix size = 288 × 256, and slice thickness = 3.0 mm, gap = 1.0 mm). The PET portion of the hybrid PET-MRI is based on the magnetic compatibility of the good solid phase array-type optoelectronic digital converter (Silicon Photomultiplier, SiPM) of the PET detector, using time-of-flight (TOF) technology. Digital MRI information and PET image information, together with TOF technology, significantly improve the accuracy and precision of MR-based attenuation correction (MRAC), and sequentially, accurately, and quantitatively display lesions associated with epilepsy. The acquisition protocol and other detailed parameters can be obtained from previous publications (Shang et al., 2018).

Imaging Review

Two experienced radiologists who were blinded to the location of the resected regions separately reviewed the images and marked abnormal areas showing obvious hypometabolism. Differences in assessments between the radiologists were resolved by consensus.

Fluid and White Matter Suppression Examination

FLAWS imaging was conducted on a 3T MAGNETOM Verio MRI scanner (Siemens Healthcare, Erlangen, Germany). The output of the FLAWS sequence consisted of two sets of images: the 3D volume acquired using the TI1 sequence (FLAWS1) and the volume acquired using the TI2 sequence (FLAWS2). Detailed parameters for FLAWS were TR = 5,000 ms, TE = 2.88 ms, TI1 = 409 ms, TI2 = 1,100 ms, flip angel = 5°, matrix size = 256 × 256, slice thickness = 1.0 mm, and FOV = 256 mm × 256 mm (Chen et al., 2018).

The images were reviewed by two radiologists, and the final conclusions have reached a consensus. Detailed standards could be found in the paper above.

Recording and Analysis of High-Frequency Oscillation

Electrode Types and Intracranial Electroencephalogram Recordings

Subdural electrodes (contact diameter of 4 mm, 2.5-mm exposure, and 10-mm spacing between contact centers) and SEEG electrodes with 8, 10, 12, and 16 contacts (0.8-mm diameter, 2-mm length, and 1.5-mm between contacts; Beijing Huakehengsheng Healthcare Co., Ltd., Beijing, China) were implanted in the putative epileptogenic region. The iEEGs were acquired using a 256-channel Nicolet recording system (Natus Medical Incorporated, San Carlos, CA, United States) with a sampling rate of 4,096 Hz. At the same time, we recorded the submental electromyogram (EMG) and the electro-oculogram (EOG) to monitor the sleep stage.

Automatic Detection of High-Frequency Oscillations

We selected 5 min of a slow wave sleep epoch when the delta activity occupied more than 25% of background activity in 30-s epochs. We referred to the results of the EMG and EOG obtained from interictal periods that were separated by at least 2 h from seizures and were transformed to a bipolar montage composed of adjacent contacts.

For automated detection of ripples and FRs, we used the method developed by our team (Jiang et al., 2018; Ren et al., 2018). We used a zero-phase finite impulse response filter, and the cutoff frequencies were 80–200 and 200–500 Hz for ripples and FRs, respectively. As described in our previous paper, we plotted a peak point distribution curve (PPDC) by computing the absolute amplitude of all peak points in each channel and ranking them in ascending order. According to maximum distributed peak points algorithm, all peak points before the turning point of PPDC are baseline points. We assigned the mean baseline amplitude by calculating the mean peak point amplitude before the turning point with a 5-s moving window. Next, ripples and FRs were automatically detected when the corresponding frequency band of signals met our setting thresholds. We set ripples as oscillations with at least eight consecutive peaks higher than 3 standard deviations (SD) above baseline mean amplitude and six consecutive peaks higher than 10 SD above baseline mean amplitude; and FRs were set as oscillations with eight consecutive peaks higher than 3 SD above the baseline mean amplitude and six peaks higher than 9.5 SD above baseline mean amplitude. Then, we automatically removed false HFOs caused by Gibbs effect through computing the frequency offset power difference of phase space reconstruction. Only when the power difference was bigger than zero would the corresponding HFO be reserved for further analysis. Last, we ranked all channels in a descending order according to the HFO rates for each patient and the top 72% channel distribution area of FRs was considered as the EZ. When no FR was detected, we would refer to the ripples results.

Outcomes of Seizures

The postsurgical outcomes of the patients were classified using the scheme described by Engel (Jerome Engel, 2016). We defined a good postsurgical outcome as class I (seizure-free) and a poor postsurgical outcome as class II and III (recurrent seizures).

Classification of Electrode Contacts and Contacts Surgically Removed

Preimplantation MRI and post-implantation CT scans could help in locating each contact anatomically along the electrode trajectory. In addition, the postsurgical MRIs were used to determine whether electrode contacts were included in the brain tissue that was eventually removed during surgery.

Single Comparison

Comparing Results Obtained by New Techniques With Those Obtained by Traditional Methods

As some traditional inspection methods like MRI, scalp EEG, and intracranial EEG are widely used clinically, it is necessary to compare their results pertaining to the detection of suspicious epileptic areas with those of new techniques such as PET-MRI, FLAWS, and HFOs, to evaluate the diagnostic value. Techniques with more accurate marking areas were considered to have higher diagnostic values.

Comparing the Efficiency of Locating EZ

Based on the surgical outcome, we selected two groups of patients (I—no seizure and II —few seizures). For patients with a good outcome, each patient's brain area could be regarded as two parts: one part was the area marked by the method and eventually removed finally, which must belong to the EZ; the other part was the remaining area, which must be inside the non-EZ. For patients with few seizures and notable improvement, the removed marking area must be part of the EZ, and the other part must contain portions of the EZ. If the marking area was part of the EZ, it is considered true positive; otherwise, it is false positive. Because we could not define the marking areas that have not been removed as either epileptic or normal, patients with non-removing marking areas were excluded. Then we calculated the sensitivity and specificity of each method.

In addition, we also used RatioChann(ev) to evaluate their locating value. According to the PET-MRI, FLAWS, and HFO results, we separately marked the channels in the abnormal area. We calculated the ratio of the resected channels to the total channels in the abnormal areas marked using the three methods. Only patients whose implanted electrodes had covered all the abnormal areas identified using PET-MRI or FLAWS were included here. We named the ratio RatioChann(ev).

$$RatioChann(ev) = \frac{\#ChannRem(ev) - \#ChannNonRem(ev)}{\#ChannRem(ev) + \#ChannNonRem(ev)}$$

where, ev is the type of event (PET-MRI, FLAWS, or HFOs-FRs), #ChannRem is the number of removed channels marked by events, and #ChannNonRem is the number of non-removed contacts with events (Jacobs et al., 2010; Gliske et al., 2018). We compared RatioChann(ev) with outcome.

Multimodal Comparison

Comparing Abnormal Regions Marked Using the Three Methods

We compared the abnormal regions marked by PET-MRI, FLAWS, and HFOs in different combinations, and we calculated the consistencies of the different combinations. Because some factors (such as sex, onset age, onset duration, seizure frequency, and involved lobes) might affect the consistency, we also compared the consistencies in different conditions.

Furthermore, we analyzed the correlations between the overlapping areas identified using the three methods (at least two or more methods) with the removing area and outcome. We compared the correlations between completely and partially/not removing marking areas and outcome in the following four groups: (1) PET-MRI, (2) FLAWS, (3) HFOs, and (4) multimodally.

Comparison of the Extent of Areas Marked Using the Three Methods

We compared the extent of areas marked in each patient using the PET-MRI, FLAWS, and HFOs to ultimately investigate the correlations among the three methods. Because the lesions were different, we specifically selected patients with FCD confirmed by postsurgical pathology, for further comparison.

Statistical Analysis

Sensitivity = true positive/(true positive + false negative); specificity = false positive/(false positive + true negative). A Wilcoxon rank sum test was used to compare ratios between different groups. Fisher's exact test was used to test the correlation between complete removing and outcome. Statistical significance was established at $p < 0.05$.

All statistical analyses were performed using IBM SPSS Statistics 17 software (IBM Corp., Armonk, NY, United States).

RESULTS

Patient Selection and Surgical Outcomes

A total of 55 patients, 15 were ultimately enrolled in this study, and 40 patients were excluded for not undergoing PET-MRI scan or FLAWS examination. Patient characteristics are summarized in **Table 1**. Ten patients had all the methods' results, one patient had HFO and FLAWS results, and four patients had HFO and PET-MRI results. Notably, (1) among the 14 patients with available PET-MRI results, 7 patients underwent a hybrid PET-MRI scan, and the results for the other patients were derived from FDG-PET and MRI imaging coregistration; (2) Patient # 15 had no FRs detected by our detector, and the related HFO location information was given by ripples results. For the variable uniformity, the RatioChann(ev) comparisons related to FRs excluded this patient. One year after the operation, 10 patients experienced recurrent seizures after surgery (5 with Engel II, and 5 with Engel III).

Diagnostic Value of Single Method Compared With Traditional Ones

For the MRI scan, 7/15 (46.67%) patients had normal results, 1 patient had bilateral abnormalities, and 14/15 (93.33%) patients' MRI results were not consistent with scalp EEG results. For the scalp EEG monitoring, one patient had normal conclusion, two patients had bilateral locations, and others seem to have too broad locations. The iEEG results seemed to be more local and accurate but still easily missed some potential abnormalities compared with HFO analysis.

Compared with the traditional methods, PET-MRI, FLAWS, and HFOs were able to locate more potential epileptic areas or to locate the abnormal areas more focally. This meant that the new methods could provide more useful information to clinicians, and further help in locating the EZ more effectively (**Supplementary Table 1**).

Efficiency of Finding the EZs

When finding the EZs, we calculated that the sensitivity and specificity of PET-MRI were 68.75 and 80.00%, respectively. The sensitivity and specificity of FLAWS were 53.85 and 33.33%, respectively. The efficiency of HFOs seemed to be better, reaching 87.50% sensitivity and 100.00% specificity.

When comparing RatioChann(ev) of removal outcome, for PET-MRI and FLAWS, there were no significant differences in the ratios between patients with good and poor outcomes

(p = 0.6954, p = 0.6667, **Figure 2C**). The ratio observed for removed and non-removed HFO-marked contacts was significantly higher in patients with a good outcome than in patients with a poor outcome (p = 0.0270, **Figure 2C**).

Consistency of the Three Methods

Of the 14 patients who underwent PET-MRI scans, at least one of the abnormal brain regions detected using PET-MRI showed a high rate of HFOs (14/14, 100%). In 5 of these 14 patients, PET-MRI and HFOs showed exactly the same location of abnormal areas (5/14, 35.71%). In 10 of the 11 patients who had FLAWS data, at least one of the abnormal areas identified using FLAWS showed a high rate of HFOs (10/11, 90.91%); moreover, the EZ defined that using the two aforementioned methods was completely consistent in 4 of the 11 patients (4/11, 36.36%). Patients, 9 of 10, who underwent both a PET-MRI scan and a FLAWS examination had at least one matched abnormal area (9/10, 90.00%), and the suspicious areas were completely consistent in 5 patients (5/10, 50.00%) (**Figures 1**, **2A**).

By comparing the different factors (sex, onset age, onset duration, seizure frequency, and involved lobes) among patients with consistency in results from different methods, we observed a tendency toward better consistency between PET-MRI and HFOs in patients who had single involved lobes (p = 0.001) (**Figure 2B**).

In all (100%) the patients, PET-MRI and/or FLAWS could find abnormal areas. Among them, two patients' intracranial electrodes did not cover all the suspicious areas. Thus, the relative abnormal discharge could not be captured, which might contribute to their Engel III outcome. Three other patients also developed Engel III outcome due to the incomplete removal of overlapping areas marked by at least two methods. For 10 patients whose electrodes covered all suspicious zones indicated by neuroimaging, indicating a complete removal, better outcome was detected after 1 year, and 5 with few seizures had residual FRs areas (**Figure 1**).

Correlation With Outcome Individually or Multimodally

When using the method individually, we found that only patients in whom the HFO-marked areas were completely resected had larger chance of seizure freedom compared with partial groups (p = 0.007).

Considering the results shown above, we define the multimodal group as: 1) whether intracranial electrodes covered all suspicious areas indicated by neuroimaging and 2) whether the HFO-marked areas were completely removed. The results showed that the multimodal group had a significantly higher possibility of being seizure-free when both conditions were met (p = 0.002) (**Table 2**).

Comparison of the Extent of Marking

After comparing the extent of areas in each patient marked using the three methods, in most cases, PET-MRI covered the largest abnormal (hypometabolism) areas. FLAWS marked relatively smaller abnormal areas. HFOs marked the most focal meaningful areas, which were located in the core or the margin of the lesion or the perilesion marked by neuroimaging.

Interestingly, when we only focused on patients' lesions verified to be FCD indicated by pathology, HFO-marked areas were more likely to be the margins or even extended beyond the lesion. This indicated that the perilesion of FCD may contribute to epileptic seizures (**Figure 3**).

TABLE 1 | Clinical information for all patients.

Patient	Sex/Age	Onset/Fre	Electrode	PET-MRI	FLAWS	HFOs	Overlapped	Removing	Outcome
1	M/23	17/d	SEEG	LT,LPT,LMP	LT,LPT,LMP	LH,LPT	LH,LPT,LMP	LH, LPT	I
2	M/29	5/d	SEEG	RT,RH	RT, RH	RH,RA	RH,RT	RT, RH,RBF	I
3	F/42	12/m	SEEG	RSP	RP	RP, RIP	RP	RP	II
4	M/16	7/w	SEEG	RPT	Normal	RPT,LH	RPT	RPT	II
5	M/13	5/d	SEEG	RCS	RCS	RP, RCS	RCS	RCR(*)	II
6	F/17	1/w	SEEG	RT,RP	RF,RCR	RF,RCR	RF,RCR	RF	III
7	M/20	6/m	SEEG	LF,LOF,LTP,LH	LF,LOF,LT,LO,RO	LF,LH,RA	LF,LOF,LH	LOF,LTP,LH	III
8	F/26	9/w	SEEG	RF,RT,RI	RT,RI	RT	RTRI	RIO(*)	III
9	M/26	13/d	SEEG	RF	RF	RF	RF	RF	II
10	F/33	13/d	Sub/depth	LP,LI	LT	LO,LT,U	LT,LI	LT,LI	III
11	M/20	3/w	Sub/depth	/	RF,RCR	RF,RCR	RF,RCR	RF	III
12	F/26	5/w	SEEG	LF	/	LF	LF	LF	I
13	F/13	12/w	SEEG	LF	/	LF	LF	LF	I
14	F/41	19/m	SEEG	RF	/	RF,RMCC	RF	RF,RCR	II
15	M/16	15/d	SEEG	RF	/	RF(#)	RF	RF	I

LT, left temporal; LPT, left posterior temporal; LMP, left medial parietal; LH, left hippocampus; RT, right temporal; RH, right hippocampus; RA, right amygdala; RACC, right anterior cingulate cortex; RMCC, right middle cingulate cortex; RBF, right basis frontalis; RF, right frontal; RSP, right superior parietal; RP, right parietal; RIP, right inferior parietal; LH, left hippocampus; RCS, right central sulcus; RCR, right central region; LF, left frontal; LTP, left temporal pole; LOF, left orbitofrontal; LO, left occipital; RO, right occipital. FCD, focal cortical dysplasia. M, male; F, female; Fre, seizure frequency; d, having seizure every day; w, having seizure every week; m, having seizure every month; Sub, subdural electrode.

**The patient has undergone radiofrequency ablation instead of resection.*

#No fast ripple (FR) was detected (the results were from ripples).

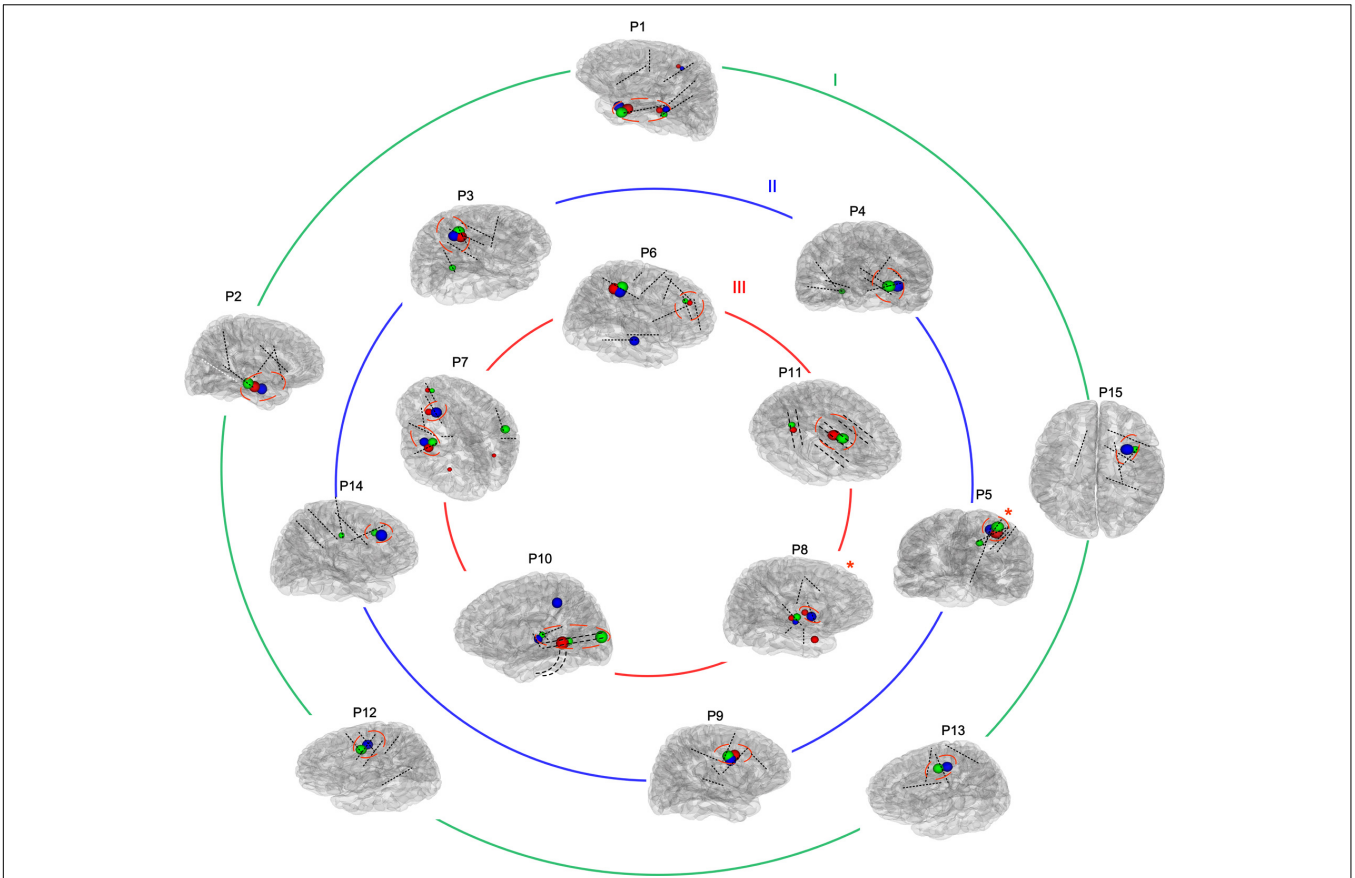

FIGURE 1 | Reconstructions of the placement of intracranial electrodes and suspicious areas mapped in all patients. The images showed the locations of subdural electrodes (P10 and P11) or SEEG locations in all 15 patients. Most electrodes are shown in black, while one contralateral electrode that was unable to be shown in the brain model is presented in white. Blue, red, and green globes mark suspicious abnormalities detected using positron emission tomography-magnetic resonance imaging (PET-MRI), fluid and white matter suppression (FLAWS), and high-frequency oscillations (HFOs), respectively, and the different volumes indicate different levels of significance. The removed volume is also marked by a red imaginary line. Moreover, all patients were divided into three groups according to their outcomes (Engel I, II, and III), as shown by the three circles. *The patient has undergone radiofrequency ablation instead of resection.

Case Studies

Patient #2 (**Figures 4A–C**), a 29-year-old male, had experienced tonic–clonic seizures for 24 years, but his MRI and 3D-FLAIR images revealed no abnormality. PET and MRI fusion results revealed hypometabolism of the right temporal lobe and right hippocampus, and FLAWS results also showed a lesion in the same area. After automatically detecting HFOs, the top 72% of the channel distribution area of HFOs covered the right hippocampus and amygdala, consistent with the PET-MRI and FLAWS results. Finally, the right hippocampus, right temporal lobe, and the right basis frontalis (little abnormal discharge) of the patient were removed, and the patient was seizure-free after 1 year of follow-up.

Patient #11 (**Figures 4D–F**), a 20-year-old male, had experienced physical convulsions or tonic–clonic seizures for 17 years. The MRI was normal. FLAWS indicated that the right frontal lobe and areas around posterior central sulcus were abnormal, as also detected by HFO analysis. However, due to the ignorance in the importance of using FLAWS and HFOs, and with the purpose of protecting the eloquent cortex, only the right frontal lobe of the patient had been removed, and the central area was not treated. As a result, the patient still had seizures after the surgery.

In addition, we must note that not all lesions are associated with EZs, such as in nodular heterotopia (NH). In this study, patient #1 (**Figure 5**), a 23-year-old man, had been suspected to have gray matter heterotopia in the left medial parietal lobe (near the ventricle), which was obvious both on PET-MRI and FLAWS images. According to the HFO analysis, channels located in this area were not the EZ. This heterotopic area was not removed. However, the patient was still seizure-free 1 year after the surgery.

DISCUSSION

For patients with drug-resistant epilepsy, removal of the EZ provides the best opportunity to eliminate seizures. However, the choice of methods that will accurately locate the EZ in a preoperative evaluation is a challenging problem that determines the success of the operation. This is particularly true for the

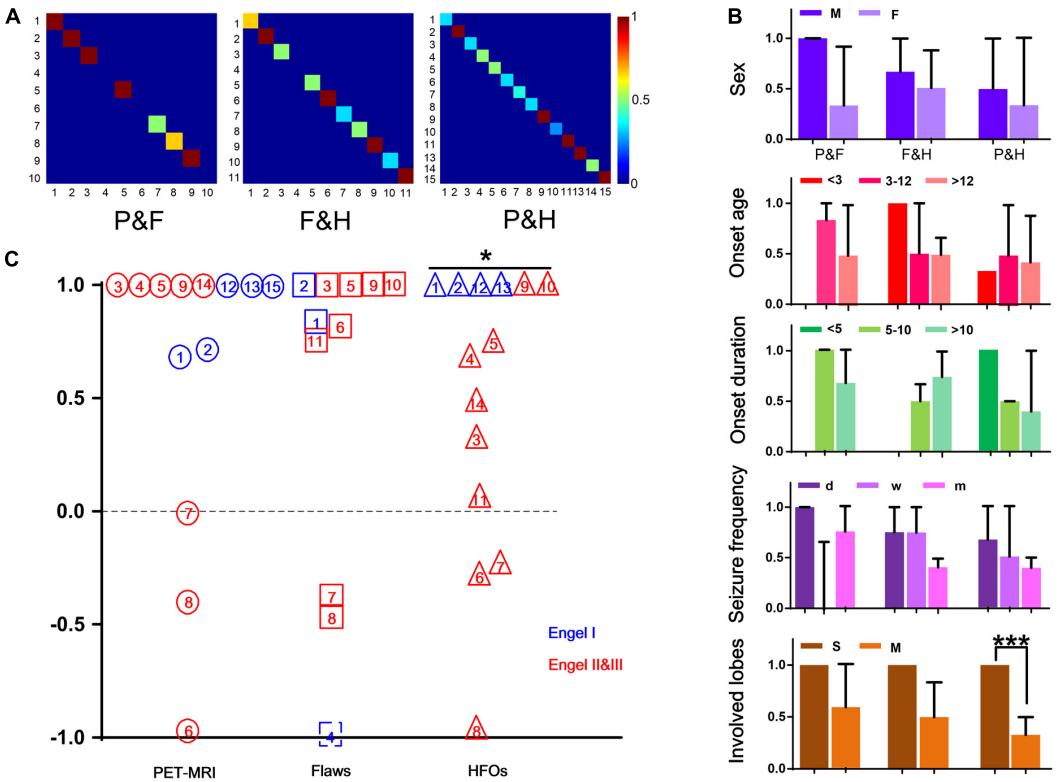

FIGURE 2 | Consistency of the three methods. **(A)** The three images show the consistency of PET-MRI and FLAWS (P&F), FLAWS, and HFOs (F&H), PET-MRI and HFOs (P&H), and colors closer to red indicate better consistency. **(B)** The consistencies in different conditions are shown here. Different colors represent different groups (sex, onset age, onset duration, seizure frequency, and involved lobe). *** $p = 0.001$. **(C)** RatioChann(ev) for each patient obtained using the three methods are listed in this figure. PET-MRI, FLAWS, and HFOs are listed from left to right and are indicated by circles, boxes, and triangles, respectively. The numbers written in the different patterns indicate different patients. Additionally, patients' outcomes are marked in different colors. For patient #4, the FLAWS examination did not identify an abnormality, and the ratio of removal was unable to be determined; therefore, we marked it with an imaginary line. For patient #10, electrodes were not implanted in all suspicious areas marked by PET-MRI, and thus, the patient was excluded from the comparison. *$p < 0.05$.

group of patients with intractable partial epilepsy who do not have an unequivocal, single, focal epileptogenic lesion on MRI (Knowlton, 2006). Multimodal methods formulated to detect the EZ have been published before, but have often focused on common imaging tests such as single-photon emission CT (SPECT), FDG-PET, diffusion tensor imaging (DTI), and so on (Pustina et al., 2015; Perry et al., 2017). When analyzing EEG results, the electrical signals analyzed usually were spikes or those at a low-frequency band. Recently, several new imaging methods have been developed to detect these MRI-invisible lesions, including PET-MRI, FLAWS, and so on. The aim of this study was to compare the accuracy of these methods to localize the EZ. To our knowledge, this clinical investigation is the first to focus on an automated analysis of HFOs, PET-MRI, and FLAWS as a multimodal method to locate the EZ.

As one of the non-invasive methods, FDG-PET is the most established functional imaging modality used to evaluate patients with epilepsy. Presurgical FDG-PET scans of patients with epilepsy are typically performed with the goal of detecting focal areas of decreased metabolism that are presumed to reflect focal functional disturbances in cerebral activity associated with EZs (Knowlton, 2006). With advances in technology, the combination of FDG-PET and MRI exams has been shown to increase the detection of the seizure focus and to improve the outcomes of epilepsy surgery to a greater extent than with either modality

TABLE 2 | Correlation with outcome individually or multimodally.

	Total	Seizure-free	Non-seizure-free	*P* value
PET-MRI areas completely removed?				
Yes	10	4	6	1
No	4	1	3	
FLAWS areas completely removed?				
Yes	6	1	5	1
No	5	1	4	
HFOs areas completely removed?				
Yes	7	5	2	0.007 (**)
No	8	0	8	
(1) Electrodes covering all neuroimaging areas; (2) Completely removing HFOs areas?				
Yes	6	5	1	0.002 (**)
No	9	0	9	

**$p < 0.01$.

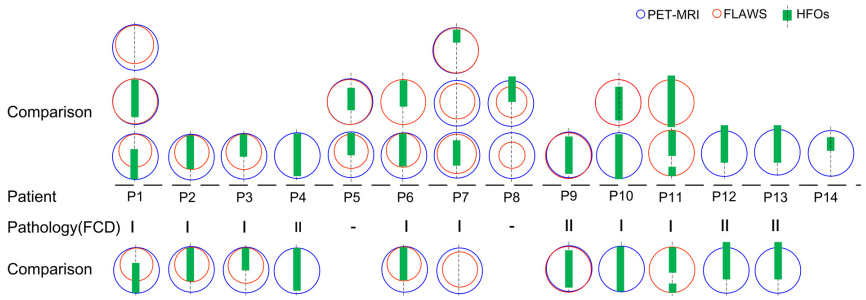

FIGURE 3 | Comparison of HFO-fast ripple (FR) marking and lesions detected by neuroimaging. A comparison of the extent of areas marked using the three methods in 14 patients is shown (patient #15 was not shown as no FR was detected); blue and red circles represent PET-MRI and FLAWS, respectively. Green rectangles represent HFO-FR-marked areas of the implanted electrodes (symbolized by the black imaginary line). Lesions classified as FCD were further compared, and HFO-FR-marked areas even extend beyond the FCD lesion.

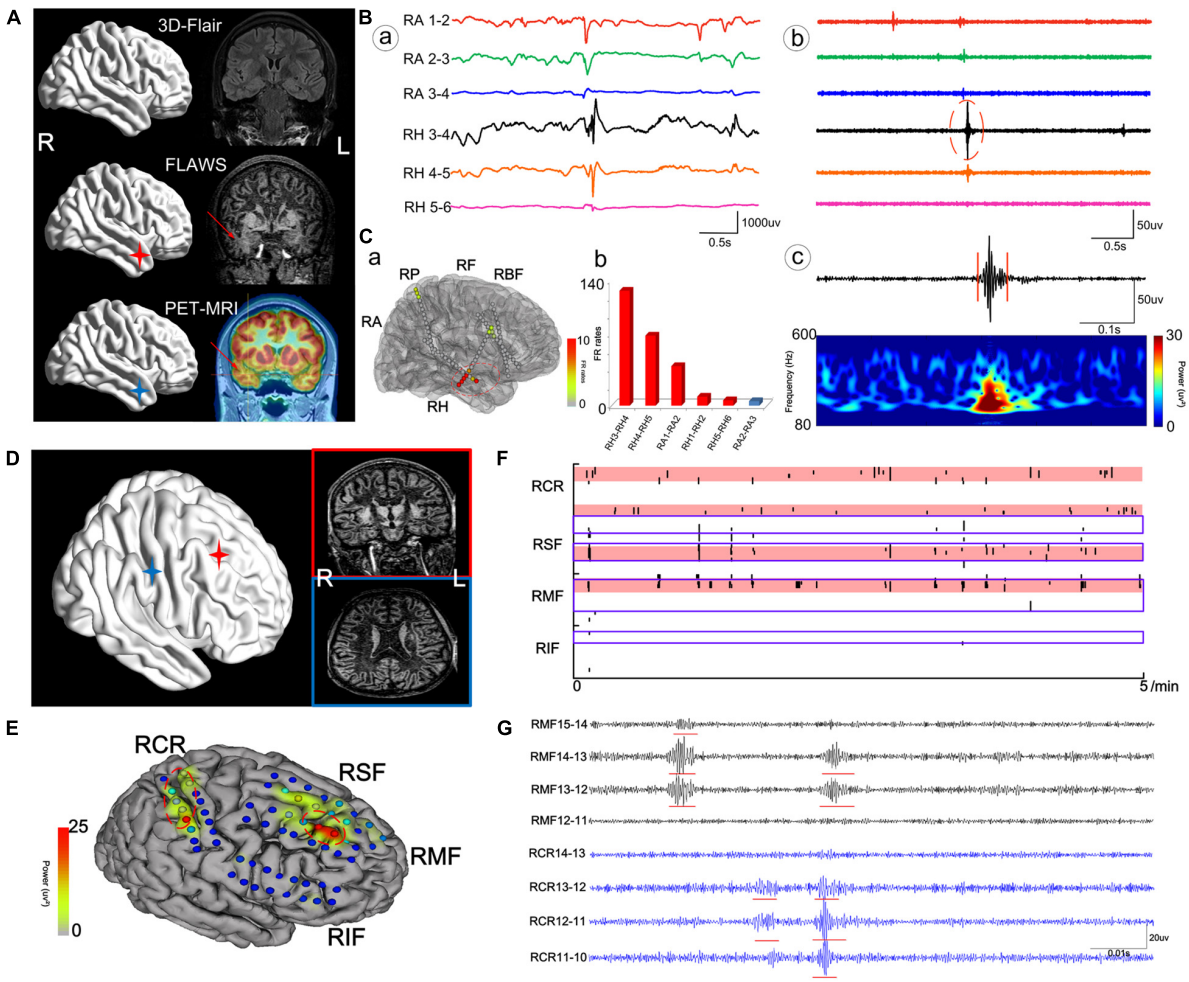

FIGURE 4 | The cases of patient #2 **(A–C)** and patient #11 **(D–G)**. **(A)** The neuroimaging results for patient #2. **(B)** Raw data (a) and intracranial electroencephalogram (iEEG) signal after the bandpass filtering (200–500 Hz) (b) of some meaningful channels. (c) One FR detected using our detector. RA, right amygdala; RH, right hippocampus. **(C)** Results of HFOs shown on the model of the brain of patient #2 (a) and the rank in a descending order according to FR rates (b). The red color marks the suspicious channels indicated by the HFO threshold. RP, right parietal lobe; RF, right frontal lobe; RBF, right basis of frontal lobe. **(D)** The neuroimaging results for patient #11. **(E)** The FR rates shown on the brain model. RCR, right central areas; RSF, right superior frontal lobe; RMF, right mesial frontal lobe; RIF, right inferior frontal lobe. **(F)** The timing of all FRs detected in each channel with our automatic detector during a 5-min iEEG segment. The time and location of each FR are presented as points. The resected area is delineated by the blue line. The pink regions show the EZ confirmed using our quantified threshold. One area marked by HFOs had not been damaged. **(G)** The detectable FRs in different channels. The red arrows indicate the marked abnormal areas.

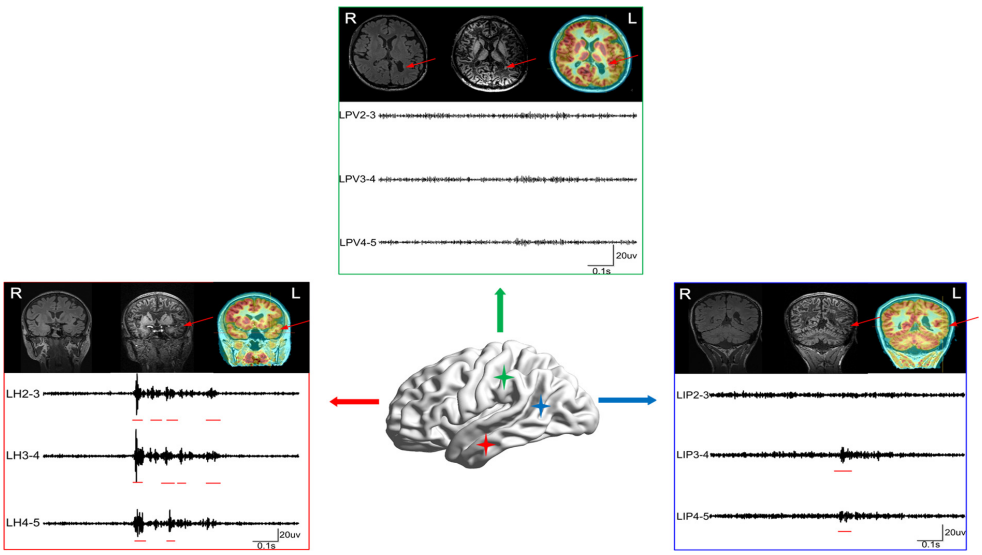

FIGURE 5 | The case of patient #1. Patient #1 was suspected to have gray matter heterotopia in the left medial parietal lobe (near ventricle) based on the MRI result, as the heterotopia was obvious both in PET-MRI and FLAWS. According to the HFO analysis, channels located in this region exhibited greatly fewer FRs than channels in left hippocampus and left posterior temporal region. The three boxes represent three lesions marked using neuroimaging (red arrows) and results of FRs (red lines). LPV, left periventricle; LH, left hippocampus; LIP, left inferior frontal gyrus. The red arrows indicate the marked abnormal areas.

alone (Lee and Salamon, 2009). In particular, new hybrid PET/MR scanners potentially combine the superior soft tissue contrast of MRI and the metabolic characterization of FDG-PET in a single exam, without the need for additional ionizing radiation inherent to PET/CT systems. According to numerous studies, PET-MRI enhances the non-invasive detection of EZ, particularly in patients with subtle lesions (Salamon et al., 2008; Chassoux et al., 2010), as well as in patients with temporal lobe epilepsy (TLE) (Lopinto-Khoury et al., 2012). When the patients' cortical lesions are more clearly identified, this technique enables a more precise localization of the borders of the EZ. However, some critical issues should be carefully addressed before drawing a diagnostic conclusion from a PET/MRI fusion image (Hu et al., 2018). First, the reduction in glucose uptake may be a physiological phenomenon that is irrelevant to epileptogenic seizures. Second, the hypometabolic areas usually appear to be larger than the real EZ because FDG uptake includes a larger area. Last, since some small FCD lesions are located at the bottom of a deep sulcus (Besson et al., 2008), PET-MRI may be insensitive to detect mild hypometabolic changes and, thus, may miss some meaningful areas that generate seizures.

Abnormalities such as FCD are often subtle, and thus, MR sequences that provide optimal contrast between normal and abnormal tissues to detect minor lesions in the cortex are urgently needed. FLAWS is a new method that clearly shows the gray matter by selectively suppressing signals from the CSF and normal white matter. The feature of acquiring two image datasets with different inversion times within the same sequence and head geometry gives the opportunity to create calculated images harnessing specific tissue contrasts, which might be helpful in segmentation algorithms and clinical diagnosis (Tanner et al., 2012). This method has the potential to detect subtle lesions that are amenable to visualization using a conventional MRI. As shown in the study by Chen et al., when the reviewers were blinded to the location of the resected regions, the FCD detection rate of the FLAWS sequence was significantly higher than that of the conventional sequences ($p = 0$) (Chen et al., 2018). However, as proved in our study, this method is only sensitive to lesions located in the cerebral cortex, but not to abnormalities in the hippocampus and other deeper brain structures.

For suspicious lesions detected using neuroimaging, clinicians usually implant intracranial electrodes into the suspicious areas and further evaluate the location of the EZ based on intracranial EEG signals. HFOs have been increasingly recognized as a promising biomarker for locating the EZ, especially for FRs (Wu et al., 2010; Zijlmans et al., 2012; Fedele et al., 2016; Fedele et al., 2017). Jiang et al. (2018) have suggested that the quantitative threshold for FR distribution to delineate the EZ is set to continuously remove at least 72% of the channels from the highest ranking. In this experiment, we used this threshold to locate the EZ. However, not every patient had FRs detected, like the patient #15, in which case ripple results would be referred.

The spatial resolution of HFOs to locate the EZ is significantly more accurate than that of PET-MRI and FLAWS, but our HFO analysis was based on the electrical signals of the intracranial electrodes, making it an invasive examination. The accuracy of localizing the epileptogenic area depended on whether the area in which the intracranial electrode was implanted had covered the entire EZ.

Since each examination has its advantages and disadvantages, a multimodal comparison that combines PET-MRI, FLAWS, and HFOs is strongly recommended to help ensure maximum precision in localizing the EZ. This may overcome the intrinsic limitations of individual modalities, particularly for patients with

a negative MRI and suspicious cortical lesions. First, using non-invasive methods such PET-MRI and FLAWS to detect metabolic changes and structural abnormalities, respectively, clinicians will be able to identify the suspicious areas related to clinical seizure semiology. Then, clinicians can implant electrodes in these areas to monitor electrical signals. According to the HFO results obtained from the intracranial electrodes, clinicians can further pinpoint the optimal boundaries of the EZ and discover some subtle lesions that might be missed by neuroimaging. Finally, overlapping areas identified in the multimodal comparison can be surgically resected.

In our study, the percentage of seizure-free was only 33.33% (5/15), lower than the effective rate reported before. This was because only patients having trouble locating the EZs would undergo these new examinations, and this research was a retrospective study, which meant that the surgery plans were not based on the results. In the future, when the results from multimodal comparing are put into practice, patients will benefit more.

In this study, when we focused on patients' lesions that were verified to be FCD, the HFO-marked area did not completely match the FCD areas. In actuality, the areas of FCD may display different degrees of epileptogenicity, ranging from electrographic silence to interictal epileptic discharges, and an initial involvement in seizure generation. The high variability in the epileptogenicity of these lesions may explain why some patients with FCD become seizure-free, despite an incomplete resection of the lesion (Fauser et al., 2009). We found that HFO-marked areas were more likely to be the margins of the dysplastic cortex and that perilesions of FCD may also be epileptic. This result is consistent with a previous study by Ferrari-Marinho et al. (2015). The occurrence of a high rate of HFOs reflects the epileptic disease activity of the underlying lesion and can be used to evaluate the different grades of epileptogenicity. This tool can help clinicians define the real extent of the EZ beyond the visible lesion observed using neuroimaging.

Compared with FCD, nodular heterotopia appears to be more complex. Nodular heterotopia results from a migration disorder characterized by the ectopic position of neurons that are frequently located along the ventricular walls (periventricular nodular heterotopia, PNH) or in the deep white matter in the form of nodules (subcortical heterotopia) (Barkovich et al., 2012). Most patients with NH suffer from drug-resistant epilepsy, but some do not show seizures (Raymond et al., 1994; Battaglia et al., 1997). In (Jacobs et al., 2009), reported that patients with NH often had SOZ areas outside the lesion, and FRs and spikes were more closely related to SOZ than to the lesion (Jacobs et al., 2009). In (Pizzo et al., 2017), found that only 6% of seizures were purely heterotopic (Pizzo et al., 2017). In (Scholly et al., 2018), recommended a combination of HFO and spike analysis to locate the EZ of PNH (Scholly et al., 2018). Our findings from patient #1 are consistent with these studies and highlight the necessity of combining results from HFO analysis and neuroimaging to analyze EZs.

A limitation of our study is that our study is an exploratory experiment. Consequently, the number of included patients is small. In the future, we will obtain data from more patients to verify the possibility of using the multimodal method to accurately locate the EZ.

DATA AVAILABILITY STATEMENT

The raw data supporting the conclusions of this article will be made available by the authors, without undue reservation.

ETHICS STATEMENT

The studies involving human participants were reviewed and approved by the Ethics Committee of Xuanwu Hospital. Written informed consent to participate in this study was provided by the participants' legal guardian/next of kin.

AUTHOR CONTRIBUTIONS

XL, TY, ZR, XW, and XC analyzed the data. XL, HZ, and XMY wrote and revised the manuscript. All authors contributed to the study and approved the submitted version.

FUNDING

This work was supported by the National Natural Science Foundation of China (81971202, 81671367, 81790653, and 81471391 to XFY) and the Beijing Natural Science Foundation (L182015 to GZ).

ACKNOWLEDGMENTS

We would like to thank Beijing Beike Digital Medical Technology Co., Ltd. for providing strong technical support for the EEG equipment used in this study.

SUPPLEMENTARY MATERIAL

The Supplementary Material for this article can be found online at: https://www.frontiersin.org/articles/10.3389/fnhum.2021.677840/full#supplementary-material

Supplementary Table 1 | Comparing the new and traditional methods' results. Lmp, left medial parietal; Lh, left hippocampus; Lt, left temporal; Lpt, left posterior temporal; Rhmei, Right Hemisphere; Racc, right anterior cingulate cortex; Rmcc, right middle cingulate cortex; Rbf, right basis frontalis; Rt, right temporal; Ri, right insula; Rh, right hippocampus; Ra, right amygdala; Rp, right parietal; Rsp, right superior parietal; Rip, right inferior parietal; Lp, left parietal; Lo, left occipital; Rpt, right posterior temporal; Rf, right frontal; Rcr, right central region; Rcs, Right central sulcus; BiF, bilateral frontal; BiT, bilateral temporal. #, No FR was detected, the results were from ripples.

REFERENCES

Akiyama, T., Mccoy, B., Go, C. Y., Ochi, A., Elliott, I. M., Akiyama, M., et al. (2011). Focal resection of fast ripples on extraoperative intracranial EEG improves seizure outcome in pediatric epilepsy. *Epilepsia* 52, 1802–1811. doi: 10.1111/j.1528-1167.2011.03199.x

Barkovich, A. J., Guerrini, R., Kuzniecky, R. I., Jackson, G. D., and Dobyns, W. B. (2012). A developmental and genetic classification for malformations of cortical development: update 2012. *Brain* 135, 1348–1369. doi: 10.1093/brain/aws019

Battaglia, G., Granata, T., Farina, L., D'incerti, L., Franceschetti, S., and Avanzini, G. (1997). Periventricular nodular heterotopia: epileptogenic findings. *Epilepsia* 38, 1173–1182. doi: 10.1111/j.1528-1157.1997.tb01213.x

Besson, P., Andermann, F., Dubeau, F., and Bernasconi, A. (2008). Small focal cortical dysplasia lesions are located at the bottom of a deep sulcus. *Brain* 131, 3246–3255. doi: 10.1093/brain/awn224

Chassoux, F., Rodrigo, S., Semah, F., Beuvon, F., Landre, E., Devaux, B., et al. (2010). FDG-PET improves surgical outcome in negative MRI Taylor-type focal cortical dysplasias. *Neurology* 75, 2168–2175. doi: 10.1212/wnl.0b013e31820203a9

Chen, X., Qian, T., Kober, T., Zhang, G., Ren, Z., Yu, T., et al. (2018). Gray-matter-specific MR imaging improves the detection of epileptogenic zones in focal cortical dysplasia: a new sequence called fluid and white matter suppression (FLAWS). *Neuroimage Clin.* 20, 388–397. doi: 10.1016/j.nicl.2018.08.010

Chugani, H. T., Shewmon, D. A., Khanna, S., and Phelps, M. E. (1993). Interictal and postictal focal hypermetabolism on positron emission tomography. *Pediatr. Neurol.* 9, 10–15. doi: 10.1016/0887-8994(93)90003-u

Erickson, K. I., Leckie, R. L., and Weinstein, A. M. (2014). Physical activity, fitness, and gray matter volume. *Neurobiol. Aging* 35 Suppl 2, S20–S28.

Fauser, S., Sisodiya, S. M., Martinian, L., Thom, M., Gumbinger, C., Huppertz, H. J., et al. (2009). Multi-focal occurrence of cortical dysplasia in epilepsy patients. *Brain* 132, 2079–2090.

Fedele, T., Burnos, S., Boran, E., Krayenbuhl, N., Hilfiker, P., Grunwald, T., et al. (2017). Resection of high frequency oscillations predicts seizure outcome in the individual patient. *Sci. Rep.* 7:13836.

Fedele, T., Van 'T Klooster, M., Burnos, S., Zweiphenning, W., Van Klink, N., Leijten, F., et al. (2016). Automatic detection of high frequency oscillations during epilepsy surgery predicts seizure outcome. *Clin. Neurophysiol.* 127, 3066–3074. doi: 10.1016/j.clinph.2016.06.009

Ferrari-Marinho, T., Perucca, P., Mok, K., Olivier, A., Hall, J., Dubeau, F., et al. (2015). Pathologic substrates of focal epilepsy influence the generation of high-frequency oscillations. *Epilepsia* 56, 592–598. doi: 10.1111/epi.12940

Frauscher, B., Bartolomei, F., Kobayashi, K., Cimbalnik, J., Van 'T Klooster, M. A., Rampp, S., et al. (2017). High-frequency oscillations: the state of clinical research. *Epilepsia* 58, 1316–1329.

Fujiwara, H., Leach, J. L., Greiner, H. M., Holland-Bouley, K. D., Rose, D. F., Arthur, T., et al. (2016). Resection of ictal high frequency oscillations is associated with favorable surgical outcome in pediatric drug resistant epilepsy secondary to tuberous sclerosis complex. *Epilepsy Res.* 126, 90–97. doi: 10.1016/j.eplepsyres.2016.07.005

Gautam, P., Nunez, S. C., Narr, K. L., Kan, E. C., and Sowell, E. R. (2014). Effects of prenatal alcohol exposure on the development of white matter volume and change in executive function. *Neuroimage Clin.* 5, 19–27. doi: 10.1016/j.nicl.2014.05.010

Gliske, S. V., Irwin, Z. T., Chestek, C., Hegeman, G. L., Brinkmann, B., Sagher, O., et al. (2018). Variability in the location of high frequency oscillations during prolonged intracranial EEG recordings. *Nat. Commun.* 9:2155.

Grieve, S. M., Korgaonkar, M. S., Koslow, S. H., Gordon, E., and Williams, L. M. (2013). Widespread reductions in gray matter volume in depression. *Neuroimage Clin.* 3, 332–339. doi: 10.1016/j.nicl.2013.08.016

Holler, Y., Kutil, R., Klaffenbock, L., Thomschewski, A., Holler, P. M., Bathke, A. C., et al. (2015). High-frequency oscillations in epilepsy and surgical outcome. A meta-analysis. *Front. Hum. Neurosci.* 9:574.

Hu, W. H., Wang, X., Liu, L. N., Shao, X. Q., Zhang, K., Ma, Y. S., et al. (2018). Multimodality image post-processing in detection of extratemporal mri-negative cortical dysplasia. *Front. Neurol.* 9:450.

Hur, Y. J., Lee, J. S., Lee, J. D., Yun, M. J., and Kim, H. D. (2013). Quantitative analysis of simultaneous EEG features during PET studies for childhood partial epilepsy. *Yonsei. Med. J.* 54, 572–577. doi: 10.3349/ymj.2013.54.3.572

Jacobs, J., Levan, P., Chatillon, C. E., Olivier, A., Dubeau, F., and Gotman, J. (2009). High frequency oscillations in intracranial EEGs mark epileptogenicity rather than lesion type. *Brain* 132, 1022–1037. doi: 10.1093/brain/awn351

Jacobs, J., Zijlmans, M., Zelmann, R., Chatillon, C. E., Hall, J., Olivier, A., et al. (2010). High-frequency electroencephalographic oscillations correlate with outcome of epilepsy surgery. *Ann. Neurol.* 67, 209–220. doi: 10.1002/ana.21847

Jerome Engel, J. (2016). *Outcome With Respect to Seizure*. Hoboken NJ: Wiley Blavkwell.

Jiang, C., Li, X., Yan, J., Yu, T., Wang, X., Ren, Z., et al. (2018). Determining the quantitative threshold of high-frequency oscillation distribution to delineate the epileptogenic zone by automated detection. *Front. Neurol.* 9:889.

Knowlton, R. C. (2006). The role of FDG-PET, ictal SPECT, and MEG in the epilepsy surgery evaluation. *Epilepsy Behav.* 8, 91–101. doi: 10.1016/j.yebeh.2005.10.015

Lee, K. K., and Salamon, N. (2009). [18F] fluorodeoxyglucose-positron-emission tomography and MR imaging coregistration for presurgical evaluation of medically refractory epilepsy. *AJNR Am. J. Neuroradiol.* 30, 1811–1816. doi: 10.3174/ajnr.a1637

Lopinto-Khoury, C., Sperling, M. R., Skidmore, C., Nei, M., Evans, J., Sharan, A., et al. (2012). Surgical outcome in PET-positive, MRI-negative patients with temporal lobe epilepsy. *Epilepsia* 53, 342–348. doi: 10.1111/j.1528-1167.2011.03359.x

Paldino, M. J., Yang, E., Jones, J. Y., Mahmood, N., Sher, A., Zhang, W., et al. (2017). Comparison of the diagnostic accuracy of PET/MRI to PET/CT-acquired FDG brain exams for seizure focus detection: a prospective study. *Pediatr. Radiol.* 47, 1500–1507. doi: 10.1007/s00247-017-3888-8

Perry, M. S., Bailey, L., Freedman, D., Donahue, D., Malik, S., Head, H., et al. (2017). Coregistration of multimodal imaging is associated with favourable two-year seizure outcome after paediatric epilepsy surgery. *Epileptic Disord* 19, 40–48. doi: 10.1684/epd.2017.0902

Pizzo, F., Roehri, N., Catenoix, H., Medina, S., Mcgonigal, A., Giusiano, B., et al. (2017). Epileptogenic networks in nodular heterotopia: a stereoelectroencephalography study. *Epilepsia* 58, 2112–2123. doi: 10.1111/epi.13919

Pustina, D., Avants, B., Sperling, M., Gorniak, R., He, X., Doucet, G., et al. (2015). Predicting the laterality of temporal lobe epilepsy from PET. MRI, and DTI: A multimodal study. *Neuroimage Clin.* 9, 20–31. doi: 10.1016/j.nicl.2015.07.010

Raymond, A. A., Fish, D. R., Stevens, J. M., Sisodiya, S. M., Alsanjari, N., and Shorvon, S. D. (1994). Subependymal heterotopia: a distinct neuronal migration disorder associated with epilepsy. *J. Neurol. Neurosurg. Psychiatry* 57, 1195–1202. doi: 10.1136/jnnp.57.10.1195

Ren, G. P., Yan, J. Q., Yu, Z. X., Wang, D., Li, X. N., Mei, S. S., et al. (2018). Automated detector of high frequency oscillations in epilepsy based on maximum distributed peak points. *Int. J. Neural. Syst.* 28:1750029. doi: 10.1142/s0129065717500290

Rosenow, F., and Luders, H. (2001). Presurgical evaluation of epilepsy. *Brain* 124, 1683–1700.

Salamon, N., Kung, J., Shaw, S. J., Koo, J., Koh, S., Wu, J. Y., et al. (2008). FDG-PET/MRI coregistration improves detection of cortical dysplasia in patients with epilepsy. *Neurology* 71, 1594–1601. doi: 10.1212/01.wnl.0000334752.41807.2f

Schick, F. (2016). Tissue segmentation: a crucial tool for quantitative MRI and visualization of anatomical structures. *Magma* 29, 89–93. doi: 10.1007/s10334-016-0549-0

Scholly, J., Pizzo, F., Timofeev, A., Valenti-Hirsch, M. P., Ollivier, I., Proust, F., et al. (2018). High-frequency oscillations and spikes running down after SEEG-guided thermocoagulations in the epileptogenic network of periventricular nodular heterotopia. *Epilepsy Res.* 150, 27–31. doi: 10.1016/j.eplepsyres.2018.12.006

Shang, K., Wang, J., Fan, X., Cui, B., Ma, J., Yang, H., et al. (2018). Clinical value of hybrid tof-pet/mr imaging-based multiparametric imaging in localizing seizure focus in patients with mri-negative temporal lobe epilepsy. *AJNR Am. J. Neuroradiol.* 39, 1791–1798. doi: 10.3174/ajnr.a5814

Soares, B. P., Porter, S. G., Saindane, A. M., Dehkharghani, S., and Desai, N. K. (2016). Utility of double inversion recovery MRI in paediatric epilepsy. *Br. J. Radiol.* 89:20150325. doi: 10.1259/bjr.20150325

Sun, K., Cui, J., Wang, B., Jiang, T., Chen, Z., Cong, F., et al. (2018). Magnetic resonance imaging of tuberous sclerosis complex with or without epilepsy at 7 T. *Neuroradiology* 60, 785–794. doi: 10.1007/s00234-018-2040-2

Tanner, M., Gambarota, G., Kober, T., Krueger, G., Erritzoe, D., Marques, J. P., et al. (2012). Fluid and white matter suppression with the MP2RAGE sequence. *J. Magn. Reson. Imaging* 35, 1063–1070. doi: 10.1002/jmri.23532

Wang, Y., Wang, Y., Zhang, Z., Xiong, Y., Zhang, Q., Yuan, C., et al. (2018). Segmentation of gray matter, white matter, and CSF with fluid and white matter suppression using MP2RAGE. *J. Magn. Reson. Imaging* 48, 1540–1550. doi: 10.1002/jmri.26014

Wu, J. Y., Sankar, R., Lerner, J. T., Matsumoto, J. H., Vinters, H. V., and Mathern, G. W. (2010). Removing interictal fast ripples on electrocorticography linked with seizure freedom in children. *Neurology* 75, 1686–1694. doi: 10.1212/wnl.0b013e3181fc27d0

Zijlmans, M., Jiruska, P., Zelmann, R., Leijten, F. S., Jefferys, J. G., and Gotman, J. (2012). High-frequency oscillations as a new biomarker in epilepsy. *Ann. Neurol.* 71, 169–178. doi: 10.1002/ana.22548

Conflict of Interest: XZ was employed by the company Siemens Healthcare.

The remaining authors declare that the research was conducted in the absence of any commercial or financial relationships that could be construed as a potential conflict of interest.

frontiers in Human Neuroscience

ORIGINAL RESEARCH
published: 08 June 2021
doi: 10.3389/fnhum.2021.624620

Ictal Occurrence of High-Frequency Oscillations Correlates With Seizure Severity in a Rat Model of Temporal Lobe Epilepsy

Nadja Birk[1], *Jan Schönberger*[1,2,3], *Karin Helene Somerlik-Fuchs*[2], *Andreas Schulze-Bonhage*[2] *and Julia Jacobs*[1,4,5]*

[1]Department of Neuropediatrics and Muscle Disorders, Medical Center—University of Freiburg, Freiburg, Germany, [2]Epilepsy Center, Medical Center—University of Freiburg, Freiburg, Germany, [3]Berta-Ottenstein-Programme, Faculty of Medicine, University of Freiburg, Freiburg, Germany, [4]Department of Paediatrics and Department of Neuroscience, Cumming School of Medicine, University of Calgary, Calgary, AB, Canada, [5]Hotchkiss Brain Institute and Alberta Children's Hospital Research Institute, University of Calgary, Calgary, AB, Canada

OPEN ACCESS

Edited by:
Xiaofeng Yang,
Bioland Laboratory, China

Reviewed by:
Tohru Okanishi,
Tottori University, Japan
Chunyan Liu,
Capital Medical University, China
Eishi Asano,
Children's Hospital of Michigan,
United States

***Correspondence:**
Julia Jacobs
julia.jacobs@gmx.de

Specialty section:
This article was submitted to Brain Imaging and Stimulation, a section of the journal Frontiers in Human Neuroscience

Received: 31 October 2020
Accepted: 16 April 2021
Published: 08 June 2021

Citation:
Birk N, Schönberger J, Somerlik-Fuchs KH, Schulze-Bonhage A and Jacobs J (2021) Ictal Occurrence of High-Frequency Oscillations Correlates With Seizure Severity in a Rat Model of Temporal Lobe Epilepsy. Front. Hum. Neurosci. 15:624620. doi: 10.3389/fnhum.2021.624620

High-frequency oscillations (HFOs, ripples 80–250 Hz, fast ripples 250–500 Hz) are biomarkers of epileptic tissue. They are most commonly observed over areas generating seizures and increase in occurrence during the ictal compared to the interictal period. It has been hypothesized that their rate correlates with the severity of epilepsy and seizure in affected individuals. In the present study, it was aimed to investigate whether the HFO count mirrors the observed behavioral seizure severity using a kainate rat model for temporal lobe epilepsy. Seizures were selected during the chronic epilepsy phase of this model and classified by behavioral severity according to the Racine scale. Seizures with Racine scale 5&6 were considered generalized and severe. HFOs were marked in 24 seizures during a preictal, ictal, and postictal EEG segment. The duration covered by the HFO during these different segments was analyzed and compared between mild and severe seizures. HFOs were significantly increased during ictal periods ($p < 0.001$) and significantly decreased during postictal periods ($p < 0.03$) compared to the ictal segment. Ictal ripples ($p = 0.04$) as well as fast ripples ($p = 0.02$) were significantly higher in severe seizures compared to mild seizures. The present study demonstrates that ictal HFO occurrence mirrors seizure severity in a chronic focal epilepsy model in rats. This is similar to recent observations in patients with refractory mesio-temporal lobe epilepsy. Moreover, postictal HFO decrease might reflect postictal inhibition of epileptic activity. Overall results provide additional evidence that HFOs can be used as biomarkers for measuring seizure severity in epilepsy.

Keywords: high frequency oscillations, epileptic seizures, seizure severity, Racine scale, mesio-temporal epilepsy

INTRODUCTION

High-frequency oscillations (HFOs) between 80 and 500 Hz are biomarkers for epileptic tissue. They were described recorded with intracranial microelectrodes and closely linked to mesio-temporal structures that generated spontaneous seizures (Bragin et al., 1999). Later, it could be shown that both ripples (80–250 Hz) and fast ripples (250–500 Hz) were linked to the seizure onset zone (SOZ) in patients with refractory epilepsy (for review, see Frauscher et al., 2017). Moreover, surgical removal of HFO-generating areas was associated with a higher likelihood of seizure freedom after epilepsy surgery (Jacobs et al., 2010, 2018; Wu et al., 2010). Most of the studies investigating whether HFOs could help to localize epileptic tissue focused on the analysis of interictal HFOs. However, ictal gamma oscillations and HFOs can also be identified during epileptic seizures (Jirsch et al., 2006; Jacobs et al., 2009; Weiss et al., 2015; Smith et al., 2020). It is known that HFO activity increases during seizures and that this increase is most prominent in the SOZ (Jirsch et al., 2006; Weiss et al., 2013). Studies have also tried to find systematic HFO increases prior to the seizure onset; however, results are currently conflicting (Jirsch et al., 2006; Khosravani et al., 2009; Jiruska et al., 2017), and no systematic approach for seizure prediction could be found using HFOs. It could also be shown that HFOs increase systematically at seizure onset independent of the seizure onset pattern and etiology (Perucca et al., 2014).

In the recent decade, increasing evidence was found that HFOs not only can be used to localize epileptic activity but also can directly reflect seizure propensity and disease severity in patients with epilepsy (Zijlmans et al., 2009). Thus, successful treatment with various antiepileptic drugs resulted in HFO reduction in patients as well as rodent animal models (for review, see Lévesque et al., 2018). HFO occurrence can be used as a predictor of seizure severity in several pediatric epilepsy syndromes (Kobayashi et al., 2015; van Klink et al., 2016). We could show that HFO occurrence around the seizure could mirror seizure severity in patients with mesio-temporal lobe epilepsy (Schönberger et al., 2019). However, in patients with mesio-temporal epilepsy, clinical assessment of seizure severity is challenged by the large variability of observed seizures. Seizure classifications successfully distinguish between seizure with and without secondary bilateral involvement, but no simple scale can be applied to assess seizure severity in patients.

The kainate rat model is an animal model for mesio-temporal epilepsy that allows studying chronic epilepsy with seizures of varying severity in a controlled environment (for review, see Lévesque and Avoli, 2013). The kainate injection provokes neuronal loss and cell dispersion resembling hippocampal sclerosis as seen in patients with temporal lobe epilepsy (Suzuki et al., 1995).

Observed spontaneous seizures show very similar semiology as in patients and can be classified, according to a modified Racine scale, into six different degrees of clinical seizure severity depending on semiology (Racine, 1972). We investigate HFO occurrence during the preictal, ictal, and postictal periods in rats with focal mesio-temporal epilepsy and hypothesized that seizure severity is mirrored by HFO occurrence.

MATERIALS AND METHODS

Animal Selection and Preparation

Adult female and male Wistar rats (250–350 g, <1 year) were used for this study. All procedures described in this study were approved by the Institutional Animal Care and Use Committee of the University of Freiburg, and experiments were performed in accordance with the relevant guidelines and regulations. It is important to note that the presented dataset was used retrospectively, and animals were originally undergoing these experiments for a separate project.

Kainate Injection and Implantation of Intracranial Electrodes

Animals were anesthetized with ketamine (100 mg/kg), xylacine (3 mg/kg), and atropine (0.1 mg/kg) and fixed into a stereotactic frame. A guide cannula was implanted into the right posterior hippocampus with the following stereotactic coordinates: AP −5.5 L −4.8 V −5.0 with regard to Bregma. Kainic acid was injected into the hippocampus by means of a Hamilton syringe, applying 0.4 μg/0.1 μl continuously over 1 min. Established status was confirmed by EEG recordings. Status epilepticus was interrupted after 2 h using diazepam.

This was followed by implanting a recording electrode with a depth of 6.5 mm, resulting in the four contacts of the electrode surrounding the region of kainate injection (see **Figure 1A** for electrode placement). The electrode consisted of 125-μm-thick Teflon-coated stainless-steel wires, which were twisted to a tetrode. The active electrode surfaces at the tips were approximately aligned with a distance of 0.5 mm between outer and inner contacts, and 1.0 mm between the two inner contacts. In addition, a single Teflon-coated tungsten wire (60-μm diameter) was used as a reference electrode, whereas the ground electrode was realized by a miniature screw placed in the skull. Prior to implantation, all electrodes were characterized by an impedance analyzer with electrochemical interface (Solartron 1260 and 1287, Farnborough Hampshire, UK) to ensure similar electrical characteristics.

Three more electrodes were implanted in the right hippocampus posterior and anterior to the injection side, and four symmetrical electrodes were implanted into the contralateral hippocampus. All electrodes were placed with their tip in the hippocampus, and only hippocampal structures were covered by the recording. The reference and ground electrodes were placed 1 mm posterior to the lambdoid suture. Electrodes were connected to the head box, and the head box was fixated on the skull using dental cement. Two hours after kainate injection, status epilepticus was interrupted by applying diazepam intraperitoneally (Somerlik et al., 2011).

At the end of the electrophysiological experiments, rats were deeply anesthetized and perfused with 2.5% paraformaldehyde. Brains were removed and placed in 2.5% paraformaldehyde for at least 48 h before histological sectioning and Nissl staining. The

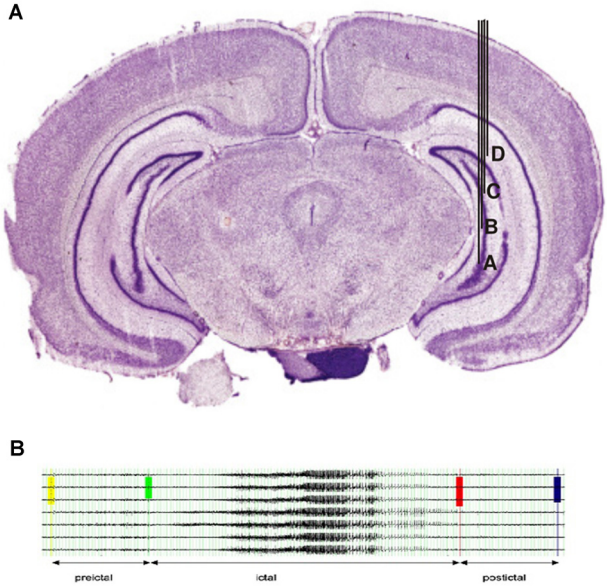

FIGURE 1 | (A) Localization of electrodes in the right hippocampus. Injection of kainate acid was placed between contacts (B&C). **(B)** Example for the selection of EEG segments in a typical seizure.

correct position of the electrodes was verified by histology after the animals were sacrificed.

Recording of Video and EEG Data

Video recordings were performed continuously for the duration of the study and screened for seizure activity on a daily basis. An EEG recording was added 72 h after implantation to allow for a postsurgical rest period for the animals. Recording devices were place on the animal's head in a way that allowed free range of movements. EEG was recorded using MPA81 recording boxes and PGA32 amplifiers (Multi Channel Systems, Reutlingen, Deutschland). The sampling rate was set at 10,000 Hz. Recording of data as well as later analysis for seizures was performed using Spike2 (Cambridge Electronic Design, Cambridge, England). This software was also used for synchronization between video and EEG recordings. Both EEG and video recordings were visually screened for seizure occurrence on a daily basis.

Behavioral Analysis of Spontaneous Seizures

Rats were included in the current analysis if they showed regular spontaneous seizure after status epilepticus and if they had at least three seizures with mild symptoms (Racine 1–4) and three seizures with severe symptoms (Racine 5&6; Racine, 1972).

Racine scales were used according to Besio et al. (2007) as follows: $R = 0$, no motor seizure activity; $R = 1$, eye closure and masticatory movements; $R = 2$, head nodding; $R = 3$, mild forelimb clonus; $R = 4$, clonus with rearing; $R = 5$, clonus with rearing and falling; and $R = 6$, wild running fit during seizure. Scoring of Racine scales was conducted by two independent reviewers, and seizures were excluded if the reviewers did not agree on scoring.

Seizures were selected according to the following criteria: 4 weeks with regular seizure activity were selected after the time of established regular seizures. In this period, the first seizure of each Racine scale was selected for each week, resulting in a maximum of 24 selected seizures per rat (4 weeks with 6 seizure types maximum). Seizures had to be at least 15 min apart from each other to be selected. All EEG samples of seizures were screened for artifacts prior to applying the high pass filer. As we were only analyzing the two contacts of an intracranial electrode that was lying deep within the hippocampus, artifacts were usually not visible even during severe seizures. Seizures with substantial artifacts have been excluded from the analysis. **Figure 1B** shows the exemplary selection of seizures for rat 1.

EEG and HFO Analysis of Seizures

EEG data were converted from the SPIKE2 format to Harmonie Monitoring System (Stellate, Montreal, QC, Canada) for the analysis of the HFO activity. Conversion was performed using the ASA software (ANT Neuro HQ, Enschede, Netherlands), as has been described in previous publications (Kuhnke et al., 2019). Two independent reviewers selected the time of seizure onset and seizure termination for all seizure periods; in cases of disagreement, seizures were discussed together to find a consensus. For each seizure, a 30-s segment directly prior to seizure onset, the whole ictal period, and a 30-s postictal segment were selected for analysis. Seizure onset and termination time were defined using the EEG recording. Seizure onset was set at the first visible ictal activity, which consisted of a high amplitude spike followed by rhythmic spiking activity in our model. Seizure termination was defined as the end of rhythmic activity in conjunction with EEG suppression. EEG analysis was performed using a bipolar montage connecting the two contacts of each electrode. Prior to filtering and HFO analysis, all segments with large and/or continuous artifacts were excluded.

All ictal HFO analysis was performed visually by two independent reviewers. Only events marked by both reviewers were used for the following analysis. In cases in which one of the events was marked differently, only the part of the event identified by both reviewers was taken into account.

For HFO identification, we used previously published criteria and methods (Zijlmans et al., 2017). The display of the computer screen was split vertically to display EEG data high-pass-filtered with 80 Hz (FIR) in the left and high-pass-filtered with 250 Hz on the right. Data were displayed with maximal temporal resolution (0.4 s per page), and the amplitude was increased to 1.5–2 μV/mm. Ripples were marked if an event was visible on the left but not on the right side of the screen. Fast ripples were marked if seen on the right side. Oscillations had to have a minimum of four oscillatory components. Additionally, all ictal spikes as visible on the unfiltered EEG were marked.

Statistical Analysis of Marked HFO

For each channel, an in-house Matlab (Mathworks, Natick, MA, USA) based program was used to calculate the number of seconds occupied by the HFO per minute for each channel for each of the seizure segments (preictal, ictal, postictal). This resulted in seconds per minute of time covered by the HFO for each segment

and each channel. This measure will be referred to as the HFO ratio in the Results section. We selected this measure as seizures were longer with increasing severity, and thus, we felt it was important to use a measure independent of the seizure length.

Different seizure segments were compared between mild seizures (Racine 1–4) and severe seizures (Racine 5&6) in regard seconds per minute of time covered by the HFO. As data were not normally distributed, a Wilcoxon rank sum test was performed for comparison between different seizure severities. The significance level was $p < 0.05$.

RESULTS

Occurrence of Spontaneous Seizures Across Animals

In total, 12 rats underwent the described experiments, which were also conducted as part of another research question. No rat died during status epilepticus or during the following observation period; two rats died during the anesthesia process and preparation prior to status epilepticus.

Six of these rats developed regular seizures after 4–8 weeks of observation after status epilepticus. Only two rats (both female) expressed seizures with both severe and mild Racine scores. Rat 1 had 232 nonsevere and 55 severe seizures; rat 9 had 42 nonsevere and 55 severe seizures within the 4-week analyzed period. Overall, time to regular seizures was long with 264 days after status epilepticus in rat 1 and 266 days in rat 2. All seizures observed in the study started over the most interior to contacts of the hippocampal electrode ipsilateral to the kainite injection site.

A total of 151 EEG channels were analyzed during 24 seizures with different Racine states. Three seizures were scored Racine 2 (two from rat 1, one from rat 9), six seizures were scored Racine 3 (three from each rat), and five seizures were scored Racine 4 (three from rat 1, two from rat 9). As all of these seizures met the criteria for focal seizure activity, they were considered mild. Six seizures were scored Racine 5 (three from each rat), and four seizures were scored Racine 6 (two from each rat). Therefore, 10 seizures were categorized as severe.

Comparison of HFO Occurrence Between Different Seizure Periods

The ratio of ripples and fast ripples was significantly higher during ictal than preictal periods ($p < 0.0001$, $n = 24$). The median duration covered increased by 150% for ictal ripples and by 300% for fast ripples compared to the preictal period. The ratios of ripples and fast ripples significantly decreased in the postictal phase in contrast to the preictal and ictal phases [$p < 0.03$, ($n = 24$)]. The median duration covered decreased by 75% for ripples and 95% for fast ripples in the postictal period compared to the ictal period. A 37% reduction was seen for ripple coverage and 80% for fast ripple coverage when comparing postictal to preictal periods. **Figure 2** demonstrates covered time per minute for ripples and fast ripples during the different seizure periods.

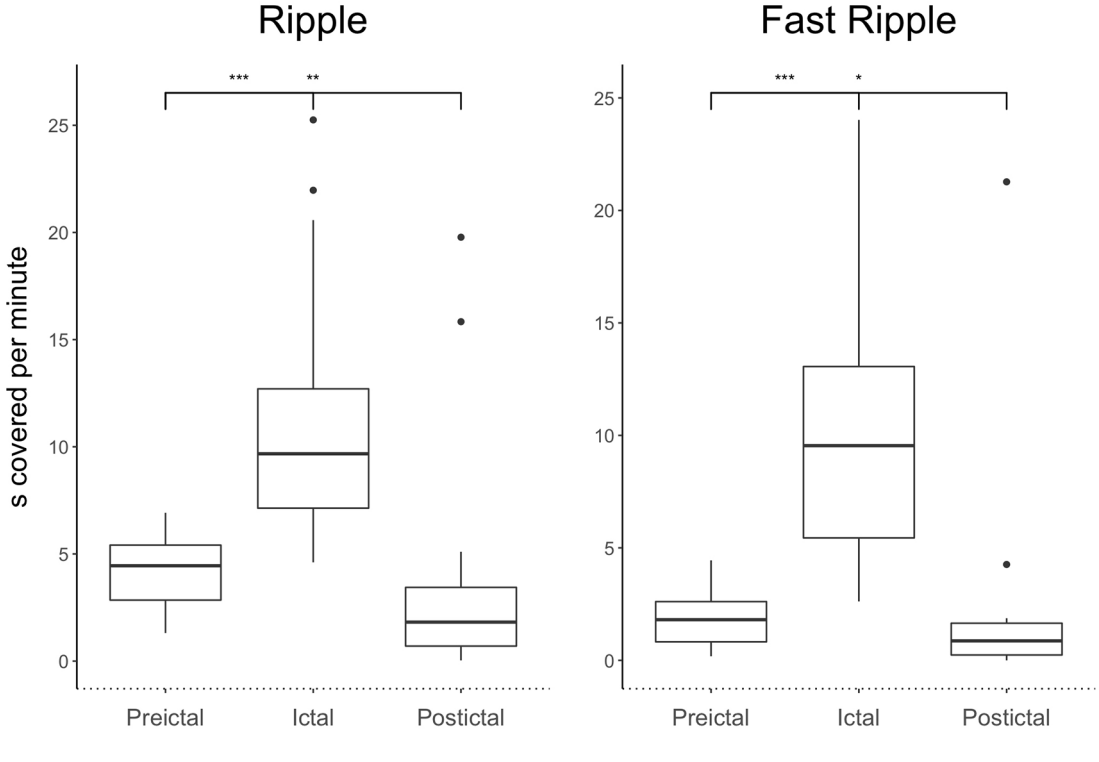

FIGURE 2 | Significant ictal increase in ripples and fast ripples compared to the preictal phase as well as significant postictal decrease across all types of seizure severity. All stars indicate significance *p*, 0.05.

Comparison of HFO Occurrence Between Mild and Severe Seizures

Ripples ratios were significantly higher during the seizure when comparing mild with severe seizures (p = 0.04, n = 10 for severe seizures, n = 14 for mild seizures; see **Figure 3A**). No difference was seen for the preictal and postictal phases.

Fast ripple ratios also were higher during the ictal period during severe compared to mild seizures (p = 0.02, n = 10 for severe seizures, n = 14 for mild seizures). Again, no differences during the preictal and postictal periods were seen for the different seizure strengths (see **Figure 3B**).

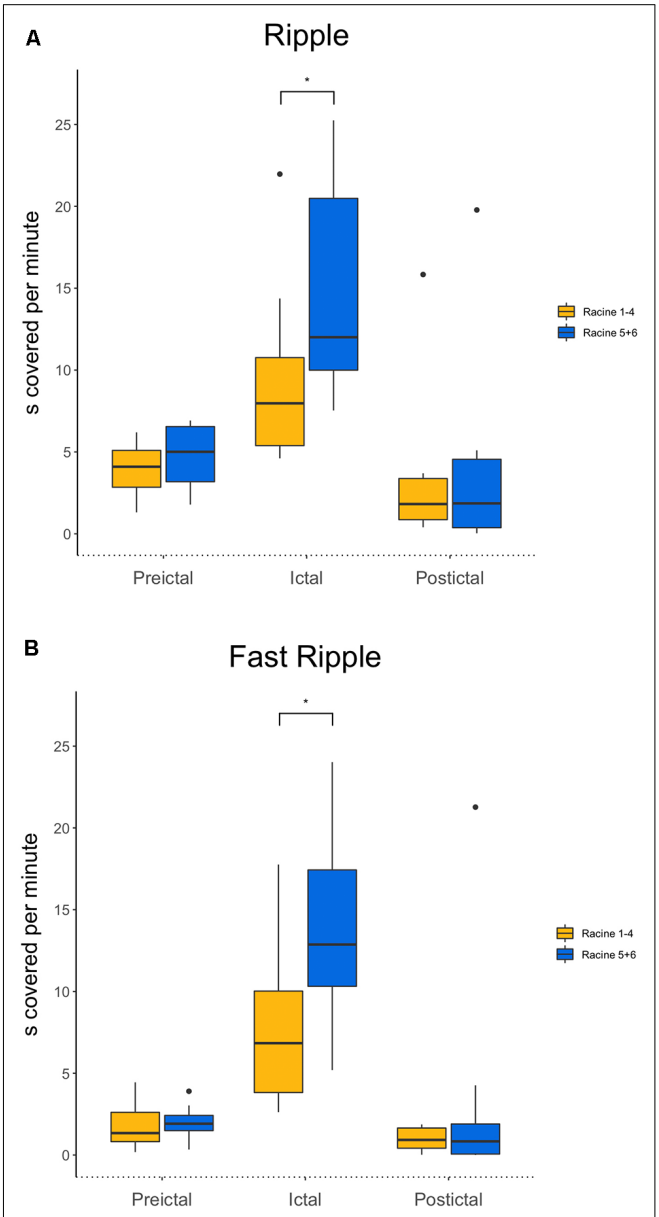

FIGURE 3 | (A) Comparison of ripples between mild and strong seizures for all three phases. Ictal ripple occurrence is significantly higher in stronger seizures. **(B)** Comparison of fast ripples between mild and strong seizures for all three phases. Ictal fast ripple occurrence is significantly higher in stronger seizures. *$p < 0.05$.

Analysis of HFO Occurrence in Individual Rats

We repeated the statistical analysis for each rat separately. Rat 1 had 232 nonsevere and 55 severe seizures, and rat 9 had 42 nonsevere and 55 severe seizures within the 4-week analyzed period. The ripple ratio was significantly higher in ictal than preictal periods (rat 1: $p < 0.001$, N = 28, Rat 2: $p < 0.008$, N = 20). Postictal segments had significantly lower ripple ratios than ictal (Rat 1: $p < 0.001$ N = 28, Rat 2: p = 0.04, N = 20) and preictal (Rat 1: $p < 0.001$, N = 28, Rat 2: p = 0.02, N = 24) periods. The fast ripple ratio was significantly higher in ictal than preictal segments (Rat 1: $p < 0.001$ N = 28, Rat 2: p = 0.007, N = 24) and significantly lower in postictal compared to preictal (Rat 1: $p < 0.001$, N = 28, Rat 2: p = 0.01, N = 24). The ripple ratio was significantly larger in both rats for severe compared to mild seizures (Rat 1: p = 0.04 N = 42, Rat 2: p = 0.03 N = 30); no difference was found for fast ripples.

DISCUSSION

Result Summary

The present study confirms our hypothesis that HFOs reflect seizure severity and ictal behavior in seizures generated over the hippocampus. HFOs were significantly more frequent during the ictal than the interictal period. After the seizure, a significant suppression of HFOs was seen. In the ictal period, HFOs were significantly higher in seizures with clinical symptoms of generalization than in those that stayed focal with mild symptoms. No difference between different seizure severities in HFO occurrence was seen in the pre- or postictal period.

Limitations

Kainate Model Limitations and Behavioral Analysis of Seizures

In the focal kainate rat model, around 60% to 80% of animals develop spontaneous seizures after a latency period of 15–10 days (Drexel et al., 2012). The majority of these animals should enter a phase of stable chronic epilepsy with regular nonconvulsive seizures around 3 months after initial status epilepticus (Lévesque and Avoli, 2013). All of our animals were observed after status, but only two reached the stadium of chronic epilepsy with regular seizures, which is a limitation of the present study. The success rate of this experiment is largely dependent on the kainate dose as well as the length of status epilepticus. We chose our approach according to previous literature, but success rates might be increased by choosing a high kainate dose in the future (Williams et al., 2009). While we had many EEG channels and seizures to analyze in this analysis, the fact that these all arrived from few animals might reduce the ability to generalize results in the same way as would be possible with more animals that had seizures. We feel, however, that this should not affect the most important information in this study, which is comparing

clinically severe to mild seizures, as we analyzed a larger number of seizures.

A rat model can always only approximate epilepsy as it occurs in patients. The kainate model used in this study is considered comparable to human temporal lobe epilepsy, especially if it focuses on a focal hippocampal injection as done here (Lévesque and Avoli, 2013). One could, nevertheless, argue whether analysis from intracranial EEG in patients would be more valuable. Our group has investigated a very similar question in patients with temporal lobe seizures previously (Schönberger et al., 2019). We have, nevertheless, chosen to replicate these findings in a kainite model for two reasons. First, this is a great opportunity to correlate neurophysiological measures like HFOs with behavioral observations in seizures. Second, seizures in rat models of epilepsy can be scored more reliably and in more detail using the Racine scale than in patients in whom seizure semiology is much more variable. Besio had described a sixth grade of severity characterized by wild running in the cage during a seizure. As we observed this phenomenon in our experiment as well, it was decided to apply the modified Racine scale in this study as suggested by Besio et al. (2007). For this study, both the EEG and the video were screened for seizure activity, which allows for maximum sensitivity when it comes to the detection of subtle clinical seizures. Video cameras allowed assessing even small mouth and upper extremity movements. Two independent reviewers were used to ensure that Racine scores were as accurate as possible.

Pitfalls of HFO Analysis

HFOs were scored visually during all three time periods around the seizure. It was decided to use visual identification even if this is more time-consuming and bears the danger of reviewer bias as we were looking at ictal HFOs and wanted to exclude the effects of regular ictal spiking on the analysis. While many automatic detection tools exist for interictal HFOs, current automatic detectors are not calibrated for ictal HFOs (Staba et al., 2002; Dümpelmann et al., 2015). Most of the ictal HFO analyses have been working with high-frequency spectra instead of distinct HFOs, and therefore, the methodology did not apply to our analysis (Ochi et al., 2007). We therefore decided to mark ictal spikes and HFOs visually by two independent reviewers and only retained those events identified by both. Ictal HFOs are often longer than interictal HFOs. To account for the large variability in length, we decided to calculate seconds covered by the HFO per minute instead of HFO rates as is usually done (Jacobs et al., 2010; Zijlmans et al., 2011). This is very similar to the methods used in previous studies with human sEEG. Another challenge is the frequency definition of HFOs. Data derived from interictal periods usually distinguish ripples (80–200/250 Hz) from fast ripples (250–500 Hz). While this distinction derived from early microelectrode studies (Staba et al., 2004) and is continuously used for current studies, some studies suggest that the separation is artificial, and many high-frequency events show a strong overlap between these frequencies (Pearce et al., 2013). Moreover, these separations were derived from interictal data, and peri-ictal HFOs might behave differently concerning frequencies. Our results are very similar for ripples and fast ripples, which might suggest that these two event types are not distinct in the way they behave during seizures.

The influence of the electrode contact size on the recording of HFOs has been debated controversially, and as in most animal models, the electrodes used for the recording in this study have a smaller contact size than the electrodes used in humans. Contact size is especially critical when using HFO recordings from different electrodes within the same study as this might bias the results. In our study, all electrodes had the same size, and the results should be comparable. Moreover, two studies on the effects of the contact size of HFO rates showed no difference between different contact sizes and HFO identification, one using human data and one in an epilepsy model (Châtillon et al., 2011, 2013).

Analysis of HFOs always struggles with the fact that both physiological and epileptic oscillations within the same frequency range can occur in humans as well as rats. Interictal- and task-related physiological HFOs have been described during eye and mouth movements in patients (Uematsu et al., 2013; Nakai et al., 2017), and occurrence of these physiological oscillations is hard to test in an animal model. We feel, however, relatively confident that the majority of events identified in the present study were epileptic as they mainly occurred within the SOZ, and our study focused on ictal HFOs, which are less likely to be physiological.

Pathophysiological Importance of HFO Mirroring Seizure Severity

Correlation Between HFO Occurrence and Different Seizure Periods

This study shows similar results in the hippocampus for rodents with chronic epilepsy as have been described in patients with refractory focal epilepsy. Several studies indicate that HFOs increase during the ictal period compared to the interictal period. In our study, no difference was found for ripples vs. fast ripples. This is similar to the data from Zijlmans et al. (2011) that showed a significant increase in ictal HFOs compared to the preictal and interictal phases. In the current study, we did not compare ictal and preictal HFOs to an interictal EEG segment. Overall data about the preictal HFO increase are less conclusive than those about the ictal HFO increase. An increase in HFOs prior to the occurrence of seizure would, of course, be clinically highly relevant as it could be used for seizure detection and warning, but most preictal HFO increases described in the literature occurred in the very few seconds directly prior to the seizure onset and therefore were clinically less relevant. This study also analyses the immediate postictal period. Similar to the data from patients with mesio-temporal epilepsy, a significant decrease in HFOs overall was seen in the postictal period. This most likely reflects a postictal suppression of epileptic activity. Similar observations have been found for interictal HFOs in the postspike slow wave (Urrestarazu et al., 2007).

Correlation Between HFO Occurrence and Seizure Severity

Data from patients with mesio-temporal epilepsy also suggested a more widespread and higher increase in HFOs in patients

who had secondary generalized compared to focal seizures (Schönberger et al., 2019). In rats, seizures were shorter and showed faster evolution from focal to generalized, which is why a separation of two ictal periods was not possible. However, ictal HFOs were clearly higher in the ictal period during severe clinical seizures than milder ones. Racine states considered severe were those whose clinical appearance equaled generalized seizures in humans. Therefore, the observed difference for HFOs for generalized vs. focal seizures during the ictal periods was similar in both rats and patients. Overall, these observations suggest that HFOs mirror the epileptic activity during active seizures. Moreover, they are an EEG correlate of seizure severity.

One could hypothesize that stronger or generalized seizures lead to a more substantial suppression of HFOs in the postictal period; however, this could neither be found for patients not in our animal model. So far, no systematic studies have investigated the length and degree of postictal HFO suppression, and this might be a future topic of discussion to better understand postictal recovery. It is important to note that the current study only focuses on the hippocampal region, which was covered during the experiments; we cannot, therefore, draw any conclusion on neocortical HFOs and seizure severity.

CONCLUSION

The present study investigated the relationship between seizure severity as determined by clinical semiology and HFO occurrence. It could be clearly shown that HFOs correlate with increasing seizure severity. This can be seen as evidence that HFOs mirror seizure severity and provides a link between the behavioral seizure observation and HFOs as a measurable EEG biomarker.

DATA AVAILABILITY STATEMENT

The raw data supporting the conclusions of this article will be made available by the authors, without undue reservation.

ETHICS STATEMENT

The animal study was reviewed and approved by Institutional Animal Care and Use Committee of the University of Freiburg.

AUTHOR CONTRIBUTIONS

NB and JS performed EEG and statistical analysis. KS-F performed animal experiments under support and supervision of AS-B. JJ supported EEG analysis, was responsible for concept and hypothesis in study and supported NB in writing the manuscript. All authors contributed to the article and approved the submitted version.

FUNDING

JS was supported by the Berta-Ottenstein-Program for Clinician Scientists from the Faculty of Medicine, University of Freiburg. JJ was supported by the German Research Foundation (DFG; JA 1725/4-1).

REFERENCES

Besio, W. G., Koka, K., and Cole, A. J. (2007). Effects of noninvasive transcutaneous electrical stimulation *via* concentric ring electrodes on pilocarpine-induced status epilepticus in rats. *Epilepsia* 48, 2273–2279. doi: 10.1111/j.1528-1167.2007.01202.x

Bragin, A., Engel, J., Wilson, C. L., Fried, I., and Buzsáki, G. (1999). High-frequency oscillations in human brain. *Hippocampus* 9, 137–142. doi: 10.1002/(SICI)1098-1063(1999)9:2<137::AID-HIPO5>3.0.CO;2-0

Châtillon, C.-É., Zelmann, R., Bortel, A., Avoli, M., and Gotman, J. (2011). Contact size does not affect high frequency oscillation detection in intracerebral EEG recordings in a rat epilepsy model. *Clin. Neurophysiol.* 122, 1701–1705. doi: 10.1016/j.clinph.2011.02.022

Châtillon, C. E., Zelmann, R., Hall, J. A., Olivier, A., Dubeau, F., and Gotman, J. (2013). Influence of contact size on the detection of HFOs in human intracerebral EEG recordings. *Clin. Neurophysiol.* 124, 1541–1546. doi: 10.1016/j.clinph.2013.02.113

Drexel, M., Preidt, A. P., and Sperk, G. (2012). Sequel of spontaneous seizures after kainic acid-induced status epilepticus and associated neuropathological changes in the subiculum and entorhinal cortex. *Neuropharmacology* 63, 806–817. doi: 10.1016/j.neuropharm.2012.06.009

Dümpelmann, M., Jacobs, J., and Schulze-Bonhage, A. (2015). Temporal and spatial characteristics of high frequency oscillations as a new biomarker in epilepsy. *Epilepsia* 56, 197–206. doi: 10.1111/epi.12844

Frauscher, B., Bartolomei, F., Kobayashi, K., Cimbalnik, J., van 't Klooster, M. A., Rampp, S., et al. (2017). High-frequency oscillations: the state of clinical research. *Epilepsia*, 58, 1316–1329. doi: 10.1111/epi.13829

Jacobs, J., Wu, J. Y., Perucca, P., Zelmann, R., Mader, M., Dubeau, F., et al. (2018). Removing high-frequency oscillations: a prospective multicenter study on seizure outcome. *Neurology* 91, e1040–e1052. doi: 10.1212/WNL.0000000000006158

Jacobs, J., Zelmann, R., Jirsch, J., Chander, R., Dubeau, C.-É.C. F., and Gotman, J. (2009). High frequency oscillations (80–500 Hz) in the preictal period in patients with focal seizures. *Epilepsia* 50, 1780–1792. doi: 10.1111/j.1528-1167.2009.02067.x

Jacobs, J., Zijlmans, M., Zelmann, R., Chatillon, C.-É., Hall, J., Olivier, A., et al. (2010). High-frequency electroencephalographic oscillations correlate with outcome of epilepsy surgery. *Ann. Neurol.* 67, 209–220. doi: 10.1002/ana.21847

Jirsch, J. D., Urrestarazu, E., LeVan, P., Olivier, A., Dubeau, F., and Gotman, J. (2006). High-frequency oscillations during human focal seizures. *Brain* 129, 1593–1608. doi: 10.1093/brain/awl085

Jiruska, P., Alvarado-Rojas, C., Schevon, C. A., Staba, R., Stacey, W., Wendling, F., et al. (2017). Update on the mechanisms and roles of high-frequency oscillations in seizures and epileptic disorders. *Epilepsia* 58, 1330–1339. doi: 10.1111/epi.13830

Khosravani, H., Mehrotra, N., Rigby, M., Hader, W. J., Pinnegar, C. R., Pillay, N., et al. (2009). Spatial localization and time-dependant changes of electrographic high frequency oscillations in human temporal lobe epilepsy. *Epilepsia* 50, 605–616. doi: 10.1111/j.1528-1167.2008.01761.x

Kobayashi, K., Akiyama, T., Oka, M., Endoh, F., and Yoshinaga, H. (2015). A storm of fast (40–150Hz) oscillations during hypsarrhythmia in West syndrome. *Ann. Neurol.* 77, 58–67. doi: 10.1002/ana.24299

Kuhnke, N., Klus, C., Dümpelmann, M., Schulze-Bonhage, A., and Jacobs, J. (2019). Simultaneously recorded intracranial and scalp high frequency oscillations help identify patients with poor postsurgical seizure outcome. *Clin. Neurophysiol.* 130, 128–137. doi: 10.1016/j.clinph.2018.10.016

Lévesque, M., and Avoli, M. (2013). The kainic acid model of temporal lobe epilepsy. *Neurosci. Biobehav. Rev.* 37, 2887–2899. doi: 10.1016/j.neubiorev.2013.10.011

Lévesque, M., Shiri, Z., Chen, L.-Y., and Avoli, M. (2018). High-frequency oscillations and mesial temporal lobe epilepsy. *Neurosci. Lett.* 667, 66–74. doi: 10.1016/j.neulet.2017.01.047

Nakai, Y., Jeong, J. W., Brown, E. C., Rothermel, R., Kojima, K., Kambara, T., et al. (2017). Three- and four-dimensional mapping of speech and language in patients with epilepsy. *Brain* 140, 1351–1370. doi: 10.1093/brain/awx051

Ochi, A., Otsubo, H., Donner, E. J., Elliott, I., Iwata, R., Funaki, T., et al. (2007). Dynamic changes of ictal high-frequency oscillations in neocortical epilepsy: using multiple band frequency analysis. *Epilepsia* 48, 286–296. doi: 10.1111/j.1528-1167.2007.00923.x

Pearce, A., Wulsin, D., Blanco, J. A., Krieger, A., Litt, B., and Stacey, W. C. (2013). Temporal changes of neocortical high-frequency oscillations in epilepsy. *J. Neurophysiol.* 110, 1167–1179. doi: 10.1152/jn.01009.2012

Perucca, P., Dubeau, F., and Gotman, J. (2014). Intracranial electroencephalographic seizure-onset patterns: effect of underlying pathology. *Brain* 137, 183–196. doi: 10.1093/brain/awt299

Racine, R. J. (1972). Modification of seizure activity by electrical stimulation: II. Motor seizure. *Electroencephalogr. Clin. Neurophysiol.* 32, 281–294. doi: 10.1016/0013-4694(72)90177-0

Schönberger, J., Birk, N., Lachner-Piza, D., Dümpelmann, M., Schulze-Bonhage, A., and Jacobs, J. (2019). High-frequency oscillations mirror severity of human temporal lobe seizures. *Ann. Clin. Transl. Neurol.* 6, 2479–2488. doi: 10.1002/acn3.50941

Smith, E. H., Merricks, E. M., Liou, J.-Y., Casadei, C., Melloni, L., Thesen, T., et al. (2020). Dual mechanisms of ictal high frequency oscillations in human rhythmic onset seizures. *Sci. Rep.* 10:19166. doi: 10.1038/s41598-020-76138-7

Somerlik, K., Cosandier-Rimele, D., Cordeiro, J., Kruger, T., Mattmueller, R., Stieglitz, T., et al. (2011). "Measuring epileptogenicity in kainic acid injected rats", in *2011 5th International IEEE/EMBS Conference on Neural Engineering* (Cancun, Mexico).

Staba, R. J., Wilson, C. L., Bragin, A., Fried, I., and Engel, J. (2002). Quantitative analysis of high-frequency oscillations (80–500 Hz) recorded in human epileptic hippocampus and entorhinal cortex. *J. Neurophysiol.* 88, 1743–1752. doi: 10.1152/jn.2002.88.4.1743

Staba, R. J., Wilson, C. L., Bragin, A., Jhung, D., Fried, I., and Engel, J. (2004). High-frequency oscillations recorded in human medial temporal lobe during sleep. *Ann. Neurol.* 56, 108–115. doi: 10.1002/ana.20164

Suzuki, F., Junier, M. P., Guilhem, D., Sørensen, J. C., and Onteniente, B. (1995). Morphogenetic effect of kainate on adult hippocampal neurons associated with a prolonged expression of brain-derived neurotrophic factor. *Neuroscience* 64, 665–674. doi: 10.1016/0306-4522(94)00463-f

Uematsu, M., Matsuzaki, N., Brown, E. C., Kojima, K., and Asano, E. (2013). Human occipital cortices differentially exert saccadic suppression: intracranial recording in children. *NeuroImage* 83, 224–236. doi: 10.1016/j.neuroimage.2013.06.046

Urrestarazu, E., Chander, R., Dubeau, F., and Gotman, J. (2007). Interictal high-frequency oscillations (100–500 Hz) in the intracerebral EEG of epileptic patients. *Brain* 130, 2354–2366. doi: 10.1093/brain/awm149

van Klink, N. E. C., van 't Klooster, M. A., Leijten, F. S. S., Jacobs, J., Braun, K. P. J., and Zijlmans, M. (2016). Ripples on rolandic spikes: a marker of epilepsy severity. *Epilepsia* 57, 1179–1189. doi: 10.1111/epi.13423

Weiss, S. A., Banks, G. P., McKhann, G. M., Goodman, R. R., Emerson, R. G., Trevelyan, A. J., et al. (2013). Ictal high frequency oscillations distinguish two types of seizure territories in humans. *Brain* 136, 3796–3808. doi: 10.1093/brain/awt276

Weiss, S. A., Lemesiou, A., Connors, R., Banks, G. P., McKhann, G. M., Goodman, R. R., et al. (2015). Seizure localization using ictal phase-locked high gamma: a retrospective surgical outcome study. *Neurology* 84, 2320–2328. doi: 10.1212/WNL.0000000000001656

Williams, P. A., White, A. M., Clark, S., Ferraro, D. J., Swiercz, W., Staley, K. J., et al. (2009). Development of spontaneous recurrent seizures after Kainate-induced status epilepticus. *J. Neurosci.* 29, 2103–2112. doi: 10.1523/JNEUROSCI.0980-08.2009

Wu, J. Y., Sankar, R., Lerner, J. T., Matsumoto, J. H., Vinters, H. V., and Mathern, G. W. (2010). Removing interictal fast ripples on electrocorticography linked with seizure freedom in children. *Neurology* 75, 1686–1694. doi: 10.1212/WNL.0b013e3181fc27d0

Zijlmans, M., Jacobs, J., Kahn, Y. U., Zelmann, R., Dubeau, F., and Gotman, J. (2011). Ictal and interictal high frequency oscillations in patients with focal epilepsy. *Clin. Neurophysiol.* 122, 664–671. doi: 10.1016/j.clinph.2010.09.021

Zijlmans, M., Jacobs, J., Zelmann, R., Dubeau, F., and Gotman, J. (2009). High-frequency oscillations mirror disease activity in patients with epilepsy. *Neurology* 72, 979–986. doi: 10.1212/01.wnl.0000344402.20334.81

Zijlmans, M., Worrell, G. A., Dümpelmann, M., Stieglitz, T., Barborica, A., Heers, M., et al. (2017). How to record high-frequency oscillations in epilepsy: a practical guideline. *Epilepsia* 58, 1305–1315. doi: 10.1111/epi.13814

Conflict of Interest: The authors declare that the research was conducted in the absence of any commercial or financial relationships that could be construed as a potential conflict of interest.

frontiers in Human Neuroscience

ORIGINAL RESEARCH
published: 10 June 2021
doi: 10.3389/fnhum.2021.682011

Application of High-Frequency Oscillations on Scalp EEG in Infant Spasm: A Prospective Controlled Study

Lisi Yan[1,2,3,4,5†], Lin Li[1,2,3,4,5†], Jin Chen[1,2,3,4,5], Li Wang[1,2,3,4,5], Li Jiang[1,2,3,4,5] and Yue Hu[1,2,3,4,5]*

[1] Department of Neurology, Children's Hospital of Chongqing Medical University, Chongqing, China, [2] Ministry of Education Key Laboratory of Child Development and Disorders, Chongqing, China, [3] National Clinical Research Center for Child Health and Disorders, Chongqing, China, [4] China International Science and Technology Cooperation Base of Child Development and Critical Disorders, Chongqing, China, [5] Chongqing Key Laboratory of Pediatrics, Chongqing, China

OPEN ACCESS

Edited by:
Jing Xiang,
Cincinnati Children's Hospital Medical Center, United States

Reviewed by:
Haiteng Jiang,
Carnegie Mellon University, United States
Lu Tang,
Nanjing Brain Hospital Affiliated to Nanjing Medical University, China

****Correspondence:***
Yue Hu
huyue915@163.com

[†] These authors have contributed equally to this work

Specialty section:
This article was submitted to Brain Imaging and Stimulation, a section of the journal Frontiers in Human Neuroscience

Received: *17 March 2021*
Accepted: *17 May 2021*
Published: *10 June 2021*

Citation:
Yan L, Li L, Chen J, Wang L, Jiang L and Hu Y (2021) Application of High-Frequency Oscillations on Scalp EEG in Infant Spasm: A Prospective Controlled Study. Front. Hum. Neurosci. 15:682011. doi: 10.3389/fnhum.2021.682011

Objective: We quantitatively analyzed high-frequency oscillations (HFOs) using scalp electroencephalography (EEG) in patients with infantile spasms (IS).

Methods: We enrolled 60 children with IS hospitalized from January 2019 to August 2020. Sixty healthy age-matched children comprised the control group. Time–frequency analysis was used to quantify γ, ripple, and fast ripple (FR) oscillation energy changes.

Results: γ, ripple, and FR oscillations dominated in the temporal and frontal lobes. The average HFO energy of the sleep stage is lower than that of the wake stage in the same frequency bands in both the normal control (NC) and IS groups ($P < 0.05$). The average HFO energy of the IS group was significantly higher than that of the NC group in γ band during sleep stage ($P < 0.01$). The average HFO energy of S and Post-S stage were higher than that of sleep stage in γ band ($P < 0.05$). In the ripple band, the average HFO energy of Pre-S, S, and Post-S stage was higher than that of sleep stage ($P < 0.05$). Before treatment, there was no significant difference in BASED score between the effective and ineffective groups. The interaction of curative efficacy × frequency and the interaction of curative efficacy × state are statistically significant. The average HFO energy of the effective group was lower than that of the ineffective group in the sleep stage ($P < 0.05$). For the 16 children deemed "effective" in the IS group, the average HFO energy of three frequency bands was not significantly different before compared with after treatment.

Significance: Scalp EEG can record HFOs. The energy of HFOs can distinguish physiological HFOs from pathological ones more accurately than frequency. On scalp EEG, γ oscillations can better detect susceptibility to epilepsy than ripple and FR oscillations. HFOs can trigger spasms. The analysis of average HFO energy can be used as a predictor of the effectiveness of epilepsy treatment.

Keywords: high-frequency oscillation, infantile spasm, quantitative analysis, time–frequency analysis, scalp electroencephalography

INTRODUCTION

Extensive high-frequency oscillations (HFOs) occur in the neural network. HFOs appear on electroencephalography (EEG) with a frequency of 40–500 Hz. HFOs include gamma (γ; 40∼80 Hz), ripple (80∼200 Hz), and fast ripple (FR; 200∼500 Hz) oscillations (Ferrari-Marinho et al., 2020). The physiological neural network (Kramer and Cash, 2012) realizes temporary synchronization by γ oscillation, synchronizes nodes in the distant and contralateral hemispheres, and facilitates rapid and complex nerve conduction. Epileptic seizures occur due to excessive neuronal excitation in an imbalanced neural network and affect other related networks paroxysmally or constantly, leading to dysfunction. The clinical applications of HFOs include preoperative evaluation of epilepsy surgery, evaluation of seizure severity, evaluation of the efficacy of various methods of epilepsy treatment, evaluation of the severity of the pathological injury, and detection of susceptibility to epilepsy and seizures. Owing to the limitations of low amplitude and spatial distribution, HFOs are recorded using intracranial electrodes with a sampling frequency of > 2,000 Hz. An artificial analysis is still the gold standard for HFO analysis (Frauscher et al., 2017). However, artificial analysis is time-consuming, and due to its inevitable subjectivity, HFOs are not routinely used in clinical practice.

Conventional EEG can only record 0.5–70 Hz of EEG activity (narrow-frequency EEG), which results from a large number of neurons (over 1 million) involved in firing and synchronization in a wide space. Because of high- and low-frequency filtering inside the amplifier, important low- or high-frequency electrical activity may be attenuated or distorted, which is important in the context of cortical signal processing. One study showed that HFOs can also be recorded using scalp EEG. Scalp EEG in children with infantile spasms (IS) can record fast activity with a frequency of between 80 and 100 Hz (Ferrari-Marinho et al., 2020). A previous study (Kobayashi et al., 2010) of 10 children with a continuous spike-and-wave pattern during sleep showed HFOs on scalp EEG, which appeared simultaneously with the spinous wave with an HFO frequency range of 97.7–140.6 Hz. Patients with focal epilepsy also demonstrate γ and ripple oscillations on scalp EEG (Andrade-Valenca et al., 2011). The HFO ratio of intracranial records in adults and children is close, but the scalp HFO rate is 100-times higher in children with epilepsy compared with adults (Frauscher et al., 2017).

We enrolled patients with IS and used time–frequency analysis to quantitatively analyze HFO energy changes in different frequency bands before and after treatment to confirm the reliability of scalp EEG to analyze HFOs. We also aimed to clarify whether HFOs recorded by scalp EEG reflect epilepsy severity and evaluate the efficacy of drugs to provide a theoretical basis for better application of HFOs in the clinic.

MATERIALS AND METHODS

Research Objects

Children who conformed to the diagnostic criteria for IS (Pellock et al., 2010) and who were hospitalized at the Children's Hospital of Chongqing Medical University from January 2019 to August 2020 were enrolled. Follow-up was conducted through outpatient visits and telephone interviews after discharge.

The inclusion criteria were as follows: (1) onset age < 12 months; (2) typical clinical symptoms, including sudden or transient spasm of the neck, trunk, and limbs, either symmetrically or asymmetrically; (3) hypsarrhythmia or atypical hypsarrhythmia on interictal EEG; (4) developmental delay or retrogression; (5) aged from 3 to 12 months.

The exclusion criteria were as follows: (1) suspected or proven neurometabolic disease or degenerative brain disease (Angappan et al., 2019); (2) proven severe disease (e.g., dysfunction of the liver, kidney, or heart); (3) lack of normative treatment for various reasons; (4) request from parents to withdraw their child from clinical observation.

The normal control (NC) group included children who attended the physical examination center of the Children's Hospital from January 2019 to August 2020. The age range of patients was 3–12 months. Video EEG (VEEG) results were reportedly normal.

This study is a prospective controlled study. The study was approved by the Ethics Committee of the Children's Hospital of Chongqing Medical University, and families of children provided written informed consent.

Collection and Analysis of Scalp EEG Data

We adopted the International 10–20 system (Nihon-Kohden, Tokyo, Japan), and the frequency of sampling was 1,000 Hz. VEEG was performed for 4 h with electromyography of the deltoid and quadriceps femoris simultaneously. Sleep persisted for at least 60 min. EEG data analysis was completed independently by two well-trained neuroelectrophysiological professionals who reached a consensus on EEG and HFO interpretation. VEEG in the IS group was graded according to Burden of Amplitudes and Epileptiform Discharges (BASED) scoring criteria (Mytinger et al., 2015). The BASED score was completed according to longitudinal bipolar montage.

The IS group were examined during the interictal period, including during the (1) sleep stage (the sleep spindle appears) with epileptic discharge (SED) and a 5-min EEG segment with the epileptic discharge with sleep spindles and low-amplitude epidermal myoelectricity; (2) wake stage with epileptic discharge (WED) and a 5-min EEG segment with the epileptic discharge with low-amplitude epidermal myoelectricity in the wake stage with the eyes closed; (3) Stages of the epileptic attack were also assessed, including pre-spasm (Pre-S) for 2 s, spasm (S) for 2 s, and post-spasm (Post-S) for 2 s. The NC group was examined during the interictal period, including during sleep stage with no epileptic discharge (SNED) and wake stage with no epileptic discharge (WNED).

A high-frequency analysis was performed using the average montage as a reference. The spike-wave analysis had the following settings: screen display, 10 s/page; sensitivity, 15∼30 μV/mm; low-frequency filtering, 0.53 Hz; high-frequency filtering, 70 Hz. Then, the spike mark was hidden and the parameters for

HFOs were adjusted as follows: chart speed, 1∼2 s/page; sensitivity, 3∼5 μV/mm; low-frequency filtering, 80 Hz; high-frequency filtering, 300 Hz. An HFO was defined as one event containing at least four consecutive and regular oscillations with a higher frequency and amplitude compared with its surrounding background (Zijlmans et al., 2012). In one EEG recording, HFOs should appear at least twice in 5 min to ensure that similar oscillatory waves can be marked in 60 s of EEG and that the marking rate of false HFOs can be reduced.

Five-min EEG signals selected at the above time points were quantitatively analyzed for HFO signals. Decomposition was performed using MATLAB wavelet analysis, and γ (40∼80 Hz), ripple (80∼200 Hz), and FR (200∼300 Hz) oscillations were examined to perform the average energy analysis. The Morlet wavelet algorithm is described in previous studies (Xiang et al., 2014, 2015).

Curative Evaluation

A short-term curative effect judgment was made after 4 weeks of treatment (Cao et al., 2011; Han et al., 2016), including clinical and EEG judgment. Clinical assessment classifications included "controlled" (seizure-free), "improved" (>50% reduction in the frequency of seizures), and "ineffective" (< 50% or no reduction in the frequency of seizures). The controlled and improved classifications were categorized as "effective." The criteria for EEG improvement (Mytinger et al., 2015) were assessed by comparing EEG results pre-treatment versus 4 weeks after treatment. A BASED score of ≤3 was considered effective, while a BASED score of ≥ 4 was considered ineffective. Efficiency was calculated as follows: efficiency = (control + improved) ÷ total number of cases × 100%.

Statistical Analysis

Statistical analysis was performed using SPSS 26.0 software. The Shapiro–Wilk method was adopted to test the normality of measurement data. Mean ± standard deviation is used to present data with a normal distribution, a paired *t*-test was used for intra-group comparison. Measurement data with a skewed distribution are expressed as median and interquartile range. Aligned Rank Transform (ART) is used to implement non-parametric liner mixed model in R (version 4.0.0) Package "ARToo" (version 0.11.0). The ARTool relies on a preprocessing step that "aligns" data before applying averaged ranks, after which point common ANOVA procedures and *post hoc* can be used (Wobbrock et al., 2011). Using Holm method to correct P value after comparison in ARTool (Elkin et al., 2021). Counting data is expressed as frequency. A P value of ≤ 0.05 was considered statistically significant.

RESULTS

General Information

Sixty children with IS met the inclusion criteria (89 children were excluded), including 33 males and 27 females with a ratio of 1.22:1. The age range of patients was 3–12 months (mean age, 6.92 ± 2.39 months) (**Table 1**). The NC group consisted of 60 healthy age-matched children (32 males and 28 females with a ratio of 1.14:1). The age range of patients in the NC group was 3–12 months (mean age, 6.28 ± 2.38 months).

Average Energy Analysis of HFOs on Scalp EEG in the IS Group Before Treatment

The HFO lead with the largest average energy is referred to as the responsible lead. Sixty children in the NC group demonstrated 204 responsible leads, with most being in the frontal lobe (79/204) and the temporal lobe (83/204). Sixty children with

TABLE 1 | Clinical features of the IS group (60 cases).

Project		Case
Sex		
	Male	33
	Female	27
Perinatal risk factors		
	Premature	4
	Asphyxia	8
	Hypoglycemia	1
	Pathological jaundice	1
Onset to start of treatment		
	< 1 month	30
	≥ 1 month	30
Mode of seizure		
	Cluster of spasms	57
	Partial, isolated spasm	3
Head MRI		
	Cerebromalacia	6
	Ventricular dilatation	4
	Delayed myelination	6
	Callosal agenesis	4
	Tuberosa sclerosis	7
	Subarachnoid hemorrhage	1
	Pachygyria	1
VEEG		
Pre-treatment	5 (BASED score)	51
	4 (BASED score)	9
Post-treatment	≥ 4 (BASED score)	14
	≤ 3 (BASED score)	16
Gene		
	14q11q12 novel copy number variation	1
	TSC2 *de novo* mutation	4
	STXBP1 *de novo* mutation	1
	SCN2A novel mutation	1
	Negative	7
Medication		
	Glucocorticoid	55
	Topiramate	44
	Valproic acid	29
	Two drugs combined	29
	More than two drugs combined	29
	Ketogenic diet	2

IS demonstrated 260 responsible leads, with most being in the temporal lobe (119/260) and the frontal lobe (94/260).

We compared the IS group with the NC group and found that the interaction effects of group (IS/NC group) × state (sleep/wake stage) × frequency (γ/ripple/FS) are statistically significant ($F_{2,590}$ = 3.13, P = 0.045). After further pairwise comparison, it was found that in γ and sleep stage, the average energy of the IS group was significantly higher than that of the NC group ($P < 0.01$) (**Figures 1–3** and **Table 2**).

In the IS group, the interaction effect of state × frequency is statistically significant ($F_{8,462}$ = 2.16, P = 0.030). After further pairwise comparison, it is found that the average energy of the sleep stage is lower than that of the wake stage in the same frequency bands ($P < 0.05$). In the γ band, the average energy of S and Post-S stage were higher than that of sleep stage ($P < 0.05$). In the ripple band, the average energy of Pre-S, S, and Post-S stage was higher than that of sleep stage ($P < 0.05$). In the FR band, only the average energy of the Post-S stage is higher than that of sleep stage ($P < 0.05$). In all frequency bands, there was no significant statistical difference between the average energy of the Pre-S/S/Post-S stage and the wake stage ($P > 0.05$) (**Table 2**).

In the NC group, the interaction effect of state × frequency was statistically significant ($F_{2,295}$ = 41.22, $P < 0.001$). After further pairwise comparison, it is found that the average energy of the sleep stage is lower than that of the wake stage in the same frequency bands ($P < 0.05$) (**Table 2**).

Average Energy Analysis of HFOs on Scalp EEG in Different Frequency Bands Between the Effective and Ineffective Groups Before and After Treatment

After normative treatment, 30 children (17 males) underwent VEEG after 4 weeks of treatment and were divided into an effective group (16 cases) and an ineffective group (14 cases) according to clinical efficacy and EEG score (**Figure 4**). The remaining 30 cases failed to complete follow-up. We statistically

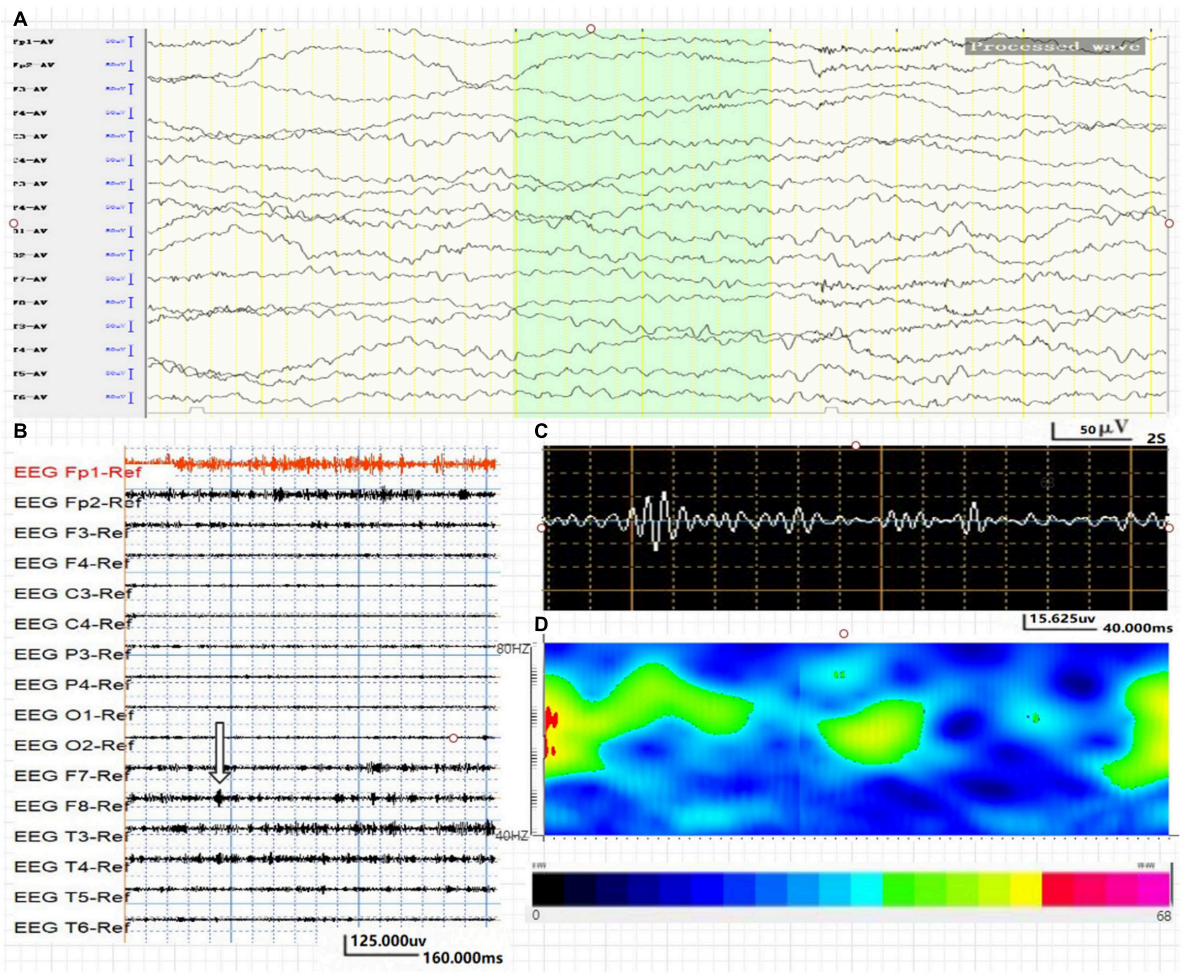

FIGURE 1 | Average energy and time characteristics of γ oscillations in WNED (NC group). The waveform and energy diagram shows the energy and time characteristics of γ oscillations (40~80 Hz) in WNED (NC group). **(A)** Scalp EEG of WNED (NC group). **(B,C)** 40~80-Hz bandpass filter. **(C)** F8 lead signals. **(D)** Spectrum diagram reflects the cumulative time–frequency of the corresponding waveform.

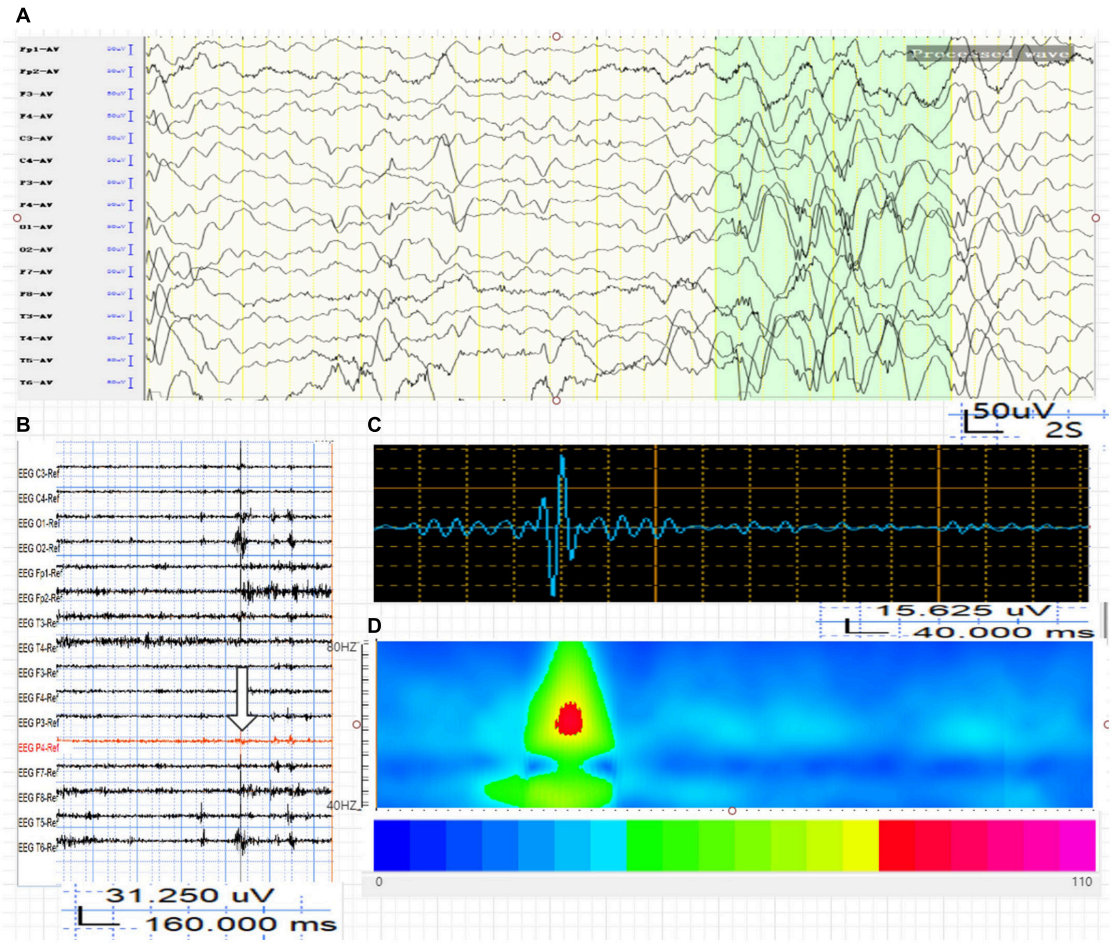

FIGURE 2 | Average energy and time characteristics of γ oscillations in WED (IS group). The waveform and energy diagram shows the energy and time characteristics of γ oscillations (40∼80 Hz) in the WED (IS group). **(A)** Scalp EEG of WED (IS group). **(B,C)** 40∼80-Hz bandpass filter. **(C)** P4 lead signals. **(D)** The spectrum diagram reflects the cumulative time-frequency of the corresponding waveform.

analyzed the average HFO energy during the interictal period in the ineffective and ineffective groups before treatment.

Before treatment, there was no significant difference in BASED score between the effective and ineffective groups [median(Q1, Q3), 5.00(5.00, 5.00) vs. 5.00(5.00, 5.00), respectively]. The interaction of curative efficacy (effective/ineffective) × state (sleep/wake stage) × frequency (γ/ripple/FS) is not statistically significant ($F_{2,140}$ = 0.76, P = 0.469). However, the interaction of curative efficacy × frequency ($F_{2,140}$ = 5.38, P = 0.005) and the interaction of curative efficacy × state ($F_{1,140}$ = 5.95, P = 0.016) are statistically significant. After further pairwise comparison, it was found that the average energy of the effective group was lower than that of the ineffective group in the sleep stage ($P < 0.05$, **Table 3**).

We further analyzed the average HFO energy before and after treatment in 16 effective children in the IS group. The results show that the BASED score before treatment (mean, 4.75 ± 0.58) was higher compared with after treatment (mean, 1.31 ± 1.25) ($P < 0.01$). The interaction between time (before/after treatment) × state (sleep/wake stage) × frequency (γ/ripple/FS) is not statistically significant ($F_{2,162}$ = 0.84, P = 0.435). The interactions of time × frequency ($F_{2,162}$ = 1.96, P = 0.145) and time × state ($F_{2,162}$ = 2.34, P = 0.128) were also not statistically significant. The main effect before and after treatment was also not statistically significant ($F_{1,162}$ = 0.03, P = 0.871).

DISCUSSION

HFOs are weaker than normal-frequency EEG signals, with lower amplitude and a shorter duration. Their characteristics cannot be accurately expressed by traditional time–domain or frequency–domain analyses (Modur, 2014; Frost et al., 2015; Zijlmans et al., 2017). The wavelet transforms in the time–frequency analysis is applied in signal analysis and processing (e.g., signal singularity detection, time-varied filtering, and pattern recognition) (Yong and Shengxun, 1996). The Morlet wavelet algorithm features good time resolution and based on Gaussian function, it allows signals to have phase fluctuations within a certain range. Using

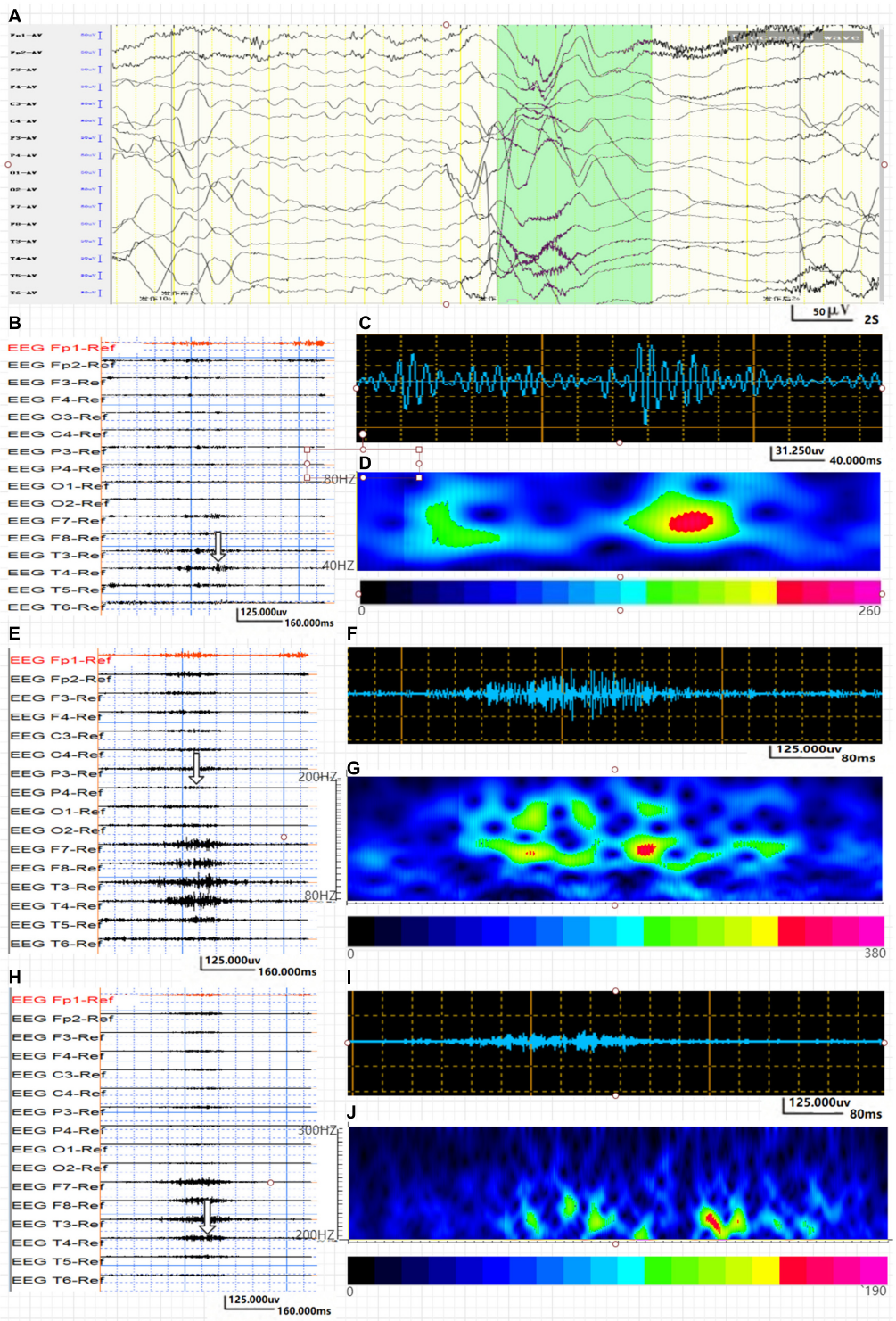

FIGURE 3 | Average energy and time characteristics of γ, ripple, and fast ripple oscillations in the IS group. The waveform and energy diagram shows the energy and time characteristics of γ, ripple, and fast ripple oscillations. **(A)** Ictal EEG of the scalp in the IS group. **(B**,**C)** 40∼80-Hz bandpass filter. **(C)** γ oscillation in the O1 lead. **(D)** The spectrum diagram reflects the cumulative time–frequency of γ oscillations of the corresponding waveform. **(E,F)** 80∼200-Hz bandpass filter. **(G)** The spectrum diagram reflects the cumulative time-frequency of ripple oscillations of the corresponding waveform. **(H**,**I)** 200∼300-Hz bandpass filter. **(J)** The spectrum diagram reflects the cumulative time-frequency of fast ripple oscillations of the corresponding waveform. The characteristic feature of ripple and fast ripple oscillations is rhythmic burst, which is different from system artifacts, such as power noise and harmonics.

this approach, the instantaneous spectral characteristics of EEG signals with non-stationary characteristics are observed, and the quantitative analysis of HFOs in epileptic brain tissue can be realized (Xiang et al., 2015). Average energy reflects the functional brain state throughout the time window, while maximum energy reflects the burst of maximum energy at a specified time point in the time window; however, maximum energy reflects different functional brain states with poor variation stability and recognizes functional changes with lower sensitivity than average energy. Therefore, average energy is used to analyze the functional brain state and to assess seizures. Non-invasive scalp EEG is disturbed by electromyographic signals, which are a well-known source of high-frequency activity, with the major signal frequency being concentrated at 20–150 Hz. We were careful to eliminate artifacts in the present data. To eliminate artifacts, EEG data analysis was completed independently by two experienced neuroelectrophysiologists who reached a consensus on EEG and HFO interpretation. Low-amplitude surface electromyographic signal segments were selected, and manual and automatic detection were performed simultaneously. The reliability and accuracy of the analysis methods were confirmed (Leiken et al., 2014). The spectrum diagram reflects the accumulated time–frequency of the HFO of the corresponding waveform, and HFO is a rhythmic outbreak that is different from system artifacts, such as power supply noise and its harmonics.

TABLE 2 | Comparison of the average HFO energy between/within the IS group and the NC group before treatment.

	γ	Ripple	FR
NC group			
Wake stage	73.99(50.16, 110.75)	37.09(23.81, 63.99)	12.44(9.41, 18.84)
Sleep stage	31.05(22.57, 51.09)▲	10.65(8.90, 14.57)▲	9.02(4.53, 9.76)▲
IS group			
Wake stage	89.87(62.67, 215.44)	40.47(26.06, 76.39)	18.59(9.48, 28.12)
Sleep stage	44.63(30.99, 170.19)△▲	12.91(10.45, 21.10)▲	9.30(4.42, 21.62)▲
Pre-S stage	92.09(45.78, 151.86)	34.28(19.30, 47.13)★	14.47(8.05, 41.56)
S stage	109.99(79.31, 144.83)★	42.26(21.45, 53.38)★	15.78(7.68, 29.69)
Post-S stage	103.17(59.50, 166.93)★	46.36(21.41, 86.68)★	23.36(8.66, 40.68)★

△, *Compared with the average HFO energy of sleep stage (NC group) in the same frequency band* $P < 0.01$.
▲, *Compared with the average HFO energy of wake stage (IS group) in the same frequency band* $P < 0.05$.
★, *Compared with the average HFO energy of sleep stage (IS group) in the same frequency band* $P < 0.05$.
P, Adjusted by Holm method.

TABLE 3 | Comparison of the average HFO energy between the effective and ineffective group before treatment.

	Ineffective group	Effective group	*P*
Stage			
Wake stage	36.62(19.55, 74.59)	51.09(21.17, 85.35)	0.486
Sleep stage	18.98(11.21, 33.55)	13.22(8.11, 38.75)	0.041
Frequency			
γ	71.93(33.90, 206.56)	82.95(40.66, 110.17)	> 0.999
Ripple	21.60(12.99, 37.13)	23.74(12.41, 50.66)	> 0.999
FR	11.43(9.43, 25.60)	11.54(5.14, 18.11)	>0.999

P, Adjusted by Holm method.

The skull does not filter high-frequency signals, but its thickness and resistance attenuate the conduction of intracranial EEG signals (Gotman, 2010). Therefore, it is generally believed that high-frequency signals are difficult to record using scalp EEG. At lower noise levels, ripples can be recorded on scalp EEG, but the amplitude is 10-times lower than with intracranial EEG (von Ellenrieder et al., 2014). Only a few studies show that scalp EEG can record FRs (Mooij et al., 2017). In this study, the average energy of HFOs confirmed that scalp EEG in patients with epilepsy and healthy children could record EEG signals in three frequency bands (γ, ripple, and FR), which mainly appear in the temporal and frontal lobes. HFOs are affected by sleep. Studies show that the HFO rate is highest during non-rapid eye movement (NREM) sleep and lowest during rapid eye movement (REM) sleep and awake stages. The area of HFOs in NREM sleep is larger (von Ellenrieder et al., 2017). Conversely, in the present study, the average HFO energy of the sleep stage is lower than that of the wake stage in the same frequency bands in both the NC and IS groups ($P < 0.05$). Thus, physiological and pathological HFOs have similar sleep balance characteristics. Besides, disturbance of scalp EEG by motor artifacts or myoelectrical activity during the waking period cannot be completely excluded.

HFOs reflect epilepsy severity. Boran et al. studied HFOs using scalp EEG before and after surgery in 11 children with intractable epilepsy undergoing surgery. The incidence of scalp HFOs positively correlated with seizure frequency and decreased after epilepsy surgery (Boran et al., 2019). In patients with atypical benign partial epilepsy, ripples recorded on scalp EEG were related to increased seizure frequency in negative myoclonus and atypical absence seizure (Qian et al., 2016). Nicole et al. discovered that the number of ripples on Rolandic spikes positively correlated with seizure frequency, suggesting that ripples on Rolandic spikes reflect seizure severity (van Klink et al., 2016). In epileptic spasms, whether clinical spasms occur is strongly linked to the amplitude of HFOs in the Rolandic area (Qian et al., 2016). In this study, it was found that in γ and sleep stage, the average HFO energy of the IS group was significantly higher than that of the NC group ($P < 0.01$). Previous intracranial electrode research in animals proved that ripple and FR oscillations can appear in the normal or epileptic hippocampus simultaneously, and the main difference between the two states is in HFO energy. Therefore, HFOs energy can more accurately distinguish physiological from pathological HFOs than frequency (Song et al., 2016). It may be considered that the origin of ripple and FR is relatively small, coupled with the distance and resistance of the skull, further leading to the attenuation of this weak signal. On scalp EEG, γ oscillations can better detect susceptibility to epilepsy than ripples and FRs.

Pathological HFOs reflect neuronal firing, which is the basis for convulsions (Lévesque et al., 2011; Zijlmans et al., 2011). From the Pre-S to the S period, the oscillation frequency gradually increases over time. Changes in ripple and FR energy coincide with epileptic seizure stages, which have an indicative effect on

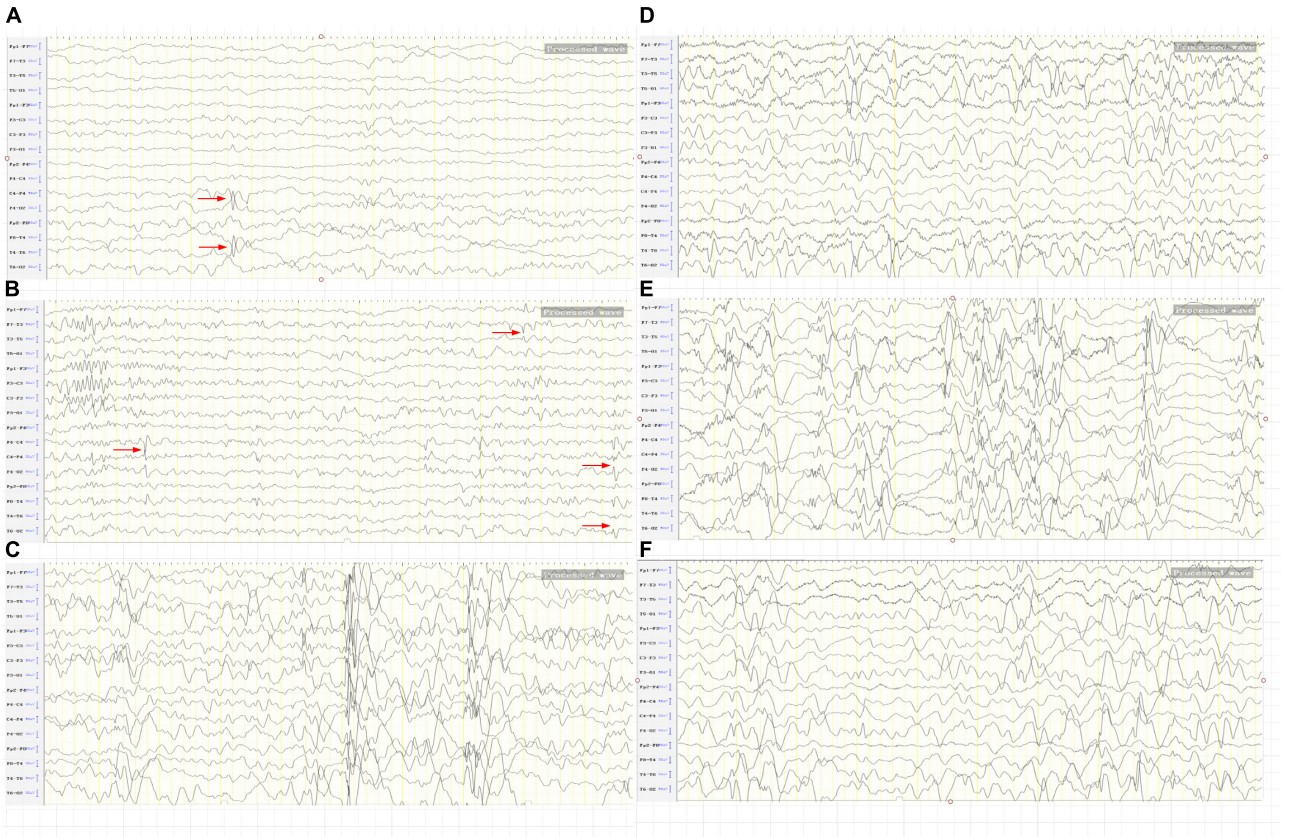

FIGURE 4 | The BASED score in the IS group. **(A)** Two points. After treatment, spikes on the right posterior temporal region. **(B)** Three points. After treatment, spikes on the right central-parietal-posterior temporal region left middle temporal region and a slow wave amplitude of $< 200\ \mu V$ on the background. **(C)** Four points. After treatment, an epilepsy discharge of $< 50\%$ within 1 s of the most severe 5 min of EEG, and a slow wave amplitude of $> 200\ \mu V$ on the background. **(D)** Four points. After treatment, an epilepsy discharge of $< 50\%$ within 1 s of the most severe 5 min of EEG, and a slow wave amplitude of $> 200\ \mu V$ on the occiput. **(E)** Five points. Before treatment, an epilepsy discharge of $> 50\%$ within 1 s of the most severe 5 min of EEG. **(F)** Five points. Before treatment, a low wave amplitude of $> 300\ \mu V$ in the bilateral parietal posterior temporal region.

seizures (Song et al., 2016). Pearce et al. (2013) discovered that HFOs begin to change 30 min before a seizure. Moreover, HFOs appear and increase significantly before spasms, suggesting that HFOs can trigger spasms (Nariai et al., 2011). The present study suggests that in the γ band, the average HFO energy of S and Post-S stage were higher than that of sleep stage ($P < 0.05$). In the ripple band, the average HFO energy of Pre-S, S, and Post-S stage was higher than that of sleep stage ($P < 0.05$).

Typical EEG traces of patients with IS manifest as hypsarrhythmia. The BASED score is a simplified EEG scoring standard based on the weight of amplitude and epileptiform discharges. A score is produced by analyzing the most severe 5 min of EEG signals in children with IS (0 and 1 point not applicable). According to the BASED score, the standard for judging hypsarrhythmia is a BASED score of 4 or 5, and no hypsarrhythmia is concluded with a score of ≤ 3. Compared with traditional EEG, the BASED score boasts better consistency among scorers (Mytinger et al., 2015); thus, a judgment of hypsarrhythmia in patients with IS is more accurate and reliable than with traditional EEG. In this study, there was no significant difference in BASED score between the effective and ineffective groups before treatment. We further analyzed the average HFO energy before and after treatment in 16 effective children in the IS group. The results show that the BASED score before treatment (mean, 4.75 ± 0.58) was higher compared with after treatment (mean, 1.31 ± 1.25) ($P < 0.01$).

Boran et al. found that the frequency of HFOs is positively correlated with the frequency of epileptic discharge (Boran et al., 2019). Patients with active partial epilepsy have a higher frequency of HFOs (accuracy rate, 88%). HFOs have clear monitoring significance for the response to drug treatment in patients with epileptic encephalopathies, such as epileptic encephalopathy with continuous spike-and-wave during sleep and variants of benign childhood epilepsy with centrotemporal spikes. The prognosis of patients with epilepsy undergoing methylprednisolone therapy is closely related to the number of HFOs on scalp EEG (Qian et al., 2016; Gong et al., 2018). Dezhi et al. studied HFOs in 22 children with persistent spike-wave encephalopathy during sleep who received methylprednisolone treatment. HFOs disappeared from scalp EEG in children treated with hormones, but children with no response or recurrence after hormone therapy showed persistent HFOs (Cao et al., 2019). In

the study, the interaction of curative efficacy × frequency and the interaction of curative efficacy × state are statistically significant. The average HFO energy of the effective group was lower than that of the ineffective group in the sleep stage ($P < 0.05$). Therefore, the evidence supports the analysis of average HFO energy can be used as a predictor of the effectiveness of epilepsy treatment. For the 16 children deemed "effective" in the IS group, the average HFO energy of three frequency bands was not significantly different before compared with after treatment. IS is a type of developmental epileptic encephalopathy. Even if seizures are controlled and EEG observations improve, varying degrees of cognitive dysfunction may still be present (Specchio and Curatolo, 2021). HFOs are involved in memory formation and information processing (Alkawadri et al., 2014). Therefore, whether the high-energy HFOs of IS patients after treatment is related to cognitive dysfunction needs to be further confirmed.

The advantages of measuring scalp HFOs include non-invasiveness and convenience. However, HFO signals are weak, and interference and artifacts are common. Some scholars have questioned the feasibility of scalp HFO recordings (Thomschewski et al., 2019). Research on the simultaneous recording of EEG signals using scalp and intracranial electrodes has confirmed that scalp HFO signals originate from the cortex. At present, scalp HFOs cannot be directly applied to guide the diagnosis and treatment of epilepsy, and their reliability and stability cannot be completely determined. However, as a non-invasive examination, this approach is highly convenient. Both animal and clinical trials have confirmed that the HFOs automatic analysis and detection system we used is fast and accurate (Xiang et al., 2014; Song et al., 2016; von Ellenrieder et al., 2017). Although the analysis results cannot completely exclude the interference of myoelectrical activity, they can provide a reference for clinical exploration of non-invasive detection of HFOs.

DATA AVAILABILITY STATEMENT

The raw data supporting the conclusions of this article will be made available by the authors, without undue reservation.

ETHICS STATEMENT

The studies involving human participants were reviewed and approved by Ethics Committee of the Children's Hospital of Chongqing Medical University. Written informed consent to participate in this study was provided by the participants' legal guardian/next of kin.

AUTHOR CONTRIBUTIONS

LY and LL were responsible for the material preparation. JC, LW, and LY collected and analyzed the data. LY and YH wrote the first draft of the manuscript. LJ reviewed the manuscript. All authors contributed to the study's conception and design, commented on previous versions of the manuscript, and read and approved the final manuscript.

ACKNOWLEDGMENTS

We sincerely thank all the children and their parents for their cooperation during this study.

REFERENCES

Alkawadri, R., Gaspard, N., Goncharova, I. I., Spencer, D. D., Gerrard, J. L., Zaveri, H., et al. (2014). The spatial and signal characteristics of physiologic high frequency oscillations. *Epilepsia* 55, 1986–1995. doi: 10.1111/epi.12851

Andrade-Valenca, L. P., Dubeau, F., Mari, F., Zelmann, R., and Gotman, J. (2011). Interictal scalp fast oscillations as a marker of the seizure onset zone. *Neurology* 77, 524–531. doi: 10.1212/WNL.0b013e318228bee2

Angappan, D., Sahu, J. K., Malhi, P., and Singhi, P. (2019). Safety, tolerability, and effectiveness of oral zonisamide therapy in comparison with intramuscular adrenocorticotropic hormone therapy in infants with West syndrome. *Eur. J. Paediatr. Neurol.* 23, 136–142. doi: 10.1016/j.ejpn.2018.09.006

Boran, E., Sarnthein, J., Krayenbühl, N., Ramantani, G., and Fedele, T. (2019). High-frequency oscillations in scalp EEG mirror seizure frequency in pediatric focal epilepsy. *Sci. Rep.* 9:16560. doi: 10.1038/s41598-019-52700-w

Cao, D., Chen, Y., Liao, J., Nariai, H., Li, L., Zhu, Y., et al. (2019). Scalp EEG high frequency oscillations as a biomarker of treatment response in epileptic encephalopathy with continuous spike-and-wave during sleep (CSWS). *Seizure* 71, 151–157. doi: 10.1016/j.seizure.2019.05.023

Cao, D., Hu, Y., Zhu, Y., Zhao, X., Li, B., Chen, L., et al. (2011). Adrenocorticotmphic hormone versus ketogenic diet therapy for infantile spasms:a randomized controlled trial. *J. Appl. Clin. Pediatr.* 26, 1442–1445.

Elkin, L. A., Kay, M., Higgins, J. J., and Wobbrock, J. O. (2021). *An Aligned Rank Transform Procedure for Multifactor Contrast Tests*. USA: University of Washington Seattle.

Ferrari-Marinho, T., Perucca, P., Amiri, M., Dubeau, F., Gotman, J., and Caboclo, L. O. (2020). High-Frequency Oscillations in the Scalp EEG of Intensive Care Unit Patients With Altered Level of Consciousness. *J. Clin. Neurophysiol.* 37, 246–252. doi: 10.1097/WNP.0000000000000624

Frauscher, B., Bartolomei, F., Kobayashi, K., Cimbalnik, J., van ′t Klooster, M. A., Rampp, S., et al. (2017). High-frequency oscillations: the state of clinical research. *Epilepsia* 58, 1316–1329. doi: 10.1111/epi.13829

Frost, J. D.Jr, Le, J. T., Lee, C. L., Ballester-Rosado, C., Hrachovy, R. A., and Swann, J. W. (2015). Vigabatrin therapy implicates neocortical high frequency oscillations in an animal model of infantile spasms. *Neurobiol. Dis.* 82, 1–11. doi: 10.1016/j.nbd.2015.04.019

Gong, P., Xue, J., Qian, P., Yang, H., Liu, X., Cai, L., et al. (2018). Scalp-recorded high-frequency oscillations in childhood epileptic encephalopathy with continuous spike-and-wave during sleep with different etiologies. *Brain Dev.* 40, 299–310. doi: 10.1016/j.braindev.2017.12.010

Gotman, J. (2010). High frequency oscillations: the new EEG frontier?. *Epilepsia* 51, 63–65. doi: 10.1111/j.1528-1167.2009.02449.x

Han, J., Zhao, W., Zhang, C., Zhang, Z., Mai, C. F., Cheng, M., et al. (2016). Comparison of the eficacy of adrenocorticotropic hormone and Methylprednisolone in the treatment of infantile spasms. *J. Appl. Clin. Pediatr.* 11, 859–862.

Kobayashi, K., Watanabe, Y., Inoue, T., Oka, M., Yoshinaga, H., and Ohtsuka, Y. (2010). Scalp-recorded high-frequency oscillations in childhood sleep-induced electrical status epilepticus. *Epilepsia* 51, 2190–2194. doi: 10.1111/j.1528-1167.2010.02565.x

Kramer, M. A., and Cash, S. S. (2012). Epilepsy is a disorder of cortical network organization. *Neuroscientist* 18, 360–372. doi: 10.1177/1073858411422754

Leiken, K., Xiang, J., Zhang, F., Shi, J., Tang, L., Liu, H., et al. (2014). Magnetoencephalography detection of high-frequency oscillations in the developing brain. *Front. Hum. Neurosci.* 8:969. doi: 10.3389/fnhum.2014.00969

Lévesque, M., Bortel, A., Gotman, J., and Avoli, M. (2011). High-frequency (80-500 Hz) oscillations and epileptogenesis in temporal lobe epilepsy. *Neurobiol. Dis.* 42, 231–241. doi: 10.1016/j.nbd.2011.01.007

Modur, P. N. (2014). High frequency oscillations and infraslow activity in epilepsy. *Ann. Indian Acad. Neurol.* 17, S99–S106. doi: 10.4103/0972-2327.128674

Mooij, A. H., Raijmann, R. C. M. A., Jansen, F. E., Braun, K. P. J., and Zijlmans, M. (2017). Physiological Ripples (± 100 Hz) in Spike-Free Scalp EEGs of Children With and Without Epilepsy. *Brain Topogr.* 30, 739–746. doi: 10.1007/s10548-017-0590-y

Mytinger, J. R., Hussain, S. A., Islam, M. P., Millichap, J. J., Patel, A. D., Ryan, N. R., et al. (2015). Improving the inter-rater agreement of hypsarrhythmia using a simplified EEG grading scale for children with infantile spasms. *Epilepsy Res.* 116, 93–98. doi: 10.1016/j.eplepsyres.2015.07.008

Nariai, H., Nagasawa, T., Juhász, C., Sood, S., Chugani, H. T., and Asano, E. (2011). Statistical mapping of ictal high-frequency oscillations in epileptic spasms. *Epilepsia* 52, 63–74. doi: 10.1111/j.1528-1167.2010.02786.x

Pearce, A., Wulsin, D., Blanco, J. A., Krieger, A., Litt, B., and Stacey, W. C. (2013). Temporal changes of neocortical high-frequency oscillations in epilepsy. *J. Neurophysiol.* 110, 1167–1179. doi: 10.1152/jn.01009.2012

Pellock, J. M., Hrachovy, R., Shinnar, S., Baram, T. Z., Bettis, D., Dlugos, D. J., et al. (2010). Infantile spasms: a U.S. consensus report. *Epilepsia* 51, 2175–2189. doi: 10.1111/j.1528-1167.2010.02657.x

Qian, P., Li, H., Xue, J., and Yang, Z. (2016). Scalp-recorded high-frequency oscillations in atypical benign partial epilepsy. *Clin. Neurophysiol.* 127, 3306–3313. doi: 10.1016/j.clinph.2016.07.013

Song, P. P., Xiang, J., Jiang, L., Chen, H. S., Liu, B. K., and Hu, Y. (2016). Dynamic Changes in Spectral and Spatial Signatures of High Frequency Oscillations in Rat Hippocampi during Epileptogenesis in Acute and Chronic Stages. *Front. Neurol.* 7:204. doi: 10.3389/fneur.2016.00204

Specchio, N., and Curatolo, P. (2021). Developmental and epileptic encephalopathies: what we do and do not know. *Brain J. Neurol.* 144, 32–43. doi: 10.1093/brain/awaa371

Thomschewski, A., Hincapié, A. S., and Frauscher, B. (2019). Localization of the Epileptogenic Zone Using High Frequency Oscillations. *Front. Neurol.* 10:94. doi: 10.3389/fneur.2019.00094

van Klink, N. E. C, van ′t Klooster, M. A., Leijten, F. S., Jacobs, J., Braun, K. P., and Zijlmans, M. (2016). Ripples on rolandic spikes: a marker of epilepsy severity. *Epilepsia* 57, 1179–1189. doi: 10.1111/epi.13423

von Ellenrieder, N., Beltrachini, L., Perucca, P., and Gotman, J. (2014). Size of cortical generators of epileptic interictal events and visibility on scalp EEG. *Neuroimage* 94, 47–54. doi: 10.1016/j.neuroimage.2014.02.032

von Ellenrieder, N., Dubeau, F., Gotman, J., and Frauscher, B. (2017). Physiological and pathological high-frequency oscillations have distinct sleep-homeostatic properties. *Neuroimage Clin.* 14, 566–573. doi: 10.1016/j.nicl.2017.02.018

Wobbrock, J. O., Findlater, L., Gergle, D., and Higgins, J. J. (2011). "The aligned rank transform for nonparametric factorial analyses using only anova procedures," in *Proceedings of the SIGCHI Conference on Human Factors in Computing Systems*. (Canada: ACM). doi: 10.1145/1978942.1978963

Xiang, J., Korman, A., Samarasinghe, K. M., Wang, X., Zhang, F., Qiao, H., et al. (2015). Volumetric imaging of brain activity with spatial-frequency decoding of neuromagnetic signals. *J. Neurosci. Methods* 239, 114–128. doi: 10.1016/j.jneumeth.2014.10.007

Xiang, J., Luo, Q., Kotecha, R., Korman, A., Zhang, F., Luo, H., et al. (2014). Accumulated source imaging of brain activity with both low and high-frequency neuromagnetic signals. *Front. Neuroinform.* 8:57. doi: 10.3389/fninf.2014.00057

Yong, L., and Shengxun, Z. (1996). "Apply wavelet transform to analyse EEG signal," in *International Conference of the IEEE Engineering in Medicine & Biology Society*. (United States: IEEE).

Zijlmans, M., Jacobs, J., Kahn, Y. U., Zelmann, R., Dubeau, F., and Gotman, J. (2011). Ictal and interictal high frequency oscillations in patients with focal epilepsy. *Clin. Neurophysiol.* 122, 664–671. doi: 10.1016/j.clinph.2010.09.021

Zijlmans, M., Jiruska, P., Zelmann, R., Leijten, F. S., Jefferys, J. G., and Gotman, J. (2012). High-frequency oscillations as a new biomarker in epilepsy. *Ann. Neurol.* 71, 169–178. doi: 10.1002/ana.22548

Zijlmans, M., Worrell, G. A., Dümpelmann, M., Stieglitz, T., Barborica, A., Heers, M., et al. (2017). How to record high-frequency oscillations in epilepsy: a practical guideline. *Epilepsia* 58, 1305–1315. doi: 10.1111/epi.13814

Conflict of Interest: The authors declare that the research was conducted in the absence of any commercial or financial relationships that could be construed as a potential conflict of interest.

frontiers in Human Neuroscience

ORIGINAL RESEARCH
published: 16 June 2021
doi: 10.3389/fnhum.2021.680295

Fast Ripples as a Biomarker of Epileptogenic Tuber in Tuberous Sclerosis Complex Patients Using Stereo-Electroencephalograph

Yangshuo Wang[1†], Liu Yuan[1†], Shaohui Zhang[1,2†], Shuangshuang Liang[2], Xiaoman Yu[2], Tinghong Liu[1], Xiaofeng Yang[3] and Shuli Liang[1]**

[1] Department of Functional Neurosurgery, Beijing Children's Hospital, Capital Medical University, Beijing, China, [2] Department of Neurosurgery, Fourth Medical Center, General Hospital of PLA, Beijing, China, [3] Bioland Laboratory, Guangzhou, China

OPEN ACCESS

Edited by:
Changming Wang,
Xuanwu Hospital, Capital Medical University, China

Reviewed by:
Zhixian Yang,
Peking University First Hospital, China
James Tao,
University of Chicago, United States

***Correspondence:**
Shuli Liang
liangsl_304@sina.com
Xiaofeng Yang
xiaofengyang@yahoo.com

[†]These authors share first authorship

Specialty section:
This article was submitted to Brain Imaging and Stimulation, a section of the journal Frontiers in Human Neuroscience

Received: 14 March 2021
Accepted: 07 May 2021
Published: 16 June 2021

Citation:
Wang Y, Yuan L, Zhang S, Liang S, Yu X, Liu T, Yang X and Liang S (2021) Fast Ripples as a Biomarker of Epileptogenic Tuber in Tuberous Sclerosis Complex Patients Using Stereo-Electroencephalograph. Front. Hum. Neurosci. 15:680295. doi: 10.3389/fnhum.2021.680295

Objectives: To evaluate the value of fast ripples (FRs) (200–500 Hz) recorded with stereo-electroencephalograph (SEEG) in the localization of epileptogenic tubers in patients with tuberous sclerosis complex (TSC).

Methods: Seventeen TSC patients who underwent preoperative SEEG examination and resective epilepsy surgery were retrospectively enrolled. They were divided into two groups according to the seizure control at 1-year postoperative follow-up. The occurrence frequencies of FRs were automatically counted, and the FR rate was calculated. The high FR rate was defined as FR rate $\geq$0.5. According to different positions, the contacts' locations were divided into three groups: inner of the tubers, the junction region of the tubers, and out of the tubers. The influence factors of postoperative seizure freedom were also analyzed.

Results: Twelve patients reached postoperative seizure freedom at 1-year follow-up. In total, FRs were found in 24.2% of the contacts and 67.1% of the tubers in all assessed patients. There were 47 high FR rate contacts localized in the junction region of the tubers, which was 62.7% of the 75 high FR rate contacts in total and was 8.4% of the total 561 contacts localized in the junction region of the tubers. Total removal of epileptogenic tubers and total resection of the high FR rate tubers/contacts were associated with postoperative seizure freedom ($P < 0.05$).

Conclusion: FRs could be extensively detected in TSC patients using SEEG, and high FR rate contacts were mostly localized in the junction region of the epileptogenic tuber, which could aid in the localization of epileptogenic tubers.

Keywords: epilepsy surgery, epileptogenic zone, fast ripples, stereo-electroencephalography(SEEG), tuberous sclerosis complex

HIGHLIGHTS

- Fast ripples can be detected extensively by stereo-electroencephalograph in tuberous sclerosis complex patients.
- Fast ripples with high rates of occurrence frequency can be used to localize epileptogenic tubers.
- Fast ripples with high rates of occurrence frequency are mostly detected in the junction region of the epileptogenic tubers.

INTRODUCTION

Tuberous sclerosis complex (TSC) is an autosomal dominant neurocutaneous syndrome: 85% of them with *TSC1* or *TSC2* gene mutation (Curatolo and Maria, 2013; Kingswood et al., 2014; Cui et al., 2018). Epilepsy is the most common neurological comorbidity, occurring in 90% of TSC patients (Liang et al., 2017; Cui et al., 2018; Liu et al., 2020). With medication-resistant epilepsy, there are additional standard-of-care approaches for seizure control in TSC patients beyond conventional antiseizure medications, and improved intellectual development has been found to be related to longer periods of seizure remission (Liang et al., 2017). Everolimus (a rapamycin analog), ketogenic diet therapy, and vagus nerve stimulation have been reported to have a greater than 50% reduction in seizure burden in more than 70% of patients with TSC (Krueger et al., 2013; Overwater et al., 2015; Park et al., 2017). Despite those treatments, more than 50% of patients with TSC still present intractable epilepsy. Several studies have demonstrated that resective surgery is the most effective treatment for TSC patients with medication-resistant epilepsy. Furthermore, systematic reviews have shown that 56–59% of TSC patients who underwent resective surgery achieved seizure freedom, and 68–75% experienced a worthwhile reduction (>90%) in seizure frequency (Jansen et al., 2007; Fallah et al., 2013; Liang et al., 2017; Liu et al., 2020).

Nevertheless, the greatest barrier to surgical intervention in TSC is the difficulty associated with localizing epileptogenic tuber(s), as multiple and bilateral cortical tubers often occur in cases with TSC (Fallah et al., 2013; Liang et al., 2017; Yu et al., 2019). High-resolution magnetic resonance imaging (MRI), magnetoencephalography, ^{11}C-positron emission tomography (PET), MRI-PET coregistration, subtraction ictal single photon emission computed tomography coregistered to MRI, and intracranial electroencephalography (EEG) have been utilized historically during preoperative assessments (Chugani et al., 2013; Kargiotis et al., 2014; Yogi et al., 2015; Sun et al., 2018; Yu et al., 2019). However, according to literatures with 10-year postoperative follow-ups, approximately 50% of TSC patients still suffered seizures following epilepsy surgery (Liang et al., 2017; Sun et al., 2018; Liu et al., 2020). To reach better postoperative seizure control, it is essential to develop newer and more efficient approaches to localize the epileptogenic tubers more accurately in TSC patients (Yu et al., 2019).

High-frequency oscillations (HFOs) (80–500 Hz) have been demonstrated to be a promising biomarker of epileptogenicity by many studies (Jacobs et al., 2008; Crépon et al., 2010; Fedele et al., 2017). The link between HFOs and the epileptogenic zone has previously been demonstrated according to clinical data indicating a correlation between the increased removal of areas with ictal HFOs and improved postsurgical outcomes (Crépon et al., 2010; Fedele et al., 2019). However, HFOs extending beyond the epileptogenic zone were reported in the majority of patients (Jacobs et al., 2010). Haegelen et al. (2013) reported that the removal of HFO-generating areas might lead to improved surgical outcomes in patients with temporal lobe epilepsy, but not in those with extratemporal lobe epilepsy. How to distinguish pathological ripples from physiological ripples is an obstacle in the clinical application of HFOs in the localization of epileptogenic zones. It is also reported that fast ripples (FRs) (200–500 Hz), but not ripples (80–200 Hz), correlate with seizure control in patients with medication-resistant epilepsy (Crépon et al., 2010; Akiyama et al., 2011; Ren et al., 2018).

In previous literatures, HFOs have been used for preoperative assessment in TSC patients with intracranial EEG recorded with subdural electrodes (Okanishi et al., 2014; Fujiwara et al., 2016). However, FRs recorded with stereo-EEG (SEEG) in TSC patients have not been studied before. Therefore, this study aims to utilize SEEG to investigate the value of FRs in localizing epileptogenic tuber(s) in TSC patients with epilepsy. We hypothesize that FRs may be a biomarker in the localization of epileptogenic tubers, and the distribution of FRs may be different in different parts of cortical tubers.

MATERIALS AND METHODS

Patient Selection and Inclusion Criteria

Patients were enrolled following the inclusion criteria: subjects who underwent preoperative evaluations with SEEG, subjects who finished resective surgeries from January 2016 to December 2018 in our epilepsy centers in Beijing, patients who had met the criteria of medication-resistant epilepsy for no less than 2 years, and subjects who had previously been diagnosed with TSC in accordance with the revised diagnostic criteria of Northrup (Northrup and Krueger, 2013). The exclusion criteria included subjects with one to three cortical tubers; subjects with obvious lymphangioleiomyomatosis, renal angiomyolipomas, and cardiac rhabdomyomas; and patients with serious cardiac, renal, or lung dysfunction (Liang et al., 2010, 2017). This study was approved by the Ethics Committee of the Fourth Medical Center, General Hospital of PLA, and the written consent was not signed for a retrospective study.

Non-invasive Preoperative Evaluation

Non-invasive preoperative evaluations included neurological history (e.g., clinical seizure semiology) and physical examination, MRI, long-term scalp video EEG recordings, PET, and neuropsychological testing. MRI scans included 3.0-T routine axial T1-weighted, T2-weighted, and diffusion-weighted imaging; sagittal T1-weighted imaging; and 1-mm thickness by zero interval axial and coronal T2–fluid-attenuated inversion recovery (FLAIR) imaging. The number of cortical tubers was counted using axial T2-FLAIR images. Neuropsychological

tests included Wechsler Intelligence Scale IV (Chinese revision) for measuring intelligence quotient and the overall subscale of quality of life on the Quality of Life in Childhood Epilepsy Questionnaire.

SEEG Examination and Epileptogenic Tuber Localization

Stereo-electroencephalograph electrodes with 8–16 contacts, 0.8 mm in diameter, 2 mm in length for contacts, and 1.5 mm in intercontact interval (Huake Company, Beijing, China) were embedded under generalized anesthesia for recording intracranial EEGs, in order to localize the epileptogenic tubers in TSC patients with multiple potential epileptogenic cortical tubers. The SEEG electrodes covered the potential epileptogenic cortical tubers, which had calcifications or cystic changes on MRI, had abnormal findings on PET images, or were localized in regions with focal ictal symptoms or focal ictal and/or interictal epileptiform discharges on scalp EEGs (Liang et al., 2017). In addition, the adjacent cortexes to those tubers were also covered with SEEG electrodes (Yu et al., 2019).

Data from a minimum of five habitual seizures episodes were required for further analysis and identification. The epileptogenic tuber was identified as the first tuber with initial rhythmical discharge on SEEG before clinical seizure attack. Propagating tubers were identified by secondary rhythmical discharges on SEEG before or after clinical seizure attack in 10 s after ictal EEG onset. If more than one tuber exhibited an initial rhythmical discharge on SEEG during the same seizure or during different seizure episodes, comprehensive analysis was performed by combining MRI-PET image fusion data and clinical semiology to distinguish independent epileptogenic tubers from propagating tubers (Yu et al., 2019; Liu et al., 2020).

FR Recording and Analysis

Interictal SEEG signals were recorded with an EEG acquisition system (Natus, United States) with a sampling frequency of 0–4,000 Hz (Ren et al., 2018). Five segments of 5-min interictal SEEGs during slow-wave sleep at midnight were used to analyze the occurrence frequency of FRs. Those segments were separated from each other and from seizure episodes by a minimum of 2 h. Slow-wave sleep was defined by the presence of more than 25% delta activity in 30-s epochs by visual inspection (Urrestarazu et al., 2007).

Bipolar montage with pairs of two adjacent EEG electrodes successively connected was used. The reference electrodes were excluded from the dataset. The automated detection of FRs was performed using software and previously described methods (Ren et al., 2018). During analysis, each contact and tuber with FRs were counted for every epoch and then averaged for a 5-min interval. The occurrence frequency of FRs was described with the number of FRs and the rate of FRs in each contact. The FR rate was calculated using the following formula: (the number of FRs in this contact/the maximum number of FRs among all contacts of this patient). A contact was defined as an FR contact when the occurrence frequency of FRs was more than 0.2/min in this contact. Similarly, a tuber with no less than one FR contact was defined as an FR tuber. In addition, when the FR rate was more than 0.5 in a certain contact (Burnos et al., 2014), we defined it as a high FR rate contact. Also, if no less than one high FR rate contact occurred in a tuber, we defined the tuber as a high FR rate tuber.

According to the positional relation of contacts and tubers, the locations of contacts were defined as inner of the tuber, junction region of the tuber, and out of the tuber. The inner of the tuber was defined as inner three-fourths of the tuber. The junction region of the tuber was defined as the outer quarter area of the tuber border on MRI-T2-FLAIR plus the adjacent cortical area of gyrus with tuber involvement. *Out of the tuber* means the cortex of gyrus without tuber involvement (**Figure 1**).

Surgical Approaches and Postoperative Medical Treatments

Patients underwent either lobectomies or tuber resections. Tuber resections were used for epileptogenic tubers within or close to eloquent areas. Lobectomies were applied when epileptogenic tubers were in the anterior temporal lobe or the frontal pole. Multiple tuber resections or lobectomies with tuber resection were considered in cases of multiple epileptogenic tubers unable to be removed by a single lobectomy. Pharmaceutical treatments were provided to all postoperative patients, utilizing optimized combinations of two to four kinds of antiseizure medications. Potential medications used in postoperative patient care were topiramate, vigabatrin, valproate, levetiracetam, lamotrigine, and oxcarbazepine.

Statistical Analysis

Statistical analysis was completed using the SPSS statistical program (version 19.0; SPSS, Inc., Chicago, IL, United States). Postoperative seizure controls were classified according to the Engel method into class I (seizure free), class II (rare seizures), class III (>90% reduction in seizure frequency), and class IV (<90 reduction in seizure frequency). Outcomes were described with percentages, means, and SD. Univariate analysis of categorical variables was performed using χ^2 and Fisher exact tests. *t*-tests and *F*-tests were used for comparison of continuous variables. When the two-tailed error probability *P* was less than 0.05, the outcome was considered to be significant.

RESULTS

Patients and Presurgical Evaluations

A total of 46 patients with TSC underwent epilepsy surgery at our hospitals from January 2016 to December 2018. Twenty-one patients received implanted SEEG electrodes and underwent resective surgery, and 17 of them with comprehensive FRs data were included in this study (**Table 1**). Both female (n = 6) and male (n = 11) patients were presented. Patient ages ranged from 2.9 to 12.6 (mean = 6.13 ± 3.06) years. Types of clinical seizures at onset included generalized epileptic spasms (n = 9), generalized tonic–clonic seizure (n = 3), focal seizure (n = 4), and generalized clonic seizure (n = 1). Seizure frequencies included

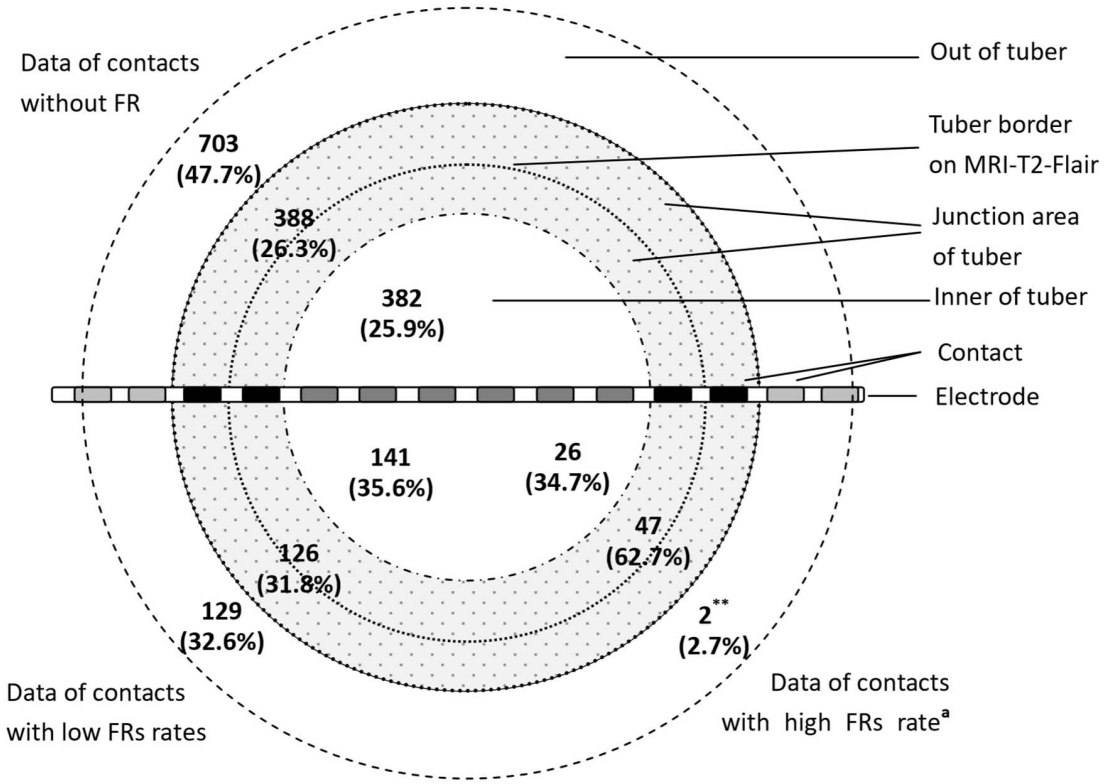

FIGURE 1 | The distribution of contacts with FRs in different parts of tubers (**$P < 0.01$, the data in this group compared with the data of contacts without FRs and data of contacts with low FR rates. [a]The ratio of the high FR rate was more than 0.5). The figure shows distribution of FRs across different parts of the tuber. The majority of the high FR rate (ratio of occurrence frequency of fast ripples $\geq$0.5) presented in the junction area of the tubers.

either daily seizures (n = 14) or weekly seizures (n = 3). Age at seizure onset ranged from 0.2 to 5.9 (mean = 1.34 ± 1.60) years. The durations of preoperative seizures ranged from 2.3 to 9.6 (mean = 4.79 ± 2.37) years. Through observation and counting, each patient had 10.18 ± 3.21 (range = 4–16) cortical tubers.

Surgical Approaches and Outcomes

A total of 25 epileptogenic tubers were identified across all patients. Patients were observed to have a single epileptogenic tuber (n = 9) or two epileptogenic tubers (n = 8); no patient was observed to have more than two epileptogenic tubers. Furthermore, 35 early propagating tubers were identified. Surgical interventions varied case by case and included epileptogenic tuber resection (n = 6), lobectomy or multilobar resection (n = 7), and a combination of lobectomy and tuber resection (n = 4). In total, 52 tubers, including 22 epileptogenic tubers and 30 propagating tubers, were removed. At 1-year follow-up, 12 patients (70.6%) achieved seizure freedom (Engel I), one reached Engel II, and the other four cases reached Engel III–IV seizure control. Significant difference was found in the percentage of total removal of epileptogenic tubers between patients with postoperative seizure freedom and those with postoperative continuous seizure at 1-year follow-up (P = 0.0239) (**Table 2**).

Interictal FRs and the Distribution

There were 471 (24.2%) FR contacts detected from the 1,944 contacts of 144 implanted SEEG electrodes, including 75 (3.9%) high FR rate contacts. Moreover, 102 (67.1%) FR tubers were observed across all covered tubers (n = 152) in all patients (**Table 1**).

The occurrence frequency of FR discharge significantly varied across the tuber anatomy ($P < 0.01$). There were 62.7% (47 of 75) high FR rate contacts located at the junction region of the tubers, and those contacts without FRs mainly located out of the tubers (n = 703, 47.7% of 1,473). High FR rate contacts included two (0.2% of 834) contacts out of the tubers, 47 (8.4% of 561) contacts in the junction region of the tubers, and 26 (4.7% of 549) contacts in the inner of the tubers (**Figure 1**). There were significant differences in the percentage of the high FR rate contacts in the three parts of cortical tubers (P = 0.0000).

Interictal FRs and Seizure Control

The tubers and contacts with FRs were compared between patients with Engel I seizure controls and those with Engel II–IV seizure controls. There was no significant difference found in percentage (or number) of FR contacts (or tubers) between those two groups ($P > 0.05$) (**Table 2**).

TABLE 1 | Patients' clinical and demographic characteristics and FR data.

No.	Gender	Age at operation (years)	Age at seizure onset (years)	Seizure type	Drugs	Number of tubers	Number of electrodes	Number of tubers covered with SEEG	Total number of contacts	Contacts containing FRs (%)	Number of FRs in contacts containing FRs (mean ± SD)	Tubers with FRs (%)	Onset tuber	Propagating tuber	Resected tubers	Follow-up (years)	Seizure free at 1 year
1	Male	8.2	5.9	GCTS CPS	VPA/LMT	4	4	4	52	8 (15.4)	125.63 ± 122.39	3 (75.0)	R-T	R-P R-F	R-T R-F	3.7	Yes
2	Female	4	0.2	CPS Tonic	OXC/LEV LMT/VPA	10	9	9	127	6 (4.7)	34.33 ± 37.25	3 (33.3)	L-F L-T	L-T L-O	L-T/L-F L-O	3.3	Yes
3	Male	5.8	0.8	Spasm GTCS/AA	VAP/LMT TMP	16	11	10	128	47 (36.7)	41.32 ± 74.50	10 (90.9)	R- R-F	R-FP R-TO	R-F/R-FP R-T/R-TO	2.7	Yes
4	Male	2.6	0.3	Spasm CPS	VPA/LMT LEV/RPM	8	7	8	104	17 (16.3)	9.35 ± 19.36	6 (75.0)	R-P	R-T R-PC	R-P/R-PC R-T	2.6	Yes
5	Female	3.8	0.5	Spasm GTCS	VPA/LEV VGB/RPM	12	9	11	122	14 (11.5)	6.07 ± 3.67	5 (45.5)	L-F R-F	L-FP L-T L-F	L-FP L-T/L-F	2.3	Yes
6	Female	3.7	0.3	Spasm CPS	VPA/LEV RPM/VGB	11	9	11	126	3 (2.4)	3.33 ± 2.31	2 (18.2)	R-P	R-I R-T	R-T/R-P R-I	1.8	Yes
7	Male	4.3	0.3	Spasm tonic	VPA/CLB RPM/VGB	14	10	12	121	26 (21.5)	28.50 ± 55.07	7 (58.3)	R-T	R-F	R-T R-F	1.7	Yes
8	Male	8.1	4	CPS GTCS	VPA/LMT RPM	9	10	9	124	33 (26.6)	55.61 ± 80.61	8 (88.9)	L-P	L-T L-PC	L-P/L-PC L-T	1.6	Yes
9	Male	3.8	0.8	Clonic/AA GCTS	VPA/TMP LEV	8	8	8	116	28 (24.1)	32.61 ± 21.86	7 (87.5)	R-F R-T	R-I R-FC	R-F/R-FC R-T/R-I	1.3	Yes
10	Male	7	0.3	Spasm GCTS	LEV/TMP VGB/LMT	11	9	10	127	24 (18.9)	157.42 ± 171.45	4 (40)	R-F	L-F R-T	R-F/L-F	1.2	Yes
11	Male	6.6	1	CPS/tonic GTCS	VPA/CBZ VGB/RPM	11	9	9	126	34 (27.0)	100.09 ± 170.57	8 (88.9)	L-F	L-P L-T	L-F/L-P L-T	1.1	Yes
12	Male	11	2	CPS GTCS	CBZ/VPA LMT	6	6	6	90	43 (47.8)	108.52 ± 218.28	6 (100)	L-P	L-F L-I	L-P/L-F L-I	1.1	Yes
13	Female	4.8	0.4	Spasm CPS	OXC/VPA VGB/RPM	7	7	7	104	51 (49.4)	77.16 ± 73.16	7 (100)	R-F L-F	R-T/R-P R-FC	R-F/R-T R-P/R-FC	2.9	No
14	Female	10.8	2	GTSC myoclonic	LEV/LMT VPA/RPM	14	8	10	116	4 (3.4)	4.75 ± 3.59	3 (30)	L-T	L-O/L-P	L-T/L-O L-P	2.8	No
15	Male	4.2	0.4	Spasm tonic AA	VPA/OXC LMT/VGB RPM	8	9	8	124	18 (14.5)	50.61 ± 41.78	6 (75.0)	R-Central R-F	R-F/L-F R-C	R-F R-Central R-C	1.8	No
16	Female	12.6	3	GCTS CPS	LEV/VGB VPA	10	9	9	110	53 (48.2)	25.45 ± 38.33	7 (77.8)	R-F L-P	R-T/R-I R-TO	R-F/R-I R-T R-TO	1.7	No
17	Male	2.9	0.5	Spasm tonic	LEV/CLB RPM/VGB	14	10	11	127	62 (48.8)	11.63 ± 22.39	10 (90.9)	L-F R-P	L-I/L-C	L-F/L-I L-C	1	No

AA, atypical absence; C, cingulate gyrus; CPS, complex partial seizure; F, frontal lobe; GTCS, generalized tonic-clonic seizure; I, insular lobe; L, left; NA, no available; O, occipital lobe; P, parietal lobe; R, right; T, temporal lobe; CBZ, carbamazepine; CLB, clobazam; LEV, levetiracetam; LMT, lamotrigine; OXC, oxcarbazepine; RPM, rapamycin; TMP, topiramate; VGB, vigabatrin; VPA, valproate.

TABLE 2 | Influence factors of postoperative seizure freedom.

Factors	Patients with seizure freedom (*n* = 12)	Patients with continuous seizure (*n* = 5)	*P*-value
Age at surgery (years)	5.53 + 2.49	7.06 + 4.34	0.3675
History of seizure (years)	4.63 + 2.21	5.80 + 3.20	0.3954
Age at first seizure (years)	1.37 + 1.79	1.26 + 1.19	0.9021
Patients with epileptic spasm (count/%)	6/50.0%	3/60.0%	0.8754
Patients with partial seizure (count/%)	7/58.3%	2/40.0%	0.7066
Number of cortical tubers	9.50 + 3.73	10.6 + 3.27	0.5758
Number of epileptogenic tubers	1.33 + 0.49	1.80 + 0.45	0.0855
Number of propagating tubers	2.00 + 0.43	2.40 + 0.55	0.1269
Number of epileptogenic tubers and early propagating tubers	3.33 + 0.78	4.20 + 0.84	0.0580
Number of removed tubers	2.92 + 0.67	3.40 + 0.55	0.1794
Total removal of epileptogenic tubers (count/%)	12/100%	2/40%	**0.0239**
Total removal of epileptogenic and early propagating tubers (count/%)	9/75%	1/20%	0.1191
Percentage of contacts with fast ripples (%)	21.01 + 12.80	32.86 + 22.18	0.1806
Percentage of tubers with fast ripples (%)	67.55 ± 27.74	74.74 + 26.97	0.6309
Number of contacts with fast ripples	23.58 + 14.33	37.60 + 25.12	0.1609
Number of tubers with fast ripples	5.75 + 2.42	6.60 + 2.51	0.5235
Total resection of contacts with high fast ripples rate (FRs rate ≥ 0.5)	11 (91.7%)	0 (0.0%)	**0.0023**
Total resection of tubers with high fast ripples rate (FRs rate ≥ 0.5)	11 (91.7%)	0 (0.0%)	**0.0023**

Bold values indicate the P < 0.05.

The removed brain tissues included 272 FR contacts (**Figure 2**) and 48 FR tubers (**Figure 3**) in all patients. Each patient removed 3–30 FR contacts, and the maximum rates of FRs occurrence frequency in remained contacts ranged from 0 to 1 in different cases (**Figure 2**). Significant differences were found in seizure freedom between patients who totally removed the high FR rate contacts and those who partially removed the high FR rate contacts (100 vs. 16.7%, $P < 0.05$) (**Table 2**).

Each patient removed two to four FR tubers, and the maximum FR rate in the remained tubers ranged from none to one in different cases (**Figure 3**). Significant differences were found in seizure freedom between those who totally removed high FR rate tubers and cases who partially removed high FR rate tubers (100 vs. 16.7%, $P < 0.05$) (**Table 2**).

Complications

One patient presented asymptomatic epidural hematoma around an electrode. No complication was identified during FR recording.

DISCUSSION

To the best of our knowledge, this study presented the first comprehensive observations of FRs detected by SEEG in cortical tubers of TSC patients. FRs were recorded in 24.2% of SEEG contacts and 67.1% of tubers covered with SEEG electrodes. The occurrence frequency of FRs varied among patients. However, areas with FRs were relatively stable in the same patient, which was consistent with previous studies (Bagshaw et al., 2009).

Fujiwara et al. (2016) and Okanishi et al. (2014) reported the presence of ictal and interictal ripples and FRs in children with TSC recorded by subdural intracranial EEG, respectively. However, the analysis of ictal HFOs was unreliable because of various potential impacts, and the ripples could not work as a biomarker for epileptogenic onset zone (Crépon et al., 2010; Akiyama et al., 2011; Fedele et al., 2019). Fujiwara et al. (2016) found that complete resection of regions with HFOs led to a better surgical outcome. However, our study and the study by Okanishi et al. (2014) showed that extensive FRs were recorded in TSC patients, and complete resection of FR contact was uncommon, especially for patients with multiple tubers. Therefore, high FR rate contacts should be identified.

Clinicians faced multifaceted challenges related to thresholds and the identification of potential epileptogenic areas. Okanishi et al. (2014) applied a bootstrapping method for thresholding, which yielded a mean HFO rate and then used it to distinguish between high and low FR channels. Application of this method led to a significant correlation between removal of the high occurrence frequency FR channels and the postoperative seizure freedom in TSC patients with subdural electrode EEG. In this retrospective research, we used 0.5 as the cutoff ratio of high occurrence frequency of FRs to define the epileptogenic zone and tubers, which had been used by Burnos et al. (2014). Then, we found significant differences in seizure freedom between patients who totally removed contacts (tubers) with high FR rates and those who partially removed, which indicated that the threshold of 0.5 had practicability and reliability in the identification of epileptogenic tuber in TSC patients, but more data were still needed to test and verify.

Previously, the onset zones of TSC, localizing to TSC tuber itself vs. perituber cortex, were controversial (Ma et al., 2012; Kannan et al., 2016). TSC cortical tubers were observed to have dysmorphic cytomegalic and immature neurons, which played an important role in the generation and propagation of epileptic discharges (Abdijadid et al., 2015; Mühlebner et al., 2016). The perituber cortex was identified through abnormalities obtained through electrocorticography, diffusive tension image, histological pathology, immunohistochemical analysis, or molecular patterns (Oh et al., 2011; Ma et al., 2012; Krsek et al., 2013). Kannan et al. (2016) found that focal seizures and interictal epileptiform discharges raised at the center of epileptogenic tubers and propagated into the tuber rim, perituber cortex, and other epileptogenic tubers. With the use of SEEG, but not subdural intracranial EEG, the FRs in the inner of the tubers and junction area of the tubers could be recorded. In this study, we found that 62.6% of the high FR rate contacts presented on the junction region of the tuber and adjacent cortex, while the

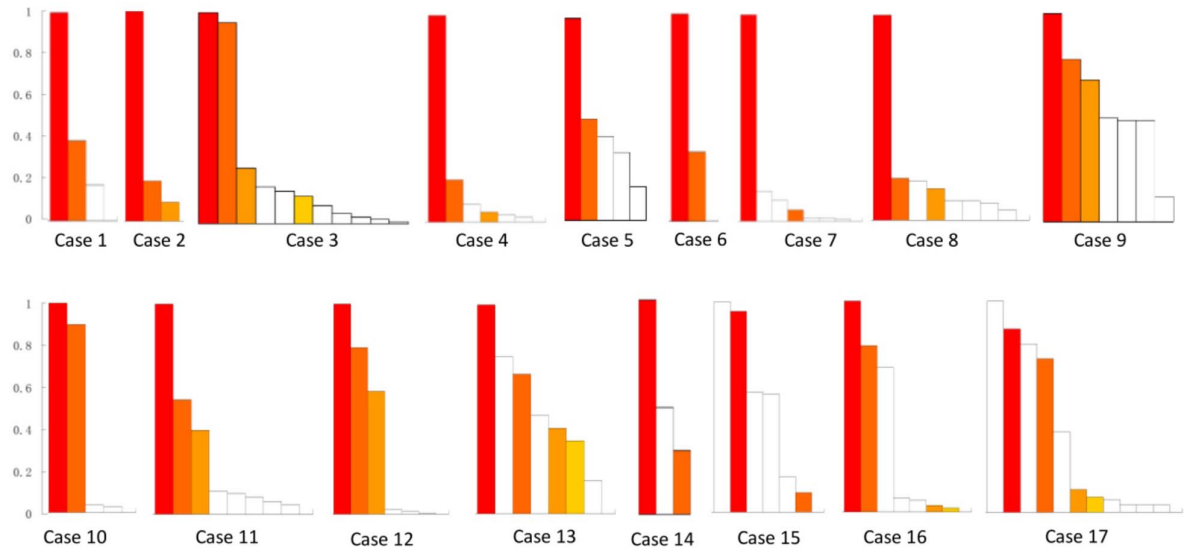

FIGURE 2 | Resective range of contacts with FRs in all of the 17 patients. This figure shows the removed contacts with FRs in each patient. There were 272 FR contacts removed in total. White bars show the reserved contacts with FR discharges. Color bars show the removed contacts with FRs. The same color bars in each patient meant the removed contacts in the same electrode, whereas the different color bars in each patient meant the contacts from different electrodes. Patients 13–17 suffered continuous seizure attack after resective operations. *y*-axis was the ratio of FRs on each contact. *x*-axis was contacts in order of the ratio of FR discharges in each patient.

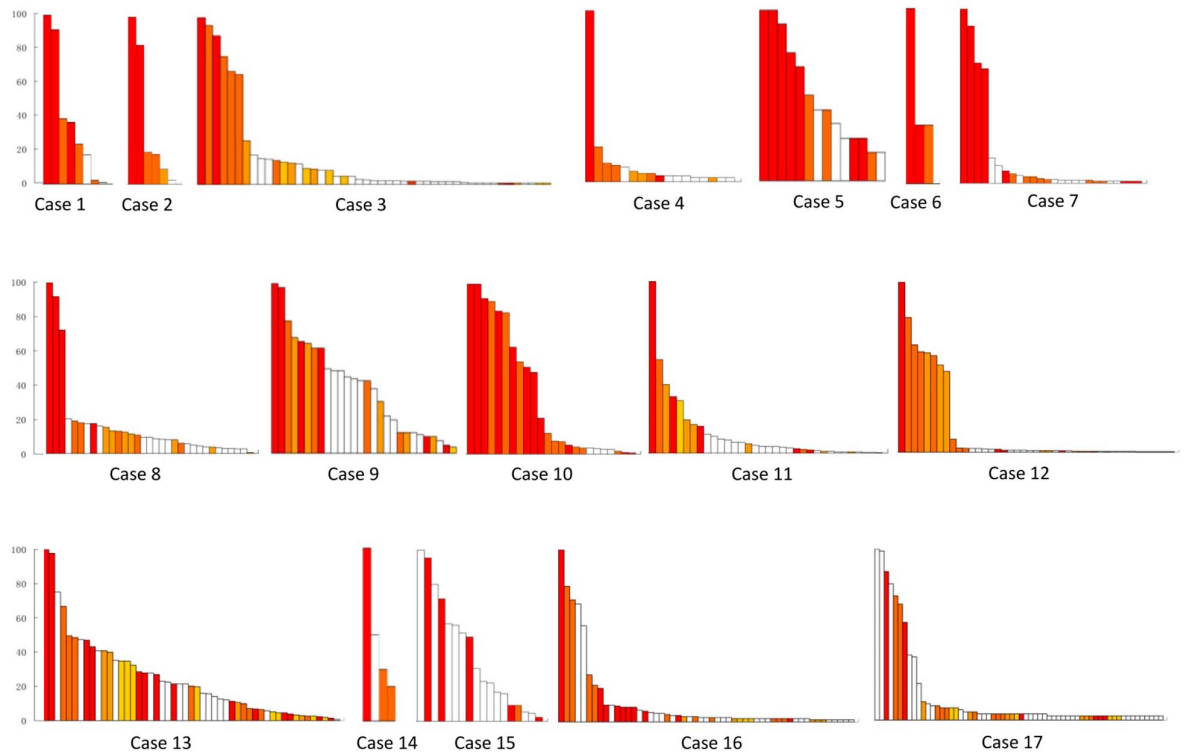

FIGURE 3 | Resective range of the tubers with FRs in all of the 17 patients. This figure shows the removed fast ripple tubers in each patient, and the number was 48 in total. White bars show the reserved tubers with FR discharges. Color bars show the removed tubers with FRs, and different color bars meant different removed tubers in each patient. Patients 13–17 suffered continuous seizure attack after resective operations. *y*-axis was the ratio of FRs on each tuber. *x*-axis was tubers in order of the ratio of FRs in different tubers in each patient.

contacts with low FR rates were almost evenly distributed in the inner of the tubers, the junction area of the tubers, and out of the tubers. Therefore, the junction area of epileptogenic tubers should be the epileptogenic zones in TSC patients.

There are some limitations to this study. First, patients with one to three cortical tubers were excluded, because the epileptogenic tuber and propagative tuber need to be defined at the same time. Second, TSC patients with three or more epileptogenic tubers were not enrolled in the study, because most of them were excluded from the resective operations. Third, the sample of enrolled subjects was small because of the low incidence of TSC.

CONCLUSION

In conclusion, FRs were extensively recorded in patients with TSC utilizing SEEG, and electrode contacts with high FR rates can be used to localize epileptogenic tubers. Furthermore, the junction areas of the tubers had most contacts with high FR rates and indicated the locations of epileptogenic zones.

DATA AVAILABILITY STATEMENT

The raw data supporting the conclusions of this article will be made available by the authors, without undue reservation.

ETHICS STATEMENT

The studies involving human participants were reviewed and approved by the Ethics Committee of Fourth Medical Center, General Hospital of PLA. Written informed consent for participation was not provided because this study is a retrospective study and patients did not provide additional information or perform other treatments or examinations.

AUTHOR CONTRIBUTIONS

SlL and SZ performed the operative and collected candidate information. LY, ShL, and XYu finished the EEG recording. XYa, YW, LY, TL, and SlL performed HFO analyses. SlL, ShL, YW, and XYa drafted the manuscript. YW, LY, SZ, and TL analyzed the datasets. All authors contributed to the article and approved the submitted version.

FUNDING

This research was supported by National Natural Science Foundation of China (81771388 and 82071448, SlL) and Beijing Nature and Science Foundation of China (7202045, SlL). Those funds did not involve the study design, data collection and analysis, interpretation of data and the writing of the report.

ACKNOWLEDGMENTS

The authors would like to show gratitude to the patients and their families for their long-term cooperation. The authors also appreciate the contribution provided by the following people: J. F. Cui from Neurosurgery Department, N. Liu, X. Y. Shang and all technicians in the Neurophysiologic Laboratory of Capital Epilepsy Therapy Center.

REFERENCES

Kingswood, J. C., Bruzzi, P., Curatolo, P., de Vries, P. J., Fladrowski, C., Hertzberg, C., et al. (2014). TOSCA - first international registry to address knowledge gaps in the natural history and management of tuberous sclerosis complex. *Orphanet J. Rare Dis*. 9:182.

Curatolo, P., and Maria, B. L. (2013). Tuberous sclerosis. *Handb. Clin. Neurol.* 111, 323–331.

Cui, J., Yu, X., Liang, S., Zhang, S., and Hu, X. (2018). First five generations Chinese family of tuberous scleroses complex due to a new mutation of the TSC1 gene. *J. Clin. Neurosci*. 54, 39–44. doi: 10.1016/j.jocn.2018.05.007

Liu, S., Yu, T., Guan, Y., Zhang, K., Ding, P., Chen, L., et al. (2020). Resective epilepsy surgery in tuberous sclerosis complex: a nationwide multicentre retrospective study from China. *Brain* 143, 570–581. doi: 10.1093/brain/awz411

Liang, S., Zhang, J., Yang, Z., Zhang, S., Cui, Z., Cui, J., et al. (2017). Long-term outcomes of epilepsy surgery in tuberous sclerosis complex. *J. Neurol.* 264, 1146–1154.

Overwater, I. E., Bindels-de Heus, K., Rietman, A. B., Ten Hoopen, L. W., Vergouwe, Y., Moll, H. A., et al. (2015). Epilepsy in children with tuberous sclerosis complex: chance of remission and response to antiepileptic drugs. *Epilepsia* 56, 1239–1245. doi: 10.1111/epi.13050

Krueger, D. A., Wilfong, A. A., Holland-Bouley, K., Anderson, A. E., Agricola, K., Tudor, C., et al. (2013). Everolimus treatment of refractory epilepsy in tuberous sclerosis complex. *Ann. Neurol.* 74, 679–687. doi: 10.1002/ana.23960

Park, S., Lee, E. J., Eom, S., Kang, H. C., Lee, J. S., Kim, H. D., et al. (2017). Ketogenic diet for the management of epilepsy associated with tuberous sclerosis complex in children. *J. Epilepsy. Res.* 7, 45–49. doi: 10.14581/jer.17008

Jansen, F. E., Van Huffelen, A. C., Algra, A., and van Nieuwenhuizen, O. (2007). Epilepsy surgery in tuberous sclerosis: a systematic review. *Epilepsia* 48, 1477–1484. doi: 10.1111/j.1528-1167.2007.01117.x

Fallah, A., Guyatt, G. H., Snead, O. C. III, Ebrahim, S., Ibrahim, G. M., Mansouri, A., et al. (2013). Predictors of Seizure Outcomes in Children with Tuberous Sclerosis Complex and Intractable Epilepsy Undergoing Resective Epilepsy Surgery: an Individual Participant Data Meta-Analysis. *PLoS One* 8:e53565. doi: 10.1371/journal.pone.0053565

Yu, X., Ding, P., Yuan, L., Zhang, J., Liang, S., Zhang, S., et al. (2019). Cortico-Cortical Evoked Potentials in Children With Tuberous Sclerosis Complex Using Stereo-Electroencephalography. *Front. Neurol.* 10:1093. doi: 10.3389/fneur.2019.01093

Sun, K., Cui, J., Wang, B., Jiang, T., Chen, Z., Cong, F., et al. (2018). Magnetic resonance imaging of tuberous sclerosis complex with or without epilepsy at 7 T. *Neuroradiology* 60, 785–794. doi: 10.1007/s00234-018-2040-2

Yogi, A., Hirata, Y., Karavaeva, E., Harris, R. J., Wu, J. Y., Yudovin, S. L., et al. (2015). DTI of tuber and perituberal tissue can predict epileptogenicity in tuberous sclerosis complex. *Neurology* 85, 2011–2015. doi: 10.1212/wnl.0000000000002202

Kargiotis, O., Lascano, A. M., Garibotto, V., Spinelli, L., Genetti, M., Wissmeyer, M., et al. (2014). Localization of the epileptogenic tuber with electric source imaging in patients with tuberous sclerosis. *Epilepsy Res.* 108, 267–279. doi: 10.1016/j.eplepsyres.2013.11.003

Chugani, H. T., Luat, A. F., Kumar, A., Govindan, R., Pawlik, K., Asano, E., et al. (2013). α-[11C]-Methyl-L-tryptophan–PET in 191 patients with tuberous sclerosis complex. *Neurology* 81, 674–680. doi: 10.1212/wnl.0b013e3182a08f3f

Jacobs, J., LeVan, P., Chander, R., Hall, J., Dubeau, F., Gotman, J., et al. (2008). Interictal high-frequency oscillations (80-500 Hz) are an indicator of seizure onset areas independent of spikes in the human epileptic brain. *Epilepsia* 49, 1893–1907. doi: 10.1111/j.1528-1167.2008.01656.x

Crépon, B., Navarro, V., Hasboun, D., Clemenceau, S., Martinerie, J., Baulac, M., et al. (2010). Le Van Quyen M. et al. Mapping interictal oscillations greater than 200 Hz recorded with intracranial macroelectrodes in human epilepsy. *Brain* 133, 33–45. doi: 10.1093/brain/awp277

Fedele, T., Burnos, S., Boran, E., Krayenbühl, N., Hilfiker, P., Grunwald, T., et al. (2017). Resection of high frequency oscillations predicts seizure outcome in the individual patient. *Sci. Rep.* 7:13836.

Jacobs, J., Zijlmans, M., Zelmann, R., Olivier, A., Hall, J., Gotman, J., et al. (2010). Value of electrical stimulation and high frequency oscillations (80-500 Hz) in identifying epileptogenic areas during intracranial EEG recordings. *Epilepsia* 51, 573–582. doi: 10.1111/j.1528-1167.2009.02389.x

Fedele, T., Ramantani, G., and Sarnthein, J. (2019). High frequency oscillations as markers of epileptogenic tissue - End of the party?. *Clin. Neurophysiol.* 130, 624–626. doi: 10.1016/j.clinph.2019.01.016

Haegelen, C., Perucca, P., Châtillon, C. E., Andrade-Valença, L., Zelmann, R., Jacobs, J., et al. (2013). High-frequency oscillations, extent of surgical resection, and surgical outcome in drug-resistant focal epilepsy. *Epilepsia* 54, 848–857. doi: 10.1111/epi.12075

Akiyama, T., McCoy, B., Go, C. Y., Ochi, A., Elliott, I. M., Akiyama, M., et al. (2011). Focal resection of fast ripples on extraoperative intracranial EEG improves seizure outcome in pediatric epilepsy. *Epilepsia* 52, 1802–1811. doi: 10.1111/j.1528-1167.2011.03199.x

Ren, G. P., Yan, J. Q., Yu, Z. X., Wang, D., Li, X. N., Mei, S. S., et al. (2018). Automated detector of high frequency oscillations in epilepsy based on maximum distributed peak points. *Int. J. Neural. Sys.* 28:1750029. doi: 10.1142/s0129065717500290

Okanishi, T., Akiyama, T., Tanaka, S., Mayo, E., Mitsutake, A., Boelman, C., et al. (2014). Interictal high frequency oscillations correlating with seizure outcome in patients with widespread epileptic networks in tuberous sclerosis complex. *Epilepsia* 55, 1602–1610. doi: 10.1111/epi.12761

Fujiwara, H., Leach, J. L., Greiner, H. M., Holland-Bouley, K. D., Rose, D. F., Arthur, T., et al. (2016). Resection of ictal high frequency oscillations is associated withfavorable surgical outcome in pediatric drug resistant epilepsy secondary totuberous sclerosis complex. *Epilepsy Res.* 126, 90–97. doi: 10.1016/j.eplepsyres.2016.07.005

Northrup, H., and Krueger, D. A. (2013). International Tuberous Sclerosis Complex Consensus Group. Tuberous sclerosis complex diagnostic criteria update: recommendations of the 2012 Iinternational Tuberous Sclerosis Complex Consensus Conference. *Pediatr. Neurol.* 49, 243–254.

Liang, S., Li, A., Zhao, M., Jiang, H., Yu, S., Meng, X., et al. (2010). Epilepsy surgery in tuberous sclerosis complex: emphasis on surgical candidate and neuropsychology. *Epilepsia* 51, 2316–2321. doi: 10.1111/j.1528-1167.2010.02669.x

Urrestarazu, E., Chander, R., Dubeau, F., and Gotman, J. (2007). Interictal high-frequency oscillations (100-500 Hz) in the intracerebral EEG of epileptic patients. *Brain* 130, 2354–2366. doi: 10.1093/brain/awm149

Burnos, S., Hilfiker, P., Sürücü, O., Scholkmann, F., Krayenbühl, N., Grunwald, T., et al. (2014). Human Intracranial High Frequency Oscillations (HFOs) Detected by Automatic Time-Frequency Analysis. *PLoS One* 9:e94381. doi: 10.1371/journal.pone.0094381

Bagshaw, A. P., Jacobs, J., LeVan, P., Dubeau, F., and Gotman, J. (2009). Effect of sleep stage on interictal highfrequency oscillations recorded from depth macroelectrodes in patients with focal epilepsy. *Epilepsia* 50, 617–628. doi: 10.1111/j.1528-1167.2008.01784.x

Kannan, L., Vogrin, S., Bailey, C., Maixner, W., and Harvey, A. S. (2016). Centre of epileptogenic tubers generate and propagate seizures in tuberous sclerosis. *Brain* 139, 2653–2667. doi: 10.1093/brain/aww192

Ma, T. S., Elliott, R. E., Ruppe, V., Devinsky, O., Kuzniecky, R., Weiner, H. L., et al. (2012). Electrocorticographic evidence of perituberal cortex epileptogenicity in tuberous sclerosis complex. *J. Neurosurg. Pediatr.* 10, 376–382. doi: 10.3171/2012.8.peds1285

Abdijadid, S., Mathern, G. W., Levine, M. S., and Cepeda, C. (2015). Basic mechanisms of epileptogenesis in pediatric cortical dysplasia. *CNS Neurosci. Ther.* 21, 92–103. doi: 10.1111/cns.12345

Mühlebner, A., van Scheppingen, J., Hulshof, H. M., Scholl, T., Iyer, A. M., Anink, J. J., et al. (2016). Novel histopathological patterns in cortical tubers of epilepsy surgery patients with tuberous sclerosis complex. *PLoS One* 11:e0157396. doi: 10.1371/journal.pone.0157396

Oh, S., Stewart, T., Miller, I., Bhatia, S., Ragheb, J., Duchowny, M., et al. (2011). In vivo optical properties of cortical tubers in children with tuberous sclerosis complex (TSC): a preliminary investigation. *Epilepsia* 52, 1699–1704. doi: 10.1111/j.1528-1167.2011.03167.x

Krsek, P., Jahodova, A., Kyncl, M., Kudr, M., Komarek, V., Jezdik, P., et al. (2013). Predictors of seizure-free outcome after epilepsy surgery for pediatric tuberous sclerosis complex. *Epilepsia* 54, 1913–1921. doi: 10.1111/epi.12371

Conflict of Interest: The authors declare that the research was conducted in the absence of any commercial or financial relationships that could be construed as a potential conflict of interest.

The handling editor declared a shared affiliation with several of the authors (YW, LY, SZ, TL, and SlL) at the time of review.

frontiers in Human Neuroscience

ORIGINAL RESEARCH
published: 30 July 2021
doi: 10.3389/fnhum.2021.709836

High-Frequency Oscillations on Interictal Epileptiform Discharges in Routinely Acquired Scalp EEG: Can It Be Used as a Prognostic Marker?

Hanan El Shakankiry and Susan T. Arnold*

UT Southwestern Medical School, Children's Health, Dallas, TX, United States

Introduction: Despite all the efforts for optimizing epilepsy management in children over the past decades, there is no clear consensus regarding whether to treat or not to treat epileptiform discharges (EDs) after a first unprovoked seizure or the optimal duration of therapy with anti-seizure medication (ASM). It is therefore highly needed to find markers on scalp electroencephalogram (EEG) that can help identify pathological EEG discharges that require treatment.

Aim of the study: This retrospective study aimed to identify whether the coexistence of ripples/high-frequency oscillations (HFOs) with interictal EDs (IEDs) in routinely acquired scalp EEG is associated with a higher risk of seizure recurrence and could be used as a prognostic marker.

Methods: 100 children presenting with new onset seizure to Children's Medical Center-Dallas during 2015–2016, who were not on ASM and had focal EDs on an awake and sleep EEG recorded with sample frequency of 500 HZ, were randomly identified by database review. EEGs were analyzed blinded to the data of the patients. HFOs were visually identified using review parameters including expanded time base and adjusted filter settings.

Results: The average age of patients was 6.3 years (±4.35 SD). HFOs were visually identified in 19% of the studied patients with an inter-rater reliability of 99% for HFO negative discharges and 78% agreement for identification of HFOs. HFOs were identified more often in the younger age group; however, they were identified in 11% of patients >5 years old. They were more frequently associated with spikes than with sharp waves and more often with higher amplitude EDs. Patients with HFOs were more likely to have a recurrence of seizures in the year after the first seizure ($P < 0.05$) and to continue to have seizures after 2 years ($P < 0.0001$). There was no statistically significant difference between the two groups with regards to continuing ASM after 2 years.

Conclusion: Including analysis for HFOs in routine EEG interpretation may increase the yield of the study and help guide the decision to either start or discontinue ASM. In the future, this may also help to identify pathological discharges with deleterious effects on the growing brain and set a new target for the management of epilepsy.

Keywords: high-frequency oscillations, ripples, scalp EEG, prognostic marker, epilepsy

OPEN ACCESS

Edited by:
Jing Xiang,
Cincinnati Children's Hospital Medical Center, United States

Reviewed by:
Duo ' Chen,
Nanjing University of Chinese Medicine, China
Li Zheng,
Peking University, China

****Correspondence:***
Hanan El Shakankiry
hshakankiry@hotmail.com

Specialty section:
This article was submitted to Brain Imaging and Stimulation, a section of the journal Frontiers in Human Neuroscience

Received: *14 May 2021*
Accepted: *28 June 2021*
Published: *30 July 2021*

Citation:
El Shakankiry H and Arnold ST (2021) High-Frequency Oscillations on Interictal Epileptiform Discharges in Routinely Acquired Scalp EEG: Can It Be Used as a Prognostic Marker? Front. Hum. Neurosci. 15:709836. doi: 10.3389/fnhum.2021.709836

INTRODUCTION

Despite all the efforts for optimizing epilepsy management in children over the past decades, controversy still exists in many areas in this field; there is no clear consensus regarding whether or not to treat epileptiform discharges (EDs), which are seen on electroencephalogram (EEG), or the duration of therapy.

For patients presenting with their first seizure, it is well known that the underlying etiology and whether the EEG is normal or abnormal are factors consistently related to the risk of recurrence; however, randomized controlled trials have demonstrated that compared to no or delayed treatment, antiepileptic drugs reduce the risk of a second seizure but do not alter longer-term seizure outcomes (Hirtz et al., 2003; Marson, 2008), and there is no existing EEG prognostic marker for intractability. In addition, when epilepsy is in remission, the optimal timing of anti-seizure medication (ASM) discontinuation is still unknown (Strozzi et al., 2015).

It is also worth mentioning that EDs have been observed in 0.6 and 7.0% of children without epileptic seizures and relatives of patients with epilepsy (Bali et al., 2007; Borusiak et al., 2010). The high incidence of abnormal patterns in the EEGs of normal people has detracted from the perceived value of EEG, perhaps unfairly. It had been postulated that subclinical discharges may be "ictal" to higher cortical functions and that many developmental or acquired defects of language or behavior (e.g., Autism) are a consequence of apparently subclinical spikes that may impair the neural processes and possibly the local plastic changes associated with learning and cognition (Guerrini et al., 2002; Laporte et al., 2002; Pressler et al., 2005; Levisohn, 2007; El Shakankiry, 2010; Bermeo-Ovalle, 2018); however, on the contrary, there are epileptic syndromes with frequent EDs in EEG but with no or minimal seizure recurrence risk and no or minimal effect on cognition. Defining what should be considered as a pathological discharge on scalp EEG is, therefore, highly needed. Clinicians rely on the location and morphology of EDs to determine the risk of seizure recurrence but identifying additional characteristics as predictive markers for prognosis could improve the yield of EEG as a tool, revolutionizing the concept of epileptogenicity and the management of epilepsy.

Over the past three decades, the rise of broadband digital systems has enabled the monitoring of electroencephalographic signals beyond the classical Berger frequency band (0.3–70 Hz), extending the recordings to frequencies as high as 500 Hz and beyond. High-frequency oscillations (HFOs) include all physiologic and pathologic oscillatory activities within the frequency band from the 80 to 500 Hz range that stands out from the baseline and persists for at least four oscillation cycles. They are classified into ripples (80–250 Hz) and fast ripples (FR, >250 Hz) (Zijlmans et al., 2017).

High-frequency oscillations were initially identified in recordings with depth and grid electrodes. In animal studies, they were linked to spontaneous seizures (Bragin et al., 2004). More recent studies have established that HFOs are more specific in identifying the seizure onset zone than traditional spikes and are more tightly linked to seizures than spikes alone (Jacobs et al., 2008).

Studies using depth electrodes, grids, or intraoperative corticography showed that resection of HFO-generating tissue and particularly disconnecting networks generating HFOs correlate with a favorable post-surgical seizure outcome (Akiyama et al., 2011; Usui et al., 2011; van Klink et al., 2014; van 't Klooster et al., 2017).

It was initially believed that the skull filters away higher frequencies, and it was not expected to find epileptic HFOs with scalp EEG; however, this proved to be incorrect, as the skull does not have low-pass filter capacities. It diminishes signal amplitude due to the greater distance between generators and sensors, but as long as the signal amplitude is greater than noise, the high-frequency signal can be distinguished on a scalp EEG recording. A comparative study with simultaneous scalp and subdural electrodes showed that HFOs co-occurred in both simultaneously (Zelmann et al., 2014; Zijlmans et al., 2017).

In the past decade, HFOs have been identified in the scalp EEG; however, investigation and clinical application of HFOs as a biomarker for epilepsy have been limited. Recent studies demonstrated that HFOs co-existing with EDs are easier to detect than HFOs alone and have greater pathological significance (Kramer et al., 2019). Physiologic ripples have not been reported in scalp recordings which may implicate that they may be attenuated before they reach the scalp (Von Ellenrieder et al., 2014).

This retrospective study aims to identify whether the electrographic finding of HFOs in coexistence with interictal spikes on routinely acquired scalp EEG is associated with a higher risk of seizure recurrence than interictal spikes alone and could therefore be used as a prognostic marker on a scalp EEG recording.

MATERIALS AND METHODS

A-Subjects

Children presenting with new onset seizure to Children's Medical Center Dallas, during 2015–2016, who were not on ASM and had focal ED on an awake and sleep EEG recorded with a sample frequency of 500 HZ, were identified by review of an electronic database. 100 children were randomly selected and enrolled in the study.

B-Methods

Charts of the included patients were reviewed with regard to the age at seizure onset, type/s of seizures, the start of ASM, brain imaging result, and diagnosed epilepsy syndrome if any.

Charts of the patient who continued to follow-up in the clinic for 2 years were reviewed with regards to the presence or absence of seizures during the 1st year and after 2 years of follow-up, identified cause for seizure recurrence and ASM after 2 years of follow-up.

EEG Acquisition and Analysis

– Awake and sleep EEG was recorded for each patient with 21 channels and a sampling frequency of 500 Hz using XLTEK Natus EEG system, CA, United States, version 988. The

standard international 10–20 electrode system was used. EEGs were analyzed blinded to data of patients.

- EEGs were reviewed in bipolar and referential montages, using as a reference the average of the 21 electrodes, unfiltered, with a time base of 15 mm/s, a high-pass filter of 0.5 Hz, a low-pass filter of 70 Hz, notch filter of 60 Hz, and a sensitivity of 15 uV/mm.
- EEGs were reviewed for the presence of background slowing and asymmetry. The EEGs were classified as either with or without background abnormality.
- Epileptiform discharges were selected from portions of the EEG which were free from any muscle artifact, often during drowsiness or sleep. We analyzed every ED in the artifact-free portions of the EEGs studied. Because in some EEGs we could not identify more than three EDs in the artifact-free portions, we decided to choose three representative EDs at least 1 s apart for each patient from an artifact-free portion of the recording to analyze.
- Channels with the highest amplitude of EDs were identified; the duration, amplitude, and topography of each discharge were recorded.
- High-frequency oscillations superimposed on EDs were identified visually by the first investigator through temporal expansion of the EEG traces with a time base of 60 mm/s, a high-pass filter of 80 Hz, and a sensitivity of 1 uV/mm, and then viewed at 1.5 s/page. HFOs were defined as oscillatory events with at least four cycles above 80 Hz, which are visible above the background signal in the filtered data (examples in **Figures 1**, **2**).
- EEGs were then reviewed by the second investigator to establish inter-observer reliability.

Statistical Analysis

Data were analyzed for the distribution and characteristics of the EDs associated with HFOs. Patients who had coexistence of HFOs with interictal EDs (IEDs) on scalp EEG were compared with those with no HFOs with regards to brain imaging results, the incidence of background abnormality in EEG, the topography of the EDs, initiation and duration of ASM, seizure recurrence after 1 year and after 2 years of follow-up. Data were analyzed for statistical significance using unpaired *t*-test comparison, a *p*-value of <0.05 was considered significant.

This study was approved by the Institutional Review Board (IRB) of The University of Texas Southwestern Medical Center, Dallas, TX, United States.

RESULTS

The average age of patients was 6.3 years (±4.35 SD). HFOs were visually identified in 19% of the studied patients (**Figure 3**). Inter-rater reliability for identification of HFO negative discharges was 99% and for identification of HFOs agreement was 78%.

High-frequency oscillations were found more often in the younger age group (22.2, 9.5, 6.58, and 4.35% of patients in age groups <2 years, 2–5 years, 5–10 years, and >10 years, respectively) (**Figure 4**).

Types of seizures in each group are shown in **Figure 5**. Most patients had focal seizures; focal non-motor seizures were the most common type seen in both groups.

High-frequency oscillations were identified with both spikes or sharp waves; however, they were more frequently associated with spikes (11.4, 8.3, and 6.6% of the EDs with a duration of

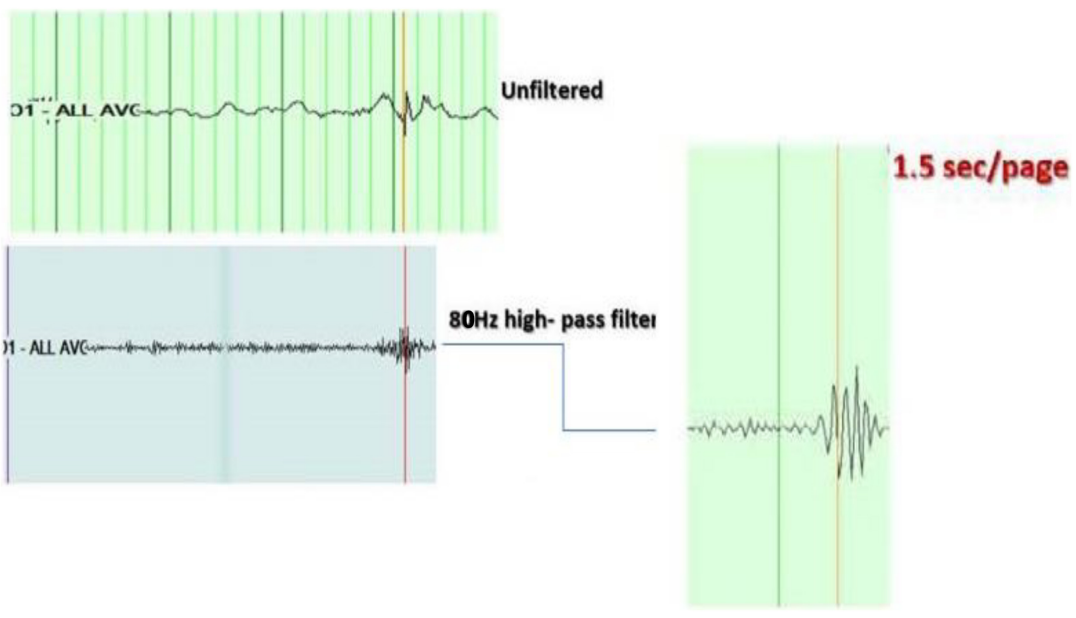

FIGURE 1 | Example of high-frequency oscillations (HFOs) on top of the spike. Top right: shows the spike at O1 in unfiltered EEG, viewed with a time base of 15 mm/s, a high-pass filter of 0.5 Hz, a low-pass filter of 70 Hz, notch filter of 60 Hz, and a sensitivity of 15 uV/mm. Middle right: shows the same spike with a time base of 60 mm/s, a high-pass filter of 80 Hz, and a sensitivity of 1 uV/mm. Left: shows the HFOs viewed with an expansion of the EEG trace to 1.5 s/page.

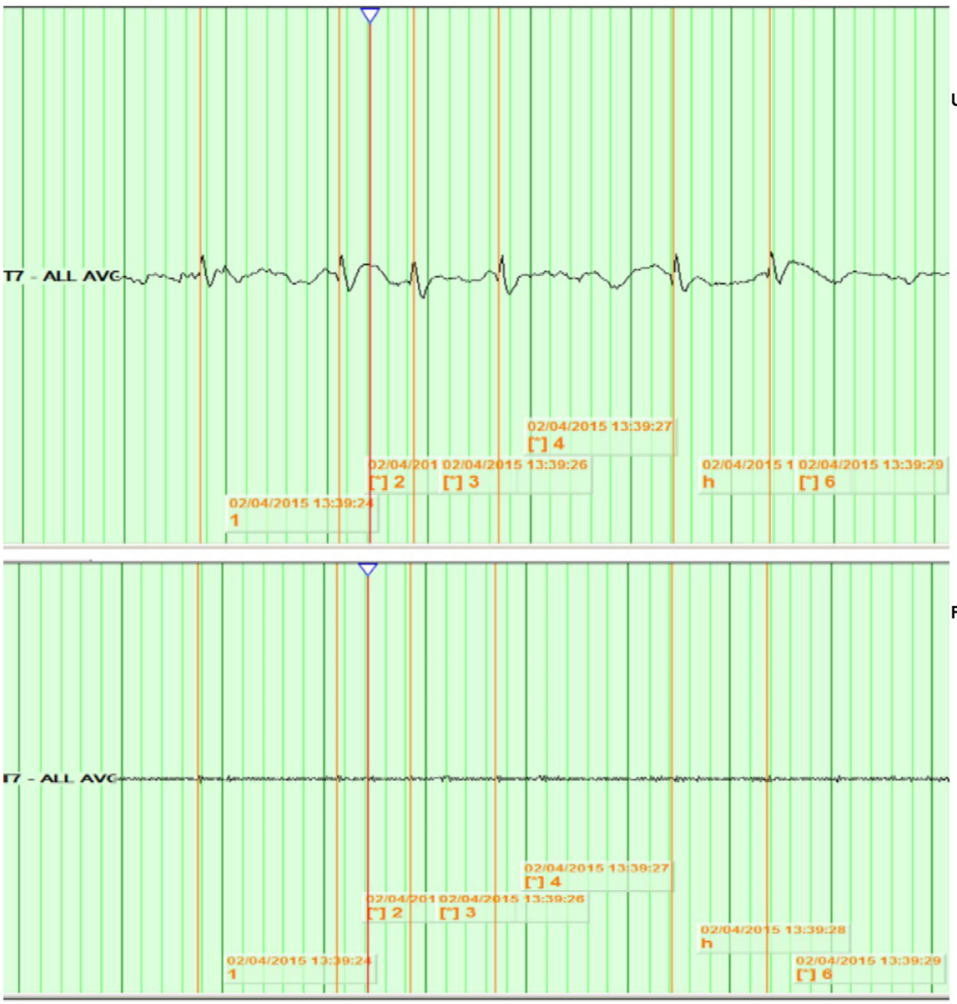

FIGURE 2 | Example of no identified HFOs. Top: shows spikes at T7 in unfiltered EEG, viewed with a time base of 15 mm/s, a high-pass filter of 0.5 Hz, a low-pass filter of 70 Hz, notch filter of 60 Hz, and a sensitivity of 15 uV/mm. Bottom: shows the same spikes with a time base of 60 mm/s, a high-pass filter of 80 Hz, and a sensitivity of 1 uV/mm.

<71, 71–100, and >100–200 ms, respectively) (**Figure 6**). They were identified more often with higher amplitude spikes/sharp waves (7.4% for EDs with amplitude 100–150 uV and 13.5% for those >150 uV compared to 4.1% for EDs < 50 uV and 5.1% for EDs 50–100 uV) (**Figure 7**). There was no significant difference in the topographic distribution of the EDs among HFO positive and negative patients (**Figure 8**).

There was no statistically significant difference between the two groups with regards to the presence of background abnormalities (7/19 of HFO positive patients and 28/81 of HFO negative patients). There was also no difference in the presence of generalized ED in addition to the focal discharges (3/19 of HFO positive patients and 8/81 of HFO negative patients) and the presence of multifocal EDs vs. a single electrographic focus (10/19 of HFO positive patients and 38/81 of HFO negative patients).

Two of the HFO positive patients (10.5%) and fifteen of the HFO negative patients (18.5%) were diagnosed with benign rolandic epilepsy with centrotemporal spikes (BECTs). Structural causes and epileptic encephalopathies were more common among the younger age group.

Brain imaging was done in 71/81 (87.7%) of the HFO negative patients (2 had brain CT and 69 had Brain MRI done). All 19 HFO positive patients had Brain MRI performed. Imaging was abnormal in 36.6% of the HFO negative patients (26/71 patients) and 52.6% of the HFO positive patients (10/19 patients). The difference between the two groups was not statistically significant ($P > 0.05$).

15/19 HFO positive and 69/81 HFO negative patients continued to follow-up for 1 year and 15/19 HFO positive and 59/81 HFO negative patients continued to follow-up for 2 years. Patients with HFOs were more likely to have recurrence of seizures during the 1st year after diagnosis, 93.3 vs. 39.1% for HFO negative patients ($P < 0.05$) (**Table 1**) and to continue to have seizures after 2 years, 86.7 vs. 15.3% ($P < 0.0001$) (**Table 2**). There was no statistically significant difference between the two groups with regards to continuing on ASM after 2 years (**Table 3**).

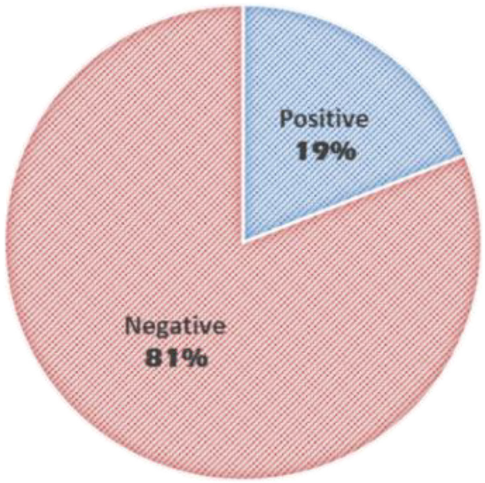

FIGURE 3 | Prevalence of HFOs among studied patients.

DISCUSSION

Scalp-recorded HFOs were reported ictally, at the onset of epileptic spasms (Kobayashi et al., 2004) and in absence seizures (Chaitanya et al., 2015), and interictally in idiopathic partial epilepsy (Kobayashi et al., 2011), epilepsy with electrical status epilepticus in sleep (ESES) (Kobayashi et al., 2010), and atypical benign partial epilepsy (ABPE) (Qian et al., 2016); however, in these studies, EEGs were either recorded with high sampling rates, utilized time-frequency power spectral analysis with Gabor transform of the signal, and/or used semiautomated or fully automated analysis. The purpose of this study was to demonstrate that a simple visual method, with no additional software, could be used to identify HFOs during routine EEG interpretation in clinical practice to help identify patients with a higher risk of seizure recurrence. The EEGs studied were routinely acquired using the standard 21 channel system. While using more channels and high-density recordings would be ideal, these methods are not used routinely and are not available in all centers. We were able to visually identify HFOs in 19% of the studied routinely acquired scalp EEGs recorded with a sample frequency of 500 HZ, with high inter-rater reliability.

It is reported that whenever filters are applied there is a chance that the spike can also degrade into an irregular oscillatory pattern (Bénar et al., 2010); therefore, in this study, only those oscillations which showed a regular ripple with at least four cycles with amplitude being distinctly different from the background were considered as HFOs; this is in accordance with other previous studies (Zelmann et al., 2009; Zijlmans et al., 2012).

High-frequency oscillations were identified more often in the younger age group, yet, they were identified in 11% of patients >5 years old. Upon chart review, patients below 5 years of age were more commonly diagnosed with epileptic encephalopathy or structural cause whereas older patients were more commonly diagnosed with idiopathic epilepsy syndrome (BECT and Panayiotopoulos syndrome). Brain imaging was more likely to be abnormal in patients who were HFO positive compared to those who were HFO negative (52.6 and 36.6%, respectively); however, this difference was not statistically significant. Seventeen of our studied patients were diagnosed with BECT; two were HFO positive. It is well known that in BECT, the EDs often persist despite

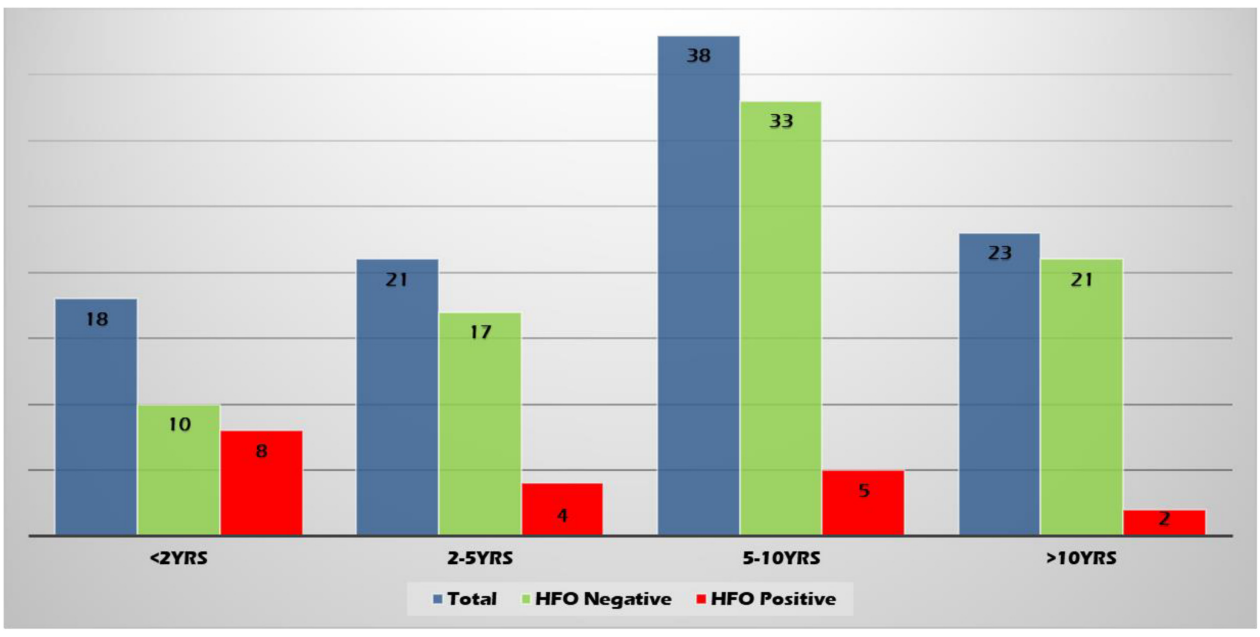

FIGURE 4 | Age group representation.

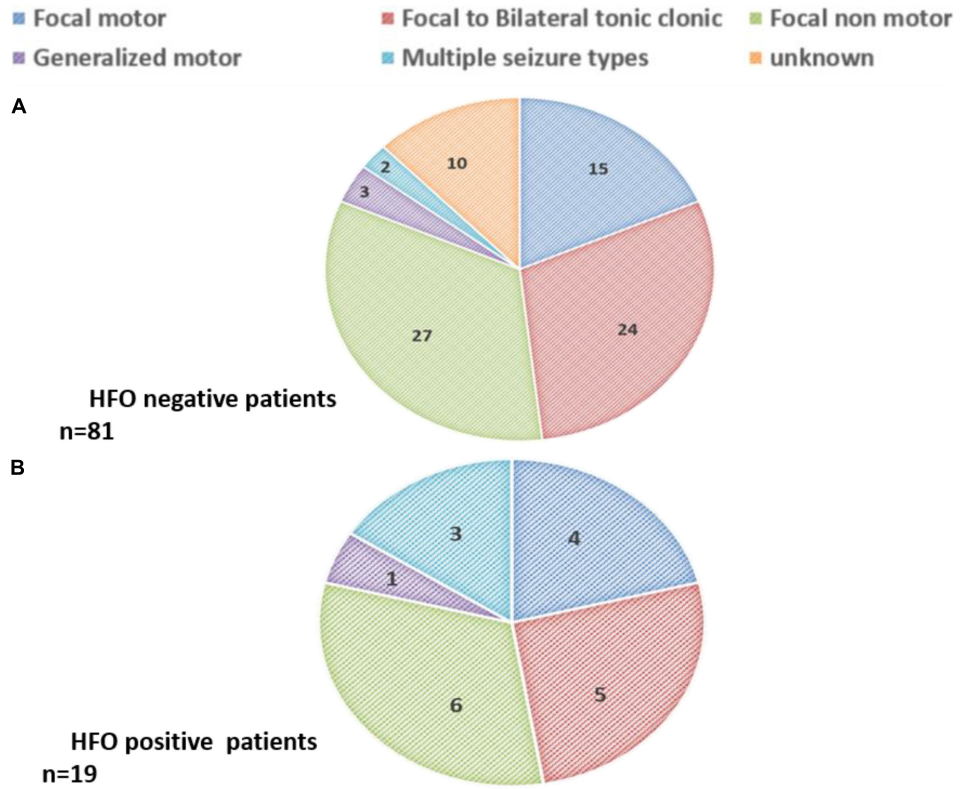

FIGURE 5 | Seizure types among **(A)** HFO negative patients ($n = 81$) and **(B)** HFO positive patients ($n = 19$).

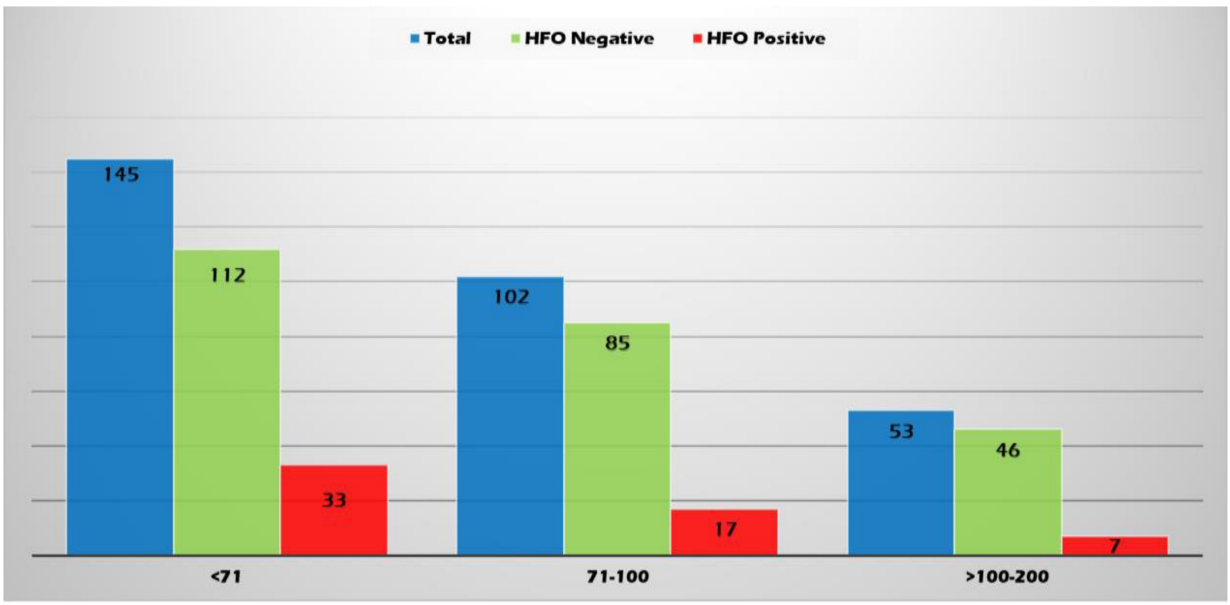

FIGURE 6 | Relationship between epileptiform discharge (ED) duration (ms) and presence of HFOs.

clinical seizure remission (Panayiotopoulos, 2007) further supporting the concept that additional factors determine ictogenesis.

On visual scanning of the unfiltered EEGs, we observed that neither the spike load nor the activation of the EDs during sleep could predict the presence of HFOs. Paroxysmal EDs augmented

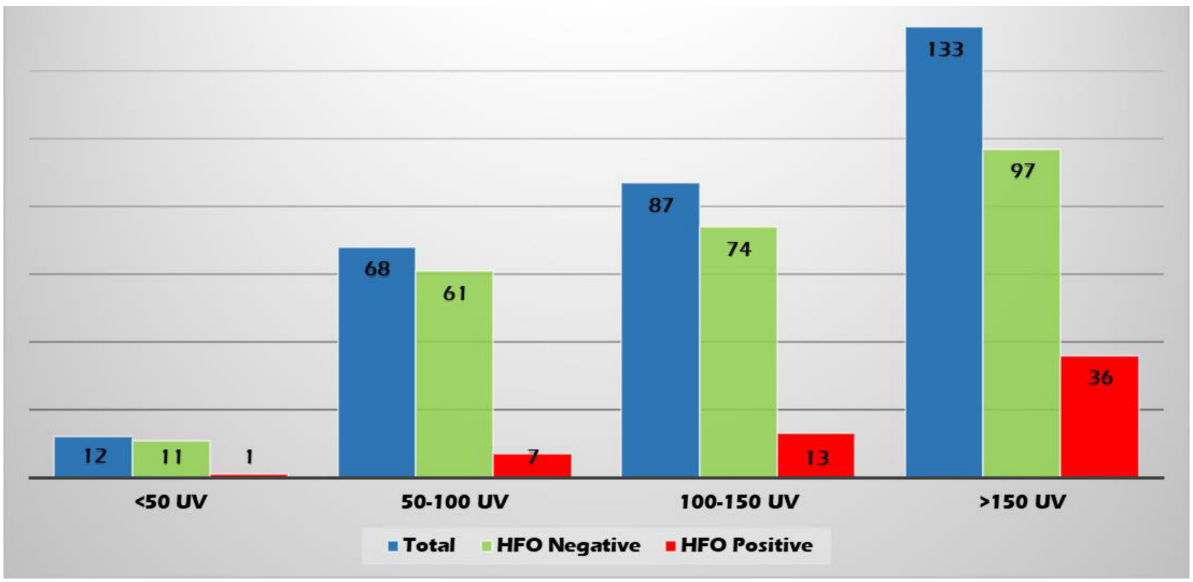

FIGURE 7 | Relationship between ED amplitude and presence of HFOs.

during sleep were previously reported in children with no clinical seizures (El Shakankiry, 2010) raising the question of how to identify active or pathological spikes that need to be treated. In this study, there was also no significant difference between HFO positive and negative patients with regards to the topographic distribution of the EDs or EEG background abnormality, this highlights that in clinical practice, one cannot predict from the appearance of interictal discharges which may have superimposed HFOs. It also implies that HFOs, when present, can be visually identified irrespective of the topographic distribution of the EDs.

High-frequency oscillations were identified with both spikes or sharp waves; however, they were more frequently associated with spikes and more often with higher amplitude EDs. Spikes and sharp waves are two types of IEDs; irrespective of their morphology both are assigned equal significance in the evaluation of a patient with epilepsy (Jaseja and Jaseja, 2012). In a study by van Klink et al. (2016) investigating the spatiotemporal relation between spikes and ripples and the difference between spikes that do and do not co-occur with ripples, spikes with ripples were reported to be shorter and had higher amplitude and higher slope than spikes without ripples.

The co-existence of HFOs with spikes or sharp waves was correlated with seizure recurrence. Patients with HFOs were

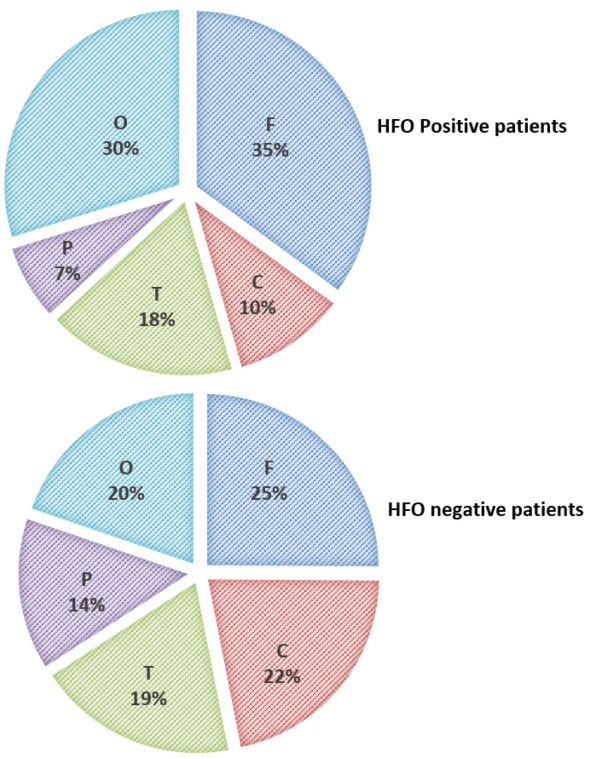

FIGURE 8 | Topographic distribution of ED in HFO positive and negative patients (F, Frontal; C, Central; T, Temporal; P, Parietal; and O, Occipital).

TABLE 1 | Seizure recurrence during the 1st year of follow-up.

Seizure recurrence during 1st year	HFO positive ($n = 15$)	HFO negative ($n = 69$)	
No	1 (6.7%)	42 (60.9%)	
Yes			
Unprovoked			
Single	1	10	
Multiple	10	9	
Provoked	3	8	
Total	14 (93.3%)	27 (39.1%)	***P*-value < 0.05**

Bold represents that the values are statistically significant.

TABLE 2 | Seizure recurrence after 2 years of follow-up.

Seizure recurrence after 2nd year	HFO positive ($n = 15$)	HFO negative ($n = 59$)	
No	2 (13.3%)	50 (84.7%)	
Yes			
Unprovoked	13	5	
Provoked	0	4	
Total	13 (86.7%)	9 (15.3%)	***P*-value < 0.0001**

Bold represents that the values are statistically significant.

more likely to have a recurrence of seizures during the 1st year after diagnosis and to continue to have seizures after 2 years. This agrees with previous studies reporting that HFOs were related to the epileptic disease activity (Zijlmans et al., 2009; Kerber et al., 2013; Kobayashi et al., 2015; Qian et al., 2016), respond to therapy more than the spikes (Qian et al., 2016), and could be a valuable predictor of the course of the disease (van Klink et al., 2016). HFOs and spikes were suggested to be two independent entities. From the perspective of cellular mechanisms, spikes reflect excitatory postsynaptic potentials (De Curtis and Avanzini, 2001), while HFOs likely reflect synchronized co-firing of small clusters of principal cells (Bragin et al., 2002, 2011). Recently, strategies aimed at improving the ability of principal neurons to maintain a *trans*-membrane chloride gradient in the face of excessive network activity were suggested to prevent interneurons from contributing to seizure perpetuation (Magloire et al., 2019; Raimondo and Dulla, 2019). Shifting target in epilepsy management to inhibition of principal cells cofiring is therefore worth studying, particularly that despite the availability of many new ASMs with differing mechanisms of action, the overall outcomes in newly diagnosed epilepsy have not improved (Chen et al., 2018).

There was no statistically significant difference between the two studied groups with regards to the initiation of ASM at presentation or continuing ASMs after 2 years; 57.6% of HFO negative patients were still on ASM after 2 years even though 84.7% of them were seizure-free. Hixson (2010) reported that after initiation of an ASM and achieving a sustained period of seizure freedom, the bias toward continuing therapy indefinitely can be substantial, and the required duration of antiepileptic therapy is much less concrete and remains controversial (Strozzi et al., 2015). This highlights the importance of applying HFO analysis as a marker of disease activity to guide the decision about discontinuing ASM to avoid undue prolonged duration of therapy without increasing the risk of seizure recurrence after discontinuing ASM.

TABLE 3 | Number of patients on anti-seizure medication (ASM) after 2 years of follow up.

ASM after 2nd year	HFO positive ($n = 15$)	HFO negative ($n = 59$)	
No ASM	3 (20%)	25 (42.4%)	
On ASM	12 (80%)	34 (57.6%)	***P*-value > 0.05**

Bold represents that the values are statistically significant.

CONCLUSION

In this retrospective study, we found that patients with HFOs were more likely to have recurrence of seizures during the 1st year after diagnosis, 93.3 vs. 39.1% for HFO negative patients ($P < 0.05$) and to continue to have seizures after 2 years, 86.7 vs. 15.3% ($P < 0.0001$). Despite that, we found out that there was no statistically significant difference between the two groups with regards to the initiation of ASM at presentation or continuing ASMs after 2 years. The fact that there was no difference in the use of ASM between the two groups emphasizes the need for a prognostic marker to guide the clinical decision regarding starting or discontinuing ASM.

The international league against epilepsy defines epilepsy as two or more unprovoked seizures or a single unprovoked seizure if the recurrence risk is similar to the general risk after two unprovoked seizures (Fisher et al., 2014). The findings of this study suggest that the presence of HFOs superimposed on EDs is a significant risk factor for seizure recurrence. We, therefore, propose that the presence of HFOs in interictal discharges will be a helpful marker for clinicians to assess the recurrence risk. If the EEGs were analyzed for the presence or absence of HFOs prospectively, the two groups would have been treated differently; the HFO positive patients would have been on ASM, while many HFOs negative patients might have not been started on ASM or might have had the ASM discontinued earlier.

A limitation of this study arises from its retrospective design, and while the sample size of 100 children appeared adequate, the group with HFOs and 2 years follow-up was relatively small. Although a larger study would be ideal, we believe that the strong statistical significance in seizure recurrence rates between the groups shows that including analysis for HFOs in routine EEG interpretation may increase the yield of the EEG and help guide the decision to either start or discontinue ASM.

Further prospective studies applying this observation are needed to decide whether to start ASM after a new onset seizure or discontinue ASM after a period of seizure freedom and to identify pathological discharges with deleterious effects on the growing brain. This may also help set a new target for the management of refractory epilepsy.

DATA AVAILABILITY STATEMENT

The raw data supporting the conclusions of this article will be made available by the authors, without undue reservation.

ETHICS STATEMENT

The studies involving human participants were reviewed and approved. The study was approved by the Institutional Review Board (IRB) The University of Texas Southwestern Medical Center, Dallas, TX, United States. Written informed

consent for participation was not required for this study in accordance with the national legislation and the institutional requirements.

AUTHOR CONTRIBUTIONS

HE: research proposal, data collection, and preparation of the manuscript. SA: principal investigator, provided oversight, review, and mentorship. Both authors contributed to the article and approved the submitted version.

SUPPLEMENTARY MATERIAL

The Supplementary Material for this article can be found online at: https://www.frontiersin.org/articles/10.3389/fnhum.2021.709836/full#supplementary-material

REFERENCES

Akiyama, T., McCoy, B., Go, C. Y., Ochi, A., Elliott, I. M., Akiyama, M., et al. (2011). Focal resection of fast ripples on extraoperative intracranial EEG improves seizure outcome in pediatric epilepsy. *Epilepsia* 52, 1802–1811. doi: 10.1111/j.1528-1167.2011.03199.x

Bali, B., Kull, L. L., Strug, L. J., Clarke, T., Murphy, P. L., Akman, C. I., et al. (2007). Autosomal Dominant Inheritance of Centrotemporal Sharp Waves in Rolandic Epilepsy Families. *Epilepsia* 48, 2266–2272.

Bénar, C. G., Chauvière, L., Bartolomei, F., and Wendling, F. (2010). Pitfalls of high-pass filtering for detecting epileptic oscillations: a technical note on "false" ripples. *Clin. Neurophysiol.* 121, 301–310. doi: 10.1016/j.clinph.2009.10.019

Bermeo-Ovalle, A. (2018). Cognitive problems in epilepsy: are interictal epileptiform discharges to blame? *Epilepsy Curr.* 18, 31–32. doi: 10.5698/1535-7597.18.1.31

Borusiak, P., Zilbauer, M., and Jenke, A. C. (2010). Prevalence of epileptiform discharges in healthy children-new data from a prospective study using digital EEG. *Epilepsia* 51, 1185–1188. doi: 10.1111/j.1528-1167.2009.02411.x

Bragin, A., Benassi, S. K., Kheiri, F., and Engel, J. Jr. (2011). Further evidence that pathologic high-frequency oscillations are bursts of population spikes derived from recordings of identified cells in dentate gyrus. *Epilepsia* 52, 45–52. doi: 10.1111/j.1528-1167.2010.02896.x

Bragin, A., Mody, I., Wilson, C. L., and Engel, J. Jr. (2002). Local generation of fast ripples in epileptic brain. *J. Neurosci.* 22, 2012–2021. doi: 10.1523/jneurosci.22-05-02012.2002

Bragin, A., Wilson, C. L., Almajano, J., Mody, I., and Engel, J. Jr. (2004). High-frequency oscillations after status epilepticus: epileptogenesis and seizure genesis. *Epilepsia* 45, 1017–1023. doi: 10.1111/j.0013-9580.2004.17004.x

Chaitanya, G., Sinha, S., Narayanan, M., and Satishchandra, P. (2015). Scalp high frequency oscillations (HFOs) in absence epilepsy: an independent component analysis (ICA) based approach. *Epilepsy Res.* 115, 133–140. doi: 10.1016/j.eplepsyres.2015.06.008

Chen, Z., Brodie, M., Liew, D., and Kwan, P. (2018). Treatment outcomes in patients with newly diagnosed epilepsy treated with established and new antiepileptic drugs: a 30-year longitudinal cohort study. *JAMA Neurol.* 75, 279–286. doi: 10.1001/jamaneurol.2017.3949

De Curtis, M., and Avanzini, G. (2001). Interictal spikes in focal epileptogenesis. *Prog. Neurobiol.* 63, 541–567. doi: 10.1016/s0301-0082(00)00026-5

El Shakankiry, H. M. (2010). Epileptiform discharges augmented during sleep: is it a trait with diverse clinical presentation according to age of expression? Accepted for publication. *Epilepsy Res.* 89, 113–120. doi: 10.1016/j.eplepsyres.2009.10.004

Fisher, R., Acevedo, C., Arzimanoglou, A., Bogacz, A., Cross, H., Elger, C., et al. (2014). ILAE official report: a practical clinical definition of epilepsy. *Epilepsia* 55, 475–482. doi: 10.1111/epi.12550

Guerrini, R., Arzimanoglou, A., and Rrouwer, O. (2002). Rationale for treating epilepsy in children. *Epileptic Disord.* 4, S9–S21.

Hirtz, D., Berg, A., Bettis, D., Camfield, C., Camfield, P., Crumrine, P., et al. (2003). Quality Standards Subcommittee of the American Academy of Neurology; Practice Committee of the Child Neurology Society. Practice parameter: treatment of the child with a first unprovoked seizure: report of the Quality Standards Subcommittee of the American Academy of Neurology and the Practice Committee of the Child Neurology Society. *Neurology* 60, 166–175.

Hixson, J. D. (2010). Stopping antiepileptic drugs: when and Why? *Curr. Treat. Options Neurol.* 12, 434–442. doi: 10.1007/s11940-010-0083-8

Jacobs, J., Le Van, P., Chander, R., Hall, J., Dubeau, F., and Gotman, J. (2008). Interictal high-frequency oscillations (80-500 Hz) are an indicator of seizure onset areas independent of spikes in the human epileptic brain. *Epilepsia* 49, 1893–1907. doi: 10.1111/j.1528-1167.2008.01656.x

Jaseja, H., and Jaseja, B. (2012). EEG spike versus EEG sharp wave: differential clinical significance in epilepsy. *Epilepsy Behav.* 25:137. doi: 10.1016/j.yebeh.2012.05.023

Kerber, K., LeVan, P., D€umpelmann, M., Fauser, S., Korinthenberg, R., Schulze-Bonhage, A., et al. (2013). High frequency oscillations mirror disease activity in patients with focal cortical dysplasia. *Epilepsia* 54, 1428–1436. doi: 10.1111/epi.12262

Kobayashi, K., Akiyama, T., Oka, M., Endoh, F., and Yoshinaga, H. (2015). A storm of fast (40–150 Hz oscillations during hypsarrhythmia in West syndrome. *Ann. Neurol.* 77, 58–67. doi: 10.1002/ana.24299

Kobayashi, K., Oka, M., Akiyama, T., Inoue, T., Abiru, K., and Ogino, T. (2004). Very fast rhythmic activity on scalp EEG associated with epileptic spasms. *Epilepsia* 45, 488–496. doi: 10.1111/j.0013-9580.2004.45703.x

Kobayashi, K., Watanabe, Y., Inoue, T., Oka, M., Yoshinaga, H., and Ohtsuka, Y. (2010). Scalp-recorded high-frequency oscillations in childhood sleep-induced electrical status epilepticus. *Epilepsia* 51, 2190–2194. doi: 10.1111/j.1528-1167.2010.02565.x

Kobayashi, K., Yoshinaga, H., Toda, Y., Inoue, T., Oka, M., and Ohtsuka, Y. (2011). High-frequency oscillations in idiopathic partial epilepsy of childhood. *Epilepsia* 52, 1812–1819. doi: 10.1111/j.1528-1167.2011.03169.x

Kramer, A. M., Ostrowski, L. M., Song, D. Y., Thorn, E. L., Stoyell, S. M., Parnes, M., et al. (2019). Scalp recorded spike ripples predict seizure risk in childhood epilepsy better than spikes. *Brain* 142, 1296–1309. doi: 10.1093/brain/awz059

Laporte, N., Sebire, G., Gillerot, Y., Guerrini, R., and Ghariani, S. (2002). Cognitive epilepsy: ADHD related to focal EEG discharges. *Pediatr. Neurol.* 27, 307–311. doi: 10.1016/s0887-8994(02)00441-1

Levisohn, P. M. (2007). The autism-epilepsy connection. *Epilepsia* 48, 33–35. doi: 10.1111/j.1528-1167.2007.01399.x

Magloire, V., Cornford, J., Lieb, A., Kullmann, D. M., and Pavlov, I. (2019). KCC2 overexpression prevents the paradoxical seizure-promoting action of somatic inhibition. *Nat. Commun.* 10:1225.

Marson, A. G. (2008). When to start antiepileptic drug treatment and with what evidence? *Epilepsia* 49, 3–6. doi: 10.1111/j.1528-1167.2008.01920.x

Panayiotopoulos, C. P. (2007). "Benign childhood focal seizures and related epileptic syndromes," in *A Clinical Guide to Epileptic Syndromes and their Treatment*, 2nd Edn, Chap. 12, ed. C. P. Panayiotopoulos (Springer-Verlag London Ltd: London), 285–318.

Pressler, R. M., Robinson, R. O., Wilson, G. A., and Binnie, C. D. (2005). Treatment of interictal epileptiform discharges can improve behavior in children with behavioral problems and epilepsy. *J. Pediatr.* 146, 112–117. doi: 10.1016/j.jpeds.2004.08.084

Qian, P., Li, H., Xue, J., and Yang, Z. (2016). Scalp-recorded high-frequency oscillations in atypical benign partial epilepsy. *Clin. Neurophysiol.* 127, 3306–3313. doi: 10.1016/j.clinph.2016.07.013

Raimondo, J. V., and Dulla, C. (2019). When a Good Cop Turns Bad: the Pro-Ictal Action of Parvalbumin Expressing Interneurons During Seizures. *Epilepsy Curr.* 19, 256–257. doi: 10.1177/1535759719853548

Strozzi, I., Nolan, S. J., Sperling, M. R., Wingerchuk, D. M., and Sirven, J. (2015). Early versus late antiepileptic drug withdrawal for people with epilepsy in remission. *Cochrane Database Syst. Rev.* 11:CD001902.

Usui, N., Terada, K., Baba, K., Matsuda, K., Nakamura, F., Usui, K., et al. (2011). Clinical significance of ictal high frequency oscillations in medial temporal lobe epilepsy. *Clin. Neurophysiol.* 122, 1693–1700. doi: 10.1016/j.clinph.2011.02.006

van Klink, N. E., van 't Klooster, M. A., Leijten, F. S., Jacobs, J., Braun, K. P., and Zijlmans, M. (2016). Ripples on rolandic spikes: a marker of epilepsy severity. *Epilepsia* 57, 1179–1189. doi: 10.1111/epi.13423

van Klink, N. E., Van't Klooster, M. A., Zelmann, R., Leijten, F. S., Ferrier, C. H., Braun, K. P., et al. (2014). High frequency oscillations in intra-operative electrocorticography before and after epilepsy surgery. *Clin. Neurophysiol.* 125, 2212–2219. doi: 10.1016/j.clinph.2014.03.004

van 't Klooster, M. A., van Klink, N. E. C., Zweiphenning, W. J. E. M., Leijten, F. S. S., Zelmann, R., and Ferrier, C. H. (2017). Tailoring epilepsy surgery with fast ripples in the intra-operative electrocorticogram. *Ann. Neurol.* 81, 664–676. doi: 10.1002/ana.24928

Von Ellenrieder, N., Beltrachini, L., Perucca, P., and Gotman, J. (2014). Size of cortical generators of epileptic interictal events and visibility on scalp EEG. *NeuroImage* 94, 47–54. doi: 10.1016/j.neuroimage.2014.02.032

Zelmann, R., Lina, J. M., Schulze-Bonhage, A., Gotman, J., and Jacobs, J. (2014). Scalp EEG is not a blur: it can see high frequency oscillations although their generators are small. *Brain Topogr.* 27, 683–704. doi: 10.1007/s10548-013-0321-y

Zelmann, R., Zijlmans, M., Jacobs, J., Châtillon, C., and Gotman, J. (2009). Improving the identification of high frequency oscillations. *Clin. Neurophysiol.* 120, 1457–1464.

Zijlmans, M., Jacobs, J., Zelmann, R., Dubeau, F., and Gotman, J. (2009). High-frequency oscillations mirror disease activity in patients with epilepsy. *Neurology* 72, 979–986. doi: 10.1212/01.wnl.0000344402.20334.81

Zijlmans, M., Jiruska, P., Zelmann, R., Leijten, F. S., Jefferys, J. G., and Gotman, J. (2012). High-frequency oscillations as a new biomarker in epilepsy. *Ann. Neurol.* 71, 169–178. doi: 10.1002/ana.22548

Zijlmans, M., Worrell, G. A., Dümpelmann, M., Stieglitz, T., Barborica, A., Heers, M., et al. (2017). Le Van Quyen M: how to record high-frequency oscillations in epilepsy: a practical guideline. *Epilepsia* 58, 1305–1315. doi: 10.1111/epi.13814

Conflict of Interest: The authors declare that the research was conducted in the absence of any commercial or financial relationships that could be construed as a potential conflict of interest.

frontiers in Human Neuroscience

CASE REPORT
published: 24 September 2021
doi: 10.3389/fnhum.2021.699556

Role of High-Frequency Oscillation in Locating an Epileptogenic Zone for Radiofrequency Thermocoagulation

*Xin Xu[1], Xingguang Yu[1], Guixia Kang[2], Zhiqi Mao[1], Zhiqiang Cui[1], Longsheng Pan[1], Rui Zong[1], Yuan Tang[2], Ming Wan[1] and Zhipei Ling[1]**

[1] Department of Neurosurgery, General Hospital of PLA, Beijing, China, [2] Key Laboratory of Universal Wireless Communications, Ministry of Education, Beijing University of Posts and Telecommunications, Beijing, China

Radiofrequency thermocoagulation (RFTC) has been proposed as a first-line surgical treatment option for patients with drug-resistant focal epilepsy (DRE) that is associated with gray matter nodular heterotopia (GMNH). Excellent results on seizures have been reported following unilateral RFTC performed on ictal high-frequency-discharge, fast-rhythm, and low-voltage initiation areas. Complex cases (GMNH plus other malformations of cortical development) do not have good outcomes with RFTC. Yet, there is little research studying the effect of high-frequency oscillation in locating epileptogenic zones for thermocoagulation on unilateral, DRE with bilateral GMNH. We present a case of DRE with bilateral GMNH, treated using RFTC on unilateral GMNH and the overlying cortex, guided by stereotactic electroencephalogram (SEGG), and followed up for 69 months. Twenty-four-hour EGG recordings, seizure frequency, post-RFTC MRI, and neuropsychological tests were performed once yearly. To date, this patient is seizure-free, the electroencephalogram is normal, neuropsychological problems have not been found, and the trace of RFTC has been clearly identified on MRI. His dosage of antiepileptic medication has, furthermore, been significantly reduced. It is concluded that RFTC on unilateral DRE with bilateral GMNH may achieve good long-term effects, lasting up to, and perhaps longer than, 69 months. Ictal high-frequency oscillation (fast ripple) inside the heterotopia and the overlying cortex may be the key to this successful effect.

Keywords: high-frequency oscillation, radiofrequency thermocoagulation, gray matter nodular heterotopia, epilepsy, stereotactic-electroencephalogram

OPEN ACCESS

Edited by:
Jing Xiang,
Cincinnati Children's Hospital Medical Center, United States

Reviewed by:
Ailiang Miao,
Nanjing Brain Hospital Affiliated to Nanjing Medical University, China
Qian Wang,
Peking University, China

***Correspondence:**
Zhipei Ling
zhipeilxx@163.com

Specialty section:
This article was submitted to Brain Imaging and Stimulation, a section of the journal Frontiers in Human Neuroscience

Received: *23 April 2021*
Accepted: *13 August 2021*
Published: *24 September 2021*

Citation:
Xu X, Yu X, Kang G, Mao Z, Cui Z, Pan L, Zong R, Tang Y, Wan M and Ling Z (2021) Role of High-Frequency Oscillation in Locating an Epileptogenic Zone for Radiofrequency Thermocoagulation. Front. Hum. Neurosci. 15:699556. doi: 10.3389/fnhum.2021.699556

INTRODUCTION

Epilepsy is one of the most prevalent neurological disorders, with around 70 million individuals affected worldwide. It can cause severe neurological disorders, leading to significant morbidity and increased mortality. Surgery should be considered in patients with drug-resistant focal epilepsy (DRE) and lesion-based epilepsy. Histopathology is an important determinant of seizure outcome (Lamberink et al., 2020). Gray matter nodular heterotopia (GMNH) often leads to DRE as a result of malformations arising during cortical development (Guerrini and Filippi, 2005; Battaglia et al., 2006). However, the relative roles of the nodular tissue and the overlying cortex in the generation of seizures can be complex and variable (Aghakhani et al., 2005; Tassi et al., 2005;

Abbreviations: DRE, drug-resistant focal epilepsy; EEG, electroencephalogram; GMNH, gray matter nodular heterotopia; MRI, magnetic resonance imaging; NH, nodular heterotopia; RFTC, radiofrequency thermocoagulation; SEEG, stereotactic electroencephalogram; VEEG, video scalp electroencephalogram.

Thompson et al., 2016). Radiofrequency thermocoagulation (RFTC) has been proposed as a surgical treatment option in patients with DRE associated with GMNH (Cossu et al., 2015, 2018), with excellent outcomes reported. Cossu et al. (2014) indicated that four out of five patients experienced sustained seizure freedom for 33.5 months following the coagulation of a single, unilateral GMNH. Mirandola et al. (2017) showed that stereotactic-electroencephalogram (SEEG)-guided RFTC was effective in 15/20 (76%) patients with DRE related to GMNH.

Radiofrequency thermocoagulation was performed in the region of ictal high-frequency, mainly in the fast-rhythm and low-voltage initiation area, guided by SEEG, which is a key factor in achieving a long-term effect (Guenot et al., 2004; Scherer et al., 2005; Cossu et al., 2018). RFTC, especially if guided by SEEG evaluation, should be considered as a first-line treatment option in single, unilateral GMNH-related epilepsy (Bourdillon et al., 2017). Outcomes with complex cases (GMNH plus other malformations of cortical development) are, however, not as good as those in other patterns of GMNH (Cossu et al., 2018). Furthermore, a worse result is obtained with bilateral GMNH, especially when the nodules are asymmetric and likely to be due to the presence of multifocal epilepsy, as a result of which the patients tend to experience multiple seizures (Battaglia et al., 2006; Thompson et al., 2016). There is, therefore, a need to study the role of high-frequency oscillation in locating the epileptogenic zone for RFTC in DRE cases with bilateral GMNH.

In this study, we present a case of DRE in which the seizure frequency was two to three times per month. The main seizure semiology was dizziness → blurred vision, with bilateral GMNH, treated using monolateral SEEG-guided RFTC, and followed up for 69 months. Twenty-four-hour electroencephalography (EEG) recordings identifying seizure frequency, post-RFTC MRI, and neuropsychological tests were performed per year. The patient and his mother provided written informed consent for the details of this case to be used for publication.

CASE DESCRIPTION

An 18-year-old male patient with a 4-year history of epilepsy visited the Department of Neurosurgery, General Hospital of PLA, in July 2015. He had undergone normal gestation and development and had no family history of epilepsy, febrile convulsions, encephalitis, or brain trauma. MRI of his brain showed bilateral periventricular heterotopia with overlying polymicrogyria of the bilateral temporal lobes (**Figure 1**). Neuropsychological and visual field tests were normal. The antiepileptic drug oxcarbazepine (450 mg/300 mg/450 mg) had been administered for 1 year. The seizure frequency was two to three times per month at the time of his examination.

CASE PROGRESSION TIMELINE

This patient experienced a seizure for the first time when he was 14 years old. It occurred one night in the summer of that year when he suddenly turned his head to his left side and was unconscious for 2 min. However, he did not have any tonic-clonic movements during this seizure. He reported that he had an aura before turning, with dizziness and blurred vision. From this time onward, he continued to have similar seizures. At times, he had left arm tonic-clonic movements after his head turned to the left side during a seizure. He did not stop having these seizures even though he tried many different antiepileptic drugs in different doses in the preceding 4 years.

DIAGNOSTIC ASSESSMENT, THERAPEUTIC INTERVENTIONS, AND OUTCOMES

A preoperative evaluation was performed by two epileptic specialist doctors, and a long-term video scalp electroencephalogram (VEEG) (NicoletOne, Middleton, WI, United States) was administered. The main semiology of the seizures was dizziness → blurred vision → decreased movement (stunned, accompanied by disorders of consciousness) → head deviation to left side → left arm tonic-clonic movements, sometimes followed by general tonic-clonic movements. Ictal discharge shown in the right posterior temporal T6-partial P4-occipital O_2 area was fast rhythm (ripple) → spike-wave (10/20 international system). Considering the combined MRI results, clinical manifestations, and the epileptic EEG pattern of the patient, we performed implantation using the Robotech-ROSA machine navigation system (Medtech, France). Six electrodes (HuaKe, Beijing, China) were implanted on the right side of the brain. The implantation site included the right temporal lobe, right hippocampus, amygdala, and insula—the anterior, middle, and posterior parts of the heterotopia—and heterotopia in the occipital lobe. No electrodes were implanted in the heterotopic area of the left side because the onset of the seizures and clinical signs were completely on the right side, although there was obvious heterotopia on the left side too (**Figure 2**).

The patient was transferred to the VEEG room for long-term video monitoring after the implantation. The two epilepsy specialists determined the epilepsy ictal discharge by the SEEG electrodes, which had a total of 74 contacts. Interictal discharges were fast ripples and were only situated at the contacts inside and around the tail end of the heterotopia. The semiology of the seizures was similar to that of the scalp EEG, namely, fast ripple (high-frequency oscillation), maximum 300 Hz, at the initiation of seizure onset, and only situated at the contacts that were the same inside and around the tail end of the heterotopia. Following closely (1 s), the contacts that were within and around the middle of the heterotopia demonstrated a fast rhythm (**Figure 3**).

Radiofrequency thermocoagulation was used in this patient because of the bilateral GMNH. The patient was not considered to be a suitable candidate for resection. However, high-frequency oscillations (HFOs) were clearly identified in the unilateral heterotopia and the overlying cortex. RFTC was used in those contacts that demonstrated HFOs in interictal and ictal onset, including the posterior parts of the heterotopia and the overlying cortex. Two adjacent contacts were used to perform RFTC (Bei-Qi, China). The stage one pre-RFTC parameters were

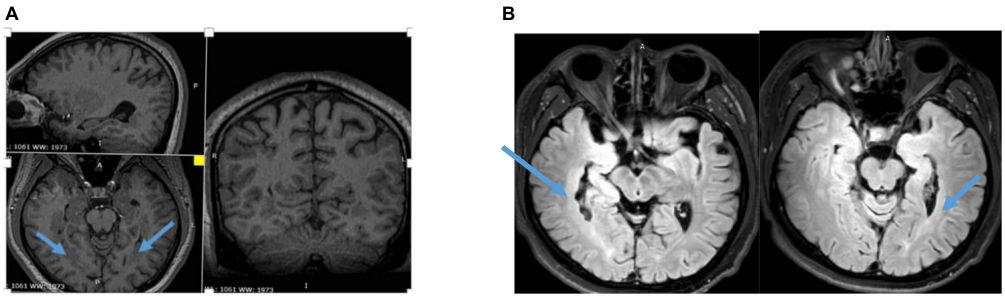

FIGURE 1 | (A) Three-dimensional (3D) MRI showing bilateral periventricular heterotopia and overlying polymicrogyria. **(B)** T2 Flair of MRI showing asymmetry bilateral periventricular heterotopia and overlying polymicrogyria.

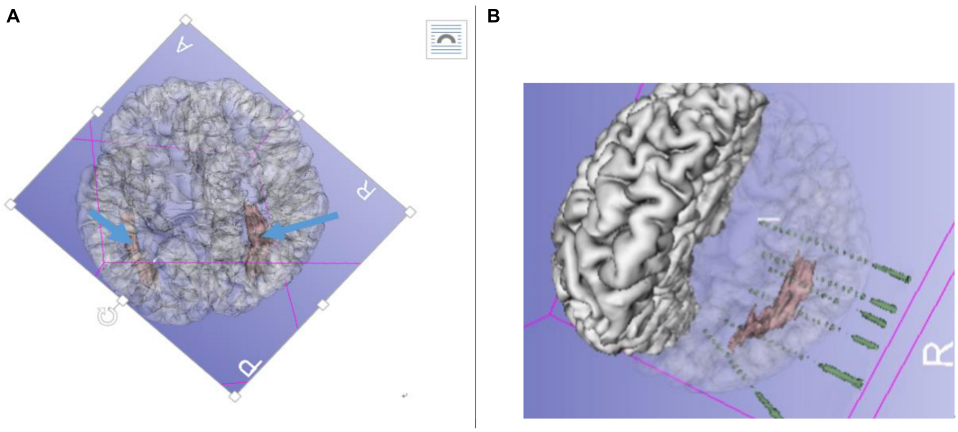

FIGURE 2 | (A) Pre-radiofrequency thermocoagulation (RFTC) 3D reconstruction MRI showing bilateral gray matter nodular heterotopia (GMNH), arrow. **(B)** Reconstruction of electrodes superimposed on GMNH.

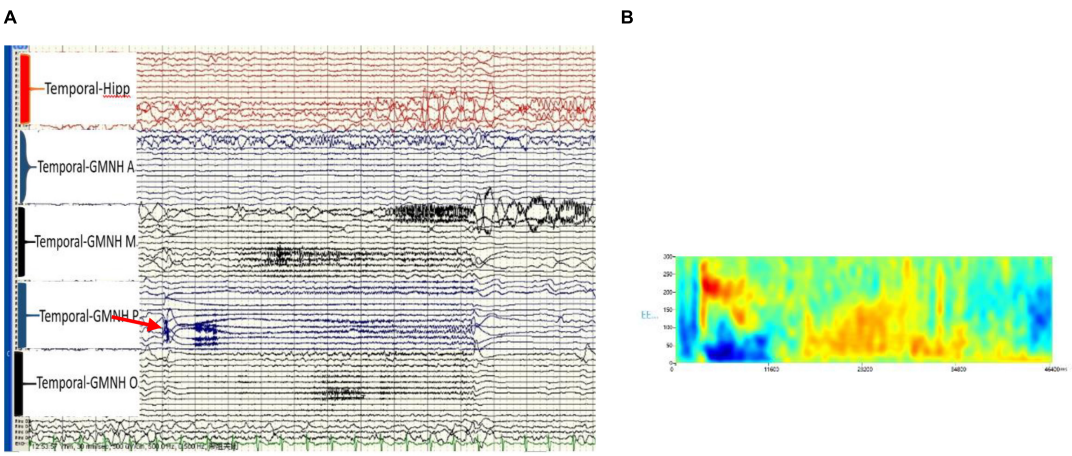

FIGURE 3 | (A) Ictal high-frequency oscillation (HFO) of the stereotactic-electroencephalogram (SEEG), post-GMNH showing HFO (ripple), arrow. **(B)** Time frequency showing direct current (DC) shift and HFO, maximum at 300 Hz of the initiation discharge of SEEG. Hipp, hippocampus; GMNH A, anterior part of heterotopia; GMNH M, middle part of heterotopia; GMNH P, posterior part of heterotopia; GMNH O, occipital lobe part of heterotopia.

2.8 W, temperature of 75°C, continued for 20 s; the stage two sustainability RFTC parameters were 4.8–5.2 W, temperature of 75°C, continued for 30–40 s.

At the time of writing this study, 69 months have passed since the RFTC was performed. The patient has had no seizures since then. Twenty-four-hour EEGs, post-RFTC MRIs, and

neuropsychological tests have all been performed once yearly. The EEG results have been normal, and the post-RFTC MRI clearly showed the RFTC site (**Figure 4**). Neuropsychological tests and visual campimetry test were normal.

Thirty-six months after the RFTC, oxcarbazepine was gradually decreased by one-half tablet every 3 months. At present, the patient is prescribed 150 mg/300 mg of oxcarbazepine and has continued to be seizure-free.

DISCUSSION

This is a report of a long-term (>69 months) follow-up of a case of DRE with bilateral GMNH and with polymicrogyria within the bilateral temporal region after unilateral RFTC of the GMNH and the overlying cortex guided by SEEG. The patient has been seizure-free for 69 months after the RFTC was performed. Twenty-four-hour VEEG results have been normal, as have neuropsychological tests and a visual campimetry test, despite bilateral GMNH with polymicrogyria within the bilateral temporal lobes.

The SEEG-guided RFTC was key to a successful outcome in this case because SEEG permits the identification of the relationship between nodular heterotopia and the cortex (Stefan et al., 2007). Excellent RFCT results on seizures have been reported following coagulation of only a single, unilateral periventricular nodular heterotopia (Thompson et al., 2016). Heterotopic tissue has been shown to play a leading role in the ictal network in seizures with simultaneous nodular and cortical onset (Dubeau and Tyvaert, 2010; Wu et al., 2012; Agari et al., 2012). However, Mirandola et al. (2017) reported that patients with complex cortical malformations, including GMNH, had less benefit from SEEG-guided RFTC alone. Previous studies have, furthermore, indicated that worse outcomes may occur with multifocal epilepsy, as these patients typically have multiple seizures with bilateral GMNH, especially when the nodules are asymmetric (Cossu et al., 2015). Tassi et al. (2005) reported that ictal onset involves nodules and the overlying cortex. The majority of network seizures (73.4%) arise simultaneously from nodular heterotopia and the overlying cortex (Mirandola et al., 2017).

Unfortunately, not all heterotopia-causing epilepsy information could be obtained from the patient under discussion. However, Acar et al. (2012) also presented a case with unilateral GMNH associated with ipsilateral hippocampal atrophy, but GMNH was not involved in the actual ictal onset zone. The implantation schedule of SEEG in this type of case aims at an intensive sampling of the epileptogenic network for effective RFTC (Cossu et al., 2017). HFOs have been detected in nodular recordings. GMNH may be central to the epileptogenic zone (Jacobs et al., 2009). Wang et al. (2020) suggested that HFOs can be a potential biomarker of epileptogenicity and epileptogenesis due to the strong correlation between HFOs (HFOs > 80 Hz) and the epileptogenic zone.

We present this case of seizures with simultaneous onset in nodular tissue and the overlying cortex with HFO (fast ripple), and a maximum of 300 Hz at the initiation of onset. The patient remained seizure-free for 69 months after RFTC, which was used at the center of the epileptogenic zone, including the heterotopia and the overlying cortex. No treatments, other than RFTC, were provided to these contacts, which demonstrated HFOs at the onset of seizures and included the posterior parts and overlying cortex on only one side of the heterotopia. Our report indicates that not all patients with bilateral GMNH are able to benefit from RFTC. The role of HFOs in locating the epileptogenic zone for RFTC was a very important factor in this case.

PATIENT PERSPECTIVE

Since only a small amount of brain tissue was removed by RFTC, and there was no neuropsychological or visual functional damage, both the patient and his parents were very satisfied with the treatment. They were particularly gratified that he has remained seizure-free, despite a reduction in his dose of antiepileptic medication, and that he takes only 150 mg/300 mg of oxcarbazepine at present.

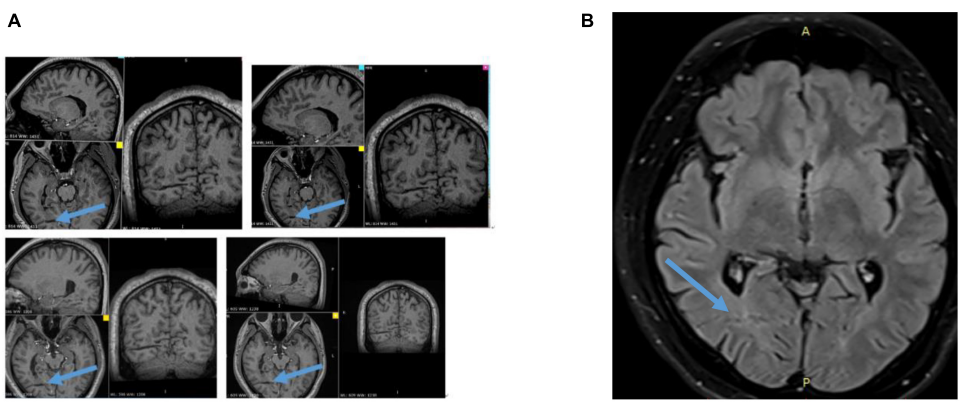

FIGURE 4 | (A) Follow-up for 58 months, 3D MRI showing a trace of RFTC at the post-GMNH every year from 2016 to 2019. **(B)** T2 Flair of MRI showing a trace of RFTC at the POST-GMNH and overlying cortex. Blue colored arrow showing a trace of RFTC.

DATA AVAILABILITY STATEMENT

The original contributions presented in the study are included in the article/supplementary material, further inquiries can be directed to the corresponding author.

ETHICS STATEMENT

Ethical review and approval was not required for the study on human participants in accordance with the local legislation and institutional requirements. The patients/participants provided their written informed consent to participate in this study. Written informed consent was obtained from the individual(s) for the publication of any potentially identifiable images or data included in this article.

AUTHOR CONTRIBUTIONS

XX contributed to the design, construction, and program of the manuscript. ZL contributed to the design and revision of the manuscript. XY contributed to revising the manuscript. GK and YT were involved in data analysis and interpretation. ZM, ZC, and LP contributed to the operation. RZ and MW acquired the data. All authors approved the final version of the manuscript and agreed to be accountable for all aspects of the work and qualify for authorship.

ACKNOWLEDGMENTS

The authors thank their technicians Li Wei Zhang, Xie Guang, and Xu Zhang for their assistance with data acquisition.

REFERENCES

Acar, G., Acar, F., Oztura, I., and Baklan, B. (2012). A case report of surgically treated drug resistant epilepsy associated with subependymal nodular heterotopia. *Seizure* 21, 223–226. doi: 10.1016/j.seizure.2011.11.002

Agari, T., Mihara, T., Baba, K., Kobayashi, K., Usui, N., Terada, K., et al. (2012). Successful treatment of epilepsy by resection of periventricular nodular heterotopia. *Acta Med. Okayama* 66, 487–492. doi: 10.18926/AMO/49045

Aghakhani, Y., Kinay, D., Gotman, J., Soualmi, L., Andermann, F., Olivier, A., et al. (2005). The role of periventricular nodular heterotopia in epileptogenesis. *Brain* 128, 641–651. doi: 10.1093/brain/awh388

Battaglia, G., Chiapparini, L., Franceschetti, S., Freri, E., Tassi, L., Bassanini, S., et al. (2006). Periventricular nodular heterotopia: classification, epileptic history, and genesis of epileptic discharges. *Epilepsia* 47, 86–97. doi: 10.1111/j.1528-1167.2006.00374.x

Bourdillon, P., Isnard, J., Catenoix, H., Montavont, A., Rheims, S., Ryvlin, P., et al. (2017). Stereoelectroencephalography-guided radiofrequency thermocoagulation (SEEG-guided RF-TC) in drug resistant focal epilepsy: Results from a 10-year experience. *Epilepsia* 58, 85–93. doi: 10.1111/epi.13616

Cossu, M., Cardinale, F., Casaceli, G., Castana, L., Consales, A., D'Orio, P., et al. (2017). Stereo-EEG guided radiofrequency thermocoagulations. *Epilepsia* 58, 66–72. doi: 10.1111/epi.13687

Cossu, M., Fuschillo, D., Cardinale, F., Castana, L., Francione, S., Nobili, L., et al. (2014). StereoEEG-guided radiofrequency thermocoagulations of epileptogenic greymatter nodular heterotopy. *J. Neurol. Neurosurg. Psychiatry* 85, 611–617. doi: 10.1136/jnnp-2013-305514

Cossu, M., Fuschillo, D., Casaceli, G., Pelliccia, V., Castana, L., Mai, R., et al. (2015). Stereoelectroencephalography-guided radiofrequency thermocoagulation in the epi-leptogenic zone: a retrospective study on 89 cases. *J. Neurosurg.* 123, 1358–1367. doi: 10.3171/2014.12.JNS141968

Cossu, M., Mirandola, L., and Tassi, L. (2018). RF-ablation in periventricular heterotopia-related epilepsy. *Epilepsy Res.* 142, 121–125. doi: 10.1016/j.eplepsyres.2017.07.001

Dubeau, F., and Tyvaert, L. (2010). Understanding the epileptogenicity of lesions: a correlation between intracranial EEG and EEG/fMRI. *Epilepsia* 51, 54–58. doi: 10.1111/j.1528-1167.2009.02447.x

Guenot, M., Isnard, J., Ryvlin, P., Fischer, C., Mauguière, F., and Sindou, M. (2004). SEEG-guided RF thermocoagulation of epileptic foci: feasibility, safety, and preliminary results. *Epilepsia* 45, 1368–1374. doi: 10.1111/j.0013-9580.2004.17704.x

Guerrini, R., and Filippi, T. (2005). Neuronal migration disorders, genetics, and epileptogenesis. *J. Child Neurol.* 20, 287–299. doi: 10.1177/08830738050200040401

Jacobs, J., Levan, P., Chatillon, C. E., Olivier, A., Dubeau, F., and Gotman, J. (2009). High frequency oscillations in intracranial EEGs mark epileptogenicity rather than lesion type. *Brain* 132, 1022–1037. doi: 10.1093/brain/awn351

Lamberink, H. J., Otte, W. M., Blümcke, I., and Braun, K. P. J. (2020). Seizure outcome and use of antiepileptic drugs after epilepsy surgery according to histopathological diagnosis: a retrospective multicentre cohort study. *Lancet Neurol.* 19, 748–757. doi: 10.1016/S1474-4422(20)30220-9

Mirandola, L., Mai, R. F., Francione, S., Pelliccia, V., Gozzo, F., Sartori, I., et al. (2017). Stereo-EEG: diagnostic and therapeutic tool for periventricular nodular heterotopia epilepsies. *Epilepsia* 58, 1962–1971. doi: 10.1111/epi.13895

Scherer, C., Schuele, S., Minotti, L., Chabardes, S., Hoffmann, D., and Kahane, P. (2005). Intrinsic epileptogenicity of an isolated periventricular nodular heterotopia. *Neurology* 65, 495–496. doi: 10.1212/01.wnl.0000172350.25380.c7

Stefan, H., Nimsky, C., Scheler, G., Rampp, S., Hopfengartner, R., Hammen, T., et al. (2007). Periventricular nodular heterotopia: a challenge for epilepsy surgery. *Seizure* 16, 81–86. doi: 10.1016/j.seizure.2006.10.004

Tassi, L., Colombo, N., Cossu, M., Mai, R., Francione, S., Lo Russo, G., et al. (2005). Electroclinical. MRI, and neuropathological study of 10 patients with nodular heterotopia, with surgical outcomes. *Brain* 128, 321–337. doi: 10.1093/brain/awh357

Thompson, S. A., Kalamangalam, G. P., and Tandon, N. (2016). Intracranial evaluation and laser ablation for epilepsy with periventricular nodular heterotopia. *Seizure* 41, 211–216. doi: 10.1016/j.seizure.2016.06.019

Wang, Y. P., Zhou, D., Yang, X. F., Xu, X., Ren, L. K., Yu, T., et al. (2020). Expert consensus on clinical applications of high-frequency oscillations in epilepsy. *Acta Epileptol.* 2:8. doi: 10.1186/s42494-020-00018-w

Wu, C., Sperling, M. R., Falowski, S. M., Chitale, A. V., Werner-Wasik, M., Evans, J. J., et al. (2012). Radiosurgery for the treatment of dominant hemisphere periventricular heterotopia and intractable epilepsy in a series of three patients. *Epilepsy Behav. Case Rep.* 1, 1–6. doi: 10.1016/j.ebcr.2012.10.004

Conflict of Interest: The authors declare that the research was conducted in the absence of any commercial or financial relationships that could be construed as a potential conflict of interest.

Publisher's Note: All claims expressed in this article are solely those of the authors and do not necessarily represent those of their affiliated organizations, or those of the publisher, the editors and the reviewers. Any product that may be evaluated in this article, or claim that may be made by its manufacturer, is not guaranteed or endorsed by the publisher.

frontiers in Human Neuroscience

ORIGINAL RESEARCH
published: 08 March 2022
doi: 10.3389/fnhum.2022.759103

Altered Neuromagnetic Activity in Persistent Postural-Perceptual Dizziness: A Multifrequency Magnetoencephalography Study

Weiwei Jiang[1†], Jintao Sun[1†], Jing Xiang[2], Yulei Sun[1], Lu Tang[1], Ke Zhang[1], Qiqi Chen[1] and Xiaoshan Wang[1]*

[1] *Department of Neurology, The Affiliated Brain Hospital of Nanjing Medical University, Nanjing Medical University, Nanjing, China,* [2] *Division of Neurology, MEG Center, Cincinnati Children's Hospital Medical Center, Cincinnati, OH, United States*

Objective: The aim of our study was to investigate abnormal changes in brain activity in patients with persistent postural-perceptual dizziness (PPPD) using magnetoencephalography (MEG).

Methods: Magnetoencephalography recordings from 18 PPPD patients and 18 healthy controls were analyzed to determine the source of brain activity in seven frequency ranges using accumulated source imaging (ASI).

Results: Our study showed that significant changes in the patterns of localization in the temporal-parietal junction (TPJ) were observed at 1–4, 4–8, and 12–30 Hz in PPPD patients compared with healthy controls, and changes in the frontal cortex were found at 1–4, 80–250, and 250–500 Hz in PPPD patients compared with controls. The neuromagnetic activity in TPJ was observed increased significantly in 1–4 and 4–8 Hz, while the neuromagnetic activity in frontal cortex was found increased significantly in 1–4 Hz. In addition, the localized source strength in TPJ in 1–4 Hz was positively correlated with DHI score ($r = 0.7085$, $p < 0.05$), while the localized source strength in frontal cortex in 1–4 Hz was positively correlated with HAMA score ($r = 0.5542$, $p < 0.05$).

Conclusion: Our results demonstrated that alterations in the TPJ and frontal cortex may play a critical role in the pathophysiological mechanism of PPPD. The neuromagnetic activity in TPJ may be related to dizziness symptom of PPPD patients, while the neuromagnetic activity in frontal lobe may be related to emotional symptoms of PPPD patients. In addition, frequency-dependent changes in neuromagnetic activity, especially neuromagnetic activity in low frequency bands, were involved in the pathophysiology of PPPD.

Keywords: persistent postural-perceptual dizziness, magnetoencephalography, cortical dysfunctions, multifrequency bands, accumulated source imaging

OPEN ACCESS

Edited by:
Changming Wang,
Capital Medical University, China

Reviewed by:
Guoping Ren,
Capital Medical University, China
Tianfu Li,
Capital Medical University, China

****Correspondence:***
Xiaoshan Wang
wangxiaoshan52@163.com

† These authors have contributed equally to this work

Specialty section:
This article was submitted to Brain Imaging and Stimulation, a section of the journal Frontiers in Human Neuroscience

Received: *15 August 2021*
Accepted: *10 January 2022*
Published: *08 March 2022*

Citation:
Jiang W, Sun J, Xiang J, Sun Y, Tang L, Zhang K, Chen Q and Wang X (2022) Altered Neuromagnetic Activity in Persistent Postural-Perceptual Dizziness: A Multifrequency Magnetoencephalography Study. Front. Hum. Neurosci. 16:759103. doi: 10.3389/fnhum.2022.759103

INTRODUCTION

Persistent postural-perceptual dizziness (PPPD) is considered a chronic functional vestibular disorder with clinical symptoms and has been defined by the World Health Organization (WHO) and the Bárány Society (Staab et al., 2017). The clinical characteristics of PPPD were persistent dizziness and/or unsteadiness for more than 3 months. Several factors, such as active/passive

motion, upright posture, and exposure to a complex environment, can aggravate the symptoms of PPPD (Staab et al., 2017). A previous study demonstrated that PPPD was one of the most common causes of chronic vestibular symptoms (Dieterich and Staab, 2017). However, the potential pathogenesis of PPPD remains unclear and has received much attention from clinical researchers.

Importantly, postural unsteadiness and visual dizziness are the core features of PPPD (Sun and Xiang, 2020). Patients with PPPD adopt a stiffened postural control strategy in response to dizzying trigger events and persistently maintain this adaptation even if the trigger factors disappear (Cao et al., 2021). In addition, researchers found that the ability to control posture through multisensory information inputs was impaired in patients with PPPD (Sohsten et al., 2016). PPPD patients were more dependent on visual or somatosensory inputs than vestibular inputs to control their body posture (Staab et al., 2017). Thus, cortical integration dysfunction involving multisensory inputs may be suggested as a potential pathophysiological mechanism of PPPD.

Recently, with the development of neuroimaging techniques, several neuroimaging methods have been used to investigate alterations in brain function in patients with PPPD. Two studies investigating structural alterations in the brain in PPPD patients using magnetic resonance imaging (MRI) found that both gray matter volume and structural networks were changed in specific brain regions (Wurthmann et al., 2017; Popp et al., 2018). Another study using single-photon emission computed tomography (SPECT) to explore regional cerebral blood flow (rCBF) in PPPD patients showed that the changes in rCBF were significantly different in several brain regions (Na et al., 2019). Moreover, several studies investigating brain activity in PPPD patients using functional MRI (fMRI) showed that the functional connectivity was altered in brain regions involved in the processing of multisensory vestibular information (Lee et al., 2018; Li et al., 2020b). In sum, the above studies indicated that cortical dysfunction could be observed in patients with PPPD using neuroimaging methods.

Magnetoencephalography (MEG) is a relatively new non-invasive technique that can be used to detect neuromagnetic signals. Recently, MEG was used to study epilepsy, migraine, and schizophrenia (Liu et al., 2015; Tang et al., 2016; Wu et al., 2016; Lottman et al., 2019; Sun et al., 2020) and used in the clinical evaluation of epileptogenic foci before epileptic surgery (De Tiege et al., 2017; Tamilia et al., 2017). MEG has a higher spatial resolution than electroencephalography (EEG) and can detect magnetic signals that are unaffected by the skull and skin (Babiloni et al., 2009). Moreover, MEG can detect signals with time resolution of milliseconds in wider frequency ranges (Moradi et al., 2003; Babiloni et al., 2009). Given the abovementioned findings, MEG could be an ideal tool to investigate cortical dysfunction in PPPD patients.

The aim of the present study was to investigate the abnormal spatial changes in brain activity in patients with PPPD. In this investigation, neuromagnetic signals were analyzed in low- to high-frequency bands using MEG. To the best of our knowledge, our study is the first to explore abnormal spatial alterations in brain activity in patients with PPPD using MEG. The investigation of alterations in brain function in patients with PPPD could improve the present understanding of the pathogenesis of PPPD and contribute to the development of treatments for PPPD in the future.

MATERIALS AND METHODS

Subjects

Eighteen right-handed patients diagnosed with PPPD were enrolled from Nanjing Brain Hospital. The inclusion criteria were as follows: (1) the clinical diagnosis of PPPD was in line with the diagnostic criteria of the Classification Committee of the Bárány Society (Staab et al., 2017), (2) no history of medication before enrollment, and (3) no abnormal MRI results. The exclusion criteria were as follows: (1) PPPD coexisting with peripheral vestibular lesions or other diseases and (2) the presence of metal implants in the head. In addition, eighteen age- and sex-matched healthy volunteers were included as controls. All healthy volunteers had no history of headache, dizziness, or other serious medical diseases. The present study was approved by the Medical Ethics Committees of Nanjing Brain Hospital and Nanjing Medical University. Informed assent was signed by all subjects. All methods were performed in accordance with the relevant guidelines and regulations of the Declaration of Helsinki for human experimentation.

Magnetoencephalography Recording

Magnetoencephalography data were recorded by a whole-head CTF 275 Channel MEG system (VSM Medical Technology Company, Coquitlam, BC, Canada) in a magnetic-shielded room in the MEG Center of Nanjing Brain Hospital. Background noise was identified by recording MEG signals in an empty room. Before formal MEG data recording, each subject was required to remove all metals from his or her body. Then, three coils were attached to the nasion and to the right and left preauricular points of each subject to locate the subject's position head relative to the MEG recording system. During MEG recording, each subject was asked to stay still with his or her eyes closed slightly and was monitored by an audio-visual system from an MEG recording device. At least five continuous MEG data files with a duration of 120 s were recorded for each subject. Each subject's head movement was limited to 5 mm for each MEG recording. The MEG data were collected at a sample of 6,000 Hz, with noise cancelation of third-order gradients.

Magnetic Resonance Imaging Scans

A 3.0-T MRI scanner (Siemens, Germany) was used to acquire three-dimensional structural images. A rapid gradient echo sequence was used to obtain anatomic 3D T1-weighted images. The imaging parameters were as follows: field of view 250 mm × 250 mm; flip angle 9°; matrix = 512 × 512. A total of 176 sagittal slices were collected for each subject. All subjects were required to minimize their head movements during MRI scanning. For each subject, markers were placed on the same three fiducial positions used for MEG recording to coregister the MRI data with the MEG data.

Data Analysis

For each MEG segment, magnetic noise and artifacts were identified by visual inspection. MEG segments without any artifacts and noise were viewed as clean MEG data and selected for further analysis. The duration of each clean MEG segment for further analysis was 100 s. The selected segments were analyzed in seven frequency bands: delta (1–4 Hz), theta (4–8 Hz), alpha (8–12 Hz), beta (12–30 Hz), gamma (30–80 Hz), ripple (80–250 Hz), and fast ripple (250–500 Hz). Notch filters for 50 Hz and its harmonics were performed to eliminate power-line noise from the MEG data.

Accumulated source imaging (ASI), which was defined as the volumetric summation of source activity over a period of time, was used to localize neuromagnetic activity (Xiang et al., 2014). The neuromagnetic sources were localized by ASI using node-beam lead fields (Xiang et al., 2014). Since each node-beam lead field indicated a form of either source-beamformer or subspace solution, the ASI had multiple source beamformers to separate correlated sources. Several previous studies have verified the reliability of this method (Xiang et al., 2014, 2015a,b; Liu et al., 2015; Tang et al., 2016; Li et al., 2020c; Sun et al., 2020).

Similar to previous studies (Xiang et al., 2009; Tang et al., 2016; Sun et al., 2020), we analyzed neuromagnetic activity based on individual MRI head models at the source level. The whole brain was scanned at 3 mm resolution (approximately 17,160 brain voxels, depending on the size of the brain) (Xiang et al., 2014). Volumetric source imaging was computed for each frequency band for each MEG data. The formula was defined as follows:

$$\mathrm{Asi}\,(r, s) = \sum_{t=1}^{t=n} Q(r, t) \quad (1)$$

In Equation (1), Asi represents the accumulative source strength at location r, s indicates the time slice, t represents the MEG data point in the selected slice s, Q indicates the source activity at location r and time point t, and n represents the number total time points included in the MEG data. Detailed mathematical algorithms and validations were demonstrated in previous publications (Xiang et al., 2014, 2015a). In addition, each voxel of source imaging contained a specific parameter to quantify neuromagnetic activity strength. Since the source strength was analyzed statistically, no units were provided for parameters (Xiang et al., 2015a). MEG source imaging was coregistered to MRI according to the three fiducial points used for MEG recording and then normalized spatially for group analyses.

Statistical Analysis

Fisher's exact test was used to identify the difference in neuromagnetic source locations between patients with PPPD and healthy controls. Student's *t*-test was performed to compare source strength between two groups. Partial correlation was applied to estimate the correlations between the source strength and clinical sores after adjustment for sex and age. The *p*-value threshold in the present study was defined as 0.05. A false discovery rate controlling procedure was used to solve type I errors. Bonferroni correction was used for multiple comparisons. Statistical analyses and computations were performed in SPSS version 20.0 for Windows (SPSS Inc., Chicago, IL, United States).

RESULTS

Clinical Characteristics

Eighteen patients with PPPD and eighteen healthy controls were enrolled in this study. The Dizziness Handicap Inventory score (DHI), the Hamilton Anxiety scale (HAMA), and the Hamilton Depression scale (HAMD) were applied to assess symptoms in patients with PPPD. The average age of PPPD patients was 55.39 $\pm$ 12.52 years. The mean duration of disease was 8.17 $\pm$ 4.38, mean DHI score was 52.72 $\pm$ 7.4, mean HAMA score was 16.61 $\pm$ 4.23, and mean HAMD was 13.44 $\pm$ 5.07. The detailed characteristics of PPPD patients are shown in **Table 1**. A total of 18 MEG segments from patients and 18 MEG segments from healthy controls were selected for further analysis.

Source Localization Pattern

At 1–4 Hz, the neuromagnetic source was mainly localized in the frontal cortex and temporal-parietal junction (TPJ) (7 in right TPJ, 4 in left TPJ, and 4 in bilateral TPJ) in patients with PPPD compared with that in healthy controls ($p < 0.05$). At 4–8 Hz, neuromagnetic activity was mainly localized in the TPJ (5 in right TPJ, 5 in left TPJ, and 4 in bilateral TPJ) in patients with PPPD compared with that in healthy controls ($p < 0.05$). At 8–12 Hz, neuromagnetic activity was mainly localized in the occipital cortex in both PPPD patients and healthy controls ($p > 0.05$). At 12–30 Hz, neuromagnetic activity was mainly localized in the TPJ (4 in right TPJ, 3 in left TPJ, and 5 in bilateral TPJ) in patients with PPPD compared with that in healthy controls ($p < 0.05$). In 30–80 Hz, neuromagnetic activity was mainly localized in deep brain areas (DBA) in both PPPD patients and healthy controls ($p > 0.05$). In the high-frequency ranges (80–250 and 250–500 Hz), PPPD subjects had a significantly higher odds ratio in the frontal cortex than healthy controls ($p < 0.05$). See **Figures 1–3** for details.

Source Strength in Neuromagnetic Activity

There was no significant difference in source strength in whole brain level between patients with PPPD and controls in all seven frequency bands (**Table 2**). However, significant changes in the localized source strength of specific brain areas were observed in low frequency bands between PPPD patients and healthy controls. In 1–4 Hz, the localized source strength in TPJ and frontal cortex in PPPD was significantly higher than corresponding brain regions in controls ($p < 0.05$). In 4–8 Hz, the localized source strength in TPJ in PPPD was significantly higher than healthy controls ($p < 0.05$). See **Figure 4** for details.

Correlations Between the Source Strength and Clinical Scores

In the present study, significant correlations were observed between the localized source strength in specific brain regions

TABLE 1 | Characteristics of the patients with PPPD.

Patient	Sex (F/M)	Age (years)	Duration of disease (months)	DHI	HAMA	HAMD	Dizziness	Unsteadiness	Non-spinning vertigo
1	F	79	5	54	11	9	+	+	+
2	M	39	12	62	18	17	+	+	+
3	F	63	8	48	16	12	+	+	+
4	F	49	3	44	10	7	+	+	+
5	F	42	14	57	20	20	+	+	+
6	F	57	9	49	16	11	+	+	+
7	F	70	4	39	13	6	+	+	+
8	F	48	7	52	17	10	+	+	
9	M	57	4	57	15	13	+	+	+
10	F	54	2	55	18	16	+	+	+
11	M	51	7	49	12	9	+	+	+
12	F	50	9	58	19	15	+	+	+
13	F	57	15	66	26	24	+	+	+
14	F	54	18	64	24	21	+	+	
15	F	75	10	51	16	18	+	+	+
16	F	33	4	47	19	11	+	+	+
17	M	47	8	42	12	9	+	+	
18	F	72	8	55	17	14	+	+	

F, female; M, male; DHI, Dizziness Handicap Inventory score; HAMA, Hamilton Anxiety scale; HAMD, Hamilton Depression scale. +indicates symptoms exist.

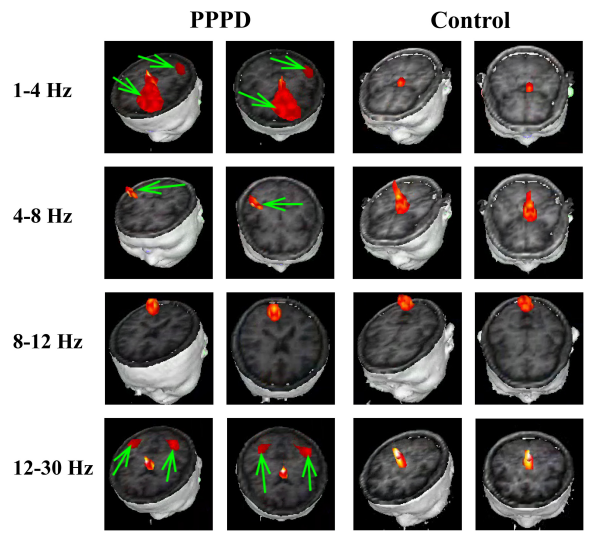

FIGURE 1 | Typical distribution of neuromagnetic source localization in 1–30 Hz frequency bands in PPPD patients and controls. Green arrows indicate the significant difference in source localization in PPPD patients compared with the controls.

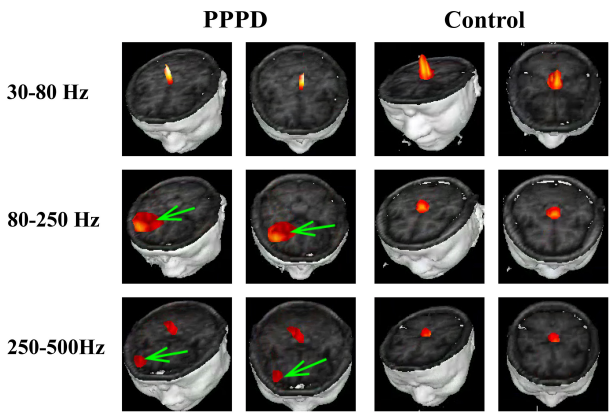

FIGURE 2 | Typical distribution of neuromagnetic source localization in 30–500 Hz frequency bands in PPPD patients and controls. Green arrows indicate the significant difference in source localization in PPPD patients compared with the controls.

in low frequency band and clinical scores in PPPD patients. Specifically, in 1–4 Hz, the localized source strength in TPJ was positively correlated with DHI score ($r = 0.7085$, $p < 0.05$), while the localized source strength in frontal cortex was positively correlated with HAMA score ($r = 0.5542$, $p < 0.05$). No significant correlation was observed between the local source strength and clinical scores in other frequency bands. The details are shown in **Figure 5**.

DISCUSSION

In the present study, we explored cortical neuromagnetic activity in patients with PPPD by multifrequency analysis using MEG. The results showed that frequency-dependent alterations in neuromagnetic activity were observed in patients with PPPD compared with healthy controls. To the best of our knowledge, this is the first study to investigate neuromagnetic activity in PPPD patients using MEG.

Our results found that the abnormal neuromagnetic source localization in patients with PPPD was more likely to be located in the TPJ than in healthy controls, indicating that the function of this brain region was disordered in patients with PPPD.

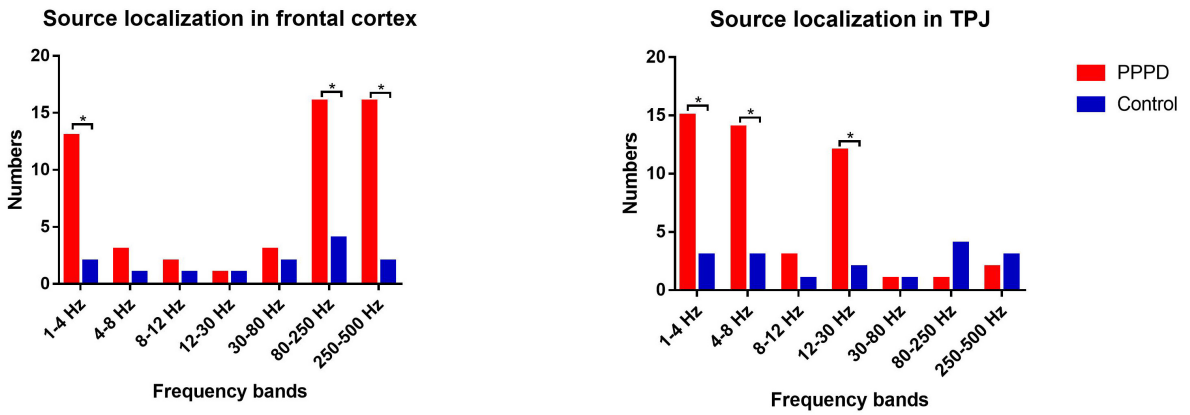

FIGURE 3 | Difference in the number of neuromagnetic source localization between PPPD patients and the controls in seven frequency bands. The number of source locations is located on the *y*-axis. Seven frequency bands are listed on the *x*-axis. *$p < 0.05$ after Bonferroni correction.

Our study also founded that the neuromagnetic source strength in TPJ in PPPD patients was significantly higher than healthy controls indicating that the neural activity of TPJ in PPPD patients was increased abnormally. In addition, in our research, a positive correlation between neuromagnetic source strength in TPJ and DHI score shown that the abnormal activity of TPJ may be related to the dizziness symptom of PPPD patients. Therefore, we speculate that the abnormal increase of neural activity in TPJ might be a potential factor contributing to dizziness symptom of PPPD patients. This finding was consisted with several studies. A study using resting-state fMRI showed that functional connectivity in the superior temporal gyrus (STG) was decreased in PPPD patients compared to healthy controls (Van Ombergen et al., 2017; Lee et al., 2018). Another study using task-based fMRI reported that functional connectivity was decreased between the STG and other brain regions in patients with PPPD (Indovina et al., 2015). In addition, a structural MRI study found decreased gray matter volume in the STG and parietal cortex in PPPD patients (Wurthmann et al., 2017). According to previous studies, the TPJ, including adjacent areas of the temporal and parietal lobes, is an important component of the parieto-insular vestibular cortex (PIVC) and plays a critical role in the integration and processing of multisensory information (Eickhoff et al., 2006; Wurthmann et al., 2017). A previous study found that the TPJ has bidirectional connections with frontal and temporal lobes and receive the sensory inputs from subcortical, visual and auditory areas (Decety and Lamm, 2007). The TPJ participates in motor and posture control by transmitting multisensory information to motor areas based on connections between posterior brain regions and the frontal cortex (Hoshi and Tanji, 2007). In addition, vestibular and visual

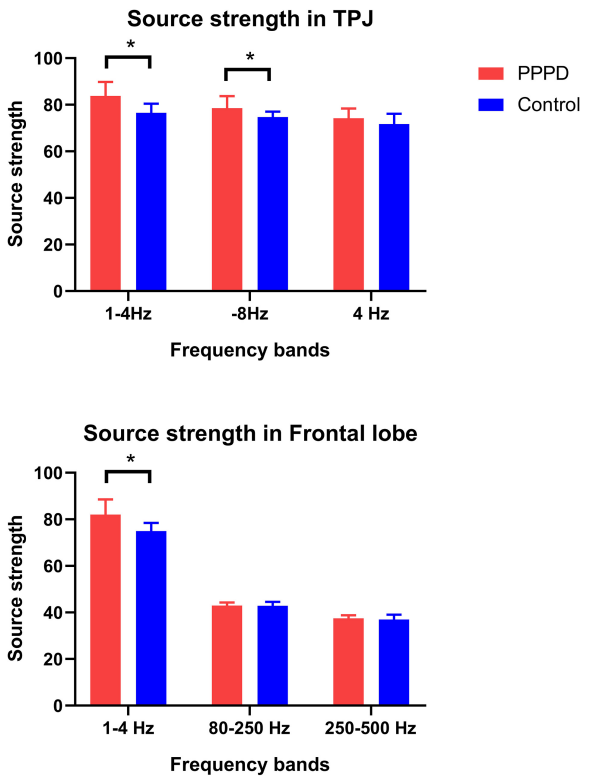

FIGURE 4 | Changes in neuromagnetic source strength in specific brain regions between two groups. *$P < 0.05$ after Bonferroni correction.

TABLE 2 | Comparison of neuromagnetic source strength between PPPD patients and controls.

Frequency bands	PPPD patient	Control	*P* value
1–4 Hz	84.29 ± 5.99	84.45 ± 8.61	$P > 0.05$
4–8 Hz	78.65 ± 5.39	79.58 ± 5.55	$P > 0.05$
8–12 Hz	82.24 ± 12.79	84.03 ± 17.03	$P > 0.05$
12–30 Hz	74.51 ± 4.68	74.79 ± 7.62	$P > 0.05$
30–80 Hz	57.39 ± 6.97	54.88 ± 9.17	$P > 0.05$
80–250 Hz	43.27 ± 1.80	43.52 ± 2.15	$P > 0.05$
250–500 Hz	38.29 ± 1.02	38.59 ± 2.54	$P > 0.05$

There was no significant difference between two groups after Bonferroni correction.

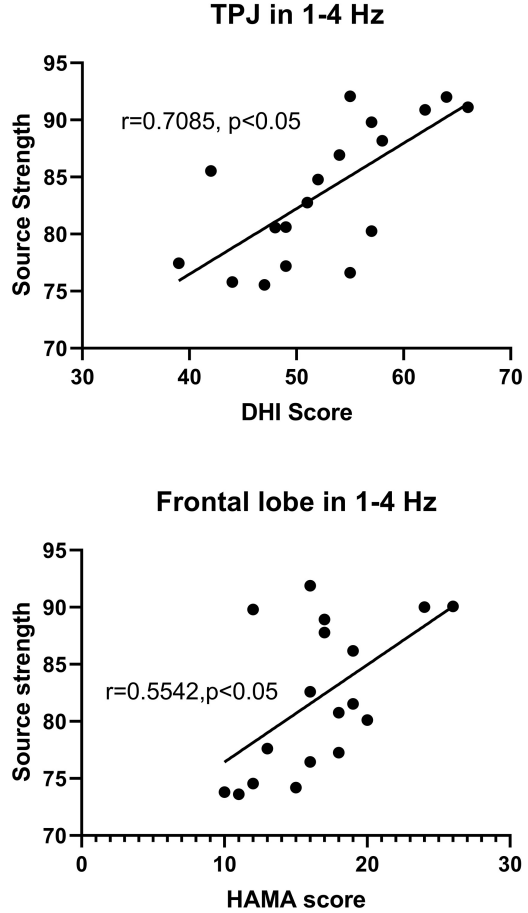

FIGURE 5 | The *y*-axis represents the neuromagnetic source strength. The *x*-axis represents clinical scores. Partial correlation analysis showed that the neuromagnetic source strength in TPJ in 1–4 Hz was positively correlated with DHI score ($r = 0.7085$, $p < 0.05$), and the neuromagnetic source strength in frontal cortex in 1–4 Hz was positively correlated with HAMA score ($r = 0.5542$, $p < 0.05$) after adjustment for sex and age.

sensory information are also integrated and processed via the TPJ (Takeuchi et al., 2018). A neuroimage study found that the abnormal activation was observed in TPJ when sensory integration conflict existed (Balslev et al., 2005). A previous study reported that patients whose lesions were localized in the TPJ presented with deficits in vestibular spatial orientation, also suggesting an association between the TPJ and the processing of vestibular spatial information (Kaski et al., 2016). In addition, dysfunction of the TPJ was also a potential pathophysiological mechanism of virtual reality sickness, a disease which was involved in vestibular-visual information mismatch (Takeuchi et al., 2018). Thus, we speculate that dysfunction in the TPJ weakens PPPD patients' ability to process and integrate vestibular spatial inputs and causes them to experience persistent dizziness and unsteadiness.

Furthermore, in our study, abnormal brain activity in the frontal cortex was also observed in patients with PPPD compared with healthy controls. We founded that the neuromagnetic source strength in frontal cortex was significantly higher than controls indicating that the abnormal neural activity of frontal cortex might be another potential pathological imaging feature of PPPD patients. This finding was in line with previous literature. Several studies confirmed that brain activity in the frontal cortex was altered in PPPD patients (Indovina et al., 2015; Van Ombergen et al., 2017; Lee et al., 2018; Li et al., 2020b). One study using structural MRI also found that gray matter volume was decreased in the frontal lobe in PPPD patients, suggesting that these individuals have a structural impairment in the frontal lobe (Wurthmann et al., 2017). Moreover, a SPECT study showed hypoperfusion in the frontal lobe in PPPD patients (Na et al., 2019). Pertinently, the frontal lobe participates in diverse cortical functions, including executive function, motivation, and working memory processing, in the brain, as reported by previous publications (Pochon et al., 2001; du Boisgueheneuc et al., 2006). The motor regions of the frontal cortex regulate posture and complex movements by receiving information from sensory regions of the parietal cortex (Wurthmann et al., 2017). Therefore, when the TPJ is dysfunctional, the motor areas of the frontal lobe cannot obtain accurate multisensory information from the external environment and patients' ability to regulate their body posture is affected. In addition, the frontal cortex is involved in emotion modulation (Lee et al., 2018). Previous studies reported that functional alterations in the frontal cortex were observed in patients with several psychiatric diseases, such as schizophrenia and autism spectrum disorder (Xiang et al., 2016; Lee et al., 2017). An fMRI study found that alterations in the frontal cortex were not observed after adjusting for anxiety and depression in patients with PPPD, indicating that abnormal changes in the frontal cortex appeared to be related to coexisting pathological psychiatric states, such as anxiety and depression, in PPPD patients (Lee et al., 2018). In our study, we founded that the neuromagnetic source strength in frontal cortex was positively correlated with HAMA score suggesting that the abnormal increase in neural activity of frontal cortex may be related to emotional symptom of PPPD patients. Our results indicated that emotional symptoms of PPPD patients, such as anxiety, may be resulted from a potential pathological basis in the frontal lobe, not just emotional feedback caused by dizziness symptoms of PPPD patients. Thus, we speculate that the functional impairment of the frontal lobe plays an important role in postural balance disturbance and emotional disorders in patients with PPPD.

For the first time, our study used MEG to demonstrate frequency-dependent alterations in cortical localized patterns in PPPD patients. We found that alterations in cortical localized patterns in the TPJ were observed in low-frequency bands (mainly in 1–4, 4–8, and 12–30 Hz), and alterations in the frontal cortex were observed in both low- and high-frequency bands (mainly in 1–4, 80–250, and 250–500 Hz). However, it is worth noting that the significant increase in neuromagnetic source strength of specific brain areas in PPPD patients compared with healthy controls was observed in low frequency (mainly in 1–4 and 4–8 Hz), while in other frequency bands the significant changes in the localized neuromagnetic source strength of specific brain regions between two groups were not founded.

According to previous studies, frequency-dependent changes in brain activity were observed in patients with other diseases, such as epilepsy, migraine, schizophrenia, and autism spectrum disorder (Tenney et al., 2014; Xiang et al., 2015a; Wu et al., 2016; Lee et al., 2017). As reported by several studies, the types of connections and information interactions at the temporal-spatial level among neurons were different in different frequency bands (Tenney et al., 2014). It was presumed that the speed of information transmission was restricted by the frequency of oscillations. In lower frequency bands, oscillations were suited to integrate information from large regions (Sauseng and Klimesch, 2008). However, in higher frequency ranges, oscillations were used to interact with neighboring neurons (Engel and da Silva, 2012). The research mentioned above could partially explain our findings in different frequency bands. We speculate that the function of information integration in large brain regions in lower frequency bands could support the processing and integration of sensory information from the external environment in the TPJ. The abnormal changes of neuromagnetic activity involving TPJ and frontal lobe in low frequency bands may be an important pathological imaging feature of PPPD. However, the specific mechanism underlying frequency-dependent changes found in the present study should be further investigated in the future.

Abnormal changes in cortical function were observed in patients with PPPD in fMRI studies (Indovina et al., 2015; Li et al., 2020a). To our knowledge, the basis of neuronal activity in the brain is electrical activity. The electrical activity of the brain in cell level is accompanied by changes in the magnetic field leading to corresponding changes in the neuromagnetic signal. Therefore, we believe that the cortical dysfunction in PPPD could cause changes in neuromagnetic signals in specific brain regions, which can be detected by MEG. In addition, a previous study using EEG have found that patients with dizziness can find abnormal brain activity in the low frequency bands, which suggested that although there is no epileptic activity in patients with dizziness, other forms of abnormal brain activity could be detected by EEG, such as abnormal brain activity in the low frequency bands (Nürnberger et al., 2021). MEG has higher spatial resolution than EEG and the magnetic signal is not affected by skull and skin. Therefore, using MEG to analyze the brain activity in patients with PPPD can get more accurate and reliable results than EEG. Source localization is an analytical method used to quantify neuromagnetic signals in the brain (Xiang et al., 2014, 2015b). By this method, subtle brain activity can be detected and located in the cortical region. We believe that using this method, we can accurately detect subtle changes in neural activity of specific brain regions and localize the cortical pathological changes in PPPD patients. In addition, source localization can also provide quantitative parameters to evaluate the subtle changes in cortical function, which could provide an objective basis for the study of the relationship between specific cortical functions and clinical symptoms. Through this method, we have studied several kinds of diseases, such as childhood absence epilepsy, migraine and so on, and obtained several localization and quantitative research results (Liu et al., 2015; Tang et al., 2016; Sun et al., 2020). Therefore, we think that the application of MEG and source localization method could obtain ideal results in PPPD research.

Limitations

There were several limitations in our study. First, the sample size of the present study is relatively small and might influence the results in our study. A larger sample size of study could be necessary to further validate our research in the future. Second, MEG is not sensitive to magnetic signals in DBA. Therefore, we only analyzed and discussed the changes in cortical functions in PPPD patients. With the application of wearable MEG devices, the above problem can be resolved. Third, due to the limitation of software, we did not analyze, and process negatively activated brain regions in patients with PPPD. Therefore, we only discussed the results of activated brain regions localized by MEG in this paper. With the progress of software technology, this problem could be solved in the future. Fourth, in this study, we found neuromagnetic localization in the right, left and bilateral TPJ at 1–4, 4–8, and 12–30 Hz. However, there was no significant difference among these locations of TPJ. We believe that the sample size could be the reason for the above results. In the future study, with the further expansion of sample size, we will be able to further understand the location characteristics of TPJ in those frequency bands. Although frequency-dependent changes were found in the present study, we also believed that the above results were only preliminary conclusion, and the specific relationship between these changes and PPPD needs further research using other methods to explore. In addition, we also agree that the study of brain networks in patients with PPPD can further deepen the understanding of the pathophysiological mechanism of PPPD. Indeed, the analysis of abnormal neuromagnetic localizations in patients with PPPD was a preliminary study of functional imaging of PPPD. Therefore, in the future, we will further investigate the brain network of PPPD based on the results of neuromagnetic source localization in PPPD patients in the present study, in order to further explore the pathophysiological mechanism of PPPD. Finally, although various methods were used to minimize artifacts, our results may still have been affected by residual artifacts. Further research is needed to verify whether the artifacts have been completely eliminated.

CONCLUSION

For the first time, our study using MEG demonstrated that abnormal changes in neuromagnetic localization in the TPJ and frontal lobe were found in low- and high-frequency bands in patients with PPPD. The localized neuromagnetic activity in TPJ and frontal cortex was abnormally increased in low frequency bands in PPPD patients compared with healthy controls. In addition, the neuromagnetic activity in TPJ may be related to dizziness symptom of PPPD patients, while the neuromagnetic activity in frontal lobe may be related to emotional symptoms of PPPD patients. These findings suggest that the TPJ and frontal lobe may play a critical role in the pathophysiological mechanism of PPPD. Our results could provide novel insights into the pathophysiology of PPPD.

DATA AVAILABILITY STATEMENT

The original contributions presented in the study are included in the article/supplementary material, further inquiries can be directed to the corresponding author.

ETHICS STATEMENT

The studies involving human participants were reviewed and approved by the Medical Ethics Committees of Nanjing Brain Hospital and Nanjing Medical University. The patients/participants provided their written informed consent to participate in this study.

AUTHOR CONTRIBUTIONS

JS, WJ, JX, and XW designed the research. JS, YS, and KZ analyzed the data. JS, WJ, QC, and LT recruited the participants and acquired the images. JS wrote the manuscript. XW revised the manuscript. All authors approved the final submitted version and agreed to be accountable for its content.

FUNDING

This study was supported by the General Program of Natural Science Foundation of Jiangsu Province (Grant No. BK20191127), Health Department of Jiangsu Province (Grant No. H2018062), Medical and Health International Cooperation Project of Nanjing Municipal Science and Technology Bureau (Grant No. 201911044), and National Natural Science Foundation of China (Grant No. 82071455).

ACKNOWLEDGMENTS

We would like to thank the physicians and researchers at the NBH. We are very grateful for support from all participants and the controls.

REFERENCES

Babiloni, C., Pizzella, V., Gratta, C. D., Ferretti, A., and Romani, G. L. (2009). Fundamentals of electroencefalography, magnetoencefalography, and functional magnetic resonance imaging. *Int. Rev. Neurobiol.* 86, 67–80. doi: 10.1016/S0074-7742(09)86005-4

Balslev, D., Nielsen, F. A., Paulson, O. B., and Law, I. (2005). Right temporoparietal cortex activation during visuo-proprioceptive conflict. *Cerebral Cortex* 15, 166–169.

Cao, Z., Liu, X., Ju, Y., and Zhao, X. (2021). Neuroimaging studies in persistent postural-perceptual dizziness and related disease: a systematic review. *J. Neurol.* doi: 10.1007/s00415-021-10558-x [Epub ahead of print].

De Tiege, X., Lundqvist, D., Beniczky, S., Seri, S., and Paetau, R. (2017). Current clinical magnetoencephalography practice across Europe: are we closer to use MEG as an established clinical tool? *Seizure* 50, 53–59. doi: 10.1016/j.seizure.2017.06.002

Decety, J., and Lamm, C. (2007). The role of the right temporoparietal junction in social interaction: how low-level computational processes contribute to meta-cognition. *Neurosci. Rev. J. Bringing Neurobiol. Neurol. Psychiatry* 13, 580–593.

Dieterich, M., and Staab, J. P. (2017). Functional dizziness: from phobic postural vertigo and chronic subjective dizziness to persistent postural-perceptual dizziness. *Curr. Opin. Neurol.* 30, 107–113. doi: 10.1097/WCO.0000000000000417

du Boisgueheneuc, F., Levy, R., Volle, E., Seassau, M., Duffau, H., Kinkingnehun, S., et al. (2006). Functions of the left superior frontal gyrus in humans: a lesion study. *Brain* 129, 3315–3328. doi: 10.1093/brain/awl244

Eickhoff, S. B., Weiss, P. H., Amunts, K., Fink, G. R., and Zilles, K. (2006). Identifying human parieto-insular vestibular cortex using fMRI and cytoarchitectonic mapping. *Hum. Brain Mapp.* 27, 611–621. doi: 10.1002/hbm.20205

Engel, J. Jr., and da Silva, F. L. (2012). High-frequency oscillations - where we are and where we need to go. *Prog. Neurobiol.* 98, 316–318. doi: 10.1016/j.pneurobio.2012.02.001

Hoshi, E., and Tanji, J. (2007). Distinctions between dorsal and ventral premotor areas: anatomical connectivity and functional properties. *Curr. Opin. Neurol.* 17, 234–242. doi: 10.1016/j.conb.2007.02.003

Indovina, I., Riccelli, R., Chiarella, G., Petrolo, C., Augimeri, A., Giofre, L., et al. (2015). Role of the insula and vestibular system in patients with chronic subjective dizziness: an fMRI study using sound-evoked vestibular stimulation. *Front. Behav. Neurosci.* 9:334. doi: 10.3389/fnbeh.2015.00334

Kaski, D., Quadir, S., Nigmatullina, Y., Malhotra, P. A., Bronstein, A. M., and Seemungal, B. M. (2016). Temporoparietal encoding of space and time during vestibular-guided orientation. *Brain* 139, 392–403. doi: 10.1093/brain/awv370

Lee, J., Hudson, M. R., O'Brien, T. J., Nithianantharajah, J., and Jones, N. C. (2017). Local NMDA receptor hypofunction evokes generalized effects on gamma and high-frequency oscillations and behavior. *Neuroscience* 358, 124–136. doi: 10.1016/j.neuroscience.2017.06.039

Lee, J. O., Lee, E. S., Kim, J. S., Lee, Y. B., Jeong, Y., Choi, B. S., et al. (2018). Altered brain function in persistent postural perceptual dizziness: a study on resting state functional connectivity. *Hum. Brain Mapp.* 39, 3340–3353. doi: 10.1002/hbm.24080

Li, K., Si, L., Cui, B., Ling, X., Shen, B., and Yang, X. (2020b). Altered spontaneous functional activity of the right precuneus and cuneus in patients with persistent postural-perceptual dizziness. *Brain Imaging Behav.* 14, 2176–2186. doi: 10.1007/s11682-019-00168-7

Li, Y., Sun, Y., Niu, K., Wang, P., Xiang, J., Chen, Q., et al. (2020c). The relationship between neuromagnetic activity and cognitive function in benign childhood epilepsy with centrotemporal spikes. *Epilepsy Behav.* 112:107363. doi: 10.1016/j.yebeh.2020.107363

Li, K., Si, L., Cui, B., Ling, X., Shen, B., and Yang, X. (2020a). Altered intra- and inter-network functional connectivity in patients with persistent postural-perceptual dizziness. *Neuroimage Clin* 26:102216. doi: 10.1016/j.nicl.2020.102216

Liu, H., Ge, H., Xiang, J., Miao, A., Tang, L., Wu, T., et al. (2015). Resting state brain activity in patients with migraine: a magnetoencephalography study. *J. Headache Pain* 16:525. doi: 10.1186/s10194-015-0525-5

Lottman, K. K., Gawne, T. J., Kraguljac, N. V., Killen, J. F., Reid, M. A., and Lahti, A. C. (2019). Examining resting-state functional connectivity in first-episode schizophrenia with 7T fMRI and MEG. *Neuroimage Clin.* 24:101959. doi: 10.1016/j.nicl.2019.101959

Moradi, F., Liu, L. C., Cheng, K., Waggoner, R. A., Tanaka, K., and Ioannides, A. A. (2003). Consistent and precise localization of brain activity in human primary visual cortex by MEG and fMRI. *Neuroimage* 18, 595–609. doi: 10.1016/s1053-8119(02)00053-8

Na, S., Im, J. J., Jeong, H., Lee, E. S., Lee, T. K., Chung, Y. A., et al. (2019). Cerebral perfusion abnormalities in patients with persistent postural-perceptual dizziness (PPPD): a SPECT study. *J. Neural. Transm.* 126, 123–129. doi: 10.1007/s00702-018-1948-3

Nürnberger, M., Klingner, C., Witte, O. W., and Brodoehl, S. (2021). Mismatch of visual-vestibular information in virtual reality: is motion sickness part of the brains attempt to reduce the prediction error? *Front. Hum. Neurosci.* 15:757735. doi: 10.3389/fnhum.2021.757735

Pochon, J. B., Levy, R., Poline, J. B., Crozier, S., Lehericy, S., Pillon, B., et al. (2001). The role of dorsolateral prefrontal cortex in the preparation of forthcoming actions: an fMRI study. *Cereb. Cortex* 11, 260–266. doi: 10.1093/cercor/11.3.260

Popp, P., Zu Eulenburg, P., Stephan, T., Bogle, R., Habs, M., Henningsen, P., et al. (2018). Cortical alterations in phobic postural vertigoa multimodal imaging approach. *Ann. Clin. Transl. Neurol.* 5, 717–729. doi: 10.1002/acn3.570

Sauseng, P., and Klimesch, W. (2008). What does phase information of oscillatory brain activity tell us about cognitive processes? *Neurosci. Biobehav. Rev.* 32, 1001–1013. doi: 10.1016/j.neubiorev.2008.03.014

Sohsten, E., Bittar, R. S., and Staab, J. P. (2016). Posturographic profile of patients with persistent postural-perceptual dizziness on the sensory organization test. *J. Vestib. Res.* 26, 319–326. doi: 10.3233/VES-160583

Staab, J. P., Eckhardt-Henn, A., Horii, A., Jacob, R., Strupp, M., Brandt, T., et al. (2017). Diagnostic criteria for persistent postural-perceptual dizziness (PPPD): consensus document of the committee for the classification of vestibular disorders of the barany society. *J. Vestib. Res.* 27, 191–208. doi: 10.3233/VES-170622

Sun, J., Gao, Y., Miao, A., Yu, C., Tang, L., Huang, S., et al. (2020). Multifrequency dynamics of cortical neuromagnetic activity underlying seizure termination in absence epilepsy. *Front. Hum. Neurosci.* 14:221. doi: 10.3389/fnhum.2020.00221

Sun, L., and Xiang, K. (2020). A review on the alterations in the brain of persistent postural-perceptual dizziness patients and non-pharmacological interventions for its management. *Rev. Neurosci.* 31, 675–680. doi: 10.1515/revneuro-2019-0109

Takeuchi, N., Mori, T., Suzukamo, Y., and Izumi, S. I. (2018). Modulation of excitability in the temporoparietal junction relieves virtual reality sickness. *Cyberpsychol. Behav. Soc. Netw* 21, 381–387. doi: 10.1089/cyber.2017.0499

Tamilia, E., Madsen, J. R., Grant, P. E., Pearl, P. L., and Papadelis, C. (2017). Current and emerging potential of magnetoencephalography in the detection and localization of high-frequency oscillations in epilepsy. *Front. Neurol.* 8:14. doi: 10.3389/fneur.2017.00014

Tang, L., Xiang, J., Huang, S., Miao, A., Ge, H., Liu, H., et al. (2016). Neuromagnetic high-frequency oscillations correlate with seizure severity in absence epilepsy. *Clin. Neurophysiol.* 127, 1120–1129. doi: 10.1016/j.clinph.2015.08.016

Tenney, J. R., Fujiwara, H., Horn, P. S., Vannest, J., Xiang, J., Glauser, T. A., et al. (2014). Low- and high-frequency oscillations reveal distinct absence seizure networks. *Ann. Neurol.* 76, 558–567. doi: 10.1002/ana.24231

Van Ombergen, A., Heine, L., Jillings, S., Roberts, R. E., Jeurissen, B., Van Rompaey, V., et al. (2017). Altered functional brain connectivity in patients with visually induced dizziness. *Neuroimage Clin.* 14, 538–545. doi: 10.1016/j.nicl.2017.02.020

Wu, D., Zhou, Y., Xiang, J., Tang, L., Liu, H., Huang, S., et al. (2016). Multi-frequency analysis of brain connectivity networks in migraineurs: a magnetoencephalography study. *J. Headache Pain* 17:38. doi: 10.1186/s10194-016-0636-7

Wurthmann, S., Naegel, S., Schulte Steinberg, B., Theysohn, N., Diener, H. C., Kleinschnitz, C., et al. (2017). Cerebral gray matter changes in persistent postural perceptual dizziness. *J. Psychosom Res.* 103, 95–101. doi: 10.1016/j.jpsychores.2017.10.007

Xiang, J., Korman, A., Samarasinghe, K. M., Wang, X., Zhang, F., Qiao, H., et al. (2015a). Volumetric imaging of brain activity with spatial-frequency decoding of neuromagnetic signals. *J. Neurosci. Methods* 239, 114–128. doi: 10.1016/j.jneumeth.2014.10.007

Xiang, J., Tenney, J. R., Korman, A. M., Leiken, K., Rose, D. F., Harris, E., et al. (2015b). Quantification of interictal neuromagnetic activity in absence epilepsy with accumulated source imaging. *Brain Topogr.* 28, 904–914. doi: 10.1007/s10548-014-0411-5

Xiang, J., Korostenskaja, M., Molloy, C., deGrauw, X., Leiken, K., Gilman, C., et al. (2016). Multi-frequency localization of aberrant brain activity in autism spectrum disorder. *Brain Dev.* 38, 82–90. doi: 10.1016/j.braindev.2015.04.007

Xiang, J., Liu, Y., Wang, Y., Kotecha, R., Kirtman, E. G., Chen, Y., et al. (2009). Neuromagnetic correlates of developmental changes in endogenous high-frequency brain oscillations in children: a wavelet-based beamformer study. *Brain Res.* 1274, 28–39. doi: 10.1016/j.brainres.2009.03.068

Xiang, J., Luo, Q., Kotecha, R., Korman, A., Zhang, F., Luo, H., et al. (2014). Accumulated source imaging of brain activity with both low and high-frequency neuromagnetic signals. *Front. Neuroinformatics* 8:57. doi: 10.3389/fninf.2014.00057

Conflict of Interest: The authors declare that the research was conducted in the absence of any commercial or financial relationships that could be construed as a potential conflict of interest.

Publisher's Note: All claims expressed in this article are solely those of the authors and do not necessarily represent those of their affiliated organizations, or those of the publisher, the editors and the reviewers. Any product that may be evaluated in this article, or claim that may be made by its manufacturer, is not guaranteed or endorsed by the publisher.

Advantages of publishing in Frontiers

OPEN ACCESS
Articles are free to read for greatest visibility and readership

FAST PUBLICATION
Around 90 days from submission to decision

HIGH QUALITY PEER-REVIEW
Rigorous, collaborative, and constructive peer-review

TRANSPARENT PEER-REVIEW
Editors and reviewers acknowledged by name on published articles

Frontiers
Avenue du Tribunal-Fédéral 34
1005 Lausanne | Switzerland

Visit us: www.frontiersin.org
Contact us: frontiersin.org/about/contact

REPRODUCIBILITY OF RESEARCH
Support open data and methods to enhance research reproducibility

DIGITAL PUBLISHING
Articles designed for optimal readership across devices

FOLLOW US
@frontiersin

IMPACT METRICS
Advanced article metrics track visibility across digital media

EXTENSIVE PROMOTION
Marketing and promotion of impactful research

LOOP RESEARCH NETWORK
Our network increases your article's readership